Magnetic and structural studies of sputtered metallic multilayers

Lafford, Tamzin Amanda

Award date:
1994

Awarding institution:
University of Bath

MAGNETIC AND STRUCTURAL STUDIES OF SPUTTERED METALLIC MULTILAYERS

submitted by

Tamzin Amanda LAFFORD

for the degree of PhD

of the University of Bath

1994

ProQuest LLC
789 East Eisenhower Parkway
P.O. Box 1346
Ann Arbor, MI 48106-1346

Abstract

Metallic multilayers were deposited by radio-frequency magnetron sputtering. Magnetic, magnetoelastic and structural properties were investigated, using techniques including quasi-d.c. magnetometry, Small Angle Magnetisation Rotation and X-ray diffraction in the θ-2θ configuration. Experimental apparatus and methods were developed according to the requirements of the thin films studied. The aim was to produce multilayers simultaneously magnetically soft and highly magnetostrictive for sensor and transducer applications.

Two Fe-Co alloys were multilayered with Ag: HiSat50® (as deposited, 45wt.% Fe, 55wt.% Co, <0.2wt.% Ta) and Permendur24® (as deposited, 72wt.% Fe, 28wt.% Co, trace Cr). Saturation magnetostriction values calculated for random polycrystalline alloys of these compositions from single-crystal magnetostriction constants were $\overline{\lambda_s}$ = +84±4ppm and $\overline{\lambda_s}$ = +42±4ppm, respectively. Published experimental λ_s data were lower. Certain multilayers exhibited λ_s equal to the calculated values. These multilayers were also the softest observed in the series, with corresponding coercivities of $H_c = 340 Am^{-1}$ and $H_c = 560 Am^{-1}$, significantly softer than plain alloy films.

The magnetostriction results on (111)-textured Co-Pd/Ag multilayers were in line with published data on a similar Co-Pd alloy ($\lambda_s \approx -160$ppm). The Co-Pd/Ag multilayers had coercivities of a few tens of kAm^{-1}; suggestions have been made for improving softness whilst utilising the highly magnetostrictive Co-Pd alloy.

The saturation magnetostriction results on all the magnetic/non-magnetic multilayers were understood by considering λ_s to be the volume average of contributions from the magnetic layers and interface regions. This interpretation was developed from a published expression for the magnetostriction of magnetic/magnetic multilayers. Fits to experimental data yielded physically reasonable values of the magnetostriction of the magnetic layers.

X-ray diffraction patterns from Co-Pd/Ag multilayers were fitted using the kinematic theory of diffraction. Layer thicknesses, lattice plane spacings and interface roughness parameters were returned by the fitting program. Further development is required for the program to become a routine tool for structural analysis.

Publications and Presentations

The following papers have arisen from the work presented in this thesis:

Lafford, T. A., M. R. J. Gibbs and C. Shearwood, "Magnetic, magnetostrictive and structural properties of iron-cobalt/silver multilayers", *J. Magn. Magn. Mat.* **132** (1994) 89-94.

Lafford, T. A. and M. R. J. Gibbs, "Magnetic, magnetostrictive and structural properties of iron-cobalt/silver multilayers", MagNews, Summer 1993.

Lafford, T. A., R. Zuberek and M. R. J. Gibbs, "Magnetic Properties of $Co_{32}Pd_{68}$/Ag multilayers", ICM Conference 1994, Warsaw, Poland. Oral presentation by TAL. Proceedings to be published in *J. Magn. Magn. Mat.*

Lafford, T. A., M. R. J. Gibbs, R. Zuberek and C. Shearwood, "Magnetostriction and magnetic properties of iron-cobalt alloys multilayered with silver", MMM/Intermag Conference, June 1994, Albuquerque, New Mexico. Poster presentation. Proceedings to appear in *J. Appl. Phys.*

Shearwood, C., T. A. Lafford and M. R. J. Gibbs, "Magnetic, magnetostrictive and structural properties of multilayer films of iron-cobalt alloys with metallic interlayers", Condensed Matter and Materials Physics Conference 1993, Leeds. Oral presentation given by TAL.

Lafford, T. A. and M. R. J. Gibbs, "Magnetic, magnetostrictive and structural properties of iron-cobalt/silver multilayers", Departamento de Electricidad y Electrónica, Universidad del País Vasco, Bilbao, Spain, June 1993. Seminar given by TAL.

Lafford, T. A. and M. R. J. Gibbs, "Magnetic, magnetostrictive and structural properties of iron-cobalt/silver multilayers", UK Magnetics Club, London, April 1993. Oral presentation by TAL.

Thomas, A. P., T. A. Lafford and M. R. J. Gibbs and P. T. Squire, "Magnetic and magnetostrictive properties of iron/silver and iron-cobalt/silver multilayers", Condensed Matter and Materials Physics Conference 1992, Sheffield. Poster presentation.

Contents

1. Introduction

The motivation for the work presented here is to find new materials suitable for magnetostrictive sensor and transducer applications. Magnetic materials with simultaneously low coercivity and high magnetostriction (preferably under relatively low fields) are desirable. Low coercivity means that power requirements will be low. A high field-dependence of the magnetostriction is a characteristic desirable for micro-actuation applications. A large stress-dependence of the permeability is required for stress sensors, which is a property arising from high magnetostriction.

Multilayers, consisting of layers typically a few nanometres thick of different compositions, can have properties different from those of bulk materials. These differences arise because of the broken symmetry of atoms at the interfaces between the layers. As in alloys, neighbouring atoms in a multilayer are not necessarily alike, having different size or electronic configurations, giving rise to mechanical and electronic interactions, as well as magnetic effects in appropriate systems. Crystal orientation may be controlled, and phases of matter not stable in bulk form may exist in stable states in thin layers. Magnetic coupling between layers may also be used to control properties, as might atomic strain imposed at interfaces between unlike-sized species. The possibility exists, therefore, of manufacturing new materials with properties tailored to requirements, once the components and conditions required to produce them have been established.

In this project, metallic multilayers were produced by radio-frequency magnetron sputtering and the principal measurements taken were magnetic, magnetostrictive and structural. The initial target was to produce a multilayer with a saturation magnetostriction of 100ppm (positive or negative) combined with a coercivity of $100Am^{-1}$. A mechanism suggested for enhancing magnetostriction

over values attainable in bulk materials is by making magnetic multilayer materials with each layer only a few atoms thick, and causing the magnetic moments on atoms to be more localised than in the bulk by straining or mixing of magnetic atoms at the interface with other atoms. These mechanisms and the work springing from them are the subject of U.K. and world-wide patent applications. The proposals are detailed in Chapter 2, where factors affecting coercivity are also discussed.

Basic principles of magnetism and the hypotheses on which the work is based are presented in Chapter 2. Chapter 2 also contains a survey of literature in the area of magnetic multilayers and their uses, of production and analysis techniques and results obtained by other workers. In Chapters 3 and 4, the experimental methods and tools for analysis of structural and magnetic data are detailed. This is followed by the presentation and discussion of results obtained (Chapter 5). Conclusions are drawn together in Chapter 6, where future prospects are commented on, and suggestions made for further work in the field. In particular, different layer type and thickness combinations have been investigated here, but deposition conditions have not been optimised for producing the softest, most highly magnetostrictive multilayers. Such optimisation is the subject of current investigations within the research group.

Some terms and nomenclature appear frequently in the body of this thesis, and are defined here. *Lattice strain*, ε, is the strain of a crystallographic lattice compared to the bulk lattice plane spacings, or the plane spacings in a thick deposited film. It is defined as:

$$\varepsilon = \frac{d_{ml} - d_{bulk}}{d_{bulk}} \qquad 1.1$$

where d_{ml} is the lattice plane spacing in the multilayer and d_{bulk} is the bulk unstrained lattice plane spacing.

An allied term is *lattice mismatch* which occurs between at the interface between two unlike species. The mismatch is defined as:

$$mismatch = \frac{a_1 - a_2}{\frac{1}{2}(a_1 + a_2)} \qquad 1.2$$

where a_1 is the appropriate unstrained atomic spacing (nearest neighbour distance) of the first species and a_2 is the unstrained atomic spacing of the second.

In referring to multilayers, the following terms are used: substrate, buffer layer, bilayer, multilayer, interface, cap layer or overlayer, layer thickness, t, and modulation period, Λ. These are illustrated in Figure 1.1. The *substrate* is the pre-fabricated material on which the subsequent film is grown. A *buffer layer* may or may not be included: this is the layer between the substrate and the rest of the multilayer film, and may affect the crystal growth of the subsequent film. The *multilayer* is deposited on top, consisting in the simplest case of repeats of two different types of layer. The surface of contact between any two layer types is the *interface* between them. The smallest repeat unit of two layers is termed the *bilayer* (a three-layer repeat would be called a trilayer). Each single layer has a thickness t_n, and the sum of the thicknesses of the single layers in one repeat unit is the modulation period, Λ, i.e. $\Lambda = \Sigma t_n = t_a + t_b$ for the bilayer case. A top layer (a *cap layer* or *overlayer*) may or may not be deposited on the multilayer. If it is, it is usually to prevent oxidation of the multilayer surface. *Superlattice* is another term frequently encountered in talking of multilayer materials. It usually refers to higher quality multilayers, that is, those with few or no structural defects, likely to have strong crystallographic texture or even have the layers grown epitaxially one on another such that the crystallinity is maintained throughout the deposit. Lattice strain may exist.

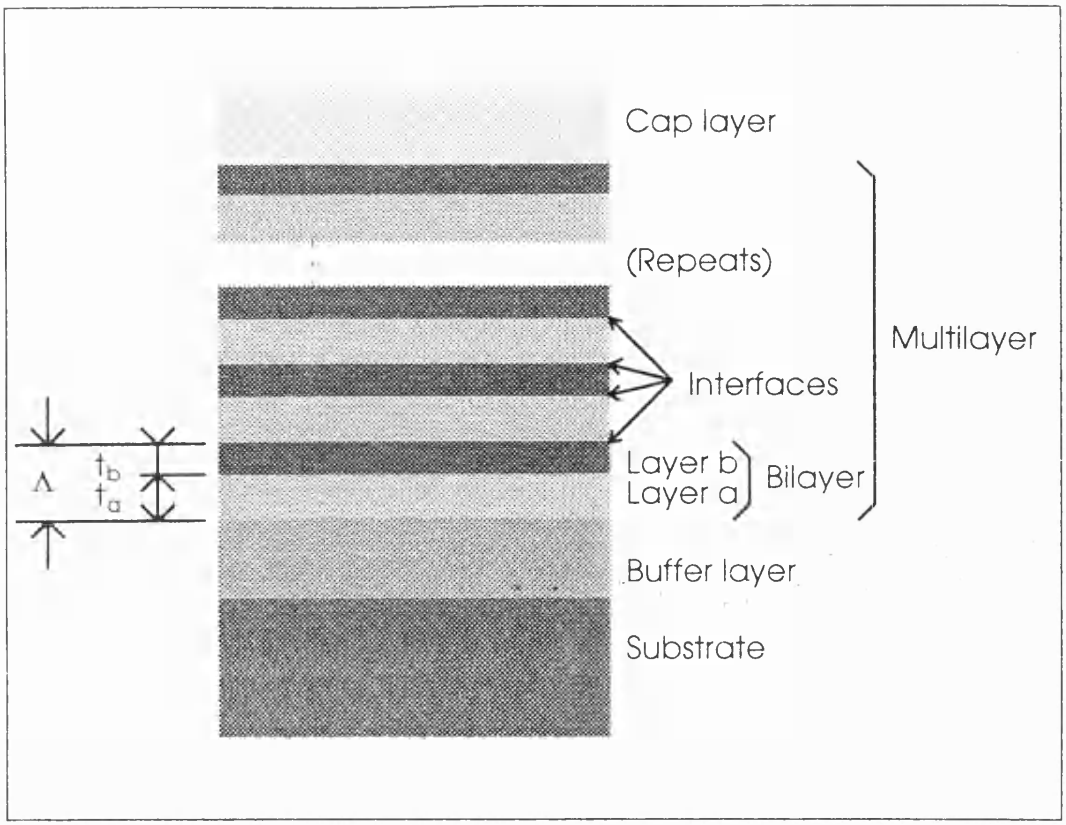

Figure 1.1 Schematic diagram of a multilayer with buffer and cap layers.

In writing the composition of a multilayer, a typical form would be: "50(2nm Fe/4nm Co)". This indicates that 50 bilayers were deposited, which consisted of layers of iron 2nm thick and layers of cobalt 4nm thick. In dealing with a series of multilayers containing iron and cobalt, the series would be described as "Fe/Co multilayers", as distinct from iron-cobalt alloys, written as "Fe-Co alloys". If a buffer layer had been included in the multilayer, its thickness and composition would be put before the above expression, and the nature of a cap layer would be described after, e.g. "40nm Au + 50(2nm Fe/4nm Co) + 10nm Au". If the same multilayer composition is deposited on each side of a substrate, then the description would become 2×50(2nm Fe/4nm Co). This is the nomenclature used in this thesis; expressions vary in published literature.

2. Literature Survey

Presented in this chapter is a brief description of some aspects of magnetic behaviour, with comments on the effects that thin film geometry might have. Following that, sputtering and other thin film deposition techniques are described. General interest in magnetic multilayers is reviewed before the last section surveys literature published on multilayers of particular interest to this project.

More information on magnetism, magnetic behaviour and magnetic properties in general can be found in many textbooks. Particular reference is made here to Cullity (1971 and 1972), Kittel (1949), Jiles (1991) and Callen and Chase (1993). For information regarding magnetism in thin films, and thin film deposition techniques, Chopra (1969), Chopra and Kaur (1983), Vossen and Kern (1978), Bunshah (1982) and Grundy *et al.* (1993) have been consulted. More details can be found in these references and the references cited therein.

2.1. Basic Magnetic Properties

The magnetic moment on an atom arises from the motion of its electrons. (The nucleus also has a magnetic moment, but this is extremely small compared to the electronic contribution). Electron spin gives rise to a spin magnetic moment, and the orbital motion causes an orbital magnetic moment. The vector sum of all contributions is the total magnetic moment of the atom. In bulk material, the total net moment is the vector sum of all the atomic contributions. This amounts to being the sum of the spin moments only in most ferromagnetic materials, since the orbital moment is *quenched*, that is, the electron orbitals are used in bonding and become effectively filled shells, and the strong orbit-lattice coupling prevents the orbital moments from contributing to the net moment. Where the vector sum is zero, the material is said to be *diamagnetic*; this is generally the case in atoms and

molecules with filled electron shells. If the electronic moments only partially cancel, in, for example, substances with incomplete electron shells, *paramagnetism*, *ferromagnetism*, *antiferromagnetism* or *ferrimagnetism* occur. The net interactions between the atomic moments determine which is the case in a given situation.

In a ferromagnet, strong exchange coupling between electron spins on neighbouring atoms in a region (called a *domain*) tends to align the spins in the same sense, giving a non-zero net magnetisation for that domain. In a paramagnet, this co-operative alignment does not occur, although the size of the atomic moment is not necessarily smaller. If the ferromagnetic sample is heated above a critical temperature (the Curie point, T_c) thermal energy overcomes the exchange coupling energy and the net moment is destroyed; the sample becomes paramagnetic.

A bulk ferromagnetic sample can be demagnetised to have a zero net magnetisation. In zero applied field, the domains, consisting of thousands of atoms, are locally magnetised to saturation, i.e. all the atomic magnetic moments within a domain are oriented in the same sense. The magnetisation vector is said to lie in an "easy direction" within the domain, i.e. in a direction which is energetically preferential in the given situation. Over the whole sample, however, the vector sum of the domain magnetisations is zero. Between the domains are *domain walls*. These consist in a narrow region (width a few tens of nanometres, depending on the substance) where the magnetic moment on each atom is not aligned exactly parallel to its neighbour, but rotated slightly, so that, over a hundred atoms or so, the direction of magnetisation is changed.

A ferromagnetic sample can become magnetised under the influence of an external magnetic field, H. There are two mechanisms by which this takes place, and the actual process is a combination of these in most cases; it depends on the

initial magnetic state of the specimen. The processes are *domain wall motion* and *moment rotation* and they are illustrated in Figure 2.1.

When a magnetic field is applied to a sample, domains with moment orientations parallel to the direction of the field "grow" at the expense of other domains. This occurs by the movement of domain walls. Note that, in talking of the motion of domain walls, there is no physical displacement of atoms; atomic magnetic moments merely realign, and the region in which the rotation of moments from one atom to another takes place appears to move. In this way, the net magnetisation of the sample increases in the field direction. The domain wall moves from its original position at an energy minimum, overcoming the potential barrier to motion by the energy supplied from the external field. That there is a threshold of energy required to overcome the barrier and move the wall is indicated by the non-zero width of the hysteresis loop (see Figure 2.1a - the special case of a single pinning site is shown).

Moment rotation within a domain occurs as shown in Figure 2.1b below. As the external field is increased in a given direction, the magnetic moments rotate until they are aligned parallel to H.

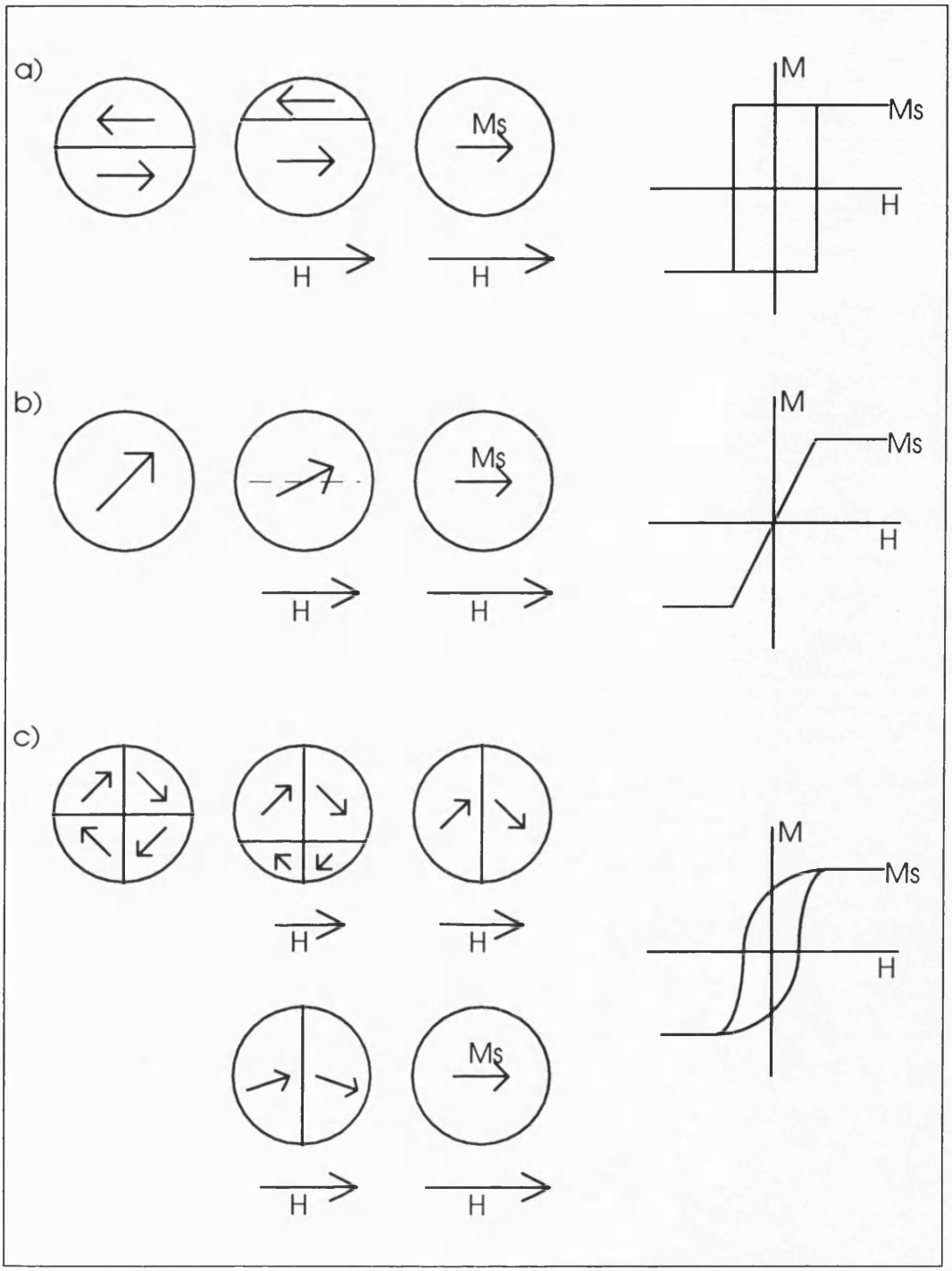

Figure 2.1 Schematic samples are shown with magnetisation loops arising from the different magnetisation mechanisms. Arrows represent the magnetisation directions. a) pure domain wall motion (single pinning site), b) pure moment rotation, c) general, for a typical ferromagnetic material, showing the influence of a) and b).

Magnetisation of a typical ferromagnet proceeds by both these mechanisms (Figure 2.1c). At extremely low H (in the so-called Rayleigh region), domain walls move reversibly such that domains in which the magnetisation is most closely aligned with the external field grow larger at the expense of domains not favourable oriented. If the field were removed, domain walls would return to their original positions. As the field is increased beyond the Rayleigh region, irreversible domain wall motion occurs, in small steps called Barkhausen jumps; the walls move from one energy minimum to the next. Once the sample has become a single domain, further magnetisation occurs as the moments rotate to align with H (if they are not already parallel) until the sample reaches technical saturation, where M = M_s. On applying extremely high fields, magnetisation can be increased further as moment misalignment due to thermal motion is overcome, but this effect is generally negligible, since the increase in M is so small and such high fields are required to attain it. Absolute saturation cannot be achieved at finite temperatures in a finite field.

The direction in which the magnetisation within a domain lies in the absence of any applied field is called the *easy direction* or *easy axis*. It is determined by *anisotropy*. There are several sources of anisotropy, each being dominant in different circumstances. Magnetocrystalline anisotropy is intrinsic to a magnetic material in a given crystalline state. It arises from spin-orbit coupling (that is, the interaction which links the motions of the electron orbits and the electron spins; also called Russell-Saunders coupling) and orbit-lattice coupling. Spin-orbit coupling is weak; relatively low fields (low energies) are required to rotate spins away from the easy direction. Orbit-lattice coupling is very strong, however; even high fields cannot re-orient the orbits with respect to the crystal lattice. The orbit geometry is linked to the crystal structure. Hence, in a spontaneously magnetised state, the magnetisation vector will tend to lie along some preferred

crystallographic axis, in the absence of an external field. Equally, there may be an *easy plane* of magnetisation, a plane in which any given direction is an easy direction.

Stress anisotropy is induced in magnetostrictive samples when stress is applied, as a consequence of magnetoelastic coupling between the lattice and the magnetisation. Shape anisotropy plays a part in the magnetisation of bulk samples, where the geometry of a sample means that it is more easily magnetised in a particular direction. The sample geometry may allow the formation of free poles, and domains (each saturated in a given direction) will form such as to eliminate or reduce in number the free poles and to separate them, to reduce their interaction energy. Figure 2.2 illustrates unfavourable and favourable domain configurations for a bulk ferromagnetic sample.

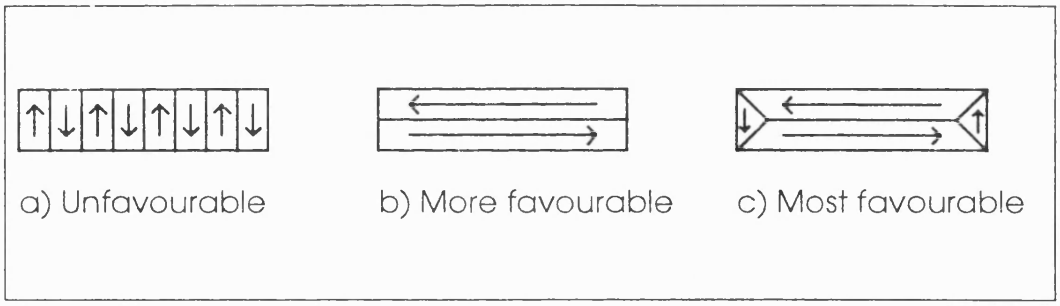

Figure 2.2 Unfavourable and favourable domain configurations from shape considerations. a) is unfavourable because there are many free poles; b) is more favourable because the number of poles is reduced, and the poles are farther apart; c) is the most favourable because the *closure domains* at the sample ends ensure that there are no free poles.

In thin films, domain walls exist through the entire film thickness. Walls parallel to the film plane are prohibited when the film thickness is less than the

thickness of a domain wall. Domain walls can be Bloch or Néel walls, depending on the film thickness. Magnetostatic energy considerations mean that Néel walls tend to form for film thicknesses less than about 35nm (Chopra and Kaur (1983)). It is energetically unfavourable for the magnetisation to point out of plane, creating free poles on the film surface. There is a thickness region where the type of domain walls which form are neither Bloch- nor Néel-like; in this region, cross-tie walls form, which have a complex structure in terms of the magnetisation directions.

Shape anisotropy usually determines that a thin film (less than a few microns thick, say) is most easily magnetised in a direction in the plane of the film. In a random polycrystalline film, it would be expected that, within the plane, there would be no preferential orientation of the magnetisation vector. (Within a crystallite, however, magnetocrystalline anisotropy may determine a preferred direction). It is possible to achieve an easy axis normal to the film plane if, for example, a polycrystalline film grows with columnar growth, in which the magnetocrystalline anisotropy can be strong along the columns (perpendicular to the film plane). Perpendicular anisotropy is important in the advance of magnetic recording technology and magnetic bubble memories in computer applications, since there is always a drive towards storing information more densely. The greater density is achieved since the lateral domain size may be smaller when there is a larger perpendicular anisotropy (see Section 2.3). Also, the magnetic flux density at the surface of the medium due to stray fields is increased, making readout easier. The direction of the easy axis in the sample is determined overall by the balance between all the anisotropy energies.

The coercivity, H_c, of a sample is defined as the reverse external field required to reduce its magnetisation to zero from the saturated state. In the simplest of models, it is proportional to the maximum gradient of the domain wall energy, γ,

with respect to wall position, x, in the sample: $H_c \propto \{d\gamma(x)/dx\}_{max}$. The value of H_c is not intrinsic to a substance, and may be affected by the treatment history. In the magnetisation loop (MH loop) it is irreversible magnetisation changes which cause coercivity and hysteresis. Above, it was mentioned that domain walls can move in small Barkhausen jumps from one energy minimum to the next. In a perfect single crystal, there would be no energy minima; these are created by imperfections in the lattice, such as dislocations, impurity inclusions, stress centres or grain boundaries. At such sites, the wall can become "pinned", such that more energy is required to move it than if it had been in a pure region of the sample, and, once over the potential barrier, it will be pinned at a new site, and so on. Consequently, it will require more than the removal of the initial field to return the wall to its original position, hence the hysteretic (irreversible) nature of the typical MH loop (Figure 2.1c). A sample is said to be magnetically *hard* if it is difficult to magnetise (permeability, $\mu = \mu_0(M + H)/H$, low, where μ_0 is the permeability of free space) and H_c is high. The sample is *soft* if H_c is low and it is easily magnetised (μ high).

Magnetostriction, λ, is the term which refers to the mechanical strain a magnetic material experiences when an external magnetic field is applied. The strain can vary with field up to magnetic saturation. The linear saturation magnetostriction, λ_s, is usually used in making comparison between materials; this is the strain observed on magnetising a sample to saturation from the demagnetised state. Spin-orbit coupling is responsible for magnetostriction as well as for magnetocrystalline anisotropy. As λ is the coupling of the magnetic moment direction and the strain, λ is the strain derivative of the anisotropy constants, K. Figure 2.3. crudely illustrates the situation; the picture is grossly exaggerated. The electron clouds are not as ellipsoidal as represented, nor rotatable by such large angles.

Engineering magnetostriction, λ_e, is an allied term: λ_e is the dimensional change observed on magnetising a sample from any initial magnetic state, and so is not an absolute quantity. The maximum λ_e is $(3\lambda_s/2)$ as observed, for example, when the magnetisation of a sample is changed from saturation in an easy direction to saturation in a perpendicular direction.

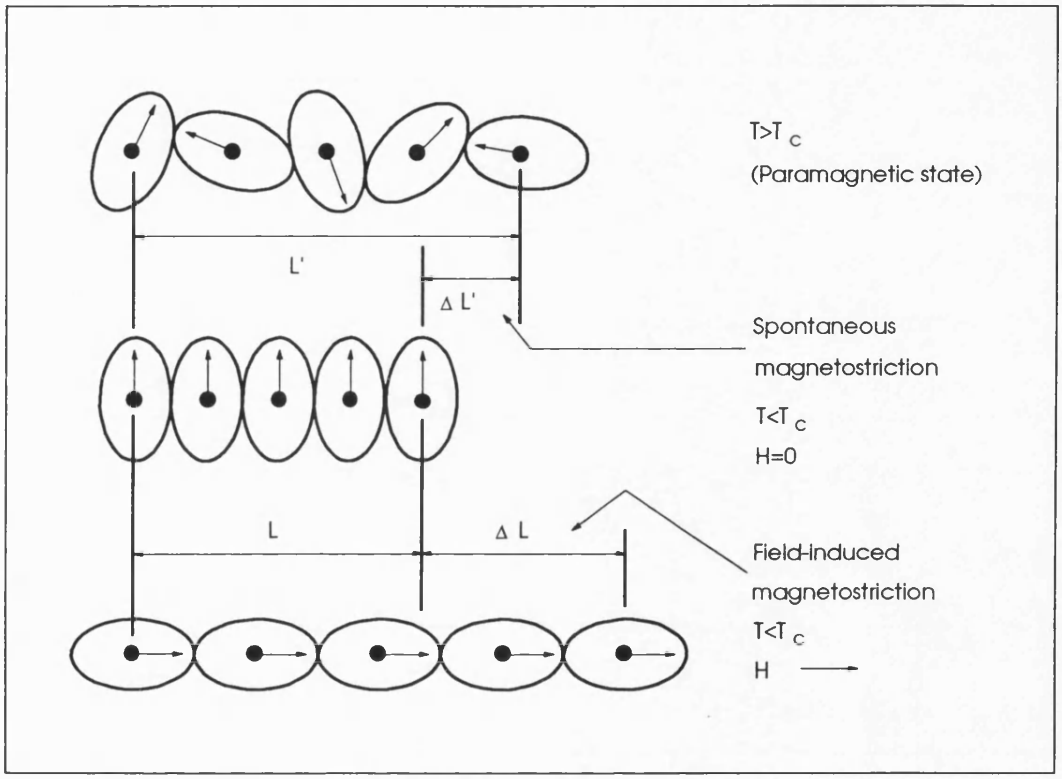

Figure 2.3 Pictorial representation of the mechanism of magnetostriction, after Cullity (1972). The dots represent the atomic nuclei; the arrows, the net atomic magnetic moment and the ellipses, the non-spherical electron clouds around the nuclei.

As the external field is applied, the spins rotate. The reorientation of the electron charge cloud is only small, since orbit-lattice coupling is strong and spin-orbit coupling is weak. The crystal lattice distorts to accommodate the rotated

charge cloud. The magnetostrictive effect is small, with strains of the order of 10^{-6} to 10^{-4}. This is the case in "localised moment" materials where the magnetic moments of atoms are localised to the atomic sites. Rare-earth metals are strong local-moment materials as a result of their unfilled 4f electron shells being within filled shells. As such, their magnetocrystalline anisotropy is high. At temperatures at which they are ferromagnetic, spin-orbit coupling is strong, and the electron charge cloud is pronouncedly non-spherical. An applied field rotates the spins *and* the orbits, resulting in large strains, e.g. λ_s of dysprosium is $\approx$ 4500ppm in the basal plane.

Fe, Co and Ni are "itinerant" ferromagnets, though only weakly so. The valence electrons are not constrained to remain near their original host atom. As electron spins are rotated in an external field, the electron energies change. The crystal then strains so that electrons at the Fermi level can relax to states of lower energy. (The band theory of metals applies here). Addition of low proportions of Si, Al or Co to Fe increases the magnetostriction over the value for pure Fe (Chin and Wernick (1980)). This is possibly due to the enhanced localisation of the Fe moments.

Expressions for the magnetostriction of cubic single crystals and polycrystals are given in Section 4.3.

It is the coupling between spins in a ferromagnet that causes them to align. This coupling is known as the *exchange force* and its strength is characterised by the *exchange integral*, J_{ex}. The exchange energy, E_{ex}, is related to this, and the resultant spin alignment in a material is determined by the condition for minimisation of E_{ex}. For $J_{ex} > 0$, E_{ex} is a minimum with spins aligned parallel, leading to ferromagnetism (provided the sample is below its Curie temperature).

For $J_{ex} < 0$, E_{ex} is a minimum with spins aligned antiparallel, which is the more common situation.

Bethe and Slater (see Jiles (1991)) postulated the variation of the exchange integral with the ratio r_a/r_{3d}, where r_a is the atomic radius (= half the separation between neighbouring atoms) and r_{3d} is the radius of the unfilled 3d electron shell. The Bethe-Slater curve (Figure 2.4) correctly separated ferromagnetic and antiferromagnetic elements, and the relative positions of Fe, Co and Ni are correct. Quantitative calculations of J_{ex} were not satisfactory, however.

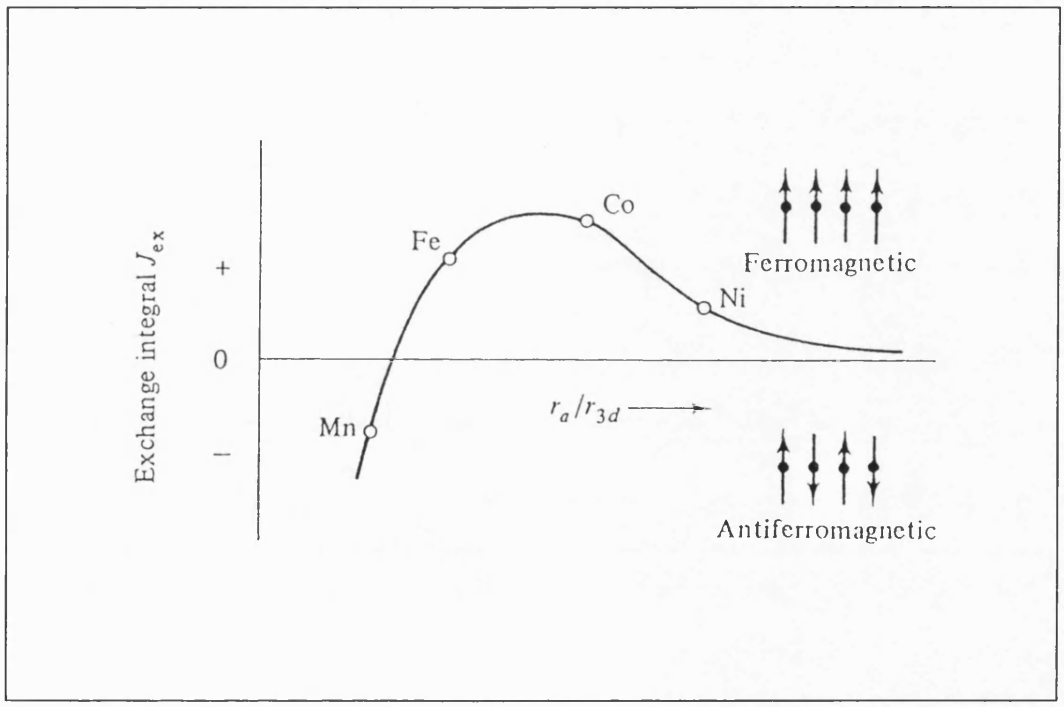

Figure 2.4 Schematic Bethe-Slater curve (after Cullity (1972)).

It has been found possible to make ferromagnetic alloys from non-ferromagnetic elements. In MnBi, for example, Mn atoms are strained apart, raising r_a/r_{3d} enough to make J_{ex} positive (Cullity (1972)). This is a further example of the manipulation of magnetic characteristics by altering atomic

arrangements. Exchange forces depend on atomic separation, not positional regularity; therefore, crystallinity is not a condition for a magnetic material.

Summary. A multilayer of all magnetic layers may behave as a thin film, or, if magnetic layers are separated by non-magnetic layers, each layer may behave as an ultra-thin film. Anisotropy considerations mean that the magnetic easy axis is likely lie in the film plane, although it is possible to fabricate films with out-of-plane easy axes. Domain walls may exist through the entire thickness of a thin film.

The magnetic and magnetostrictive properties of a magnetic material may be affected by alloying or mixing with other elements. For example, the alloy MnBi is ferromagnetic while neither element is, as the separation of the Mn atoms is increased. The addition of a small amount of Si, Al or Co to Fe enhances the magnetostriction. In a multilayer of elemental layers, these mechanisms would be localised at the interfaces. Besides such behaviour in multilayers, there may be effects from magnetic dipolar and exchange coupling between layers.

2.2. General Manufacture and Applications of Metallic Multilayers

After describing the process of sputtering, brief accounts are given of other processes of thin film deposition. Different processes yield films with different structural and other properties, which are suitable for various applications. Sputtering is a quick deposition method, and, with suitable arrangements of load-locks and other facilities, is suitable for industrial mass production of components and devices.

Sputtering is a process in which a target is bombarded with energetic ions. Non-reactive ions ensure the deposition of the plain target material. Reactive ions

may be used to deposit films of the reaction products of the ions with the target; nitrides such as AlN are often deposited in this way. The ions are accelerated towards the target anode by an applied electric field (typically a few hundred kVm^{-1}). Momentum transfer in secondary collision processes at the target causes atoms to be sputtered off it, along with secondary electrons. These atoms then travel in line-of-sight until they hit the substrate cathode, or the chamber walls (for example) and adhere. The deposition profile is approximately cosinusoidal. The high energy of sputtered species tends to result in highly adherent films. The process is carried out at a gas pressure of a few to about a hundred millitorr, introduced into a vacuum chamber. The vacuum minimises contamination from unwanted gas species.

The sputtered species is generally neutral. The source of ions is either a glow discharge (created by applying a voltage of the order of 1kV across a gas to break it down into a plasma) or an ion beam. Glow discharge sputtering tends to give higher deposition rates since ions can strike the target obliquely, so that primary collisions can cause sputtering rather than the secondary processes required for normal incidence. Deposition does not necessarily occur in a line-of-sight, since the sputtered atoms have to travel through the discharge, and so undergo collision. This scattering can tend to make deposition thicknesses more uniform across a sample.

In magnetron sputtering, a magnet is fitted behind the target to increase sputtering efficiency. Electrons are trapped to spiral around the magnetic flux lines (Figure 2.5). The electrons are thus restricted to remain near the plasma region, increasing the number of ionising collisions. This results in a more dense plasma confined near the target. There is increased erosion, therefore, in the "race-track" area defined by the magnetron. The deposition profile is altered by the presence of the magnetron and films can have a more uniform thickness (see Section 3.2 for a

measured deposition profile). Targets of magnetic materials spread the flux, giving a wider racetrack and more even erosion.

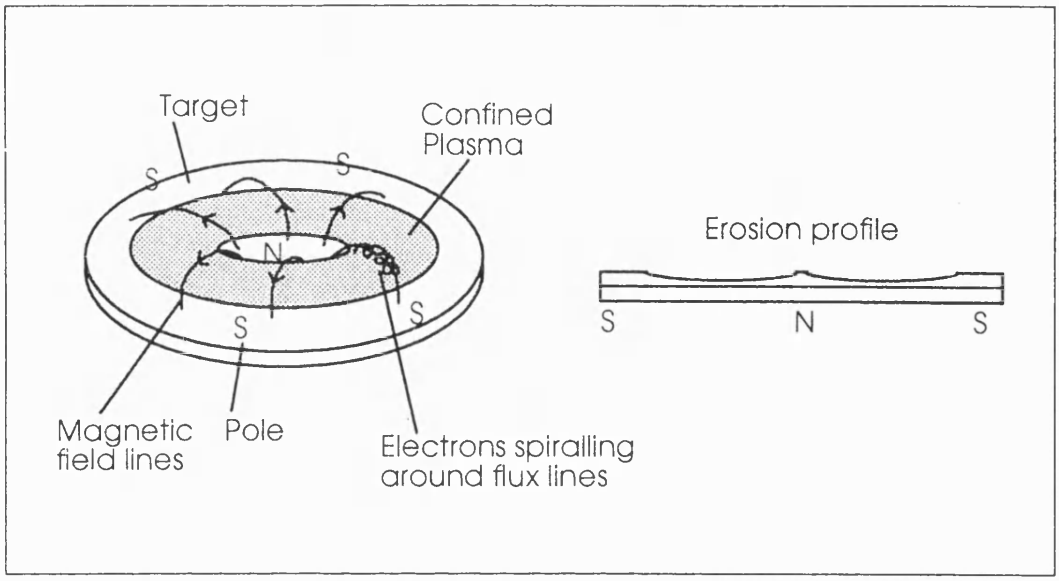

Figure 2.5 Effect of the presence of a magnetron behind a sputtering target.

D.c. sputtering is confined to the deposition of conductors, since, on an insulating target, charge would build up and eventually repel the bombarding ions. This limitation is overcome in the radio frequency sputtering technique. A field which reverses polarity periodically ensures that there is no charge build-up. Thus insulators, semiconductors and refractory materials can be sputtered, as well as metallic elements and alloys.

Energy to strike the plasma is drawn from the r.f. field. The ions created are accelerated in this field towards the target, and atoms are sputtered off. For half the r.f. cycle, the ions are accelerated towards the substrate and sputtering occurs here. For net deposition, therefore, it is necessary that the sputtering rate from the target be greater than the sputtering rate from the substrate. A magnetron helps here. A d.c. bias field could also be applied.

The plasma is sustained as electrons oscillate in the r.f. field, colliding with and ionising atoms from the sputtering gas (usually argon). A lesser contribution comes from ionising collisions of atoms with secondary electrons ejected when atoms are sputtered from the target. Since gas ionisation is enhanced over the d.c. case, where secondary electrons are essential to sustain the plasma, lower gas pressures are viable, usually in the millitorr range. High cathode voltages are also avoided. Deposition rates are of the order of 1nm/min to 100nm/min.

There are other variants on the sputtering method. Radio frequency and magnetron sputtering have been mentioned here because the deposition technique used to fabricate films and multilayers in this project was radio frequency magnetron sputtering. For details of other sputtering methods, the reader is referred to the books cited above (page 5).

Another method of depositing thin films and multilayers is **Molecular Beam Epitaxy (MBE)**. This is carried out under ultra-high vacuum (typically 10^{-9} to 10^{-10} torr) in stringently clean conditions. Source materials are held in crucibles which are heated; the vapour escapes through a tiny hole, making effectively a point source giving a beam of evaporant directed towards the substrate. The evaporation rate can be controlled by the temperature of the crucible, within limits. Deposition rates are slow (up to a few nm/min), the base pressure is low and there is no plasma region to be crossed, so deposited films are of high quality and purity even at low substrate temperatures. This method is suitable for making epitaxial films and multilayer superlattices, and complicated small-scale structures (e.g. quantum wells). Crystal quality is better and interfaces are sharper than in sputtered multilayers (Dekoster *et al.* (1993)).

Vacuum Evaporation is conducted in a high vacuum chamber with a pressure in the milli- to microtorr range. A solid or liquid source is held in a crucible, which is heated by direct resistance, radiation, eddy currents, electron beam, laser beam

or arc discharge. Alternatively, a resistively heated wire may provide the source atoms. The evaporated particles travel in line-of-sight to condense on the substrate. Uneven deposition may be smoothed by moving the substrate in complicated patterns during deposition, or by introducing into the chamber a gas with which the evaporated particles collide, randomising their flight path. Deposition rates of 1nm/min to 75μm/min. are possible.

Ion Plating is a variation on vacuum evaporation. Source particles are produced in the same way and then pass through a gas discharge created by introducing a gas into the chamber and applying a few kV of negative bias to the substrate. The purpose of the discharge, leading to ion bombardment, is to modify the deposition surface beneficially. On passing through the discharge, some of the evaporated particles are ionised by collisions. Particles incident on the substrate may stick and ions may pick up electrons from it. The incident, accelerated ions sputter impurities off the substrate, but also some deposited matter, so the net deposition rate is reduced from the vacuum evaporation case. The purity of the film is, however, improved, and the adhesion properties are enhanced. Film uniformity is improved, since collisions in the discharge scatter the evaporated particles to give a more even spatial distribution. Polycrystalline films are generally produced, possibly crystallographically textured. The ion bombardment of the substrate causes it to heat up, which may not be desirable, especially as the temperature reached may not be known. Heating can be reduced if an extra source of electrons is introduced to sustain the discharge, enabling the bias on the substrate to be reduced.

In **Laser Ablation**, powerful radiation from a laser evaporates material from a target and interacts with the evaporation products to form a high temperature plasma. Thermal energy converts to kinetic and the material is transported to the substrate, where it condenses. The arriving material has high energy, which may

lead to re-sputtering and, in multilayers, interface mixing. A wide range of target materials can be used, and many parameters influence deposition rate. Deposition rates can vary from hundredths of a nanometre to nanometres per laser pulse. Working at typically tens of hertz, this gives deposition rates around a nanometre to a micron or so per minute (Jackson and Palmer (1994), Lindley (1994)).

Electrodeposition is essentially electrolysis, with the electrolyte the source material and one electrode the substrate. Metal ions in the electrolyte are reduced to atoms at the electrically conducting substrate, as they gain electrons from the external circuit. To deposit on non-conducting substrates, metal ions are reduced on picking up electrons from a chemical reducing agent, not an external electric circuit (electroless deposition). The deposition rate is hard to control in this situation. It is easier in the conventional electrodeposition system, where the electric potential between the electrodes is the major factor in determining the deposition rate, but the geometry of the system and the nature of the electrode-electrolyte interfaces also influence it. Since different materials require different activation potentials, it is possible to make compositionally modulated films. It is not possible to have more than one layer pure, since, at the higher potential (considering a two-component system) both materials will be deposited. The electrolyte would be made up of a very dilute solution of the component requiring the lower potential in order that, at the higher potential, the deposit would consist mostly of the major component.

Chemical Vapour Deposition (CVD) is the technique where, generally, a thermally-activated chemical reaction is the process which transfers material from the source to the substrate. The substrate is often the surface at which the reaction occurs. The temperature of the source with respect to the substrate determines the rate of deposition. The process is widely used in the electronics industry to deposit semiconducting, conducting, insulating and resistive coatings. Given a suitable

system, it is possible to coat all shapes and sizes at high rates. It is possible to control the grain structure and orientation of deposits. A wide variety of atmospheres is employed, from gases to packed particulate materials. In Plasma Assisted Chemical Vapour Deposition (PACVD), a chemical reaction is started between gases by an electric discharge. Lower substrate temperatures may be used than would be required for CVD. This enables the deposition of materials for which the thermal mismatch between film and substrate would cause severe film stresses if CVD were used. Other materials may be deposited which would not be stable at higher temperatures. The deposition of pure materials is, however, difficult. Since the substrate temperature is low, the desorption of product gases is slow, so they tend to be incorporated into the film. Film uniformity is also harder to control, since it now depends on the plasma profile. The PACVD process is not yet well understood.

The **Thin Film Growth Process** proceeds as follows, in a general sense. Firstly, the individual particles impinging on the substrate lose their component of velocity normal to the substrate and are adsorbed. If the incident energy is too high, condensation may not occur. Initially, the adsorbed material is not in thermal equilibrium with the substrate, and so is mobile. In the course of the motion, particles interact and form larger units ("clusters" or "nuclei"). Desorption of the clusters is possible unless they collide with other clusters and grow too large for this. Newly incident material may also increase the cluster size. Above a critical size, the nuclei become thermodynamically stable. The nuclei grow in size and number until a saturation nucleation density is reached. This density and the average size of the clusters depend on the deposition conditions. Generally, growth parallel to the substrate proceeds more quickly than in the perpendicular direction. These larger nuclei are called *islands*. Islands are still mobile, and, as

more material is deposited, the islands agglomerate. This reduces surface area relative to volume and so is a lower energy state. Agglomeration may be enhanced by increasing the mobility of the islands by, for example, heating the substrate. In r.f. sputtering, mobility may also be increased by reducing the sputtering pressure (Glocker *et al.* (1986)). New nuclei may form in bare areas revealed as islands coalesce. Larger islands then join together and the deposit becomes a network rather than a discontinuous film. The film becomes completely continuous as the holes and channels in the network are filled.

Initial nucleation and growth of a film may be classified as layer-like, island-like or mixed (Stranski-Krastanov growth). These are illustrated in Figure 2.6. Which process occurs depends on the thermodynamic parameters of the deposit and substrate surface.

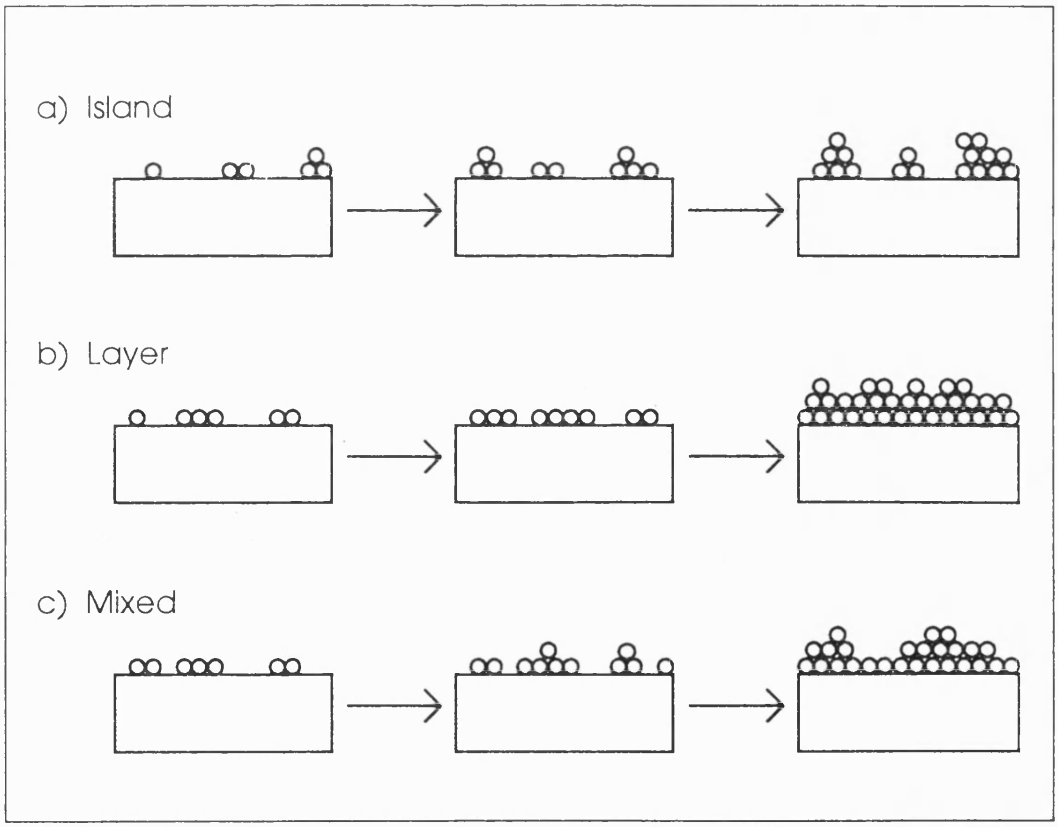

Figure 2.6 Basic growth processes: a) island, b) layer-by-layer, and c) mixed type (Stranski-Krastanov). After Chopra and Kaur (1983).

2.3. General Interest in Magnetic Multilayers

There are many applications of thin films and multilayers, magnetic and otherwise. Thin films are generally of the order of 1μm thick, and layer thicknesses in a multilayer are typically 0.1nm to a few nanometres. Non-magnetic uses include optical coatings, X-ray monochromators, solar cells, thin-film microelectronic devices and superconducting tunnelling devices (see Ruggiero (1985)). Chopra and Kaur (1983) cover all these and more, along with applications of magnetic films. Applications of magnetic thin films and multilayers include magnetic and magneto-optic recording media and devices, magnetoresistive devices and computer memory elements. Many research groups around the world are investigating numerous aspects of magnetic thin films and multilayers. The aims are to understand the fundamental magnetic behaviour and properties of these artificial, synthesised materials, and some groups have potential applications in view. There has been interplay between theory and experiment. Theorists predict certain modes of behaviour in particular systems, which are then investigated experimentally; experimentalists, in studying given systems, discover new trends and patterns in magnetic behaviour requiring theoretical understanding.. Falicov *et al.* (1990) have produced a review of theory of magnetism relating to thin films and multilayers, of materials and methods of deposition and characterisation, applications and prospects for future developments. A large bibliography is included.

Before proceeding in the next section to a more detailed discussion of published literature regarding magnetoelastic multilayers, a brief review of some of the research activity in other areas of magnetic multilayers and thin films will be given.

Much of this research has centred on data storage media and read/write devices for magnetic and magneto-optic recording. For data to be stored more densely,

storage media require perpendicular anisotropy (i.e. easy axis of magnetisation normal to the film plane). The domain storing the "bit" is then magnetised perpendicular to the plane, which may occupy less lateral area than a domain magnetised parallel to the plane and which has higher stray field at the medium surface. Shape anisotropy acts against this arrangement, however. A high coercivity, H_c, is required, so that the bit may not be wiped out accidentally by magnetic fields in the normal environment. It is also necessary that the magnetostriction of the material be small (preferably zero) so that data may not be lost via the inverse magnetostrictive effect under strain due, for example, to thermal expansion. A square hysteresis loop with a high remanent magnetisation is required, so that the bit may be easily read by a conventional soft magnetic head, or so that the domain gives a large Kerr rotation in the magneto-optic case.

Co/Pd and Co/Pt multilayer systems have been the basis of much of the research in this area. The properties of the multilayers can be controlled by a variety of parameters (see below). Many papers are devoted to the study of perpendicular anisotropy and the effective anisotropy is often considered as the sum of volume and surface (interface) contributions, after Néel (1954) postulated the existence of surface anisotropy in binary alloy and multilayered systems (see Section 2.4).

General observations are given below, with references. The films and multilayers were deposited by a variety of sputtering techniques.

a) Thinner Co layers give films with higher H_c and squarer MH loops: Carcia and Zeper (1990, Pt/Co), Bennett *et al.* (1991, $Co_{25}Pd_{75}$ alloy films), Wan and Hadjipanayis (1991, Co-Ni alloy films, MH loop measured parallel to the plane), de Haan *et al.* (1992, Co/Pd). Hashimoto *et al.* (1990, Co/Pt and Co/Pd) also note that Kerr rotation, θ_K, is enhanced in multilayers with smaller total thickness, even when the individual layer thicknesses are the same.

b) H_c is increased as the pressure and mass of the sputtering gas is increased: Hashimoto *et al.* (1989b, Co/Pt and Co/Pd multilayers - K_u is reduced, however; 1989a, Co-Pd alloys) - this they attribute to fine columnar growth which pins domain walls; de Haan *et al.* (1992) who suggest that there is less interface mixing at higher sputtering pressures, as do Carcia and Zeper (1990); He *et al.* (1991, Co/Pt) - they also note that θ_K is increased as sputtering pressure is raised, and they attribute the higher H_c to a rougher top surface at higher sputtering pressures.

c) Anisotropy, K_u, depends on Co layer thickness, tending to perpendicular orientation for $t_{Co} < 0.8$nm: Bennett *et al.* (1991, Pd/Co), de Haan *et al.* (1992), Greaves *et al.* (1992, Pt/Co), Hashimoto *et al.* (1989b). Similar spontaneous behaviour was observed for Au/Co/Au(111) sandwiches by Bruno and Renard (1989). Daalderop *et al.* (1992) predicted and confirmed perpendicular anisotropy in Co/Ni multilayers for $\Lambda < 1.5$nm. A high $\mu_0 M_s$ of 1T was obtained.

d) Sharp, flat interfaces enhance K_u and reduce H_c: Honda *et al.* (1991, Co/Pt).

e) Co/Pd and Co/Pt-based systems tend to have (111) crystallographic texture. This texture enhances the perpendicular anisotropy and buffer layers between the substrate and the multilayer can enhance this texturing: Tsunashima *et al.* (1991, Pt/Co and Pd/Co).

Hashimoto *et al.* (1989a) have studied the range of Co-Pd alloys in thin film form. They find the highest H_c for ≈75at%Pd, 25at%Co and maximum K_u for ≈ 68at%Pd in Co. The greatest λ_s occurs around these compositions, however, being about -170ppm. They attribute high K_u in Co/Pd multilayers (1989a) to the magnetostrictive nature of Co-Pd at interfaces.

Yamaguchi *et al.* (1993) have investigated a more complex multilayer system, after the suggestion that K_u is linked to lattice strain via magnetostriction. (A

similar note was made by de Haan *et al.* (1992)). They studied multilayers with repeat units of Ag/Co/Pd and Pd/Co/Ag on Pd buffer layers. They found that having Ag as the first layer gave sharper multilayer interfaces, and that the order of deposition and the thickness of Co affected K_u. A further, more complicated system was examined by Bloemen and de Jonge (1992), attempting to produce perpendicular anisotropy in multilayers containing Ni. This they achieved for $t_{Ni} \approx$ fractions of nm, at which thicknesses the largest H_c, M_r and θ_K were found.

Detailed structural analyses of Pt/Co multilayers have been carried out by Greaves *et al.* (1992) and Li *et al.* (1993).

For read/write magnetic heads for magnetic recording, soft magnetic materials are required. They should have low H_c (of a few tens Am^{-1}), high saturation magnetisation, high permeability, μ, ($\mu > 1000$ at frequencies of 10MHz and above; Dirne *et al.* (1989)), good thermal stability and λ_s zero. Attention has focused on magnetic/magnetic type multilayers, with components chosen to produce soft films with low λ_s. Amorphous alloys exist which have very low λ_s values, but they often have low values of saturation magnetisation and poor thermal stability. To improve this situation, some groups have tried to make multilayers with Fe in these alloys (Dirne *et al.* (1989, Fe/Co-Nb-Zr and Fe/Fe-Cr-B) and Jimbo *et al.* (1991, Fe/Co-Zr)). For low H_c and high μ, they aim for small grain sizes. Dirne *et al.* found that H_c was reduced and μ increased with thicker Fe layers ($t_{Fe} > 2$-4nm), and that B_s could be raised to 1.8T. Jimbo *et al.* maintained a fixed thickness ratio for their layers, but did find that λ_s was not the same for each sample. On annealing, they found that, at higher temperatures, H_c was reduced, λ_s was increased and anisotropy became more pronounced; the Fe grain size grew, but remained small. Ohnuma *et al.* (1993) have found good μ-frequency responses by multilayering Co-B-N and Fe-B-N with Fe-N and AlN, respectively, which also improved the soft magnetic properties. Krishnan *et al.* (1991a), studying Fe/AlN

multilayers, found that M and θ_K were increased by increasing the Fe layer thickness, which also reduced H_c until a thickness of 12nm was reached ($H_c \approx$ 320Am^{-1}), when H_c increased again. Opposite behaviour was found when Fe/Ni and Fe/Co multilayers were studied (Krishnan *et al.* 1991b). Fixing the layer thickness ratios, they observed that H_c was lower in the Fe/Ni system when the multilayer period, Λ, was small ($<\approx$4nm; $H_c \approx$120Am^{-1}). M increased to a maximum value as Λ increased. The Fe/Co multilayers were hard, which they attribute to a large anisotropy of FeCo alloy formed at the interfaces. Nagai *et al.*, studying Ni/Fe multilayers, also found H_c decreased as Λ decreased. They observed a minimum H_c of around 80Am^{-1}. They observed an increase in B_s as the proportion of Ni in the multilayer was increased, and for given layer thicknesses of Ni and Fe, zero λ_s could be achieved. The λ_s behaviour was interpreted as the volume average of contributions from the individual layers and the mixed alloy region at the interface. The elements have negative values of bulk λ_s while NiFe alloy has a positive λ_s. It is therefore possible to balance the contributions to give a resultant zero magnetostriction. Dirne and Denissen (1989) have applied a similar interpretation to Fe/Co multilayers. (See also Section 2.4). The multilayers discussed in this section were deposited by various methods on different substrates under different conditions. The details can be found in the references cited. A review of soft magnetic multilayers has been written by de Wit (1992).

Another major focus for magnetic multilayer research is giant magnetoresistance (GMR), where the resistance of a sample can change up to tens of percent on the application of an external field, even at room temperature. Large fields of a few tesla are often required, however. Parkin *et al.* (1991) have observed 65% magnetoresistance at room temperature in Co/Cu multilayers fabricated by d.c. sputtering. Such materials have potential application in magnetoresistive sensors and recording heads. (See also Grundy *et al.* (1993)).

The structural characteristics required for a multilayer to exhibit GMR are the subject of ongoing debate. Magnetic layers separated by non-magnetic layers are required. It was thought at first that rough interfaces were needed from which the electrons scattered, but this was demonstrated not to be entirely the case when GMR was observed in MBE-grown Co/Cu multilayers by Greig *et al.* (1992) and Hall *et al.* (1992), who observed GMR up to -26%; they attribute the behaviour to interface scattering, supported by their data on annealed samples. Furthermore, it appears that layered structures are not required, as GMR has been observed in granular films, by Xiao *et al.* (1993, Fe-Ag) and Maeda *et al.* (1993, various compositions) and in discontinuous multilayer films, where Hylton *et al.* (1993) see GMR in Ni-Fe/Ag films at low fields of a few hundred Am^{-1}. An explanation of the latter has been put forward by Slonczewski (1994).

In multilayers, antiferromagnetic alignment of adjacent magnetic layers across the non-magnetic spacer layers results in the spin-dependent scattering of electrons (the "spin-valve" effect). Whether or not this alignment occurs depends on the spacer thickness in an oscillatory manner, with an oscillation period of a few atomic layers. The oscillatory nature of the exchange behaviour and its correlation with values of magnetoresistance have been the subject of much theoretical and experimental research, e.g. Grünberg *et al.* (1991, 1992, Fe/Cr), Celinski and Heinrich (1991), Coehoorn (1991), Fuß *et al.* (1992, Fe/Al, Fe/Au), Mathon *et al.* (1992) and Bruno and Gyorffy (1993). Dieny *et al.* (1991) emphasise the rôle of bulk spin-dependent scattering rather than interfacial scattering in their uncoupled sputtered multilayers (various components). Le Dang *et al.* (1993) say that the magnetoresistance in their sputtered Co/Cu multilayers is more sensitive to the crystal structure than the fraction of Co layers that are antiferromagnetically coupled, and, for thin Co, the magnetoresistance is higher for multilayers with higher crystal quality.

Enhancement of magnetic moments at surfaces or multilayer interfaces has been predicted theoretically and observed experimentally in a variety of systems. Calculations have been carried out using various models. Fu *et al.* (1985) predicted enhanced moments on 3d bcc transition metals as overlayers on, or in sandwiches or superlattices with, Au and Ag, arising from the 2D nature of the atomic arrangement. This might be due to the reduction in co-ordination number and symmetry, causing narrowing of the electron d-bands leading to a higher partial density of states at the Fermi energy. This was suggested by Fabricius *et al.* (1991), working on Cu/Ni-like superlattices with sharp interfaces; they suggest that more Ni and less Cu is required for higher moments; and Aldén *et al.* (1992), Fe, Co and Ni surfaces, who, however, find no enhanced moment on the fcc (111) surface of Ni.

In several cases, following the work of Fu *et al.*, Pan *et al.* (1992, 1993a, b, c) have found enhanced magnetic moments for thin layers of magnetic materials: in Fe/Ag multilayers, moment enhancement on the Fe atom was found for all Fe layer thicknesses (up to 10nm), being greater for thinner t_{Fe}; in Fe/Cu multilayers, the moment was enhanced for $t_{Fe} < 7.5$nm ($t_{Cu} = 7.5$nm) with a maximum moment of $3.44\mu_B$ per Fe atom when $t_{Fe} = 4.5$nm (1993a); in Fe/Pd multilayers, an enhanced moment was observed for $t_{Fe} < 6.5$nm ($t_{Pd} = 6.5$nm), which they attributed to the formation of an non-equilibrium iron-rich fcc phase at the interfaces; an enhanced moment was seen for $t_{Fe} < 8$nm ($t_{Au} = 7.5$nm) in Fe/Au multilayers (NB Fe and Au are miscible), for which they cite an "active layer" model. Wu *et al.* (1992) have observed enhanced orbital moments on Co in Co/Pd multilayers where the individual layer thicknesses were less than 1nm. Reduction of magnetic moments has been observed by Peng *et al.* (1992) in Ag/Ni multilayers, in contrast to other workers they cite. They attribute the reduction to interdiffusion at the multilayer interfaces, to interlayer exchange and charge transition from Ag to the 3d bands of

Ni atoms near the interfaces. All the multilayers mentioned here were deposited by electron beam evaporation.

Another property that can be altered in thin films and multilayers is the elastic modulus. This may have consequences for magnetoelastic behaviour in multilayers. Both enhancement and softening have been reported, and several explanations have been put forward. Yang *et al.* (1977) observed an increase in the biaxial modulus of a factor of 2 to 4 in Au-Ni and Cu-Pd compositionally modulated films with period < 2.5nm (NB the compositional modulation is not step-like, as it would be in a good quality multilayer). They tentatively suggest that this is caused by the interaction of an additional Brillouin zone with the Fermi surface. Richardson *et al.* (1992) say that this is not the likely cause of the *softening* they observe in non-periodic Mo/Ni superlattices, but that the cause of the softening may be local to the interfaces, and possibly linked to strain in the Ni lattice. Such an interpretation is also put forward by Khan *et al.* (1983) who observed elastic constant softening in periodic Mo/Ni superlattices, for smaller periods where the Ni lattice was expanded.

A "coherency strain model" has been developed by Jankowski and Tsakalakos (1985) and Jankowski (1988), indicating that compressive strain should increase elastic constants. In multilayers, this could be achieved by lattice mismatch at interfaces. Jankowski (1989, 1992) has shown that lattice strain indeed occurs in Au/Ni multilayer systems. Delsanto *et al.* (1992) have shown that the theoretical strains required for a significant enhancement of the elastic constants is small (of the order of 1%). In Ag/Ni multilayers, Carlotti *et al.* (1992) have observed shear elastic constant, c_{44}, softening by up to 40% for periodicities down to 1.3nm (c_{11} was unaffected). This they attribute to the lattice parameter variations: expansion of the Ag and Ni lattices in the growth direction, contraction of the Ag lattice and expansion of the Ni lattice parallel to the film plane.

2.4. Magnetostrictive Multilayers

The aim of this project was to investigate the magnetoelastic and soft magnetic properties of metallic multilayers, with a view to producing soft magnetic, highly magnetostrictive materials for sensor and transducer applications. Targets were set at the start of $|\lambda_s|$ = 100ppm and H_c = 100Am^{-1}. Such values have been reported in the literature, but not simultaneously on the same multilayer.

It is an empirical observation that substances with greater localisation of the magnetic moment at atom sites are more highly magnetostrictive (see the case of the rare-earth metals, Section 2.1). By introducing strain, therefore, to the magnetic lattice, by the proximity of atoms of a different size at the interfaces in a multilayer, it is hoped to enhance the magnetostriction. Mixing of component layers at the interfaces may be another mechanism by which to enhance λ_s. Although Fe, Co and Ni are itinerant ferromagnets, they are only weakly so, and it has been demonstrated that moving the atoms apart can increase the magnetostriction by enhancing the moment localisation. Alloys of Fe with Si, Al or Co show increased λ_s (Chin and Wernick (1980)).

O'Handley and Sun (1992) report that large internal [atomic] strains may exist in thin films and at surfaces, of the order of 1-10%. In highly strained layers, the magnetoelastic coefficients can change magnitude and sign. They find that the surface magnetoelastic coupling constant in some amorphous alloys is three times the bulk value (Sun and O'Handley (1991)). Kozono *et al.* (1987), working with multilayers of Fe with various materials, attribute the λ_s behaviour they observe to lattice strain, the formation of γ-iron and alloying at the interfaces.

Crystallographic structures may be stabilised in thin layers which are not stable in the bulk. For example, fcc Co may be found in thin layers (Nafis *et al.* (1991)). Thomassen *et al.* (1992) have grown thin films of Fe on Cu(100). They have grown ferromagnetic pseudo-fcc-type Fe where the magnetism is a surface

property apparently correlated with the expansion of the Fe interatomic distance near the surface. Fcc Fe is not usually ferromagnetic.

Nagai *et al.* (1988) have proposed that the magnetostriction of a multilayer can be expressed as the volume average (effectively) of the magnetostriction values of the component layers and any interdiffusion layers. This, they apply to multilayers consisting of two magnetic component materials, such that:

$$\lambda_s = \left(\frac{1}{\Lambda}\right)\left\{(t_a - t_{int})\lambda_s^a + (t_b - t_{int})\lambda_s^b + 2t_{int}\lambda_s^{int}\right\} \qquad 2.1$$

The subscripts *a*, *b* and *int* refer to the two magnetic layers and the interface region, respectively; t_i are the thicknesses of the respective layers and λ_s^i the corresponding saturation magnetostriction constants (see Figure 2.7). Dirne and Denissen (1989) consider this expression applicable while the elastic moduli of the component layers are not dissimilar. Both groups fitted their data assuming an interface mixed region of either a 50-50 alloy of the two components or a linear variation of alloy composition across the interface, using t_{int} as the fitting parameter (see Section 2.4.1 below). The inverse of the modulation period, i.e. $1/\Lambda$, is also proportional to the number of layers (or the number of interfaces) per unit thickness of the total multilayer.

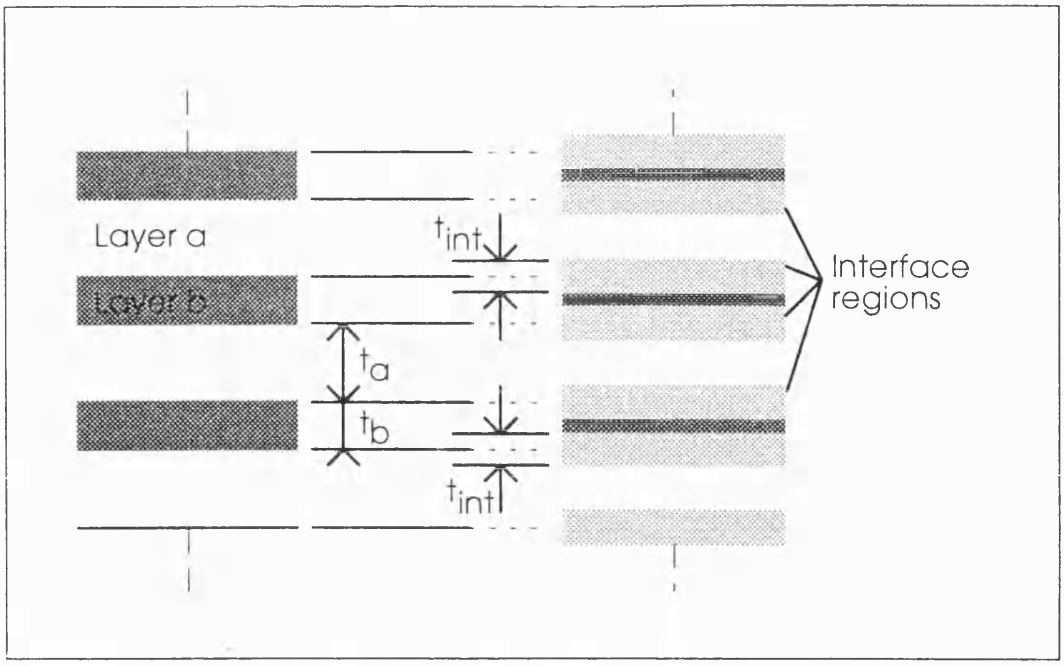

Figure 2.7 Schematic multilayer showing interface regions.

A different approach arises from the work of Néel (1954). Néel developed a theory of magnetostriction and magnetocrystalline anisotropy, from which he deduced that there exists in ferromagnets a surface anisotropy energy. This arises from the different symmetry of the atomic arrangement at a surface compared to that in the bulk, and plays a significant rôle in the properties of ferromagnetic substances in which the components are dispersed on a scale smaller than 10nm. In his calculation of the surface anisotropy energy density, Néel considered a simplified dispersed system where plane layers of magnetic material were separated by non-magnetic layers of the same thickness. He stated that the results were analogous for materials consisting of fine, isolated grains; but the case he considered is just that of the magnetic/non-magnetic multilayer. For the magnetisation vector lying in the plane of the layers, the surface contribution to the anisotropy energy density is K_s/t_{mag}, where t_{mag} is the thickness of the magnetic layer and K_s is the newly-defined surface anisotropy constant. Since

magnetocrystalline anisotropy and magnetostriction both have their origins in spin-orbit coupling, it is expected that a similar surface (or interface) contribution to magnetostriction might exist, by analogy. Thus Szymczak *et al.* (1988) have proposed that the effective saturation magnetostriction of a multilayer can be written as:

$$\lambda_s^{eff} = \lambda_s^v + 2\frac{\lambda_s^s}{t_{mag}} \qquad 2.2$$

where λ_s^v is the "volume magnetostriction", λ_s^s is the "surface magnetostriction" (with units of length) and t_{mag} is the thickness of the magnetic layer. Szymczak *et al.* apply this expression only to multilayers consisting of magnetic layers of a single type interleaved with non-magnetic layers, and in which the interfaces may be rough but are probably not alloyed (see Section 2.4.2). They apply this interpretation to multilayers which have any thickness of the non-magnetic layer. As Dirne and Denissen (1989) have pointed out, Equation 2.2 could only apply to a magnetic/magnetic layer system when t_a/t_b is a constant. They believe that magnetostriction in magnetic/magnetic multilayer systems is mainly determined by the thickness of t_{int}. When there is mixing at the interfaces, λ_s^s becomes a difficult term to interpret.

Consider applying Equation 2.1 to a multilayer of magnetic/non-magnetic bilayers (refer to Figure 2.7). The equation would become:

$$\lambda_s = \left(\frac{1}{t_{mag}+t_{int}}\right)\left\{(t_{mag}-t_{int})\lambda_s^{mag} + 2t_{int}\lambda_s^{int}\right\}$$

$$\therefore \lambda_s t_{mag} = \lambda_s^{mag} t_{mag} + \frac{2t_{int}\left(\lambda_s^{int} - \lambda_s^{mag}\right)}{1+\frac{t_{int}}{t_{mag}}} \qquad 2.3$$

This expression can only be applied to systems where the maximum interface thickness can be supported by the two layers, i.e. it is required that $t_{int} \leq t_{mag}$ and $t_{int} \leq t_{non\text{-}mag}$. A perfectly straight line would not be expected from a plot of $\lambda_s t_{mag}$ against t_{mag}, since t_{mag} appears in the intecept. However, such a plot can be useful

in situations where $t_{int} << t_{mag}$ and linearity of $\lambda_s t_{mag}$ vs. t_{mag} would imply that that was the case. From a linear regression of the data, the magnetostriction contribution from the bulk of the magnetic layer, λ_s^{mag}, can be obtained from the gradient. Curvature of the data would suggest that the interface thickness is not negligible compared to the magnetic layer thickness. Any difference between λ_s for the multilayer and λ_s^{mag} is contained in the intercept term, c. The terms λ_s^{int} and t_{int} are not uniquely defined. If the intercept is zero, then either $t_{int} = 0$ or $\lambda_s^{int} = \lambda_s^{mag}$. Non-zero intercepts indicate influence of the interfaces on the magnetostriction of the multilayer series. An independent measure of t_{int} would be required in order to establish λ_s^{int} from the magnetostriction data.

The magnetic layer thickness when $\lambda_s = 0$ can be found: $t_{mag0} = -c/\lambda_s^{mag}$. If t_{mag0} is positive, this is the point at which the magnetic layer and interface region contributions are balanced; the magnetic layers and interface regions must be acting against one another, or the interface regions are contributing nothing to the magnetostriction and the whole thickness t_{mag0} is taken up by interface. A negative t_{mag0} indicates that the interfaces act to enhance the magnetostriction of the multilayer.

At $\lambda_s = 0$, therefore, the interface thickness can be expressed as $t_{int} = (\lambda_s^{mag} t_{mag0})/(\lambda_s^{mag} - 2\lambda_s^{int})$. Depending on the relative sign and size of the magnetostriction values λ_s^{mag} and λ_s^{int}, the interface thickness can be qualitatively related to t_{mag0} as shown in Table 2.1, below. It is interesting to note that some combinations of magnetostriction values give unphysical values for t_{int}.

Table 2.1 Effect on values of t_{int} of different volume and interface magnetostriction values.

Condition:	Result when $t_{mag0} > 0$	Result when $t_{mag0} < 0$
$\lambda_s^{mag} > 0,\ 0 < \lambda_s^{int} < \lambda_s^{mag}/2$	$0 < t_{mag0} < t_{int}$	$t_{int} < 0$, unphysical
$\lambda_s^{mag} > 0,\ 0 < \lambda_s^{mag}/2 < \lambda_s^{int} < \lambda_s^{mag}$	$t_{int} < 0$, unphysical	$t_{int} > \lvert t_{mag0} \rvert$
$\lambda_s^{mag} > 0,\ 0 < \lambda_s^{mag} < \lambda_s^{int}$	$t_{int} < 0$, unphysical	$t_{int} < \lvert t_{mag0} \rvert$
$\lambda_s^{mag} > 0,\ \lambda_s^{int} < 0$	$t_{int} < t_{mag0}$	$t_{int} < 0$, unphysical
$\lambda_s^{mag} < 0,\ \lambda_s^{int} > 0$	$t_{int} < t_{mag0}$	$t_{int} < 0$, unphysical
$\lambda_s^{mag} < 0,\ \lambda_s^{mag}/2 < \lambda_s^{int} < 0$	$t_{int} > t_{mag0}$	$t_{int} < 0$, unphysical
$\lambda_s^{mag} < 0,\ \lambda_s^{mag} < \lambda_s^{int} < \lambda_s^{mag}/2 < 0$	$t_{int} < 0$, unphysical	$t_{int} > \lvert t_{mag0} \rvert$
$\lambda_s^{mag} < 0,\ \lambda_s^{int} < \lambda_s^{mag} < 0$	$t_{int} < 0$, unphysical	$t_{int} < \lvert t_{mag0} \rvert$

A known value of t_{int} may retrospectively alter the value of λ_s calculated from measurements on the multilayer. This arises if the thickness of the magnetic layer has been used at any point, for example, in calculating saturation magnetisation from magnetic measurements and if M_s is then used in calculating λ_s, as required in

the Small Angle Magnetisation Rotation technique described in Section 3.4. In recalculating M_s in order to adjust λ_s, it would be necessary to take into account whether or not the interface region were magnetic. If the interface were not magnetic and not magnetostrictive, then the plot of $\lambda_s t_{mag}$ vs. t_{mag}, using the true magnetic layer thickness (t_{mag} - t_{int}) would be similar to the original plot except that the data points would be shifted to slightly lower t_{mag} and lower $\lambda_s t_{mag}$. If the interface were magnetic, it would be necessary to know its magnetisation in order to adjust λ_s accordingly; the contribution λ_s^{int} could then be found from the measured data.

Expressions 2.2 and 2.3 can be shown to be comparable, although their physical bases are different. Rearranging Equation 2.2 gives:

$$\lambda_s^{eff} t_{mag} = \lambda_s^v t_{mag} + 2\lambda_s^s \qquad 2.4$$

Comparing with Equation 2.3, the "volume magnetostriction" term λ_s^v is identified with λ_s^{mag}. The "surface magnetostriction", the fixed value $2\lambda_s^s$, is then to be compared with the whole of the expression for the intercept, c, which is not expected to be truly constant for finite interface thicknesses t_{int} due to the presence of t_{mag} in c. If $t_{int} << t_{mag}$, then the interface term can be simplified. Then comparison with Equation 2.4 yields $\lambda_s^s \approx t_{int}(\lambda_s^{int} - \lambda_s^{mag})$. Equation 2.3 is a volume average model of the magnetostriction of multilayers where a finite thickness interface may or may not be magnetostrictive. Equation 2.2 considers that the magnetostriction of a multilayer consists of a contribution from the volume of the magnetic layer plus a surface contribution which arises from the altered symmetry of the atomic arrangement at the interfaces, not from any finite thickness of material at the interfaces. Although the two models have different physical bases, magnetostriction data can be presented in the same form for both. If different regression coefficients, r, are encountered when data are presented as λ_s vs. $1/t_{mag}$ and $\lambda_s t_{mag}$ vs. t_{mag}, this is because the values involved in the calculations

of r are different, and in particular, the range of t_{mag} is generally greater than the range of $1/t_{mag}$. This often leads to higher correlation coefficients for data regressed as $\lambda_s t_{mag}$ vs. t_{mag}. In this thesis, both in examining published data and in discussing experimental results obtained in this work, both ways of plotting the data will be used, as both are encountered in the literature.

Below, λ_s data from published literature are presented, for various groups of multilayer systems. Methods used to measure λ_s include measuring sample deflection in a rotating magnetic field, substrate curvature in a constant magnetic field, changes in magnetic anisotropy due to sample bending or under applied stress, torque magnetometry, cantilever-capacitance methods and Strain-Modulated Ferromagnetic Resonance (SMFMR). Many of these methods are indirect, and experimental accuracies are not reported, although Dirne and Denissen (1989) quote a relative accuracy of 10%, and Zuberek 15% (1993). Small Angle Magnetisation Rotation (SAMR) is also applicable, if correction is made as necessary for the presence of a substrate (see Section 3.4.1).

2.4.1. Magnetic/Magnetic Multilayers

The literature data in this section are plotted against the inverse of the modulation period, $1/\Lambda$, after Equation 2.1. Iron, cobalt and nickel are all mutually soluble, forming alloys over the complete composition range (Hansen (1958), Hultgren *et al.* (1973)). The lines shown on the plots are regression lines for the individual data sets.

Data from different groups do not, in general, coincide, although, as can be seen in the appropriate tables, no two sets are identical. There are different layer thickness combinations, and different deposition methods and conditions used, which may affect the structural quality of the multilayers. Glass is frequently used

as a substrate, but not always the same type. Since glass is amorphous, it should not determine the crystallographic texture of the deposit; an oriented crystal such as Si(100) may do, however. Single crystals can have different magnetostriction constants in different crystallographic directions, so crystallographic texture in a multilayer could have an important influence on its magnetostriction (see Section 4.3). Published magnetostriction data on Fe/Co and Fe/Co-Fe multilayers are presented in Figure 2.8 (details of the multilayers are given in Table 2.2)

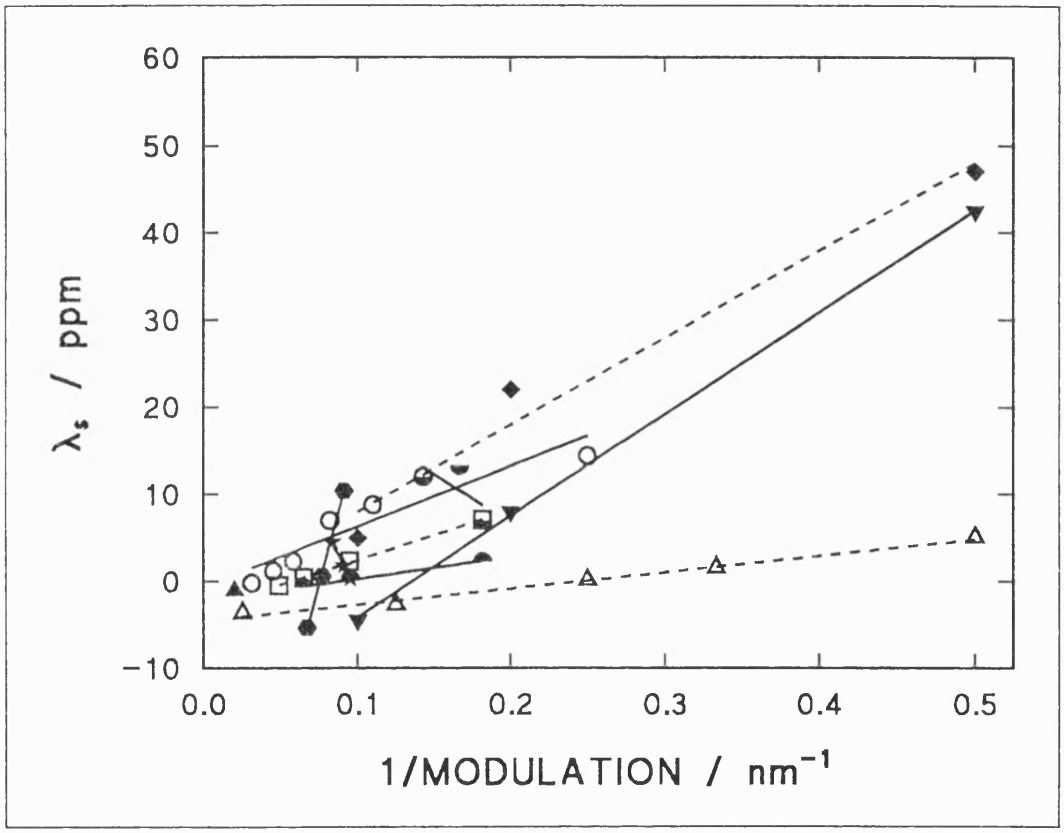

Figure 2.8 Literature data on the magnetostriction of multilayers of iron with cobalt and iron-cobalt alloy (for key, see Table 2.2).

Table 2.2 Key and information on data presented in Figure 2.8 on Fe/Co and Fe/Co-Fe multilayers. Multilayers are Fe/Co unless otherwise stated.

	Reference	Deposit	Line: λ_s =	r
○	Senda and Nagai (1989a)	t_{Co} = 2nm	69.2/Λ - 0.6	0.92883
□	Senda and Nagai (1989a)	t_{Co} = 0.5nm	57.1/Λ - 3.3	0.99966
◓	Senda and Nagai (1989a)	Fe/Co-Fe t_{CoFe} = 0.5nm	25.0/Λ -2.2	0.99695
★	Senda and Nagai (1989a)	Fe/Co-Fe t_{Fe} = 10nm	-353.2/Λ +33.9	0.99997
◒	Senda and Nagai (1989a)	t_{Fe} = 5nm	-112.0/Λ +29.1	0.66157
Δ	Okuyama and Shinjo (1992)	t_{Fe}/t_{Co} = 1 On Au buffer	18.8/Λ - 4.6	0.99527
▼	Dirne *et al.* (1990)	t_{Fe}/t_{Co} = 1	116.92/Λ - 15.8	0.99985
♦	Dirne *et al.* (1990)	t_{Fe}/t_{Co} = 1	100.0/Λ - 2.0	0.98533
⬟	Dirne and Denissen (1989)	t_{Fe} = 10nm	661.0/Λ - 49.9	0.99912
▲	Nakatani and Kobayashi (1989)	t_{Fe} = 45nm, t_{Co} = 5nm	—	—

continued...

Table 2.2 continued.

	Substrate	Deposition method	λ_s measurement	$P_{deposition}$ / torr, and gas type	$T_{substrate}$ / °C
○ □ ◗ ★ ◡	Corning 0211 glass	ion beam sputtering in 8kAm^{-1} field parallel to surface	change in substrate curvature in constant 2kAm^{-1} field	?	160
Δ	Glass, polyimide	electron-beam evaporation	?	10^{-9}	27
∇	Na glass, Ba glass (?)	ion beam sputtering	sample deflection in rotating (5Hz) field	1.5×10^{-4}, Ar	<30
◆	Na glass, Ba glass (?)	ion-assisted ion beam sputtering	sample deflection in rotating (5Hz) field	1.5×10^{-4}, Ar	<30
⬢	Na glass, Ba glass	ion beam sputtering	sample deflection in rotating (5Hz) field	1.5×10^{-4}, Ar	<30
▲	Corning 7059 glass	ion beam sputtering	torque meter	1.9×10^{-4}, Ar	post-anneal 300°C, 1hr in Ar

Most of the data are fitted well by Equation 2.1. Dirne and Denissen (1989), Dirne *et al.* (1990) and Senda and Nagai (1989a) all explain the observed variation in λ_s by considering a mixed layer of Fe-Co alloy at the multilayer interfaces, about 1nm thick. Dirne's group deduce this from fitting their data using Equation 2.1, inserting λ_s values for Fe and Co layers as measured on textured single films and assuming that each interface region is a linear concentration gradient from one component to the other. Senda and Nagai observed the λ_s behaviour in multilayers with t_{Co} down to 0.5nm. Okuyama and Shinjo (1992) found the same thickness of interface region, although evaporation would be expected to produce multilayers with less interface mixing. The more negative λ_s results would indicate a smaller mixed region; the λ_s values for Fe and Co they used in Equation 2.1, however, were calculated for oriented samples, and the resulting value for Co was three times larger than that used by Dirne and Denissen. If more similar values had been used, the calculated interface thickness would have been less. Since Okuyama and Shinjo used Au buffer layers under the Fe/Co multilayers, greater crystallographic texture would be expected. The more positive λ_s values observed by Dirne *et al.* in multilayers where additional ion bombardment was used are attributed to increased interface mixing. The greater the proportion of the multilayer that consists in a mixed, alloy region with positive λ_s, the more positive is λ_s of the multilayer, which is evidenced from Figure 2.8 (bearing in mind the layer thickness combinations). The thickness of the alloy layer can be increased on annealing, as this promotes interdiffusion between miscible materials. Dirne *et al.* (1990) report a ten-fold increase in the magnetostriction of a multilayer of 10nm Fe/5nm Co-Nb-Zr on annealing for 30 minutes in a nitrogen atmosphere at 400°C, which they attribute to mixing of the Fe and Co to form an alloy at the interfaces. Senda and Nagai (1989a) report an increased λ_s on annealing a multilayer of 20nm Fe/2nm Co in a 40kAm^{-1} field at temperatures up to 300°C, for the same reason. Annealing a

10nm Fe/0.5nm Co multilayer had no effect, as the Co was already completely mixed.

Coercivity is another property which can be affected by annealing, which can reduce film stresses and promote grain growth. Small grain sizes are expected to result in lower coercivities from magnetocrystalline anisotropy considerations, as Houdy *et al.* (1991) have observed in Fe/Co multilayers. For fixed t_{Fe} = 2.8nm, thicker Co layers result in lower H_c values, reaching a minimum of around 800Am^{-1} for t_{Co} = 5nm before increasing slightly. This is opposite to the observations of Komuro *et al.* (1988) that more Fe and less Co in a multilayer reduces H_c. Annealing reduced H_c further. Senda and Nagai (1989a) observe the same trend as Komuro *et al.*, but the conditions for lower coercivity are those for which λ_s is smaller. The lowest value seen is 300Am^{-1} by Nakatani and Kobayashi (1989) in 10(45nm Fe/5nm Co) annealed at 300°C for 1 hour in Ar to reduce the film stress (measured using a B-H loop tracer at 40Hz). Senda and Nagai observed a coercivity of about 350Am^{-1} in a 20nm Fe/2nm Co multilayer reduce to around 65Am^{-1} after a magnetic field anneal at 300°C (measured by M-H loop tracer and vibrating sample magnetometer). Both these multilayers have thick Fe layers, and the annealing could reduce film stress. Stress relief was also considered the initial cause of softening in Fe/Co-Zr multilayers by Jimbo *et al.*(1991), even though grain size increased from 10-15nm to 20nm. Further annealing increased H_c, however, indicating that grain size effects now dominated over stress effects. By inserting 5nm SiO_2 layers into 15nm Fe/0.5nm Co multilayers, Senda and Nagai decreased H_c dramatically, a minimum of about 72Am^{-1} being achieved when the thickness of Fe/Co multilayer between the SiO_2 layers was 50nm, which they suggest is due to extra magnetostatic wall energy. Jimbo *et al.* (1991), making Fe/Co-Zr multilayers, found a decrease in H_c from about 320Am^{-1} to around 40Am^{-1} on annealing, with t_{Fe} = 20-30nm. Their magnetostriction data also fits

well Equation 2.1, but λ_s values are between -5ppm and +3ppm. Dirne *et al.* (1989) found very soft multilayers ($H_c \approx 50Am^{-1}$) in the Fe/Co-Nb-Zr and Fe/Fe-Cr-B systems when the thickness of the amorphous alloy layers were greater than 4nm and 2nm, respectively.

Deposition at elevated temperatures can increase interface mixing of mutually soluble materials, reduce film stress and increase grain size in the films. Larger grain size could lead to a higher coercivity. Working on Co-Cr alloy films, Fartash and Oesterreicher (1989) and Niimura and Naoe (1985) found such behaviour. Wan and Hadjipanayis (1991) found the opposite in $Co_{80}Ni_{20}$ films, i.e. that deposition at higher temperatures reduced H_c and that larger grain sizes gave the lowest coercivities. Philipp and Tiemann (1972) report only a small effect on depositing Ni-Fe and Co-Fe alloy films at temperatures of 100-300°C. They do observe, interestingly, that the coercivity of a film depends on its composition, observing minima of approximately $140Am^{-1}$ for 70% Ni in Fe and about $1kAm^{-1}$ for 15% and 70% Co in Fe. All the films were 2.5μm thick, d.c. sputtered onto water-cooled glass.

Bulk diffusion constants indicate that negligible intermixing ought to occur at these temperatures, and yet it is observed. Gleiter (1992), however, reports that diffusion in nano-structured metals is substantially increased over self- and solute-diffusion in bulk materials. The self-diffusion of nano-structured copper is enhanced by 2-4 orders of magnitude over grain-boundary diffusion, and by 14-20 orders of magnitude over lattice diffusion in bulk Cu. For Ag and Au in Cu and Pd, solute diffusion is enhanced by 3-5 orders of magnitude over grain-boundary diffusion and by 8-18 orders of magnitude over lattice diffusion.

Coercivity can be increased by raising the sputtering pressure. This has been noted by Shearwood (1994) investigating an iron-cobalt alloy (approximately 50%-50%) multilayered with silver, deposited by r.f. magnetron sputtering. H_c was

measured parallel to the film plane. The sputtering pressure at which the magnetic layer was deposited had a significantly greater effect on H_c than the non-magnetic layer sputtering pressure. Hashimoto *et al.* (1989b), Carcia and Zeper (1990) and He *et al.* (1991), looking at Co/Pd and Co/Pt multilayers, also note that increased deposition pressure increases H_c. In these cases, the MH loops were measured perpendicular to the film plane. The effect here may be connected with the columnar growth of Co and the usual easy axis being the hexagonal *c*-axis

Data on Fe/Ni and Fe/Ni-Fe multilayers are presented in Figure 2.9, the key and details for which are given in Table 2.3.

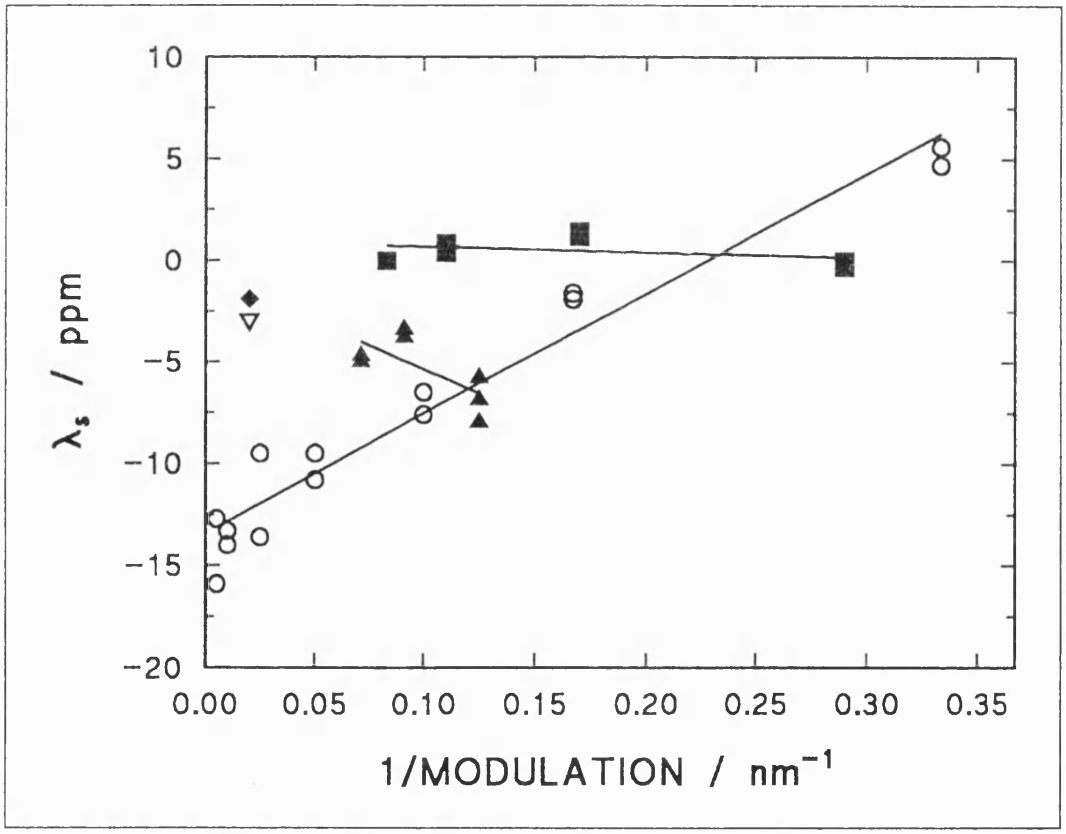

Figure 2.9 Literature magnetostriction data on Fe/Ni and Fe/Ni-Fe multilayers. See Table 2.3 for details.

Table 2.3 Details of Fe/Ni and Fe/Ni-Fe multilayers for which data are presented in Figure 2.9. Multilayers are Fe/Ni unless otherwise stated.

	Reference	Deposit	Line: λ_s =	r
○	Nagai *et al.* (1988)	$t_{Fe}/t_{Ni} = 1$	59.1/Λ - 13.4	0.97560
■	Nagai *et al.* (1988)	$t_{Ni} = 2nm$	-2.9/Λ + 1.0	0.37492
▲	Nagai *et al.* (1988)	$t_{Ni} = 4nm$	-47.5/Λ - 0.6	0.71635
♦	Nakatani and Kobayashi (1989)	$t_{Fe} = 45nm$, $t_{Ni} = 5nm$	—	—
∇	Nakatani and Kobayashi (1989)	$Fe/Ni_{80}Fe_{20}$ $t_{Fe} = 45nm$, $t_{Ni\text{-}Fe} = 5nm$	—	—

Table 2.3 continued.

	Substrate	Deposition method	λ_s measurement	$P_{deposition}$ / torr, and gas type	$T_{substrate}$ / °C
○ ■ ▲	Corning 0211 glass, Si (100) wafer	ion beam sputtering in 8kAm^{-1} field parallel to surface	change in substrate curvature in constant 2kAm^{-1} field	1×10^{-4}, Ar	160
♦ ∇	Corning 7059 glass	ion beam sputtering	torque meter	1.9×10^{-4}, Ar	post-anneal 300°C, 1hr in Ar

A poor correlation coefficient is obtained for the fit to data for which t_{Ni} = 2nm, since the gradient is small and the λ_s values are near zero. Otherwise, the fit looks reasonable. The data for t_{Ni} = 4nm is quite scattered, but for equal thicknesses of Fe and Ni, Equation 2.1 seems appropriate.

For Fe layers the same thickness as Ni layers, Nagai *et al.* (1988) observe a more positive λ_s for larger $1/\Lambda$ (thinner layers) due to the more dominant effect of the formation of Fe-Ni alloys at the interfaces. When the thickness of Ni is fixed, the trend with $1/\Lambda$ is opposite, as the relative amount of Ni in the multilayers is increased, and Ni has a more negative λ_s value than Fe (-34ppm as opposed to -7ppm for random polycrystalline samples (Cullity (1972))).

Nakatani and Kobayashi (1989) report for their Fe/Ni multilayer H_c = 160Am^{-1} and for their Fe/Ni-Fe multilayer H_c = 130Am^{-1}. Both contain thick Fe layers of 45nm and were annealed to relieve film stress. Krishnan *et al.* (1991) found $H_c \approx$ 320Am^{-1} for multilayers containing equal thicknesses of Fe and Ni layers for $t_{Ni} \leq$ 4nm while Nagai *et al.* (1988) report coercivities of less than 80Am^{-1} for multilayers with t_{Ni} = 2nm or 4nm and $t_{Fe} \geq$ 4nm. These multilayers have the smaller λ_s values of the series, however. Thicker Ni layers give higher values of H_c (t_{Fe} = 10nm) and H_c increases with the multilayer period when $t_{Fe} = t_{Ni}$. Nagai *et al.* attribute low coercivity values to poor crystallinity in the Fe layers.

Considering both Fe/Co and Fe/Ni multilayers, it seems that lower coercivities are obtained when the multilayers contain more Fe and less Co or Ni.

If Equation 2.1 applies, λ_s of the multilayer can be balanced to zero, which is what is desired in materials for magnetic recording (which is the aim of many of the groups cited here). The maximum magnetostriction achievable, however, cannot be greater than the largest value of those of the component layers or interface.

This restricts the maximum λ_s in the Fe/Co system to approximately +60ppm for 70% Co in Fe (Bozorth (1951)) for a random polycrystalline sample. The Fe/Ni system is limited to the pure nickel value of -34ppm (for an isotropic polycrystalline sample) or to -46ppm (λ_{100} for Ni) if the Ni layers are crystallographically textured (Cullity (1972)). The largest positive value of λ_s in the random polycrystalline Fe-Ni alloys is approximately +22ppm, for 20% Ni in Fe. These limits will apply unless some non-equilibrium phase can be produced, which has different properties. Otherwise, a different mechanism will have to be invoked, for example lattice strain using non-miscible materials as the interlayers. Other electronic interactions may also occur in that case. The experimental saturation magnetostriction constants of pure, random polycrystalline ferromagnetic elements are as follows: Fe: -7ppm, Ni: -34ppm and Co: ≈-16ppm (Cullity (1972)).

2.4.2. Magnetic/Non-Magnetic Multilayers

There is a wealth of data on magnetic/non-magnetic multilayers, much of which concerns Fe/non-magnetic systems. The iron-containing multilayers are not promising for large magnetostriction values, but they can be magnetically soft. Silver, copper and molybdenum are not miscible in iron, cobalt or nickel, whereas chromium, silicon and aluminium are (Hansen (1958), Hultgren (1973)). Literature magnetostriction data in this section is plotted as λ_s vs. $1/t_{mag}$ (after Equation 2.2) or as $\lambda_s t_{mag}$ vs. t_{mag} (after Equation 2.3) since both presentations are found in published literature. The comparability of the two expressions has been pointed out (Section 2.4) although their physical bases are different. Lines, where shown, are regression lines. Where indicated, not all the points for a given data set are plotted; the line, however, is the regression of all the points in the set.

Data on iron multilayered with non-magnetic interlayers are given in Figures 2.10, 2.11 and 2.12 for Fe/Cu, Fe/(C or Ti or Al_2O_3) and Fe/(Si or SiO_2) respectively. Corresponding details are given in Tables 2.4, 2.5 and 2.6.

Fe and Cu are do not normally form alloys, but interface mixing may occur, especially in sputtered multilayers, or the interfaces may be rough. The largest magnetostriction value reported for Fe/Cu multilayers is $\lambda_s \approx +4$ppm, by Awano *et al.* (1988). It can be seen from the plot that λ_s can be made to change from negative to positive values. The magnetic layer contributions to the magnetostriction, λ_s^{ν} and λ_s^{mag} according to Equation 2.2 and 2.3 respectively, are also both positive and negative in different data sets. For polycrystalline iron, λ_s = -7ppm but in a single crystal, λ_{100} = +21ppm and λ_{111} = -21ppm (Cullity (1972)) so positive or negative values of λ_s are expected in multilayers with different crystallographic texture in the iron layer (Senda and Nagai (1989b)).

The lowest H_c values quoted are around 80Am^{-1}, by Kozono *et al.* (1987) for a multilayer of about 1.5nm Fe/1.9nm Cu (H_c rises for thicker layers before dropping slightly; the layer thickness ratio is fixed) and by Senda and Nagai (1989b) for 5nm Fe/1nm Cu. Senda and Nagai have (110) textured films. They attribute the lower coercivities to smaller Fe grain sizes and to a decrease in domain wall energy due to magnetostatic coupling between iron layers.

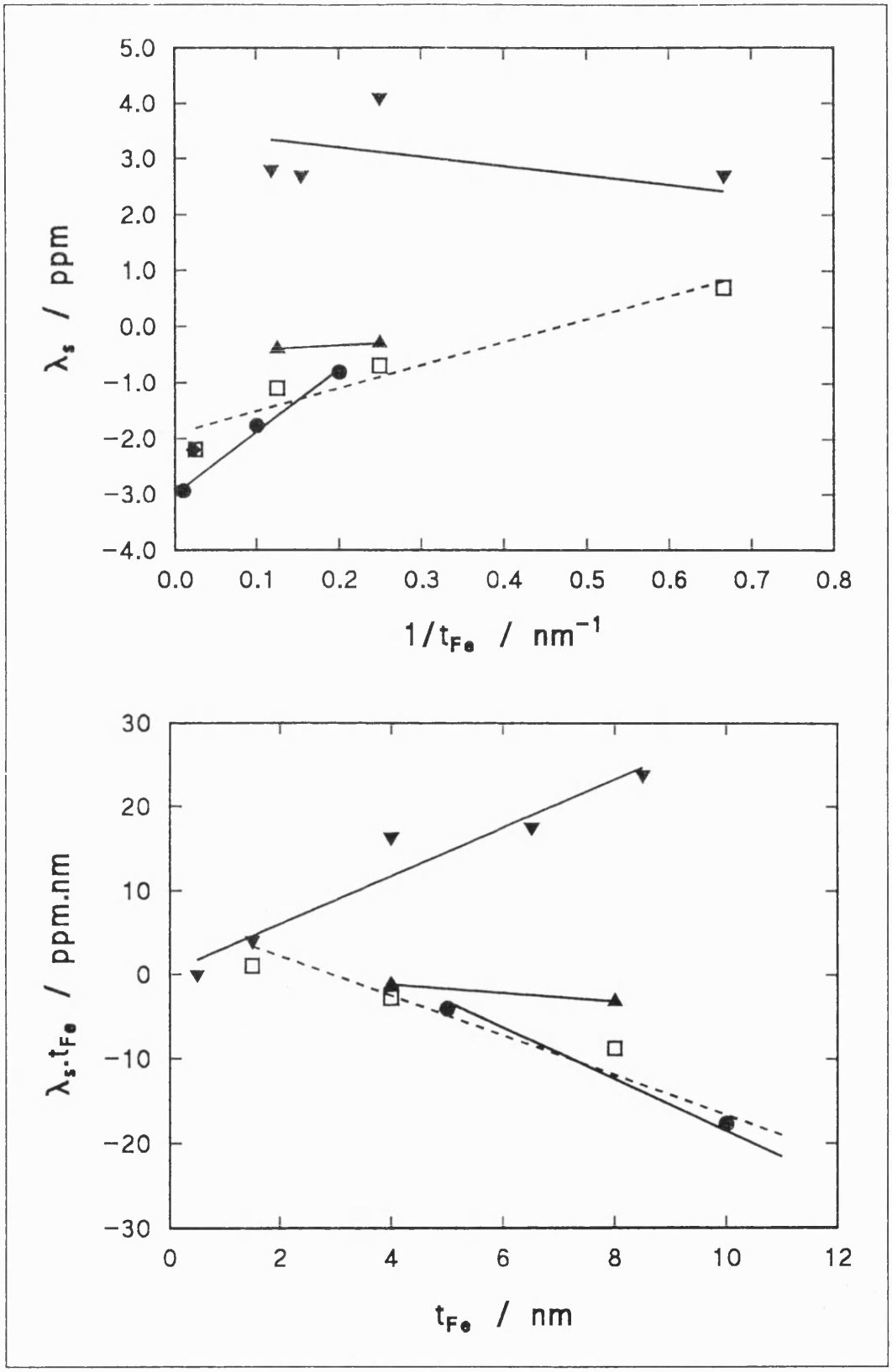

Figure 2.10 Published λ_s data on Fe/Cu multilayers. See Table 2.4 for details.

Table 2.4 Details of Fe/Cu multilayers for which magnetostriction data are presented in Figure 2.10.

	Reference	Deposit	Lines	r
●*	Senda and Nagai (1989b)	t_{Cu} = 1nm	$\lambda_s = 11.2/t_{Fe} - 3.0$	0.99620
			$\lambda_s t_{Fe} = -3.1t_{Fe} + 12.1$	0.99999
□*	Kozono *et al.* (1987)	t_{Fe}/t_{Cu} = 1/1.25	$\lambda_s = 4.1/t_{Fe} - 1.9$	0.96554
			$\lambda_s t_{Fe} = -2.4t_{Fe} + 6.9$	0.99854
▲	Kozono *et al.* (1987)	t_{Cu} = 2nm	$\lambda_s = 0.80/t_{Fe} - 0.50$	1
			$\lambda_s t_{Fe} = -0.50t_{Fe} + 0.80$	1
▼✞	Awano *et al.* (1988)	t_{Cu} = 4nm	$\lambda_s = -1.7/t_{Fe} + 3.5$	090017
			$\lambda_s t_{Fe} = 2.9t_{Fe} + 0.31$	0.96473
◆*	Nakatani and Kobayashi (1989)	t_{Fe} = 45nm, t_{Cu} = 5nm	—	—

✞ point for large $1/t_{Fe}$ not plotted, * point for large t_{Fe} not plotted.

continued...

Table 2.4 continued.

	Substrate	Deposition method	λ_s measurement	$P_{deposition}$ / torr, and gas type	$T_{substrate}$ / °C
●	Corning 0211 glass	ion beam sputtering in 8kAm^{-1} field parallel to surface	change in substrate curvature in constant 2kAm^{-1} field	1×10^{-4}, Ar (?)	160
□ ▲	Si	r.f. magnetron sputtering	change in anisotropy field under applied stress	2.0×10^{-3}, Ar	150
▼	Glass	r.f. sputtering	cantilever capacitance method in 560kAm^{-1}	1.0×10^{-2}, Ar	≈ 20 (water-cooled)
◆	Corning 7059 glass	ion beam sputtering	torque meter	1.9×10^{-4}, Ar	post-anneal 300°C, 1hr in Ar

Data on Fe/C, Fe/Ti and Fe/Al_2O_3 multilayers are presented below.

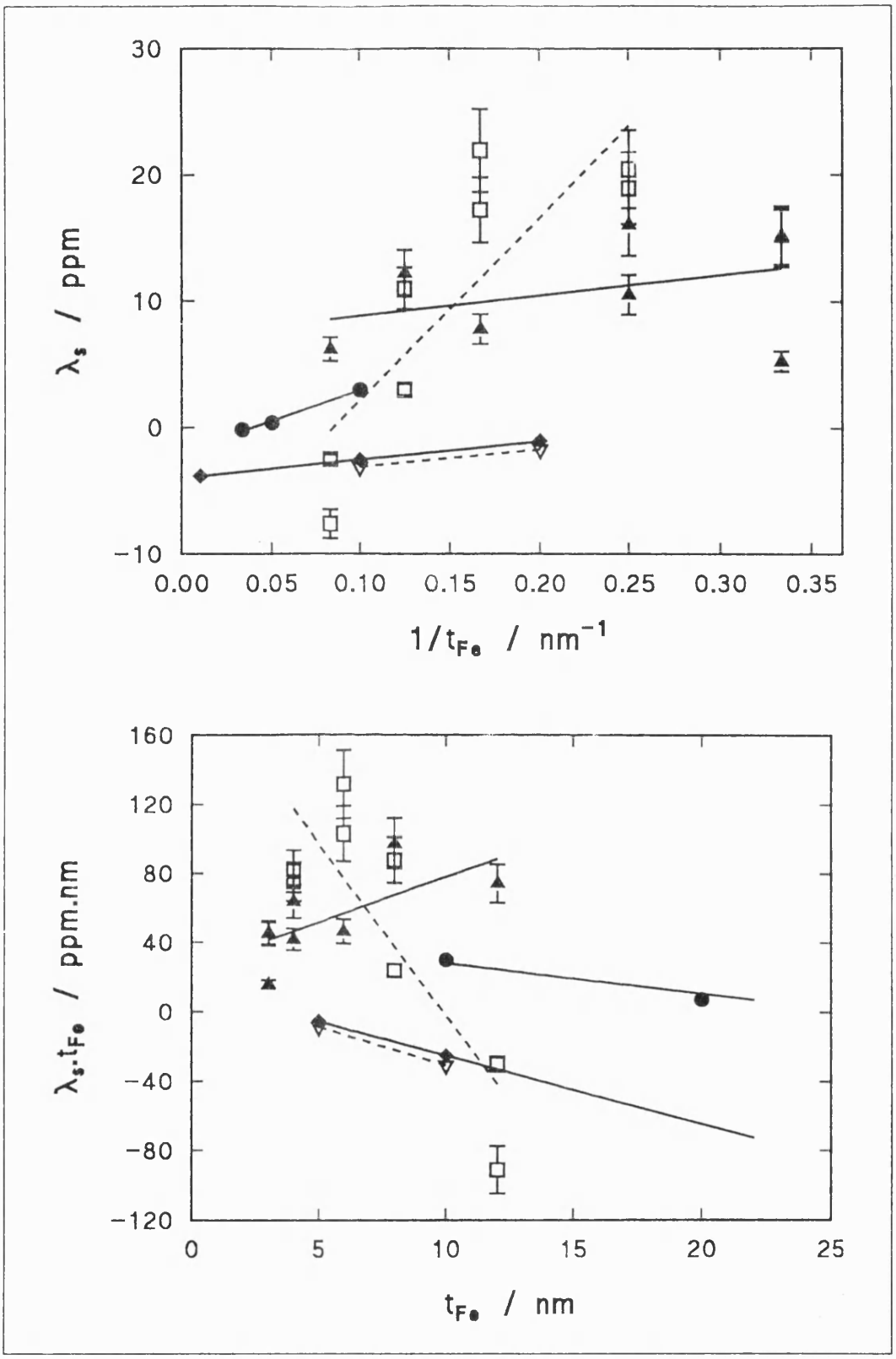

Figure 2.11 Literature magnetostriction data on Fe/C, Fe/Ti and Fe/Al_2O_3 multilayers. See Table 2.5 for details.

Table 2.5 Details for Fe/C, Fe/Ti and Fe/Al_2O_3 multilayer magnetostriction data presented in Figure 2.11.

	Reference	Deposit	Lines	r
●*	Senda and Nagai (1989b)	Fe/C	$\lambda_s = 48.7/t_{Fe} - 1.9$	0.99658
		t_C = 5nm	$\lambda_s t_{Fe} = -1.8t_{Fe} + 45.9$	0.98648
□	Zuberek *et al.* (1993)	Fe/C	$\lambda_s = 144.5/t_{Fe} - 12.3$	0.84144
		t_C = 1nm	$\lambda_s t_{Fe} = -19.9t_{Fe} + 196.9$	0.83651
▲	Zuberek *et al.* (1993)	Fe/C	$\lambda_s = 16.3/t_{Fe} + 7.2$	0.38183
		t_C = 2nm	$\lambda_s t_{Fe} = 5.3t_{Fe} + 25.5$	0.68969
∇	Senda and Nagai (1989b)	Fe/Ti	$\lambda_s = 14.2/t_{Fe} - 4.5$	1
		t_{Ti} = 5nm	$\lambda_s t_{Fe} = -4.5t_{Fe} + 14.2$	1
♦*	Senda and Nagai (1989b)	Fe/Al_2O_3	$\lambda_s = 14.8/t_{Fe} - 4.0$	0.99919
		t_{Al2O3} =5nm	$\lambda_s t_{Fe} = -4.0t_{Fe} + 14.6$	r^2 = 0.999999

* point for large t_{Fe} not plotted.

continued...

Table 2.5 continued.

	Substrate	Deposition method	λ_s measurement	$P_{deposition}$ / torr, and gas type	$T_{substrate}$ / °C
● ▽ ◆	Corning 0211 glass	ion beam sputtering in 8kAm^{-1} field parallel to surface	change in substrate curvature in constant 2kAm^{-1} field	1×10^{-4}, Ar (?)	160
□ ▲	glass, Si	d.c. triode sputtering	SMFMR	7.5×10^{-5}	water-cooled

Data from Senda and Nagai are quite well fitted by both forms of multilayer λ_s interpretation. The data from Zuberek *et al.* (1993) are poorly fitted by either expression, however, although the deposition conditions favour sharp interfaces between Fe and C and hence small t_{int}. The authors note two different crystallographic phases, however - bcc crystalline and amorphous - which have not been separated in the above treatment, and to which they assign different λ_s values. Thinner Fe layers give more amorphous structures. They also suggest that λ_s^v is affected by the thickness of the non-magnetic interlayer (they analyse the data for t_C = 1nm and t_C = 2nm together, but they have been separated above and it can be seen that the regression lines are quite different). Zuberek *et al.* achieve λ_s values between about -8ppm and +22ppm, whereas other data sets lie around $\lambda_s = 0$ with $|\lambda_s| < 5$ppm. The high values do not correspond particularly with crystal structure. There is no information on crystallographic texture in the samples, although both positive and negative values of the volume magnetostriction

contributions, λ_s^{ν} and λ_s^{mag}, obtained from the regressions may reflect differences in texture between the multilayer series. The single-crystal magnetostriction constants for Fe are $\lambda_{100} = +21$ppm and $\lambda_{111} = -21$ppm (Cullity (1972)).

Nakatani and Kobayashi (1989) and Senda and Nagai (1989b) report minimum H_c values of around 200Am^{-1}; for Senda and Nagai, this corresponds to an optimum iron layer thickness of 20nm. The multilayer has (110) texture and the grain size is about 10nm, which is not the smallest they observe. For Fe/Al_2O_3 multilayers, the minimum H_c is around 80Am^{-1} for the thinnest Fe layers. These minima all occur for multilayers with $\lambda_s \approx 0$.

Published results on Fe/Si and Fe/SiO_2 multilayers are shown below. Again, the λ_s values in these multilayers are low. The regressions according to Equation 2.3 (lower plot) indicate that the magnetostrictive contribution from bulk Fe is -2.5ppm to -3.5ppm for all the above systems. This implies similar crystallographic texture in each series, which is likely when they have been deposited under similar conditions. For Fe/Si multilayers, Nakatani and Kobayashi (1989) and Senda and Nagai (1989b) report coercivities of around 950Am^{-1}; for Senda and Nagai, this occurs at lower t_{Fe}. A very low coercivity of about 30Am^{-1} is reported by Senda and Nagai (1990) for Fe/SiO_2 multilayers with 8nm Fe and 5nm or 2.5nm SiO_2. H_c is lower for thinner Fe layers and those multilayers sputtered with a lighter gas. Again, smaller grain sizes result in lower coercivities.

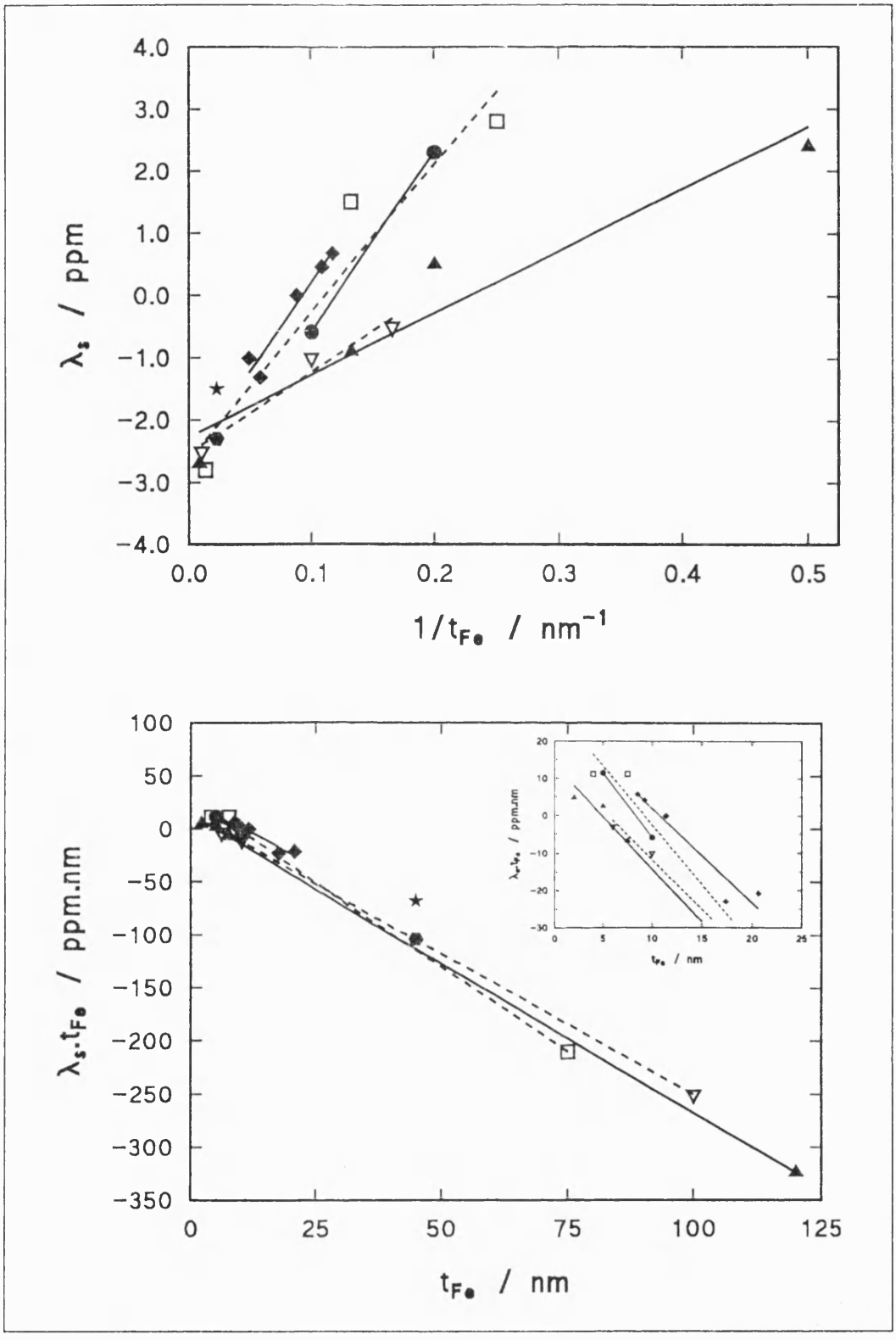

Figure 2.12 Published magnetostriction data on multilayers of Fe/Si and Fe/SiO_2. Inset shows detail for small t_{Fe}. See Table 2.6 for details.

Table 2.6 Details of Fe/Si and Fe/SiO_2 multilayers; data in Figure 2.12.

	Reference	Deposit	Lines	r
●	Senda and Nagai (1989b)	Fe/Si t_{Si} = 5nm	$\lambda_s = 28.9/t_{Fe} - 3.5$ $\lambda_s t_{Fe} = -3.5t_{Fe} + 28.9$	1 1
□	Senda and Nagai (1990)	Fe/SiO_2 (NeAr) t_{SiO2} = 5nm	$\lambda_s = 23.7/t_{Fe} - 2.6$ $\lambda_s t_{Fe} = -3.2t_{Fe} + 29.4$	0.95772 0.99904
▲	Senda and Nagai (1990)	Fe/SiO_2 (Ar) t_{SiO2} = 5nm	$\lambda_s = 10.0/t_{Fe} - 2.3$ $\lambda_s t_{Fe} = -2.8t_{Fe} + 13.7$	0.96484 0.99988
▽	Senda and Nagai (1990)	Fe/SiO_2 (Kr) t_{SiO2} = 5nm	$\lambda_s = 13.0/t_{Fe} - 2.5$ $\lambda_s t_{Fe} = -2.6t_{Fe} + 14.6$	0.98100 0.99992
♦	Senda and Nagai (1990)	Fe/SiO_2 (NeAr) t_{SiO2} = 2.5nm	$\lambda_s = 28.3/t_{Fe} - 2.6$ $\lambda_s t_{Fe} = -2.5t_{Fe} + 27.2$	0.97070 0.96263
★	Nakatani and Kobayashi (1989)	Fe/Si t_{Fe} = 45nm, t_{Si} = 5nm	—	—
⬢	Nakatani and Kobayashi (1989)	Fe/SiO_2 t_{Fe} = 45nm, t_{SiO2} = 5nm	—	—

continued...

Table 2.6 continued.

	Substrate	Deposition method	λ_s measurement	$P_{deposition}$ / torr, and gas type	$T_{substrate}$ / °C
●	Corning 0211 glass	ion beam sputtering in 8kAm^{-1} field parallel to surface	change in substrate curvature in constant 2kAm^{-1} field	1×10^{-4}, Ar (?)	160
□ ▲ ▽ ◆	Corning 0211 glass, Si	ion beam sputtering in 8kAm^{-1} field parallel to surface	change in substrate curvature in constant 2kAm^{-1} field	1×10^{-4}, $Ne_{80}Ar_{20}$, Ar and Kr resp.	160
★ ⬢	Corning 7059 glass	ion beam sputtering	torque meter	1.9×10^{-4}, Ar	post-anneal 300°C 1hr Ar

Some coercivity data are available for other multilayers containing iron. Kozono *et al.* (1988) have made Fe/Ag multilayers with t_{Ag} = 2nm. It is unlikely that the Ag layer is continuous at such thicknesses (Chopra and Randlett (1968)). In multilayers deposited by r.f. magnetron sputtering at 150°C, they observe that H_c is lower for thicker iron layers ($H_{cmin} \approx 80Am^{-1}$), where the iron becomes continuous and the d_{110} lattice plane spacing relaxes towards that of a thick Fe film. They observe the opposite trend in UHV evaporated multilayers, where the Fe

layers are always continuous and the lattice spacings relatively unaffected; they suggest this is due to some grain growth mechanism, which is not elucidated. Using d.c. sputtering, Haga *et al.* (1993) observe lower coercivities for *thinner* Fe layers; their Ag layer is thicker, and likely to be continuous, which may influence the growth of the Fe layers.

By contrast, Nagakubo *et al.* (1988) found in ion beam sputtered Fe/Al multilayers that thicker t_{Fe} (t_{Al} = 2nm) led to an increase in H_c at the same time as the d_{110} plane spacing became more like the bulk spacing. For fixed t_{Fe} = 10nm, a minimum H_c was found for $t_{Al} \approx 25$nm, thicker or thinner Al layers giving a higher value. Haeiwa *et al.* (1991), studying d.c. magnetron sputtered Fe/Al multilayers, found that the coercivity was reduced to 40-80Am^{-1} when the iron layer was increased to more than twice the thickness of the aluminium layer. This trend is opposite to that of Nagakubo *et al.*

Although some very soft Fe/non-magnetic multilayers have been produced, the saturation magnetostriction values are generally low, and the Fe/non-magnetic system does not look promising for fulfilling the aims of this project.

The next series of multilayers to be considered are those containing nickel or cobalt interleaved with non-magnetic layers. Figure 2.13 shows literature data on Ni/Ag and Ni/C multilayers. Details of the films are given in Table 2.7.

Larger λ_s values are obtained in the multilayers containing silver rather than carbon, although no value exceeds that of random polycrystalline Ni. The C layer is amorphous, while the Ag layer would be expected to be polycrystalline or crystalline. Since Ag and Ni both take the face-centred cubic structure in bulk form, it is likely that the Ni/Ag multilayer grew in the fcc structure, and may possibly be (111) textured ((111) is the close-packed plane). Silver and nickel are

mutually insoluble, so interfaces in a Ni/Ag multilayer are expected to be sharp. For Ni, λ_{100} = -46ppm, λ_{111} = -24ppm and for a random polycrystalline sample, λ_s = -34ppm (Cullity (1972)). Values of λ_s^{ν} and λ_s^{mag} obtained by fitting the data to Equations 2.2 and 2.3 respectively are all between -35ppm and -37ppm, in good agreement with the random polycrystalline value, as is λ_s of the multilayers containing 100nm Ni layers. Zuberek *et al.* give no structural data on the Ni/Ag multilayers, but they do state that, in the Ni/C multilayers, the Ni layer is hexagonal for t_{Ni} = 5nm but fcc above 6nm. The magnetisation is strongly reduced in these multilayers, which they attribute to non-magnetic layers at the interface. Such layers may also reduce the effective magnetostriction.

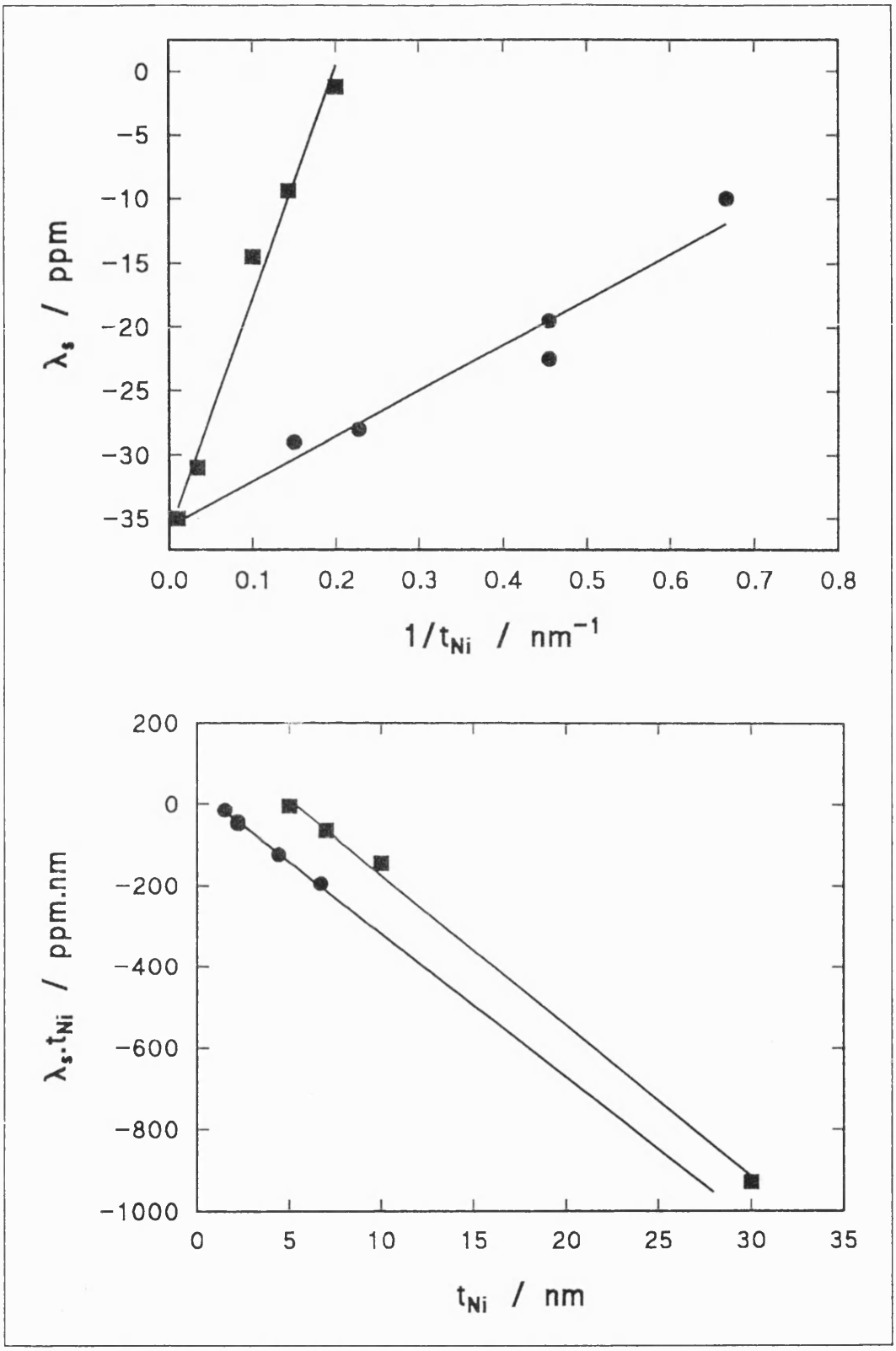

Figure 2.13 Published magnetostriction data on Ni/Ag and Ni/C multilayers.

For details, see Table 2.7.

Table 2.7 Details of Ni/Ag and Ni/C multilayers for which data are presented in Figure 2.13.

	Reference	Deposit	Lines	r
●	Zuberek *et al.* (1988)	Ni/Ag t_{Ag} = 5nm	$\lambda_s = 35.5/t_{Ni} - 35.6$ $\lambda_s t_{Ni} = -35.3t_{Ni} + 35.1$	0.98017 0.999995
■	Zuberek *et al.* (1987)	Ni/C t_C = 2nm	$\lambda_s = 182.5/t_{Ni} - 36.0$ $\lambda_s t_{Ni} = -37.0t_{Ni}$ +194.5	0.99053 0.99992

One point from each data set is omitted from the plot of $\lambda_s t_{Ni}$ vs. t_{Ni} since t_{Ni} is large. The regression lines shown take all data points into account.

Table 2.7 continued.

	Substrate	Deposition method	λ_s measurement	$P_{deposition}$ / torr, and gas type	$T_{substrate}$ / °C
●	Glass, Si	UHV electron gun evaporation	SMFMR	5×10^{-9}	water-cooled
■	Corning glass	d.c. triode sputtering	SMFMR	1.0×10^{-3}, Ar	water-cooled

Zuberek *et al.* point to the importance of interfaces in the magnetostriction of the multilayers. Gumbsch *et al.* (1991) have performed calculations on the accommodation of lattice mismatch at Ni/Ag boundaries with a (110) interface plane, and have found that the minimum enthalpy configuration corresponds to a reduction in density of 16% in the first Ni atomic plane (i.e. Ni atoms are further

apart than usual in bulk nickel). The usual Ni/Ag interface plane is (111), however, and the authors point out that the density reduction in this case may be smaller. Measurements by Ruud *et al.* (1993) on (111)-textured Ag/Ni multilayers (ion-sputtered) indicate the presence of a tensile interface stress of $2.27\pm0.67 Jm^{-2}$. The multilayers were deposited on (100)-oriented Si wafers at -156°C. At thin layers, the lattice plane spacings were strained from the bulk values, the Ni lattice being expanded and the Ag lattice contracted. The stress of the total multilayer was greater in this situation. Rodmacq and Dos Santos (1992) have deposited Ag/Ni multilayers by d.c. sputtering onto glass at -173°C. Polycrystalline, (111) textured superlattices were produced with sharp interfaces. The magnetisation lay in the film plane for all Ag and Ni layer thicknesses examined (0.5-4nm and 0.2-2nm, respectively). The magnetisation data suggested that there was a magnetically "dead" layer at each interface (cf. Zuberek *et al.*, Ni/C, above). The Curie temperature was lower for multilayers containing less Ni.

These papers do not give data on the coercivity of the multilayers.

Below are presented published data on Co/Cu, Co/C and Co/Ag multilayers (Figure 2.14). Multilayer details are given in Table 2.8. These data show a wider range of λ_s values than do the Ni/non-magnetic multilayers. For polycrystalline Co, $\lambda_s = -16$ppm, less than the value for polycrystalline Ni; in the crystalline state, $\lambda_s = 0$ parallel to the cobalt hexagonal *c*-axis, $\lambda_s \approx -50$ppm at 90° to the *c*-axis and $\lambda_s \approx -100$ppm at 60° to the *c*-axis (Cullity (1972)). Again, Zuberek's group obtains the largest values and other groups obtain values closer to zero. Crystallographic texturing may contribute to this difference (as suggested in the Fe/non-magnetic case, above) but such information is not given.

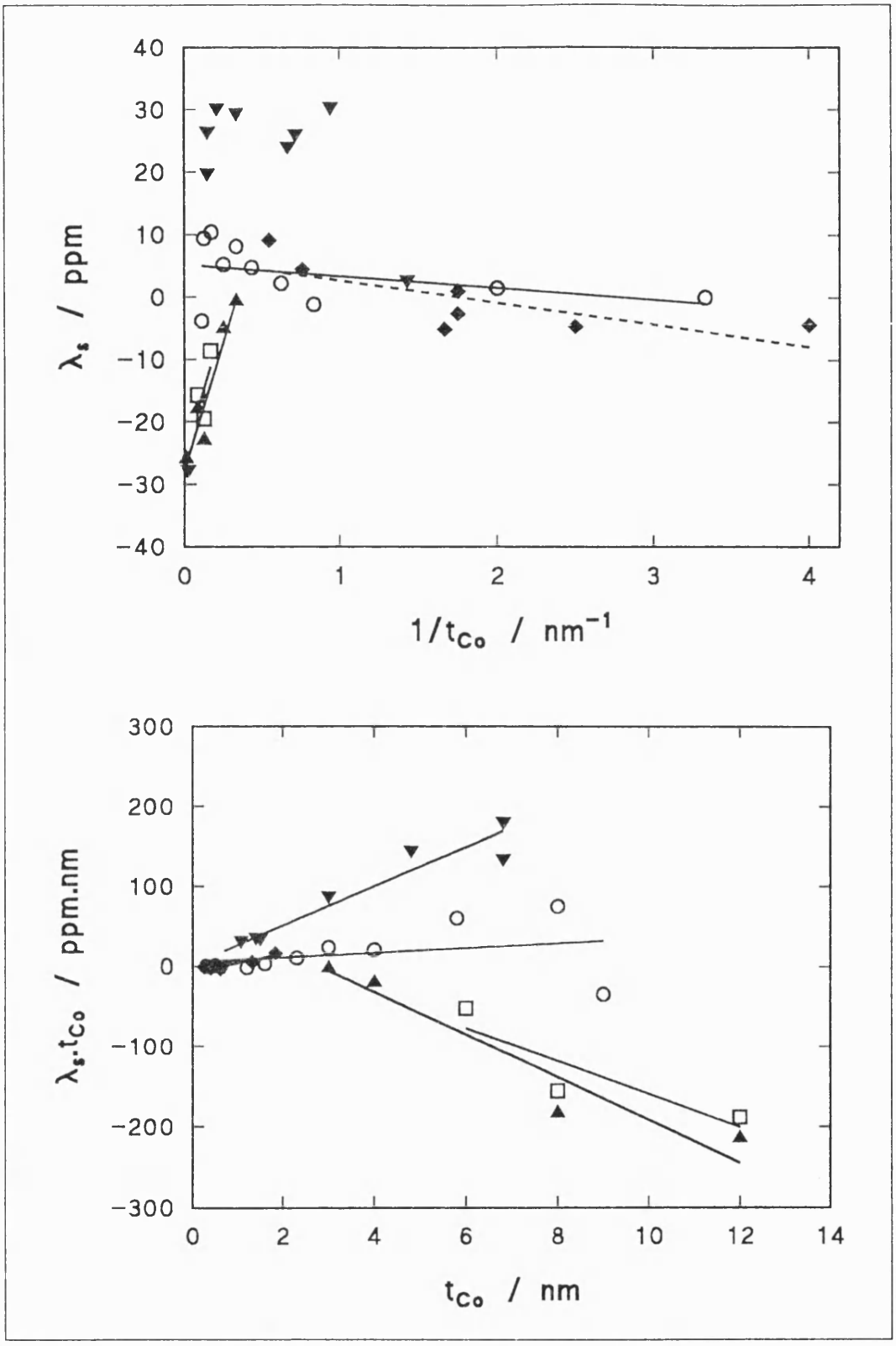

Figure 2.14 Literature magnetostriction data on Co/Cu, Co/C and Co/Ag multilayers. Details are presented in Table 2.8.

Table 2.8 Details of Co/Cu, Co/C and Co/Ag multilayers for which λ_s data are presented in Figure 2.14.

	Reference	Deposit	Lines	r
○	Awano *et al.* (1988)	Co/Cu	$\lambda_s = -1.8/t_{Co} + 5.1$	0.40411
		$t_{Cu} = 4nm$	$\lambda_s t_{Co} = 2.9t_{Co} + 5.4$	0.28524
□	Zuberek *et al.* (1991)	Co/C	$\lambda_s = 84.0/t_{Co} - 25.1$	0.63887
		$t_C = 1nm$	$\lambda_s t_{Co} = -20.6t_{Co} + 46.5$	0.88513
▲*	Zuberek *et al.* (1991)	Co/C	$\lambda_s = 81.3/t_{Co} - 27.5$	0.95423
		$t_C = 2nm$	$\lambda_s t_{Co} = -26.7t_{Co} + 74.6$	0.99968
▼*	Szymczak *et al.* (1990)	Co/Ag	λ_s vs. $1/t_{Co}$ not fitted	—
		$t_{Ag} = 5nm$	$\lambda_s t_{Co} = 24.5t_{Co} + 2.4$	0.95846
♦	Awano *et al.* (1988)	Co/Ag	$\lambda_s = -3.5/t_{Co} + 6.1$	0.74399
		$t_{Co}/t_{Ag} = 2/5$	$\lambda_s t_{Co} = -8.4t_{Co} + 7.0$	0.94260

* one point of these data sets is excluded from $\lambda_s t_{Co}$ vs. t_{Co} plot. Lines as for entire data set.

continued...

Table 2.8 continued.

	Substrate	Deposition method	λ_s measurement	$P_{deposition}$ / torr, and gas type	$T_{substrate}$ / °C
○ ♦	Glass	r.f. sputtering	cantilever capacitance method in 560kAm^{-1}	1.0×10^{-2} Ar	≈ 20 (water-cooled)
□ ▲	Glass, Si	d.c. triode sputtering	SMFMR	7×10^{-5}	water-cooled
▼	Glass	UHV electron gun evaporation	SMFMR	$2\text{-}5\times10^{-9}$	water-cooled

The data from Szymczak *et al.* (1990) is not fitted by the $1/t_{Co}$ expression (Equation 2.2). Fitting in the form of Equation 2.3 is better (although the two expressions are essentially similar), but it is clear from the plot that there is a systematic deviation from the fit (NB in the fit given, the point for the largest t_{Co} has been ignored and only the thinner layer group of multilayers has been included). Szymczak *et al.* propose adding a new phenomenological term to Equation 2.2, $\lambda_s^d/(\alpha + t_{Co})$, to model the contribution to λ_s of the reduced symmetry in a multilayer and depending on the origin of the magnetoelastic interactions, which they cite as being mainly dipolar and single-ion interactions in Co-based films. The terms λ_s^d and α have units of length. The meaning of the new term is not clarified (bearing in mind that there already exists in the expression a term for the contribution from the surfaces/interfaces which arises by the analogy drawn with Néel's concept of surface anisotropy (1954) resulting from the altered symmetry of atoms at a surface compared with those in the bulk). The fit they

obtain with the modified expression is not good, either. Apart from the data points at the extremes of the Co thickness range studied, the λ_s data seem to be scattered around a mean value of 27±8ppm, which would indicate that interface effects are very small in this multilayer series. This contrasts with the Ni/Ag data above, which is well fitted without modification of the expressions. The Co/Ag data of Awano *et al.* (1988) is also poorly fitted, but does not show the same behaviour as the data of Szymczak *et al.* The multilayers of Szymczak *et al.* were sputtered at a much lower pressure, favouring sharper, smoother interfaces than in Awano's case. Neither group gives structural information on their multilayers (although Awano *et al.* state that X-ray diffraction patterns were measured). In their Co/C multilayers, Zuberek *et al.* report an amorphous-like structure for $t_{Co} < 4$nm, and hexagonal for $t_{Co} > 8$nm, where perpendicular anisotropy is observed. In-plane anisotropy is observed for $t_{Co} < 8$nm.

Schelp *et al.* (1992) have studied the effects of annealing on a 1.5nm Co/6.0nm Ag multilayer prepared by electron beam evaporation on Si(111) with a 5nm Au buffer layer. The annealing was performed in dry hydrogen in a rapid furnace to minimise oxidation and to have a precise annealing time and temperature. The multilayer interfaces sharpened as the annealing temperature was increased up to 360°C, over which period the coercivity increased from about 25kAm^{-1} to about 250kAm^{-1} and the perpendicular anisotropy decreased. Beyond 360°C, the multilayer characteristic disappeared.

Nafis *et al.* (1991) have deposited Co/Cu and Co/Si multilayers by d.c. and r.f. sputtering. Using a SQUID magnetometer, they find that the magnetisation lies in-plane for all the Co thicknesses investigated (0.4nm to 10nm). For Co/Cu with t_{Cu} = 1.15nm, the in-plane coercivity is close to zero for $t_{Co} > 1.2$nm. The opposite H_c trend with Co thickness was found with Si interlayers. H_c being close to zero for t_{Si}

< 0.7nm. Nafis *et al.* consider that the Co in the multilayers is predominantly fcc. The Co/Cu interfaces were sharper than the Co/Si interfaces. At small t_{Co}, the group considers that a soft Co-Si alloy is formed. Measurements taken at 10K give larger H_c values. Deposition at higher temperatures also has different effects in the two cases. The coercivity of Co/Cu multilayers is increased, while that of Co/Si multilayers is decreased. The Co/Cu interfaces might be expected to sharpen on heating, and the Co/Si interfaces to blur.

Wang and Sellmyer (1991) found that thicker Co layers in Co/Cr multilayers d.c. sputtered onto Cu or glass with a 400nm Cr buffer layer gave rise to larger coercivities. This they attributed to atomic diffusion at interfaces and to crystal orientation, which could be enhanced by the deposition at an optimum temperature of 400°C. The Co layer thicknesses were varied from 2.5nm to 30nm. The easy axis was in-plane. At each boundary, 1nm of Co lost its ferromagnetism. Clarke *et al.* (1991), growing multilayers of Co/Au, Co/Cu and Co/Cr by MBE, explained their results by proposing that one monolayer of Co at each interface did not contribute to the magnetisation while the rest exhibited bulk magnetisation values. This applied when the interfaces were sharp i.e. with Au and Cu interlayers. De Gronckel *et al.* (1991), examining UHV evaporated Co/Cu multilayers, found a mixed layer at the interface, one atom thick. In their Co/Cr multilayers, Clarke *et al.* attribute the reduced moment to interdiffusion of Cr into Co. Using a Co thickness range from 0.5nm to 4.0nm, they found that the easy axis switched to perpendicular for t_{Co} < 1-2nm. The hcp structure of Co favours perpendicular anisotropy but is not strong enough to overcome the shape anisotropy until the magnetoelastic anisotropy energy dominates at low t_{Co}. Bruno and Renard (1989) have calculated that there should exist a spontaneous perpendicular magnetisation in Au/Co/Au sandwiches below a critical t_{Co}, and that interface roughness alters the

surface contribution to anisotropy, which explains the modification of the perpendicular anisotropy on annealing, as Co/Au interfaces are sharpened.

Nakatani and Kobayashi (1989) have examined multilayers of Fe with many different interlayers, magnetic and non-magnetic and of different crystal structures. They were investigating the effects of lattice mismatch on soft magnetic properties. Lattice mismatch can cause atomic strain at multilayer interfaces. The Fe layer thickness was kept at 45nm and the intermediate layers were 5nm thick; ten repeats were deposited. In plotting and interpreting their data, no account was taken of the different electronic structures or magnetic properties of the interlayers or their relative solubilities in iron. Note that the Fe layers are thick. Any strain is likely to be localised at the interfaces and most of the Fe layer would be relaxed to bulk spacings. The lowest coercive force was obtained at a mismatch of about +1% (Fe/Ni-Fe). Ni-Fe is known to be a generally soft material. H_c increases dramatically for mismatches above 3%. All the magnetostriction values are negative and lie between -4.0ppm (pure Fe film) and -0.3ppm (Fe/BN and Fe/Mn-Zn ferrite) for which the lattice mismatches are zero and not given, respectively. However, the authors comment that the magnetostriction does not appear to be correlated with the changes in soft magnetic properties. Nakatani and Kobayashi have also examined the effects of multilayering Fe with Cr-Si and Cr-Mo alloys with different amounts of Si and Mo in order to alter the amount of lattice mismatch obtained. Fe is known to mix with Cr and Si and it would be expected that there would be some interface mixing resulting from the ion beam sputtering deposition technique. This would be enhanced by the heat treatment used to relax film stress. The minimum H_c (around 200Am^{-1}) occurs for the Fe/Cr multilayer with a lattice mismatch of 0.6%, and is higher again for 1% lattice mismatch, which gave the minimum H_c in the previous series. At this point, the mean crystallite size

has almost reached the minimum of about 25nm. The crystallite size is much greater for lattice mismatches lower than about 0.4% but is fairly constant beyond that. To establish further the effects of lattice mismatch and interface strain, it might be helpful to fabricate a series of multilayers of Fe with only one type on interlayer, varying the thicknesses of each whilst remaining in a thickness region where the layer thickness itself does not determine the magnetisation direction. Thinner layers should exhibit a greater average strain, since atoms tend to relax towards bulk positions deeper into a layer. It is clear form the work of Nakatani and Kobayashi that different interlayers do affect thick Fe layers in different ways, however, and so the properties observed are not due solely to the Fe layer. It is also clear from other workers that the thickness of the interlayer does influence the characteristics of the multilayer.

The data presented above do not show any magnetostriction values approaching those aimed for in this project ($|\lambda_s|$ = 100ppm). (Many groups, however, are aiming to reduce λ_s and not to enhance it). A variety of results is seen even in the same multilayer systems, although data sets generally do not overlap and many different deposition methods, conditions and substrates have been used, which can result in different interface qualities, crystal structures and textures. Some of the multilayers are magnetically soft, however, with coercivities similar to our target value of $100Am^{-1}$. The lattice strain mechanism for enhancing λ_s might yet be pursued, as might the possibility of crystallographically texturing the magnetic layer to exploit the different values of λ_s obtainable along different crystallographic axes.

Another approach is to examine elements and alloy systems which are known to be highly magnetostrictive, but magnetically hard, and attempt to reduce the coercivity, possibly sacrificing some of the magnetostriction in the process. Below (Figure 2.15, Table 2.9) are presented published data on Co/Pd multilayers,

investigated for use in magnetic recording, since a high coercivity and strong perpendicular anisotropy can be achieved in certain circumstances. Both palladium and platinum form alloys with cobalt. Co/Pd multilayers are often polycrystalline and generally exhibit fcc (111) texturing, so the λ_{111} data from Takahashi *et al.* are more to be compared with the other data than λ_{100}.

The contributions to λ_s from the volume of the magnetic layers, λ_s^v and λ_s^{mag} according to Equations 2.2 and 2.3 respectively, range from -28ppm to -40ppm. These values are larger than λ_s of random polycrystalline Co: λ_s = -16ppm (Cullity (1972)), although single-crystal magnetostriction constants can be more negative (see comment on Co/non-magnetic multilayers, above). The more negative λ_s values for the Co/Pd multilayers than for random polycrystalline Co may also indicate a degree of alloying of the component layers at the interfaces; Co-Pd alloys can have large negative magnetostrictions (Hashimoto *et al.* (1989a)). When layer thicknesses are small, the λ_s values for the multilayers tend toward those of Co-Pd alloys of the same proportional compositions.

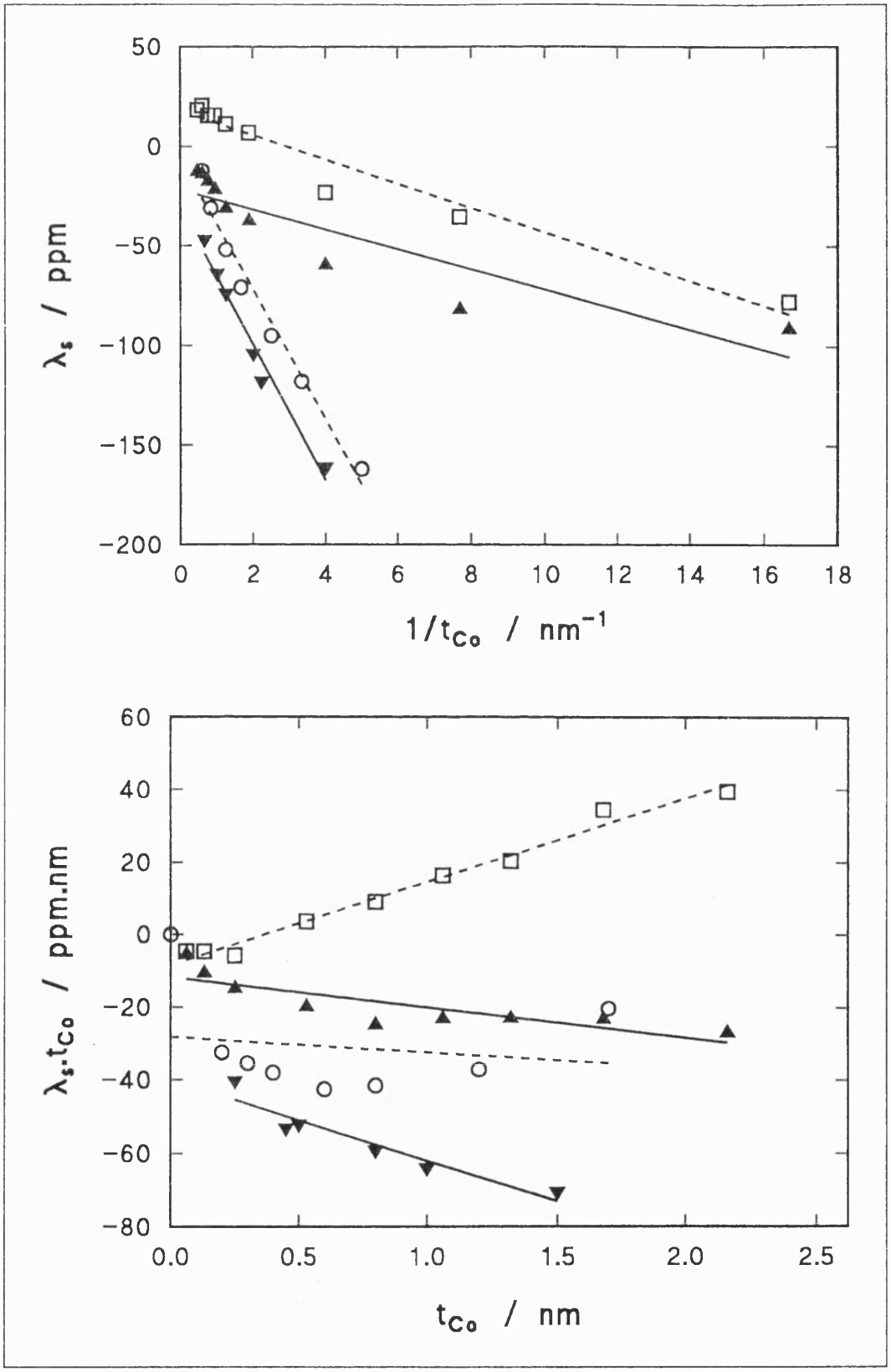

Figure 2.15 Published λ_s data on Co/Pd multilayers. Details in Table 2.9.

Table 2.9 Details of Co/Pd multilayers for which magnetostriction data are presented in Figure 2.15 above.

	Reference	Deposit	Lines	r
○	Hashimoto *et al.* (1989b)	$t_{Pd}/t_{Co}= 2$	$\lambda_s = -32.6/t_{Co} - 6.6$	0.98656
			$\lambda_s\, t_{Co} = -4.3t_{Co} - 28.2$	0.16827
□	Takahashi *et al.* (1993)	$t_{Pd}/t_{Co} \approx$ 76/24	$\lambda_{100} = -6.1/t_{Co} + 17.8$	0.97616
	(λ_{100})		$\lambda_{100}t_{Co} = 23.0t_{Co} - 8.4$	0.99119
▲	Takahashi *et al.* (1993)	$t_{Pd}/t_{Co} \approx$ 76/24	$\lambda_{111} = -5.0/t_{Co} - 21.8$	0.89849
	(λ_{111})		$\lambda_{111}t_{Co} = -8.3t_{Co} - 11.8$	0.83538
▼	Awano *et al.* (1990)	$t_{Pd} = 3.6$nm	$\lambda_s = -34.1/t_{Co} - 31.4$	0.98631
			$\lambda_s t_{Co} = -22.1t_{Co} - 39.9$	0.95242

continued...

Table 2.9 continued.

	Substrate	Deposition method	λ_s measurement	$P_{deposition}$ / torr, and gas type	$T_{substrate}$ / °C
○	Glass	d.c. magnetron sputtering	optical cantilever method in 1200kAm^{-1}	2-25×10^{-3} Ar	?
□ ▲	Glass	r.f. magnetron sputtering	estimated from anisotropy induced by uniaxial strain	1×10^{-2}	?
▼	Glass	vacuum evaporation	cantilever capacitance method in 1360kAm^{-1}	5-20×10^{-9}	?

As can be seen from the plots, saturation magnetostriction values larger than 100ppm can be achieved in this system. The coercivities are tens or hundreds of kAm^{-1}, however. Coercivities here are generally measured perpendicular to the film plane, and this is usually the easy direction; the preference for this direction becomes stronger as t_{Co} decreases (den Broeder *et al.* (1987), de Haan *et al.* (1992)). Den Broeder *et al.* report sharp interfaces between the Co and Pd layers.

It has been observed that increased sputtering pressure increases H_c in Co/Pd multilayers. De Haan *et al.* attribute this to decreased interface mixing and Hashimoto *et al.* state that domain wall pinning is an important factor. He *et al.* (1991) observe the same in Co/Pt multilayers and attribute the increased coercivity to increased grain size.

The anisotropy behaviour of the multilayers has been attributed to strain effects from the substrate and the magnetostrictive effect in strained Co layers (Hashimoto *et al.*). Awano *et al.* observed tensile stress in the Co layers of their multilayers, which was less than could be accounted for by lattice mismatch between Co and Pd.

Takahashi *et al.* and Hashimoto *et al.* have also studied magnetostriction in Pt/Co multilayers. The values are generally lower than for Pd/Co systems. Positive values are found, whereas λ_s of Co is negative. Co-Pt alloys have positive magnetostriction values over a wide range of compositions, however, so they propose that mixing of the multilayer components at the interfaces dominates the magnetostriction of the total films. Den Broeder *et al.* have looked at Fe/Pd multilayers, which have much larger coercivities perpendicular to the plane than their Co/Pd multilayers. They say that the easy direction seems to be more in-plane, but do not give H_c for that configuration.

The largest magnetostriction values are obtained in Co-Pd alloy films rather than multilayers. Hashimoto *et al.* (1989a) have investigated a wide range of compositions of r.f. magnetron sputtered Co-Pd alloy films, typically 200nm thick. The maximum λ_s is achieved at about 72at% Pd in Co, where $\lambda_s \approx -170$ppm. Perhaps this is caused by the increased localisation of the moment on the Co atoms by their dilution by Pd atoms. The perpendicular coercivity of this film is about 65kAm^{-1}. The multilayers were deposited at 25mtorr Ar pressure; a lower pressure might be expected to reduce H_c (see above).

Summary. The aim of this project is to produce multilayers which are simultaneously highly magnetostrictive and magnetically soft. From the literature reviewed above, soft magnetic properties are generally found in multilayers with relatively more Fe and less Co or Ni. Values of only a few tens of Am^{-1} have been

reported. The frequent observation has been that a smaller grain size leads to a lower coercivity in a thin film or multilayer, although the opposite has also been reported. So, iron-containing multilayers where the grain growth has been interrupted by the insertion of interlayers might be expected to be magnetically soft.

Film stress generally raises coercivity. Stress can be reduced by post-deposition heat-treatment or deposition at elevated temperatures. Heat treatments will also affect the structure at the interfaces, promoting mixing between mutually soluble components or separation of immiscible materials. This may affect the softness and the magnetostriction of the multilayer. Grains in the multilayer are also likely to grow, which may counteract the reduction in H_c due to stress relief. There would be some optimum heat treatment condition.

Plain iron layers in a multilayer give low magnetostriction. For an isotropic polycrystal of Fe, λ_s = -7ppm. Larger values may be obtained if the iron layers are crystallographically textured, since λ_s = +21ppm and λ_s = -21ppm (Cullity (1972)). Magnetostriction constants of a material are generally different along different crystallographic directions, so texture may be employed in a multilayer to give a higher λ_s. Some alloys are highly magnetostrictive - more so than the constituent elements. Thus it is expected that multilayers containing such layers would have larger values of magnetostriction than multilayers made with elemental layers. To improve softness if such films were magnetically hard, interlayers which interrupted grain growth might be used, or interlayers which were themselves magnetically soft but not necessarily so magnetostrictive.

These observations arise in addition to the lattice strain mechanism mentioned before for the enhancement of λ_s (e.g. p.14 - strain of the magnetic atoms at multilayer interfaces could enhance moment localisation). Use of a multilayered structure of appropriate components can give control over λ_s and H_c.

3. Experimental Methods

The fabrication of multilayer samples and the methods of magnetic and structural characterisation are described. Choice of materials and conditions is explained, as is the calibration of the growth system.

3.1. Sputter Deposition

Sputtering was chosen as the deposition method because deposition rates can be high, giving a high sample production rate, an important consideration in industry. Sputtering can produce polycrystalline films which may incorporate lattice strain and/or mixing at the interfaces and may have crystallographic texture. R.f. sputtering allows both conductors and non-conductors to be sputtered onto a wide range of substrates.

3.1.1. Sputtering Machine

The machine used was a Nordiko NM2000 radio-frequency magnetron sputterer, shown schematically in Figure 3.1. Its configuration was "sputter-up", i.e. the substrate was positioned directly above the target. Three 15cm-diameter targets were mounted on a turntable inside the sputtering chamber; the required target was then positioned beneath a hole in the fixed shield, directly below the substrate. Two moveable shutters were between the target and the substrate, to prevent any deposition during sputter cleaning or while the plasma was being struck. The removable copper platen on which the substrates are mounted was about 18cm diameter; there were facilities for heating or water-cooling it. The heating facility was not exploited in this present study, but is being used in on-going investigations in the research group into multilayer materials.

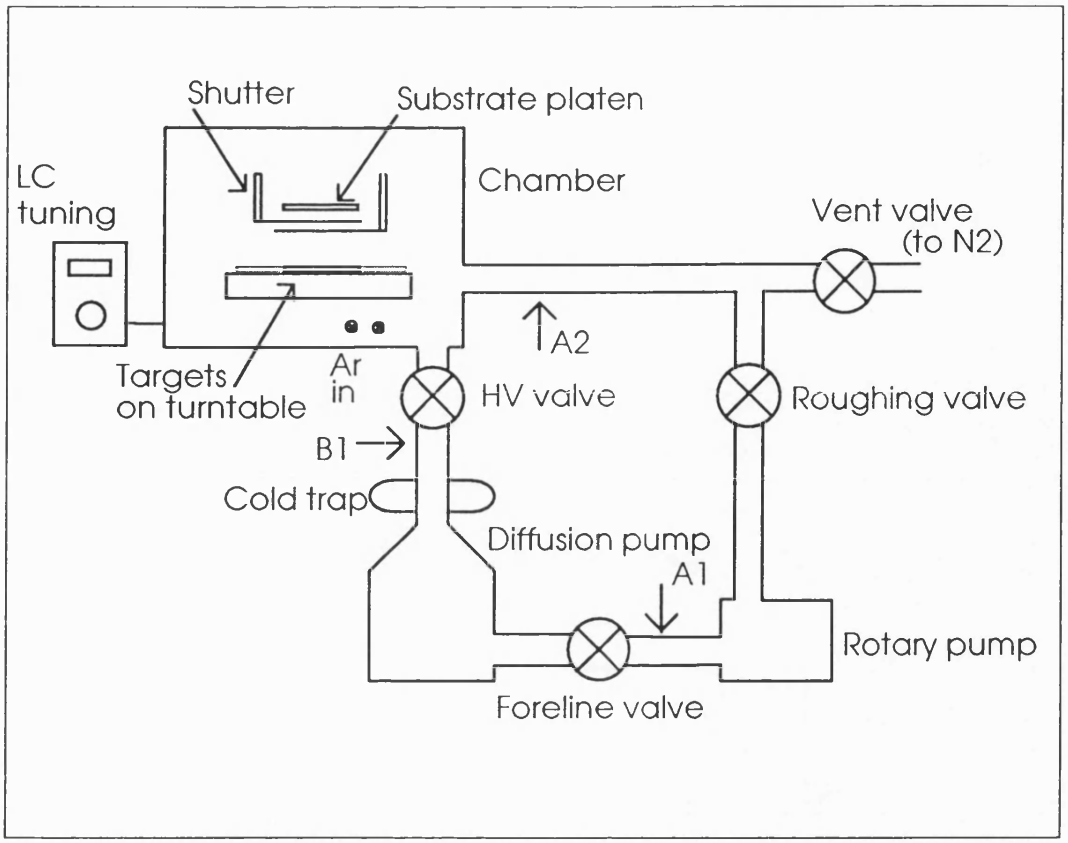

Figure 3.1 Schematic diagram of sputtering system. The arrows indicate the positions of the pressure gauges. A1 and A2 are Pirani gauges; B1 is a Penning gauge.

The r.f. power supply (maximum output 555W) operated at 13.56MHz, the frequency assigned for industrial, scientific and medical use. The magnetrons had been tuned by the manufacturer to give least reflected r.f. power when magnetic targets were in place. During deposition of pure iron, it was possible to reduce the reflected power to zero. The reflected r.f. power (displayed on the control panel) was reduced to a minimum during sputtering by a manually adjustable LC tuning circuit, which matched the impedances between the r.f. generator and the plasma discharge. Different targets had different optimum tuning positions.

The vacuum system consisted of a Balzers DIF 200 oil diffusion pump backed by a Balzers DUO 030 A mechanical rotary pump. Quality silicone oils were used in the pumps. A liquid nitrogen cold trap fixed between the diffusion pump and the sputtering chamber trapped any backstreaming oil, water vapour and other contaminants. Contaminants in the chamber increased the pumping time required to achieve a given vacuum level (or degraded the vacuum attainable) and degraded the quality of the film which could be deposited.

The sputtering chamber was 55cm diameter and 40cm deep. Two needle valves controlled the gases admitted during sputtering. Both were supplied by zero-grade argon. The foreline and roughing valves were pneumatically activated, and there was a high vacuum angle valve between the diffusion pump and the sputtering chamber. This valve controlled the effective pumping speed, and was adjusted during sputtering to maintain the required pressure.

The shutters, Ar valves, r.f. power switch, LC tuning and target turntable were all operated by hand.

3.1.2. Sputtering Parameters

Parameters were chosen initially to be in line with those of other researchers. The sputtering gas was zero-grade argon. Argon is unreactive and more readily available than other noble gases, and is widely used by other workers. Argon was introduced to the sputtering chamber at 5mtorr, a pressure typically found in the literature and within the range recommended by Nordiko. The target-substrate distance was set at 6cm to achieve uniformity across the deposited film of 5% or better over the central 5cm. This separation was the closest reasonably achievable with both moveable shutters present. Multilayers were grown at room temperature or with the substrate platen water-cooled.

Most multilayers were deposited at 75W or 100W, since these powers gave reasonable deposition times for the thicknesses of layers required (necessary since the machine is operated largely by hand, and repeatability of layer thickness is required). It was also thought that lower powers would cause less disruption at multilayer interfaces, since the sputtered atoms would impinge on the substrate with less energy, causing less re-sputtering and interface mixing, and would result in films with fewer pinholes.

Table 3.1 lists details of the targets used in the sputtering machine. Materials with low impurity levels were chosen so that multilayers with good compositional purity could be grown. Interpretation of observed characteristics can then discount the presence of impurities. The first magnetic targets used were the pure magnetic elements (Fe, Co and Ni). Magnetic alloy targets were then chosen where the magnetostriction of the polycrystalline alloy was known to be significantly higher than those of the elements, to give multilayers with higher λ_s than that attainable with elemental layers. The Fe-Co alloy targets were single sheets supplied by Telcon Ltd. HiSat50 has a composition which has one of the highest λ_s values of any polycrystalline Fe-Co alloy. The Co-Pd target was a mosaic of 99.9% pure Co sectors on a 99.95% Pd disc. The amount of Co required was calculated to give an alloy composition at the substrate of approximately 30%Co, 70%Pd, as this is the composition with the largest λ_s reported by Hashimoto *et al.*, (1989). Electron probe microanalysis of sputtered Co-Pd films showed the composition to be 32wt%Co, 68wt%Pd, which has $\lambda_s \approx -160$ppm. For non-magnetic interlayers, noble metals Ag and Cu were chosen. These are insoluble in Fe, Co or Ni, do not react with them and are larger atoms than the magnetic species; lattice strain of the transition elements might result at the interfaces and enhance λ_s. It was generally found, however, that it was the noble metal that strained rather than the magnetic species. This was attributed to the relatively low Young's moduli (E_{Ag}=76GPa,

E_{Cu}=118GPa; cf. E_{Fe} = 212GPa, E_{Co} = 207GPa and E_{Ni} = 202GPa (Tottle, 1984)). The effect of molybdenum interlayers was then examined (E_{Mo}=335GPa).

Table 3.1 Sputtering targets.

Target	Composition	Bulk crystal structure	Thickness / mm
Fe	99.9%	bcc	1
Co	99.9%	hcp	0.44
Ni	99.98%	fcc	1
HiSat50®	50wt%Fe, 50wt%Co, <0.2wt%Ta	bcc	≈0.3
Permendur24®	24wt%Co, 0.6wt%Cr, balance Fe (75.4wt%)	bcc	≈0.3
Co-Pd	99.9% Co sectors on 99.95% Pd disc	?	Co: 0.5mm, Pd: 0.125mm
Ag	99.99% Ag	fcc	1
Cu	99.99% Cu	fcc	1
Mo	99.9% Mo	bcc	0.127

The quality of the edges of the target was not critical, provided it fitted in the earthed clamping ring on the target turntable. Consequently, since commercial dedicated sputtering targets are so expensive, workshop-cut discs were purchased, or discs were cut in-house from rectangular sheets.

For making films for target calibration, glass microscope slides 1-1.2mm thick were used as the substrates. Other studies on glass used Corning 7059 (50mm× 75mm×0.5mm) which contains a low level of impurities (<0.2% alkali content). For studies of magnetostriction, however, a flexible substrate was required; Kapton® polyimide film (Du Pont Ltd.) was chosen, with a nominal thickness of 25 μm and width ≈28mm. It has a low Young's modulus compared to metals (3.5GPa cf. typically 100-200GPa) and so did not prevent measurements of magnetostriction in films deposited on it. All the substrates were amorphous in order that no crystallographic order be imposed on the deposited films.

In the early stages, multilayers of 25 bilayers were deposited as routine. It was found, however, that the magnetic signals from samples so thin were often small, and X-ray diffraction scans were poor because very little material was available to scatter the X-rays. Some films on Kapton also tended to curl up on removal from the sputterer. Multilayers were then grown with 50 bilayers (typically) on either side of a Kapton substrate, to equalise any film stresses.

3.1.3. Preparation of a Multilayer Film

Substrates, targets, the platen and anything else which is put inside the sputtering chamber were always handled with cleanroom plastic gloves to prevent grease and dirt entering the chamber. When working inside the chamber (e.g. to change a target) a cap and laboratory coat were also worn. Such cleanliness was necessary in order that a good vacuum could be achieved and that deposited films adhered well to the substrates.

Substrates were fixed to the substrate platen by means of small clamps holding a square frame (Figure 3.2). The screws had flattened sides so that air could not be trapped here and only slowly outgas during evacuation. Glass substrates were clamped directly. Kapton polyimide substrates were held around a glass

microscope slide before clamping. It was found that this arrangement made it easier to manipulate the substrates while clamping, reducing mechanical stresses imposed on the substrates, making for less-stressed multilayer films. It was not necessary to clamp the substrates tightly; just sufficiently to prevent the substrates falling during sputtering (provided thermal contact was not a critical consideration).

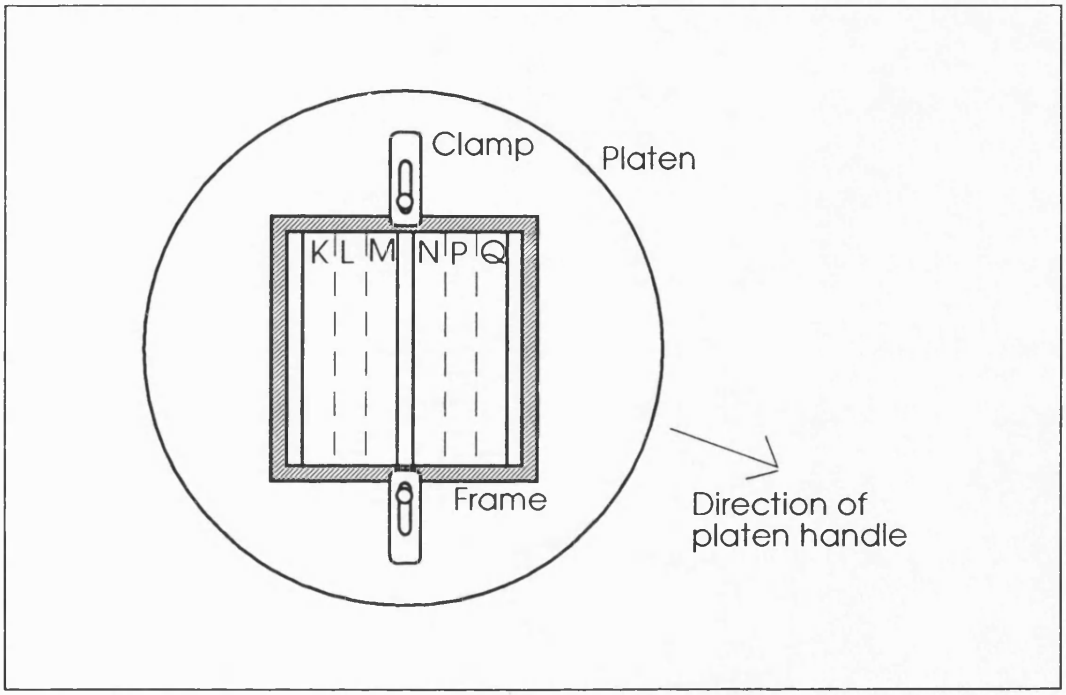

Figure 3.2 Substrates clamped to the platen. The dashed lines show where the Kapton samples were cut into strips after deposition, and the letters are the standard labels assigned to sections in those positions.

Glass substrates were cleaned with acetone and propan-2-ol (both AnalaR grade) prior to loading in the chamber. They were dried with a dust-off can or dry N_2 boil-off. Some were also baked at 80°C to ensure that all the cleaning agents had been thoroughly evaporated off. Treating the Kapton substrates in this way

often attracted dust to them, so these were usually just blown with a dust-off can or N_2. The substrate surfaces were kept grease-free, but otherwise, no detailed attention was paid to substrate surface preparation. Some authors (e.g. Celinski and Heinrich (1991); Egelhoff and Kief (1992); Mattox (1975)) maintain that meticulous surface preparation is essential for the growth of films with high structural quality. Stringent cleaning procedures are usually adopted when Molecular Beam Epitaxy and other ultra-high vacuum systems are used to produce epitaxial films and multilayers. Epitaxy was not a requirement in this project.

With the chamber at atmospheric pressure, targets and substrates could be positioned. Once the substrate platen was loaded in the chamber, the chamber was "roughed out" using the mechanical rotary backing pump until a pressure reading in the chamber of about 10^{-1} torr was reached. Roughing was then stopped. Provided the liquid nitrogen cold trap on the diffusion pump was full, the high vacuum (HV) valve to the chamber was opened by degrees, starting from 5% opening. During this time, the foreline pressure was monitored to ensure that it did not rise above about 30mtorr, to minimise backstreaming contaminants to the chamber. Once the HV valve was fully open, the system was left to pump down for about an hour, or until the pressure in the chamber (as measured by a Penning gauge) was less than 1μtorr. At this point, the targets were sputter cleaned for several minutes at 100W and 5mtorr Ar, raising the surface temperature to about 50°C, to remove any surface contamination and to aid outgassing. The shutter was in place to prevent any deposition onto the substrates. If the substrates were glass, these were also sputter cleaned, but this was not usually done for Kapton substrates. The system was then left to pump down again before deposition. The nitrogen trap was kept topped up throughout the processes of pump-down and deposition.

With the appropriate target positioned underneath the substrate and the shutter closed, argon gas was admitted. The needle valve having been set suitably, the HV angle valve was adjusted to give an Ar pressure of 5mtorr (usually around 30% open, depending on the needle valve setting. The Pirani gauge read 3.1mtorr, since it was calibrated for air). The r.f. power was then switched on. To ignite the plasma, it was necessary to raise the Ar pressure momentarily via the second needle valve. The amount required varied with the target being used: Ag required very little extra Ar, while the Fe-Co alloys often required a pressure up to 2×10^{-1}torr (uncorrected gauge reading) before the plasma ignited. Once the Ar pressure had dropped again, the shutter was moved smartly across and a timer simultaneously started. Deposition proceeded for the time required for the desired layer thickness, as found from calibration of the deposition rates. During deposition (if there was enough time) an LC circuit was tuned so that there was minimum reflected r.f. power. Deposition times for Ag were usually too short, so the tuning was left at the position required for the other target used. For example, for iron-cobalt alloys multilayered with silver, this meant the power reflected from the Ag target was 13-14W (for a 75W deposition) rather than the optimum achievable of 10-12W. The deposition rate was not noticeably affected. After the allotted time, the r.f. power was turned off at the same time as the shutter was moved smartly back between the target and the substrate (in case the r.f. power button was not hit cleanly, and the plasma did not go out.) The next required target was then moved into place, and the process repeated, until the desired multilayer had been produced. At the end of the sequence, the Ar was closed off, the HV valve shut and the chamber vented to white-spot nitrogen (dry, oxygen free, 99.998% pure). The nitrogen pressure was kept at $\approx$1bar higher than atmospheric, so that air and water vapour could not enter the chamber and contaminate it. Water vapour is especially difficult to remove. At atmospheric pressure, the door was opened and the substrate changed.

In making double-sided films, care was taken to turn the substrates over such that the edge which had been closest to the platen centre remained closest to the centre so that the films on the two sides should have equal thicknesses as far as possible. When fabrication was complete, the samples were sectioned with a sharp scalpel according to the scheme shown in Figure 3.2. As far as possible, the same section (L) was used for measurements.

If the pressure gauges were thought to be reading incorrectly, they were cleaned, according to the manufacturers recommendations. Occasional checks were also made on their calibration. The oils in the diffusion pump and rotary pump were also changed periodically. When the chamber had become very coated with deposits, it was wiped out with AnalaR acetone and propan-2-ol. Smaller components which could be removed were sand-blasted before chemical cleaning. Windows frequently became opaque with deposited metal, which was removed *ex situ* with concentrated acid.

3.2. Film Thickness Calibration

To establish the deposition rates of the various target metals, plain films were deposited on glass slides with narrow (≈1mm) Kapton strip masks stretched across them. Tight clamping was necessary to keep the strip close to the slide during deposition, so that the edges of the masked area were sharp. Since the Kapton was so thin, there were no shadowing effects.

At the r.f. power and pressure required, films were deposited for known lengths of time of between several minutes and a couple of hours. The film thickness was then measured with a Talystep® (Rank Taylor Hobson) profilometer with a nominal precision of 0.5nm. The error on an individual measurement was usually about 1-2% of the total film thickness, however, due to vibrations on the

trace and the need to extrapolate lines in the trace where the step edge was not vertical.

By eye, the sample table was checked to be level. With the vertical measurement magnification at 5×10^3, the stylus force was adjusted to be 40μN with the stylus positioned on a metal region of the sample. The sample was levelled as the stylus was drawn across the groove in one direction only. The procedure was carried out at increasingly sensitive vertical resolutions, taking care not to damage the stylus by dragging it across the sample if the stylus force might be too great (due to having raised the sample table towards it, for example).

The thickness was measured at 7 points along the film at 1cm intervals, with the fourth point being at the centre of the deposit. In calculating the average film thickness, the middle 5 points were taken, as the thickness decreases sharply at the two ends (Figure 3.3).

Thickness was plotted against deposition time (Figure 3.4). The regression line gave the deposition rate. Negative intercepts were found, attributed to deposition of Kapton in the channel when the substrate was sputter-cleaned. Calibration checks on multilayers with small numbers of repeats are consistent with other calibration checks on thicker samples (Shearwood (1994)).

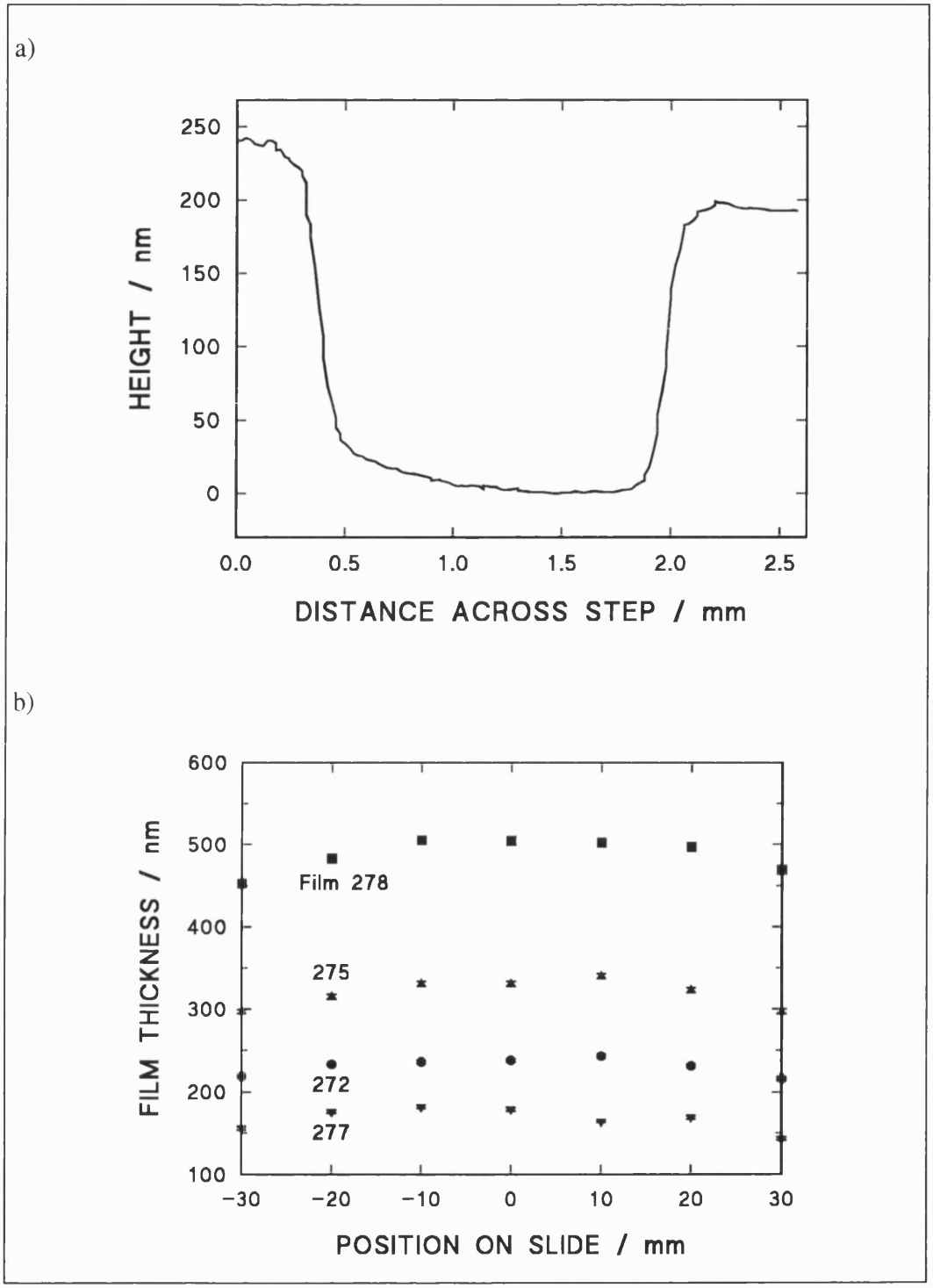

Figure 3.3 a) A typical Talystep trace (of Fe deposited at 200W for 30min). The curve and slant are due to imperfect levelling of the sample surface; b) deposition profile along a Fe-Co alloy film grown at 100W, P_{Ar} = 5mtorr. 278: 60min.; 275: 40min.; 272: 30min.; 277: 20min.

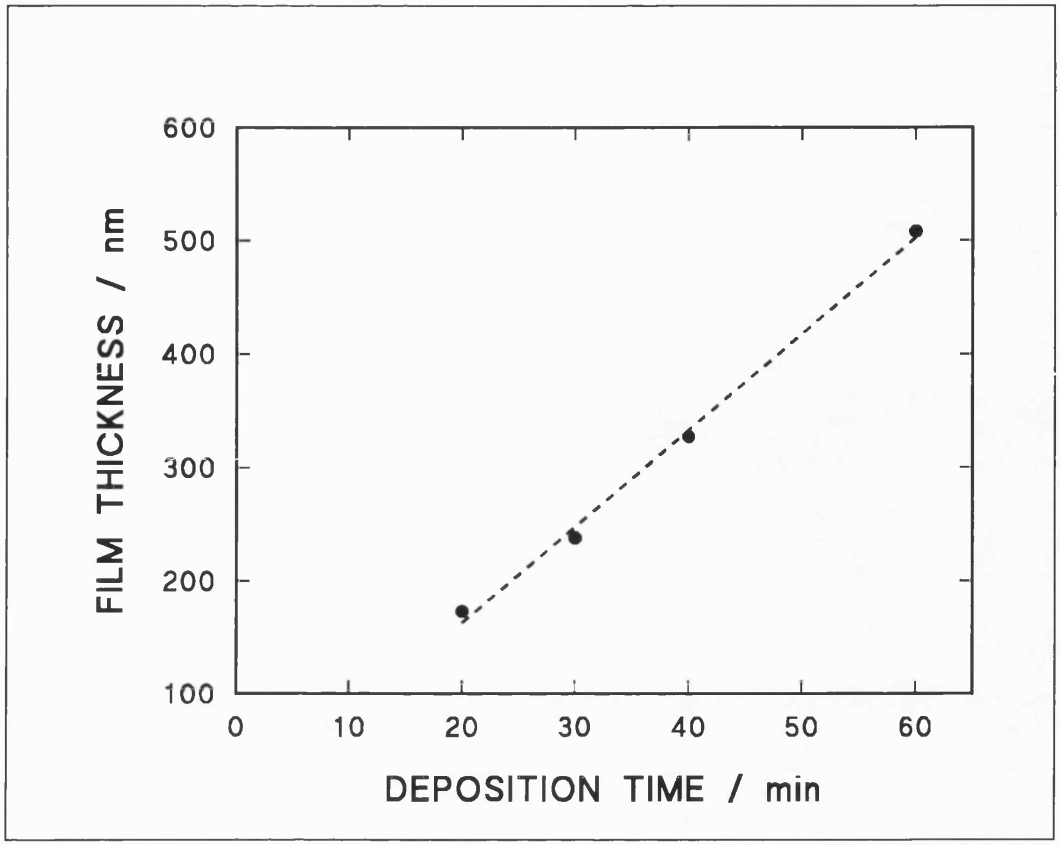

Figure 3.4 Plot for deposition rate of HiSat50 sputtered at 100W, 5mtorr Ar.

3.3. Magnetisation and Hysteresis Measurements

Magnetic hysteresis (MH) loops in the plane of the multilayer were routinely measured using a quasi-d.c. inductive magnetometer. This is suitable for thin-film geometry and especially for soft magnetic materials. Being quasi-d.c., a.c. effects on MH behaviour are avoided. Some films were also measured using the Faraday balance at the Departamento de Electricidad y Electrónica, Universidad del País Vasco, Bilbao, Spain; notably multilayers containing Co-Pd alloy, which were too magnetically hard to be usefully measured in the d.c. magnetometer. All measurements were taken with the applied field parallel to the film plane.

3.3.1. Inductive Magnetometer

The quasi-d.c. inductive magnetometer was made in-house after the original design described by Squire *et al.* (1988). It is shown schematically in Figure 3.5.

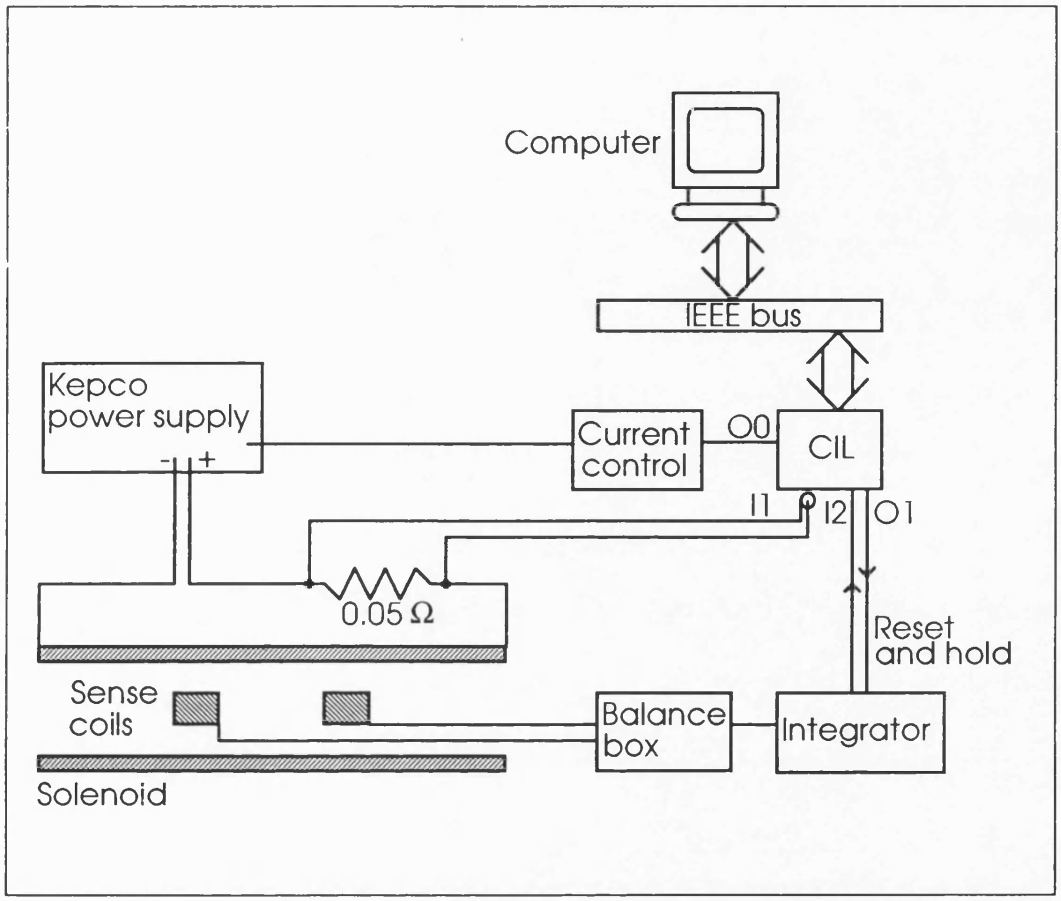

Figure 3.5 Schematic diagram of the d.c. inductive magnetometer. The CIL is an A-to-D, D-to-A converter. O0 and O1 are CIL outputs, I1 and I2 are inputs.

The applied field was supplied by a 1.3m long solenoid driven by a Kepco 2035C Bipolar Operational Power Supply/Amplifier (±20V, ±20A). The field was axial; $H_{max} \approx 28 kAm^{-1}$ (at present - this has been increased during the course of this work, so earlier measurements were taken at lower maximum fields). Two matched sense-coils (20 000 turns on formers 25mm×14mm×4mm) were mounted on a support such that they were positioned co-axially on the solenoid axis,

symmetrically about its mid-point. With a sample present in one coil, a change in its magnetisation induced a voltage in the coil, according to Faraday's Law,

$$V = -nA\frac{dB}{dt} = -n\left(A_m\frac{dB_m}{dt} + A_c\frac{dB_{air}}{dt}\right) \qquad 3.1$$

where n is the number of turns cut by the magnetic flux, A_m is the sample cross-sectional area, A_c the coil area, B_m the sample magnetic induction and B_{air} the magnetic induction of air. For a material with high permeability, $B_{air} << B_m$ and the expression reduces to:

$$V = -nA_m\frac{dB_m}{dt} \qquad 3.2$$

Since samples were generally strips a few millimetres wide and approximately 7cm long, all the sense coil turns were cut. The signal from the empty sense-coil was added in series opposition to that from the sample sense-coil. This acted to cancel common-mode signals, due to the changing magnetic field and to interference. The balance condition between the two coils (with no sample present) was set by means of a potentiometer prior to taking measurements.

The applied field, H, was stepped from the maximum negative level set, to the maximum positive level and back at a rate of the order of 0.01Hz (hence quasi-d.c.). The combined sense-coil signals were measured using the A-to-D, D-to-A converter (Computer Instruments Ltd - CIL) and integrated to give a signal proportional to the total magnetisation of the sample at that point. This signal was relayed to the computer via the IEEE 488.2 bus. The computer also controlled the system. Several loops were measured. Each loop was corrected for integrator drift and then the average was taken. This reduced the effect of random noise on the resulting loop.

The form of the time-dependence of the applied field was a truncated tangent:

$$H = \frac{\tan(2b\pi\frac{t}{T})}{\tan(2b\frac{\pi}{2})} \qquad 3.3$$

The shape factor, b ($0<b<1$), determines the sharpness of the function. This enabled data points to be crowded around H = 0 (high b) which was useful in studying low coercivity materials. A linear ramp function was achieved by putting b = 0.1. The points were spread at equal intervals in time, enabling a linear drift correction to be made. Other parameters set by the operator in the control program were the number of points per loop, the time taken for one loop (although the lower limit on this is determined by the number of points chosen), the number of loops to be measured for averaging, and the amplification range for the CIL (R=0.1, 1 or 10, depending on the size of the signal obtained). A y scaling factor was also set; this determined only the size of the real-time plot to the screen. The maximum field was set using a potentiometer.

There was always some small background signal due to the matching condition between the coils changing as they heated up. This background changed with time and was only significant when high fields were used, when the solenoid heated resistively. It was not practical to set the balance condition for the sense-coils for each single measurement, however. Having set it at the start of a series of measurements, loops of the background signal were measured at frequent intervals throughout the series. A program was written to subtract background loops from sample measurements. The same system parameters as those for the sample loops were required for the background loops, i.e. same field shape factor, number of points on loop, signal amplification factor (R), loop time and field range. An example of the effect of background correction is given in Figure 3.6.

The d.c. magnetometer control program included procedures for analysing and plotting the data. After correction, loops were read into the program, which returned the coercive field and other parameters. Magnetisation was returned in arbitrary units. For comparison between samples, it was necessary to multiply this value by R and divide by the nominal sample magnetic volume.

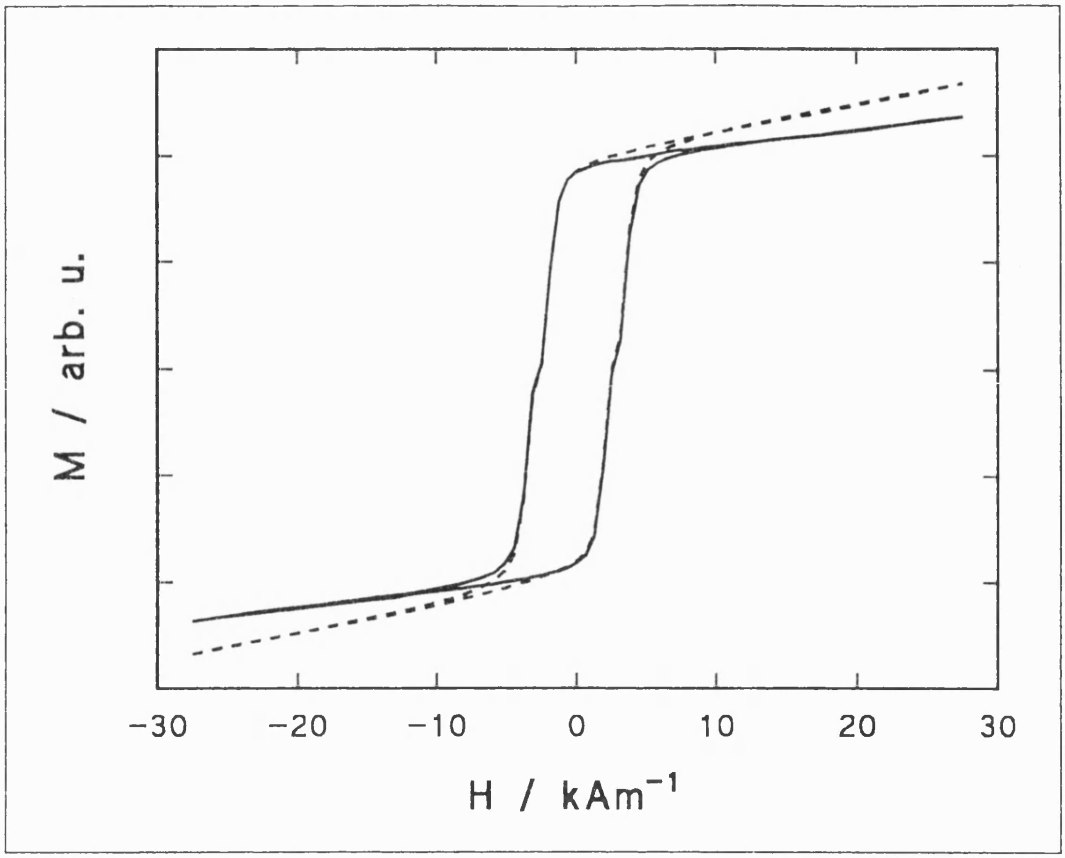

Figure 3.6 Corrected (solid line) and uncorrected (dashed line) MH loops for the multilayer 2×50(10nm Permendur24/7nm Ag).

To investigate how the MH characteristics varied along the length of a sample, a specimen of the multilayer 2×50(10nm Permendur24/3nm Ag) on Kapton was cut into pieces each about 1cm×1cm, according to the diagram below (Figure 3.7). The hysteresis loop of each section was measured both parallel and perpendicular to the long axis of the original film. The results are shown in Figure 3.8. (Detailed results on Permendur24/Ag multilayers are presented in Section 5.2.2).

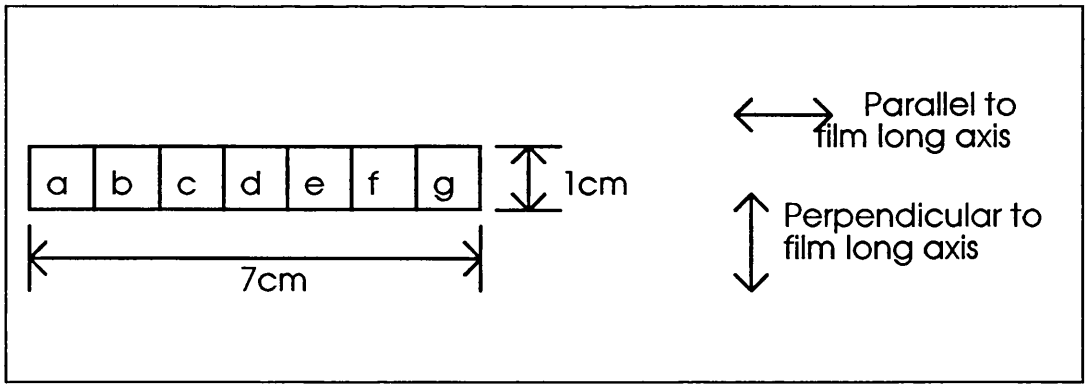

Figure 3.7 The sections cut for determination of MH characteristics along the length of the sample.

Thereis hardly any difference in anisotropy between parallel and perpendicular directions, and along the length of the film (Figure 3.8). The loops shown in other parts of this work represent the average loop in the parallel configuration.

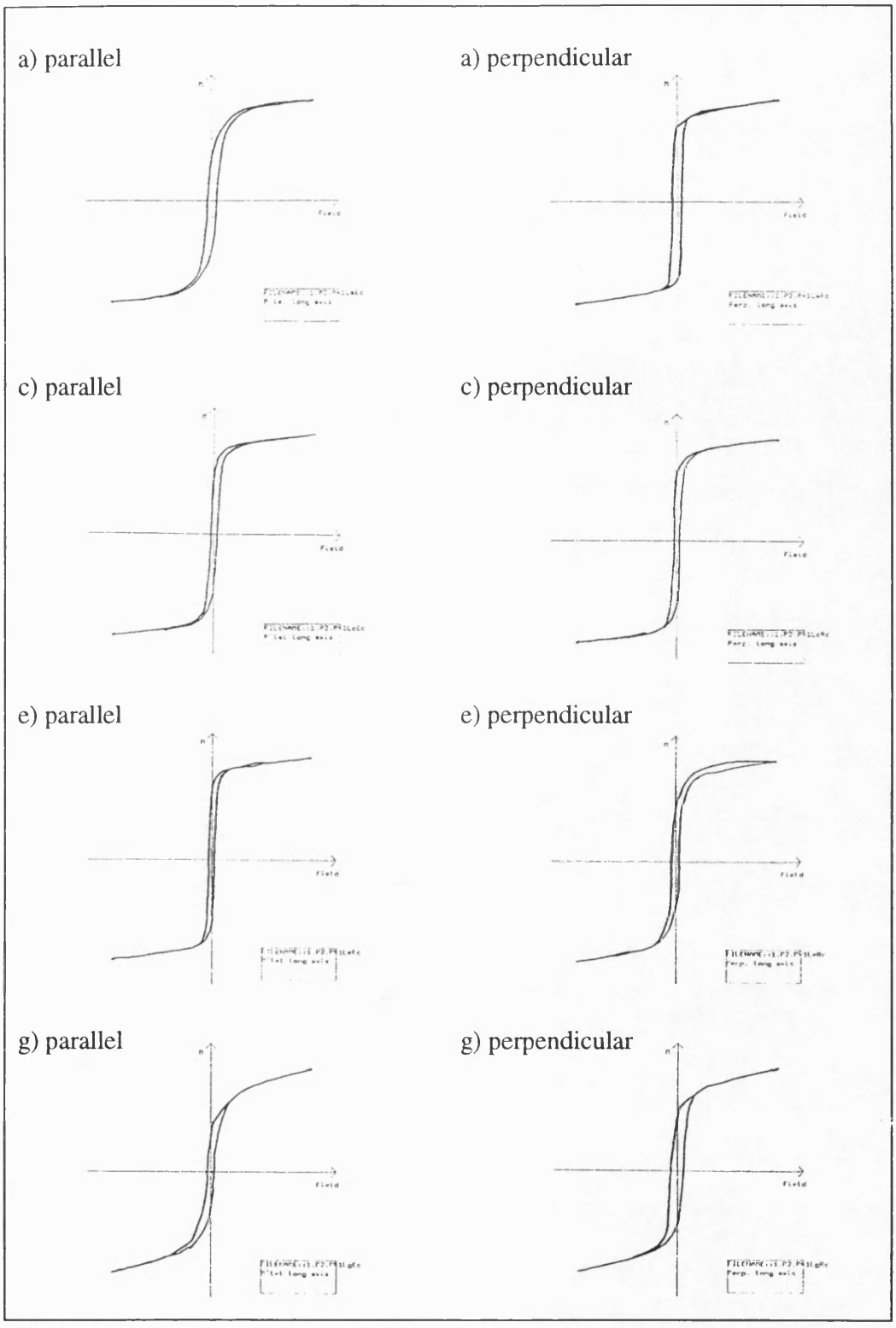

Figure 3.8 Hysteresis loops of sections along the film length for the multilayer 2×50(10nm Permendur24/3nm Ag) on Kapton. Section letters correspond with those in Figure 5.7. H_{max} = 27kAm^{-1}. Shape factor b = 0.9.

3.3.2. Faraday Balance

The Faraday balance was a DSM-8 magneto-susceptometer made by MANICS, Belgium (Figure 3.9). It was fully computer-controlled. It had a maximum field of 1.6T and facilities for cooling a sample to liquid helium temperatures, or heating to about 1000°C. The balance was calibrated with a standard iron sample.

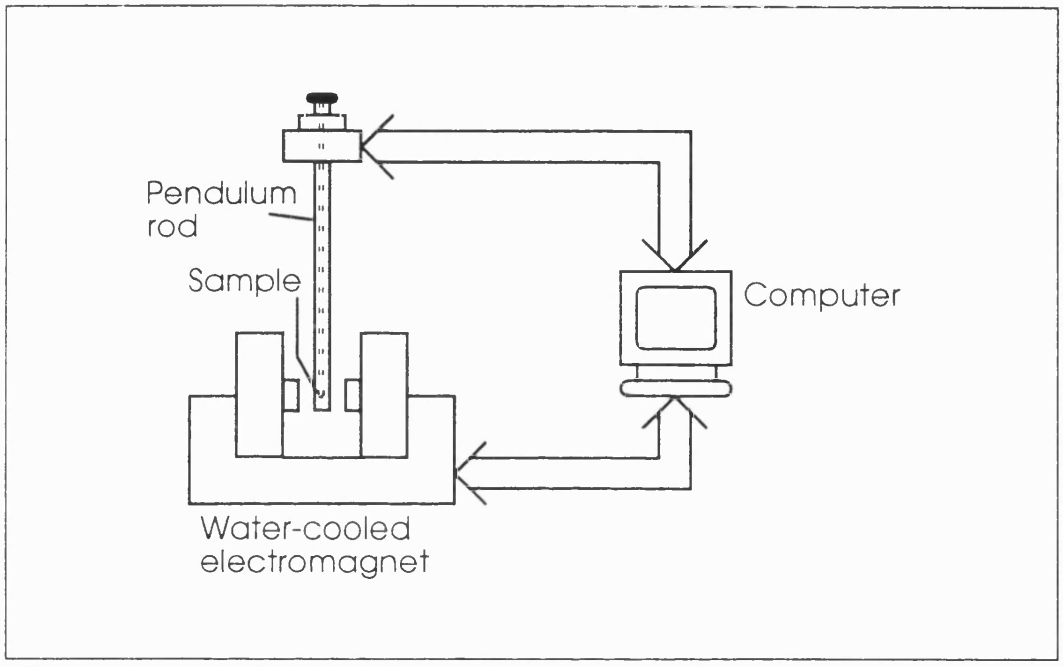

Figure 3.9 Schematic diagram of the Faraday balance (after manufacturer's manual). Heating and refrigeration facilities not shown. The field gradient is perpendicular to the page.

The sample was attached to the end of a rigid rod pendulum and subjected to an inhomogeneous field in the x direction, consisting of a steady field plus a field gradient, provided by a water-cooled electromagnet. A magnetic sample in this field experienced a force pushing it away from the central position. A servo-controlled device exerted a compensation force, F_c, to restore the pendulum to its

original position, detected by optical cells. This force was related to the magnetisation of the sample, and the field and field gradient it experienced.

$$F_c \propto \frac{d(MH)}{dx}$$
$$\propto \frac{M}{H}\left(H\frac{dH_x}{dx}\right) \qquad 3.4$$
$$\propto \chi\left(H\frac{dH_x}{dx}\right)$$

where M is the magnetisation of the sample and χ is the mass susceptibility. According to the manufacturer's literature, the Faraday balance is capable of a sensitivity of $2\times10^{-12}Am^2$.

Hysteresis loops in the plane of the samples were taken at room temperature. The sample holder was a closed tube approximately 4mm diameter and 10mm long. The sample was to sit in the bottom few millimetres while the tube was fitted to the pendulum rod for insertion into the balance. A typical desired mass of sample to give a reasonable signal was about 1mg. To approach this mass, it was necessary to stack many small squares cut from a sample on top of one another. A strip ≈ 2.5-3mm was cut from the length of a film; this was then cut into squares which were placed horizontally in the holder, padded with cotton wool. After the rod was inserted into the balance, its position was adjusted so that the sample was at the zero position. The required field steps were programmed into the computer. It was possible to split the cycle into sections, taking more frequent steps in some regions than in others. Complete loops were measured stepping from positive H_{max} to negative H_{max} and back again. For measurements of M_s only, half-loops were measured. At the end of the cycle, the raw data and background-corrected loops were displayed. Values of H_c and M_s were returned. For soft samples, H_c should be viewed with some scepticism, since around H = 0 readings are less accurate. This is because both the steady field and the field gradient go to zero as $H\rightarrow0$.

Besides measuring hysteresis loops, the Faraday balance could also measure susceptibility, χ, while the sample temperature was varied.

3.4. Magnetostriction Measurements

The Small Angle Magnetisation Rotation (SAMR) technique was used routinely to measure saturation magnetostriction, λ_s. The method was appropriate to soft samples with thin-film geometry. No special sample preparation was required; a correction was made for the presence of the substrate. The alternative technique of Strain Modulated Ferromagnetic Resonance (SMFMR) confirmed some of the SAMR results, and was used to find λ_s of Co-Pd/Ag multilayers which could not be saturated in the field available in the SAMR apparatus.

3.4.1. Small Angle Magnetisation Rotation

Apparatus was constructed after the design of Narita *et al.* (1980) and is shown schematically in Figure 3.10. A sense-coil arrangement similar to that used in the d.c. inductive magnetometer was placed inside the water-cooled solenoid, which provided a d.c. bias field, H_{dc}, of up to 18kAm^{-1} along its axis to saturate the sample in-plane. The output of the Farnell H-60/25 power supply (25A maximum) to the solenoid was controlled by a resistance box. The sense-coils sat within the uniform-field region of the rectangular Helmholtz coils, which applied a sinusoidal a.c. field, H_{ac}, of a few hundred Am^{-1} perpendicular to the d.c. field, but still in the plane of the sample. The Helmholtz coils were driven by a Thurlby Thandar TG1304 Programmable Function Generator at several hundred hertz via an Amcron M-600 Laboratory Power Amplifier, a.c. coupled. The frequency was chosen to give $2f$ non-coincident with harmonics of the mains frequency, and such that the current to the Helmholtz coils was not significantly reduced by the

increased load impedance; also that the sense-coil signal should be readily detectable (preferably several μV or above).

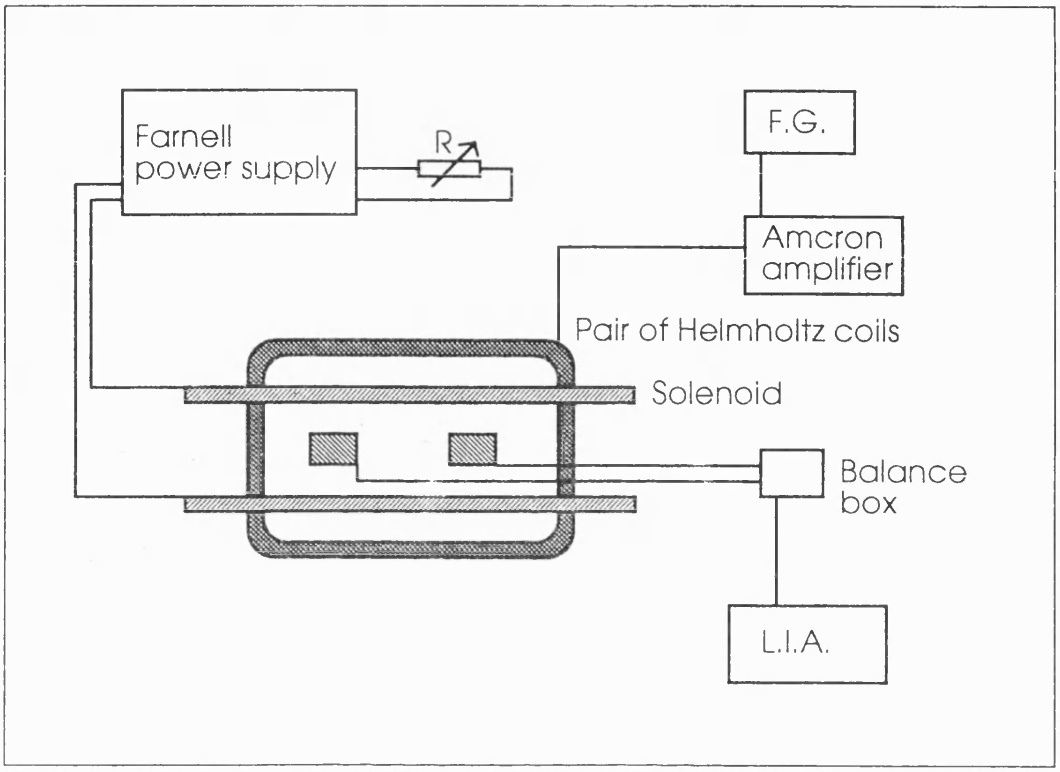

Figure 3.10 Schematic diagram of Small Angle Magnetisation Rotation apparatus. F.G. = function generator, L.I.A. = lock-in amplifier.

The sample was held in place by one fixed clamp and one clamp free to move, attached via a pulley to the load; thus stress could be applied to the sample. Under the effect of the a.c. field, the magnetic moments in the sample oscillated about their saturation direction (see Figure 3.11) inducing a voltage in the sense-coil at twice the drive frequency. (A signal at the fundamental was also induced in the search coils by the field directly, and this was never completely cancelled by adding in series opposition the signal from the empty coil.)

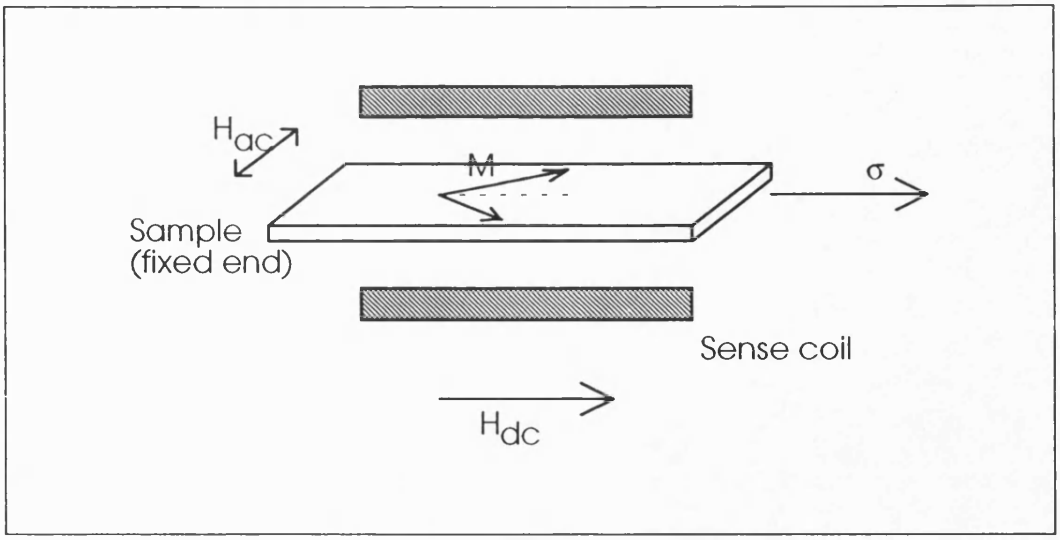

Figure 3.11 Effect of a.c. perpendicular field on sample magnetic moments.

The signal at $2f$ was detected by a Stanford Research Systems SR830 DSP Lock-In Amplifier (LIA). The amplitude of the signal, ε_{2f}, is proportional to the square of the maximum magnetisation rotation angle, θ_{max}, for small angles. (For a full analysis, see Narita *et al.* (1980)).

$$\begin{aligned} \varepsilon_{2f} &= 2\pi NAM_s\omega\sin^2\theta_{max}\sin 2\omega t \\ &\approx 2\pi NAM_s\omega\theta_{max}{}^2\sin 2\omega t \qquad 3.5 \\ \left|\varepsilon_{2f}\right| &\propto AM_s\theta_{max}{}^2 \end{aligned}$$

where N is the number of turns on the sense-coil, A is the sample cross-sectional area and $\omega = 2\pi f$ is the drive frequency. The stress-induced anisotropy field, H_k, relates to $\sin\theta_{max}$ by:

$$\sin\theta_{max} = \frac{H^{\perp}_{ac,max}}{H_{dc} + H_k + H_s} \qquad 3.6$$

where $H_s = M_s(N_D^{\perp} - N_D^{\parallel})$ is the shape anisotropy field. (N_D are the demagnetising factors).

ε_{2f} is affected by the combined strengths of the d.c. and a.c. fields and, for magnetostrictive samples, by the amount of tensile stress, σ, applied by means of

the load. Loads induce uniaxial anisotropy in magnetostrictive samples. To obtain λ_s, increasing loads were applied to the sample and the d.c. bias field was adjusted to maintain the $2f$ signal amplitude. The change ΔH_{dc} required is equal to the anisotropy field, H_k. The saturation magnetostriction was then calculated from:

$$\lambda_s = -\frac{\mu_0 M_s}{3}\frac{H_k}{\sigma} \qquad 3.7$$

In practise, values of H_{dc} were plotted against applied stress (increasing and decreasing) and λ_s was calculated from the gradient.

Before measuring H_k vs. σ, it was advisable to check the SAMR region, i.e. where, in terms of applied field and load, the above equations are valid. This was done by applying a given load and noting ε_{2f} for a series of decreasing values of H_{dc}. This was repeated for several values of σ. The quantity $\varepsilon_{2f}^{-1/2}$ was then plotted against H_{dc}. In the region where $\varepsilon_{2f}^{-1/2}$ varied linearly with H_{dc}, the SAMR condition was fulfilled.

Narita *et al.* used SAMR to measure λ_s of ribbon samples. In order to apply the principle to deposited films and multilayers, account had to be taken of the substrate. The presence of the substrate effectively altered the stress experienced by the sample. Using a uniform strain model, the modified stress is:

$$\sigma = \frac{T}{A_{f+s}}\frac{E_f}{E_{f+s}} \qquad 3.8$$

where T is the tension applied to the sample, A_{f+s} is the cross-sectional area of the film plus the substrate and E_f and E_{f+s} are the Young's moduli of the film and the film-plus-substrate, respectively. In the absence of any measurements on the multilayer, the Young's modulus of the multilayer, E_f, was calculated from a volume average of the constituent layers. E_{f+s} was calculated in a similar way. This adjustment for the substrate is similar to that of Wenda *et al.* (1987). Young's moduli for the metals used were taken from data books or manufacturers' literature (in the case of multilayers made using commercial alloys as sputtering targets).

The Young's modulus of Kapton was taken to be 3.49GPa after measurements were done using a vibrating reed apparatus (after Berry and Pritchet (1975)) on resonant modes 2, 3 and 4. These results were in line with stress-strain measurements. The manufacturer's literature gives E = 2.45GPa. It has been found that these different E values do not affect λ_s by more than the experimental error. Thus λ_s is sensitive to the measurement itself and less so to the correction applied. Some λ_s measurements on deposited multilayers taken by SAMR have been confirmed by strain modulated ferromagnetic resonance (SMFMR), an independent measurement.

The typical variation of λ_s values calculated from repeated measurements, removing and reclamping the sample in between, was 5-10%. λ_s values down to a few parts per million have been successfully measured. With a time constant τ = 300ms, the variation on the LIA output voltage, ε_{2f}, was typically 0.7μV_{pp} on a signal of 4-50μV, due to noise. The correct H_{dc} setting to maintain ε_{2f} was obtained by watching the output for a few seconds so that the range of ε_{2f} observed was the same. A longer time constant was not used because it was necessary to keep H_{dc} high for as short a time as possible, in order that the solenoid should not become too hot from resistive heating, nor the power supply overheat.

3.4.2. Strain Modulated Ferromagnetic Resonance

Saturation magnetostriction measurements by strain-modulated ferromagnetic resonance were carried out by Dr. Ryszard Zuberek at the Institute of Physics, Polish Academy of Sciences, Warsaw, Poland. Details of the SMFMR method can be found in Zuberek *et al.* (1990, 1993) and references therein, and in Nguyen Chi Thanh and Krishnan (1985). A schematic diagram of the apparatus is shown in Figure 3.12.

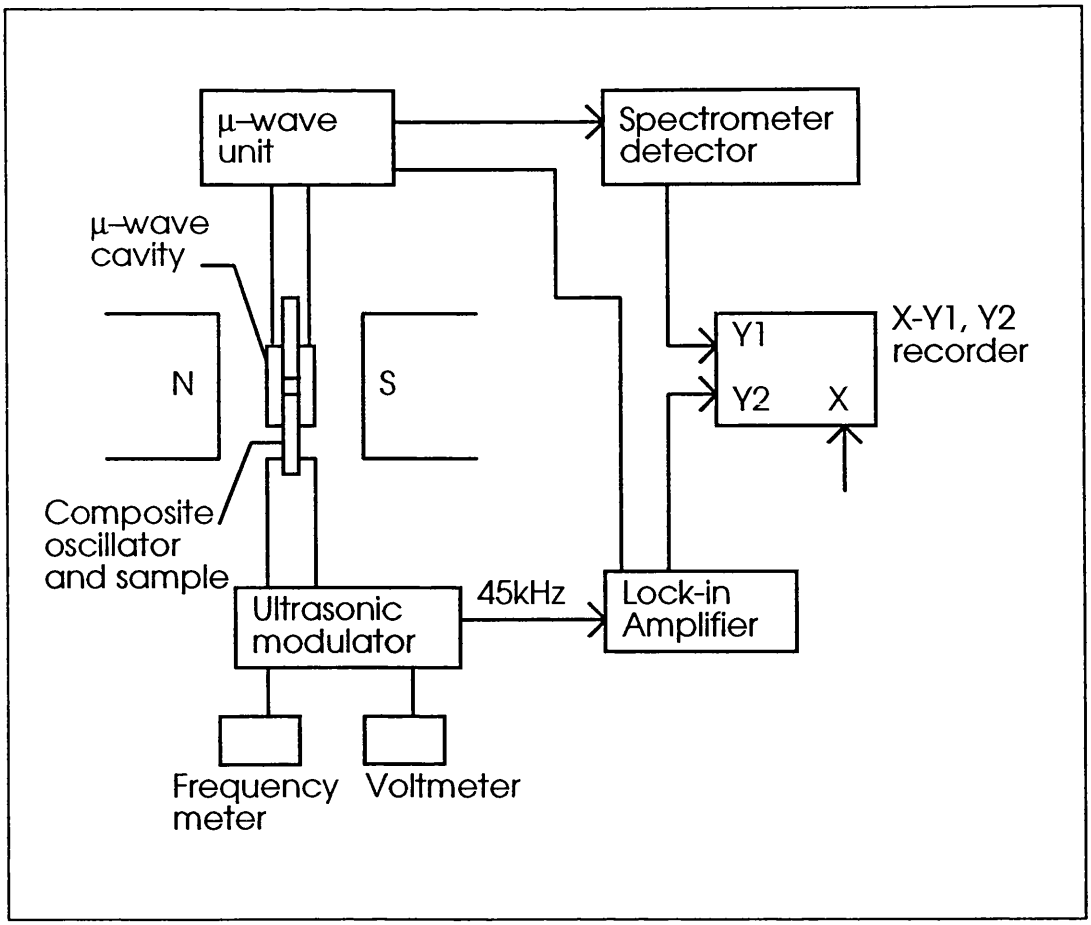

Figure 3.12 Schematic diagram of the SMFMR apparatus. Courtesy Dr. R. Zuberek, Polish Academy of Sciences.

The sample (≈3mm×4mm) was placed in a ferromagnetic resonance cavity. A time-dependent strain was applied to it which modulated the position of the ferromagnetic signal line. The straining system consisted of a sandwich transducer, amplitude transformer and piezoelectric composite resonator (to which the sample was attached) according to Wosik *et al.* (1978). λ_s was obtained from the shift $\Delta H_\sigma = H_\sigma - H_0$, where H_σ is the resonance field of the stressed sample and H_0 is the resonance field for zero applied stress:

$$\lambda_s = \frac{\mu_0 M_s}{3} \frac{\Delta H_\sigma}{\sigma} \qquad 3.9$$

It is assumed that $M_s >> H_0+H_k$ and that the magnetoelastic tensor is isotropic. The field was applied parallel to the film plane and to the induced anisotropy axis. The usual error in the measurement was 15% (Zuberek (1993)).

3.5. Structural Characterisation

3.5.1. X-Ray Diffraction

Samples were routinely investigated using high-angle X-ray diffraction in the θ-2θ configuration with reflection geometry. This is a standard technique to obtain information on crystal plane spacings, strain, approximate grain size, multilayer period and interface quality. The radiation was Cu-Kα, for which $\lambda_{\alpha 1}$ = 0.154056nm, $\lambda_{\alpha 2}$ =0.154439nm. The weighted average wavelength is λ = 0.15418nm. The generator was a Philips PW1730/10 4kW X-ray generator, typically working at 40kV, 25mA, using a PW2275/20 long fine focus 2kW Cu target. The detector was a PW1820/00 xenon proportional counter with a PW1752/00 graphite monochromator and PW1368/55 automatic divergence slit assembly. The sample was mounted in a PW1820/00 vertical diffractometer goniometer. The apparatus was controlled by microprocessor PW1710/00. During the course of this work, Philips PW1877 PC-APD 3.5b software became available, allowing spectra to be fitted, each peak with two half-Lorentzian distributions. This enabled a more precise determination of peak positions and widths, with allowances made for background signals.

Samples were clamped in position such that the scattering vector was normal to the surface, i.e. the structure in a direction perpendicular to the film surface was probed. Multilayers deposited on Kapton substrates were wrapped around a glass slide to facilitate mounting.

The position of the centroid of a diffraction peak is given by the Bragg condition:

$$\lambda = 2d \sin\theta \qquad 3.10$$

where λ is the wavelength of the X-rays, d is the spacing of the lattice planes causing the diffraction and θ is the angle between the incident beam and the diffracting planes. Homogeneous lattice strain in the sample alters the peak positions. The d-spacings of standard samples are published in the Powder Diffraction File. It was against these, or against measurements made on thick, single-component films, that comparisons were made in order to quantify the average strain in deposited films. The incident X-ray beam has an area of $\approx 1\text{cm}^2$ at the sample surface, so the reflected intensity at a given angle is the average response from this region. The angular step size was typically 0.005°.

For a perfect single crystal, the peak has width due to instrumental broadening only ($\approx 0.2°2\theta$). In polycrystals, the peak width (FWHM) is broadened due to small grain size; very thin samples also give broader diffraction peaks. Peaks may also be broadened if a range of d-spacings exists in the interrogated region (due to inhomogeneous strain). The Scherrer Equation (below - see Guinier (1963)) has been used to estimate average grain size in films (e.g. Rodmacq (1991)). It must be remembered, however, that other factors also cause diffraction peak broadening, so the results are not absolute.

$$L = \frac{0.9\lambda}{\Delta 2\theta \cos\theta} \qquad 3.11$$

L is the grain size and $\Delta 2\theta$ is the peak width (FWHM).

If a sample had crystallographic texture, i.e. one plane had grown predominantly parallel to the substrate in preference to other planes doing so, this was evidenced in the XRD spectrum. The relative intensities of peaks arising from diffraction from different planes were compared with standard spectra in the PDF.

If one peak was significantly more intense than others, the corresponding plane was oriented preferentially in the film plane. The sample may still be polycrystalline (Figure 3.13).

Texture assessment by this method is qualitative, and the information limited. Only strong texture is shown clearly in θ-2θ scans, and there is no quantitative indication of which lattice planes lie at which angles to the sample surface. For a complete assessment of the distribution of lattice plane positions in a specimen, investigation with a triple-axis goniometer would be required, to examine planes not lying parallel to the film surface. Transmission XRD would also provide useful additional information about planes lying at large angles to the film plane.

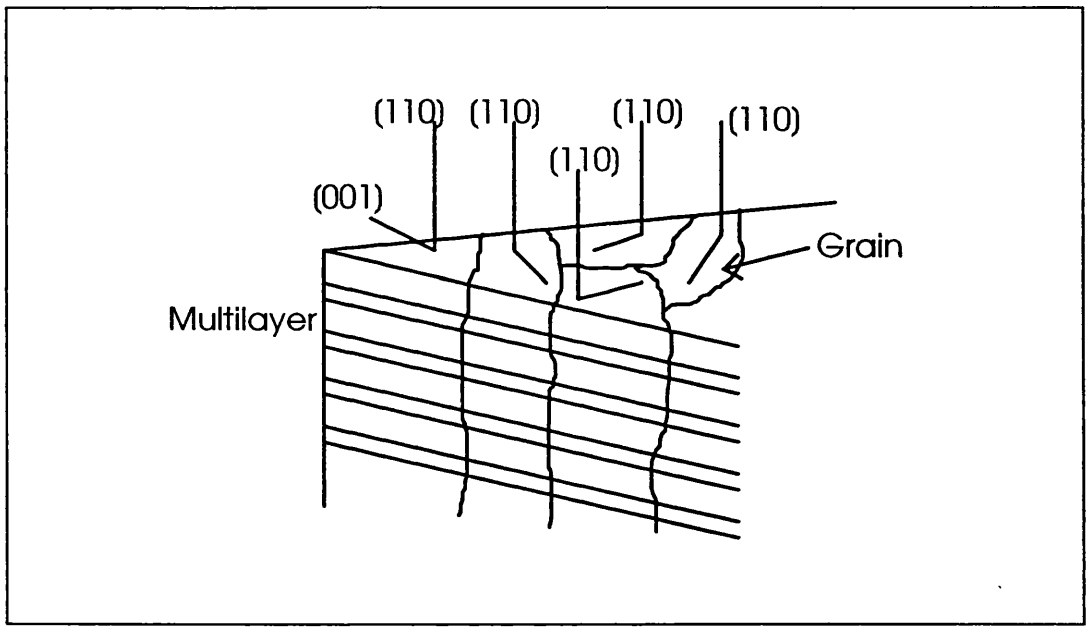

Figure 3.13 Schematic diagram of textured polycrystallinity. After Fujii (1987). The [110] directions are perpendicular to the film plane (i.e. the (110) planes lie parallel to the film plane). The direction lines in the plane represent the [001] axes.

Multilayer samples have another periodicity in addition to the lattice planes: that of the layers themselves. For low angles ($2\theta \leq\approx 4°$), the Bragg condition is satisfied with $d = \Lambda$ (Λ is the multilayer repeat distance). Low angle XRD could not be accomplished with the diffractometer used here. However, if the multilayer interfaces are sharp and flat, and the repeat distance is uniform throughout the stack, satellite peaks appear around the main peaks due to diffraction from the crystal planes. These positions are defined by:

$$\Lambda = \frac{\lambda}{2(\sin\theta_{i+1} - \sin\theta_i)} \qquad 3.12$$

(Meyer *et al.* (1981), see Section 4.1).

According to Azároff (1968), Cu-Kα radiation is not suitable for the analysis of Co, Fe or Mn. These elements fluoresce under this radiation, emitting X-rays of all wavelengths. This increases the background intensity and reduces the intensity reflected at the characteristic angles. Using Cu-Kα on these samples does not damage them. In the diffractometer used, the problem of fluorescence was reduced in three ways:

1) The incident X-ray beam is not filtered, but the reflected beam is monochromated by a graphite monochromator so that only Cu-Kα is incident on the detector.

2) The Xe in the proportional counter is particularly sensitive to wavelengths in the 0.15nm region, so acting as a filter to other wavelengths.

3) An electronic peak-height discriminator rejects all pulses below a certain amplitude, thus filtering out low-level noise.

If diffraction images on such samples were taken with a Laue powder camera, where reflections at all angles are recorded simultaneously, the fluorescence would turn the film uniformly black, and the picture would provide no information on the specimen structure.

3.5.2. Electron Microscopy

In order to look at the multilayer stack in cross-section, a few samples were prepared for investigation in a transmission electron microscope (TEM) according to the method used by Swab and Klinger (1988). Small chips were broken off samples of multilayers deposited on glass slides. These were embedded in a hard resin compound, close to the surface. Once the resin had set, the specimen was put in another mould and more resin was added, so that the multilayer sample finished sandwiched between the two resin halves, with the thinnest part of the chip closest to the tip of the block (Figure 3.14a).

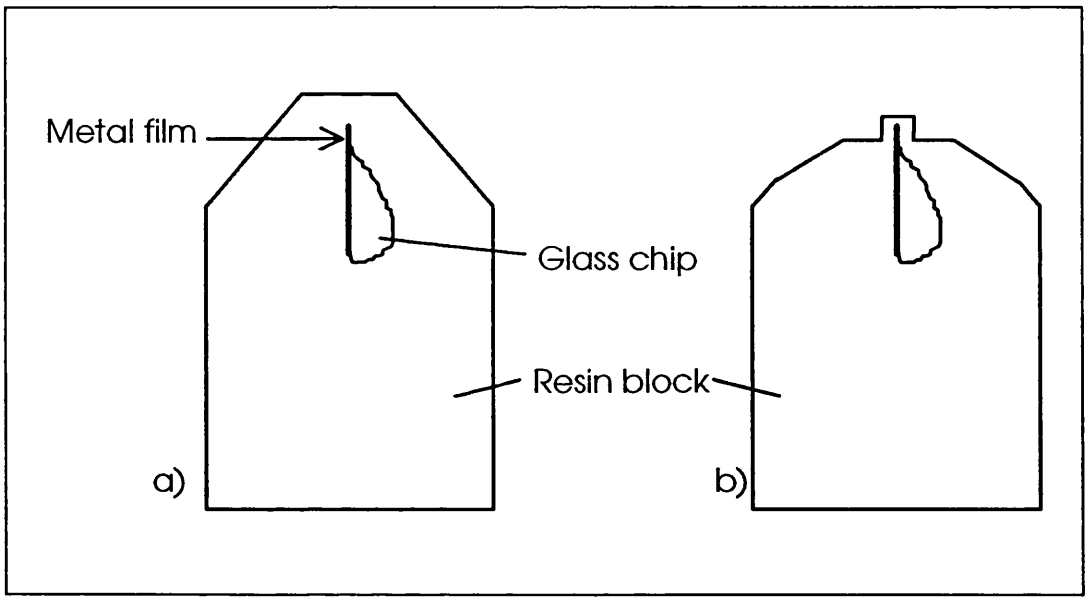

Figure 3.14 Mounting of multilayer sample in resin block. a) initially, b) after first trimming.

The block was trimmed until shaped as in Figure 3.14b. This trimming was done by hand using a sharp razor blade and by using a glass knife in an ultramicrotome. Final thin-sectioning of samples for the TEM was done using a diamond knife in the ultramicrotome. Sections were floated onto water and

collected on copper grids. This method was used successfully in imaging Ni/Ag multilayers.

Multilayers on Kapton were not successfully prepared for TEM. The Kapton did not cut cleanly. More successful was the deposition of multilayers onto 1cm diameter plastic cover slips, which were cut and examined in the Biomedical Sciences Department at the University of Sheffield. TEM could not be used routinely, although it would have made a good complement to XRD, in particular with regard to multilayer periodicity and interface quality.

3.6. Annealing

Two forms of annealing were carried out: 1) under low vacuum, 2) in a flow of Ar or forming-gas ($90\%N_2+10\%H_2$). It was desired that the samples should not oxidise. Forming-gas was most successful in this, since H_2 is a reducing agent.

Vacuum annealing. The multilayer samples were sandwiched between two aluminium plates about 10cm long. These were placed inside a Pyrex tube of about 3.5cm diameter attached to an Edwards Two-Stage rotary pump. A liquid nitrogen cold trap reduced backstream contamination to the vacuum chamber and helped to lower the pressure attainable. Before and during annealing and while the sample cooled, the chamber was evacuated.

In the cylindrical cavity in a Lenton Thermal Designs tube furnace (non-inductively wound) was placed a Pyrex tube, inside which was a 4mm thick aluminium tube acting as a thermal mass to even the temperature profile along the length of the tube. A temperature around 30° higher than required was programmed into the controller. Once the required temperature had stabilised and the sample tube had been evacuated, the sample tube was slid into the furnace for the required length of time. See Figure 3.15. It is estimated that the temperature

was stable to within ±3°C during annealing. There was a similar variation of temperature along the 10cm length of the sample.

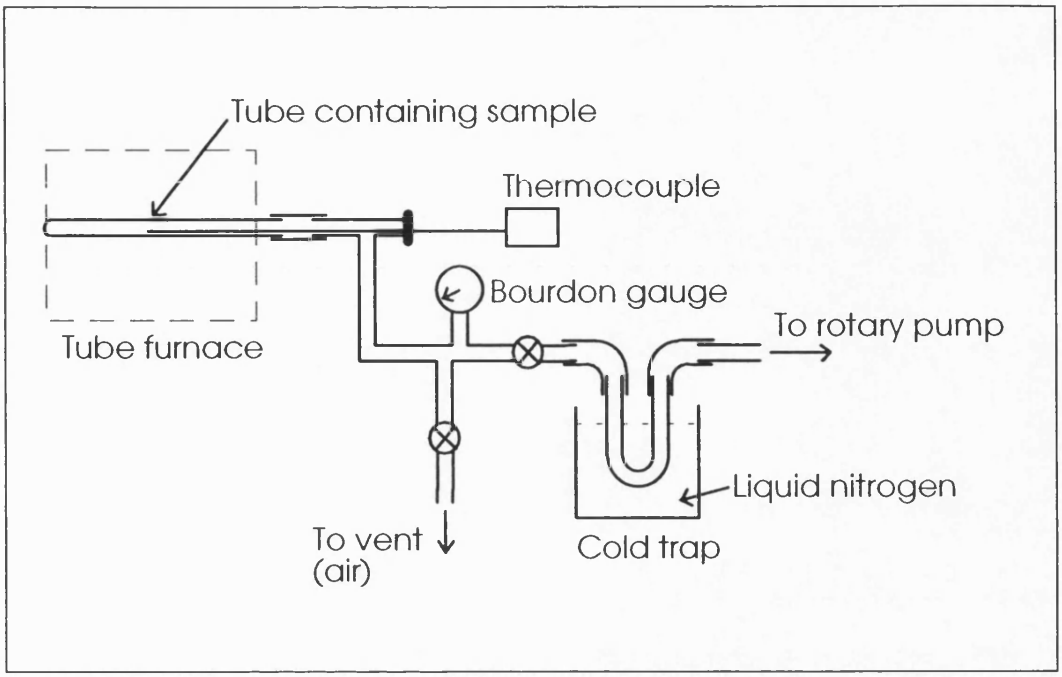

Figure 3.15 Schematic diagram of vacuum annealing apparatus.

Following cooling, the valve to the pump was closed and air was admitted to the tube. On reaching atmospheric pressure, the tube was disconnected and the sample removed.

Gas-flow annealing. The arrangement of the apparatus is shown schematically in Figure 3.16. The gas flow rate was monitored with a flow meter at the exhaust, calibrated for nitrogen. Heat was supplied by a Leister "Hotwind S" 9C1 heat gun capable of heating up to 600°C. A K-type thermocouple probed the temperature at the aluminium thermal mass in which were sandwiched the samples. Many samples were stacked at once in the holder, two side by side with a layer of plain Kapton between them and the next two. It took approximately 10 minutes for the temperature of the samples to reach the required temperature (usually 300°C), at

which point timing began. The output of the heat gun was controlled by hand throughout the anneal. The temperature generally varied by less than about ±4°C. At the end of the anneal, the heat was removed and cold air blown around the sample tube. The gas flow was maintained throughout.

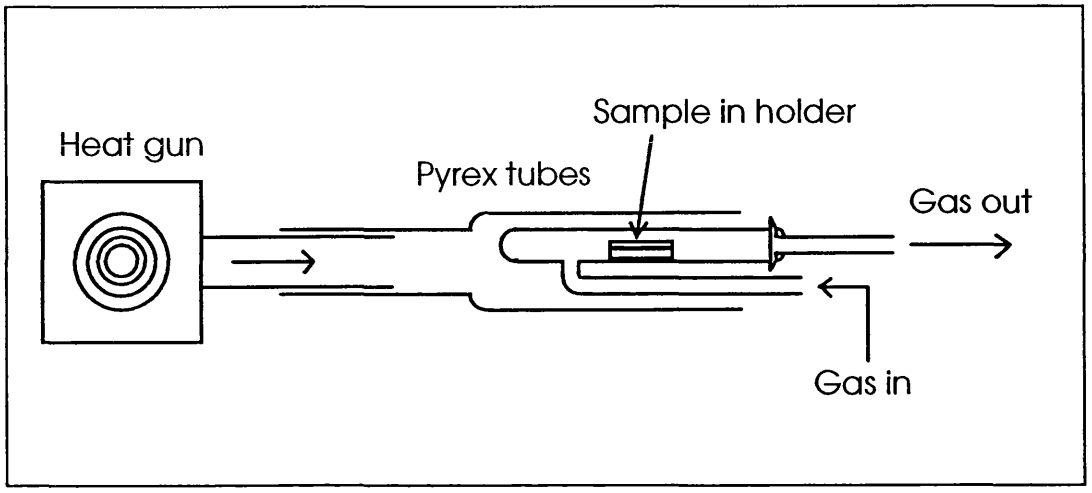

Figure 3.16 Schematic diagram of apparatus used for annealing samples in a flow of gas. The thermocouple, attached to the sample holder, is not shown.

3.7. Ferromagnetic Resonance

Ferromagnetic resonance measurements were carried out on a Brucker ESP 300 at the Universidad del País Vasco, Bilbao, Spain, operated by Mr. Luis Lezama. A sample ≈3mm×3mm was placed, free to move, in a closed glass tube which was then positioned in the cavity. The sample oriented itself such that the applied field was parallel to the film plane. The cavity was excited at 9.73GHz or 34.0GHz (in a different machine) and the signal was modulated at 100kHz. The parallel field was scanned across an appropriate range, usually from high field down to zero. (At 9.73GHz, the fields were of the order of tenths of a tesla; at 34.0GHz, around 1T). The differential absorption of the radiation was traced out; the position of the resonant field is then the point at which the response crosses the

zero line. From the resonant field, values of the Landé g-factor can be obtained. When g=2, the magnetisation of a sample is due purely to electron spin, while g=1 corresponds to pure orbital magnetic moment. For applied field parallel to the film plane, the resonance condition leads to the following relation (Kittel (1971)):

$$\gamma = \frac{-\omega_{res}}{\sqrt{B_{res}(B_{res}+\mu_0 M)}}, \qquad 3.13a$$

$$g = \frac{-\gamma\hbar}{\mu_B} \qquad 3.13b$$

γ is the gyromagnetic ratio and $H_{res} = B_{res}/\mu_0$ is the applied field at resonance for the sample. $\omega_{res} = 2\pi f$ is the oscillation frequency. Measurements taken at f = 9.73GHz were considered to be less reliable, since H_{res} was low and the true field was not known accurately, due to remanence in the electromagnet pole pieces.

3.8. Mössbauer Spectroscopy

Mössbauer spectroscopy yields information on the magnetic moment orientations in a sample. Spectra of some samples were measured by Dr. J. Z. Jiang at the University of Liverpool, and by Dr. J. M. Williams and Prof. J. Adetunji at the University of Sheffield. In the Sheffield case, samples were mounted on discs 1.5cm in diameter (sometimes several samples glued on top of one another) and placed perpendicular to the incoming γ-ray beam, in apparatus constructed in-house. Data were taken at room temperature over several days per sample (typical run-times were 100-150 hours) to improve counting statistics.

Magnetic nuclei absorb radiation at a characteristic frequency and re-emit this radiation in all directions. Because of recoil energy involved in the emission and absorption of γ-rays, the energies of emitter and absorber do not overlap in the static case and resonant absorption cannot occur. To bring the two energies into (partial) overlap, the Doppler shift is employed. The sample (absorber) is moved in

the line of the γ-rays at speeds up to $v \approx 10 mms^{-1}$. A detector behind the sample measures the transmitted γ-ray intensity and so an absorption spectrum is obtained. Troughs occur where the sample has absorbed radiation and emitted it in all directions.

For iron, a characteristic spectrum of six peaks is obtained (see Figure 3.17).

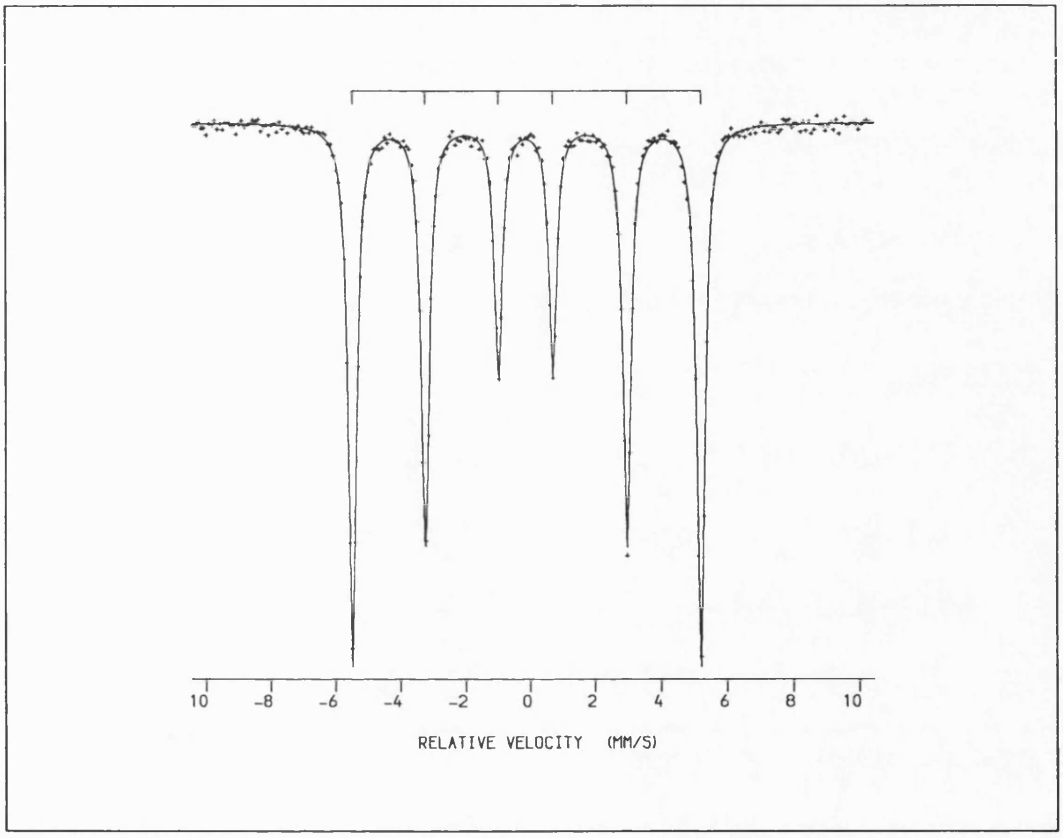

Figure 3.17 Characteristic Mössbauer spectrum of α-Fe. The points are experimental data and the line is a fit. The top scale indicates the peak positions. Courtesy Dr. C. Hawkins, University of Sheffield.

The spectrum is symmetric about v=0. The integrated intensities of the peaks are related by the following ratios, taking peak 1: peak 2: peak 3

$$3:\frac{4\sin^2\theta}{1+\cos^2\theta}:1 \qquad 3.14$$

where θ is the average angle between the atomic magnetic moment and the γ-ray beam. If measurements are taken with different sample orientations with respect to the γ-ray beam, the moment angle distribution can be determined. For the present study, however, data were taken for the γ-rays perpendicular to the film plane. Thus the average inclination of the moments to the film plane was obtained. If it is known along which crystallographic axes the moments are likely to lie, then Mössbauer data also yield structural information.

Summary. Multilayer films were deposited by r.f. magnetron sputtering as a wide variety of target and substrate materials may be used, and the resulting films may be polycrystalline, incorporating lattice strain and/or layer mixing at the interfaces. These properties are considered desirable for enhancing λ_s over that obtainable in bulk materials. Post-deposition annealing was employed to modify crystallinity and the interface structure of samples. The measurement techniques used for routine characterisation of multilayer samples were d.c. magnetometry (to measure MH loops), Small Angle Magnetisation Rotation (SAMR, to measure λ_s) and X-ray diffraction (XRD, to investigate crystal structure). The geometry of the MH loop tracer and the SAMR apparatus were particularly suited to the study of thin films, and the fields attainable were appropriate for soft magnetic materials. The fields were applied along the sample plane. The MH loops of some samples were also measured using a Faraday balance with a maximum field of 1.5T. For the magnetically hard Co-Pd/Ag multilayers, this was used exclusively. It was necessary to cut the samples into small squares, though it is not thought that this action affected the loops, considering the film thicknesses. The saturation magnetostriction of these harder films was measured by Strain Modulated

Ferromagnetic Resonance (SMFMR) as the SAMR field was insufficient. SMFMR was also used to confirm some results on other, soft samples.

High angle XRD gave information on crystal plane spacing, strain, approximate grain size, crystallographic texture, multilayer periodicity and interface quality. Some samples were examined by cross-sectional transmission electron microscopy (TEM). This technique was not available routinely, unfortunately; it would have complemented XRD, in particular with respect to multilayer periodicity and interface quality. Multilayers deposited on Kapton were not successfully prepared for TEM. If the contrast between component layers was poor, then individual layers could not be distinguished.

Ferromagnetic Resonance (FMR) measurements yield the Landé g-factor, the value of which indicates the nature of the sample magnetic moment, i.e. the degree of spin and orbital contributions. The interpretation of FMR data for multilayers is complex and was not explored in depth. Mössbauer spectroscopy was carried out on some samples with the γ-ray perpendicular to the sample plane. The data yielded the average moment angle with respect to the γ-ray beam, and it was hoped that, assuming the moments to lie on given crystallographic axes, these data would be tallied with the model for magnetostriction of textured polycrystalline samples presented in Section 4.3. Mössbauer spectroscopy is time-consuming, yet, ideally, more measurements would have been taken with the γ-ray at different angles to the sample to give more detailed information on the direction of **M**.

4. Mathematical Models

Various mathematical descriptions used in interpreting experimental data are presented in this chapter, with their derivations.

4.1. Origin of X-Ray Diffraction Satellite Peaks

The X-ray diffraction scan of a multilayer specimen may show smaller satellite peaks around a main diffraction peak, if the interfaces are sufficiently smooth and the repeat distance uniform throughout the stack.

For constructive interference of X-rays diffracted from a set of crystal planes, the path difference between rays from different planes must be an integral number of wavelengths. This condition is described by the Bragg law:

$$\lambda = 2d\sin\theta \qquad 4.1$$

where d is the plane spacing for the order of diffraction considered, λ the X-ray wavelength and θ the angle between the incident beam and the plane (Figure 4.1).

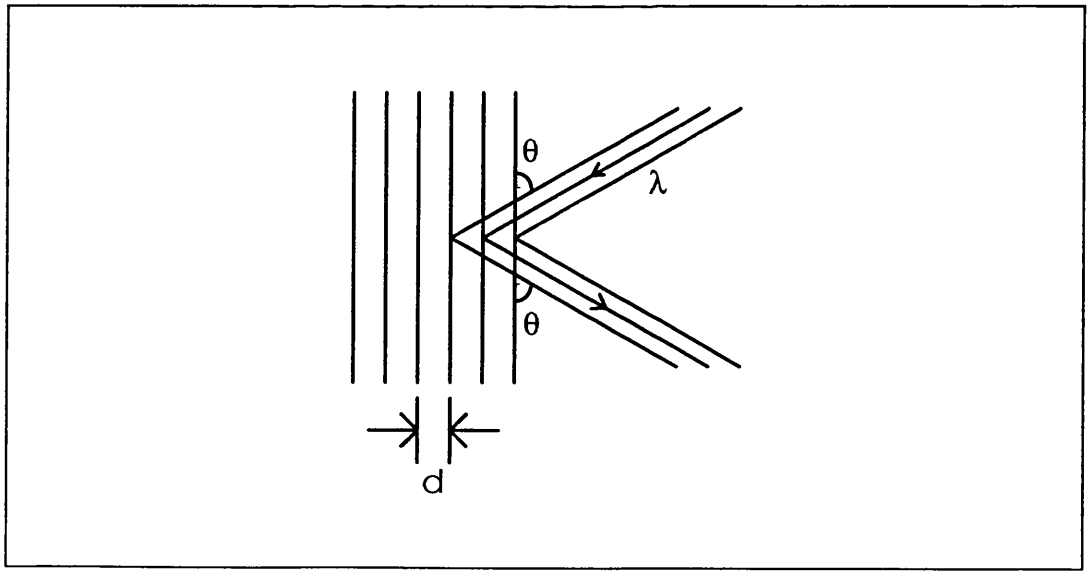

Figure 4.1 Bragg diffraction from a set of crystal planes.

Bragg diffraction can be represented in reciprocal space by the Ewald sphere construction (Figure 4.2) where **g** is the reciprocal lattice vector and $\mathbf{k}_i$ and $\mathbf{k}_r$ are the wave vectors of the incident and diffracted beams, respectively. The modulus of the **k**-vectors is $2\pi/\lambda$. The modulus $|\mathbf{g}| = 2\pi/d$ by definition. From the construction, it can be seen that, for constructive interference of diffracted X-rays, $|\mathbf{g}| = 2|\mathbf{k}|\sin\theta = 4\pi\sin\theta/\lambda$. Hence $\lambda = 2d\sin\theta$, the Bragg law. The resulting diffraction pattern, for a cubic lattice, is illustrated in Figure 4.3. For an infinite amount of substance with a perfectly periodic plane spacing, an infinite number of diffraction spots results; these are separated (in k-space) by $\Delta k = 2\pi/d$. Each spot corresponds to a different set of diffraction planes.

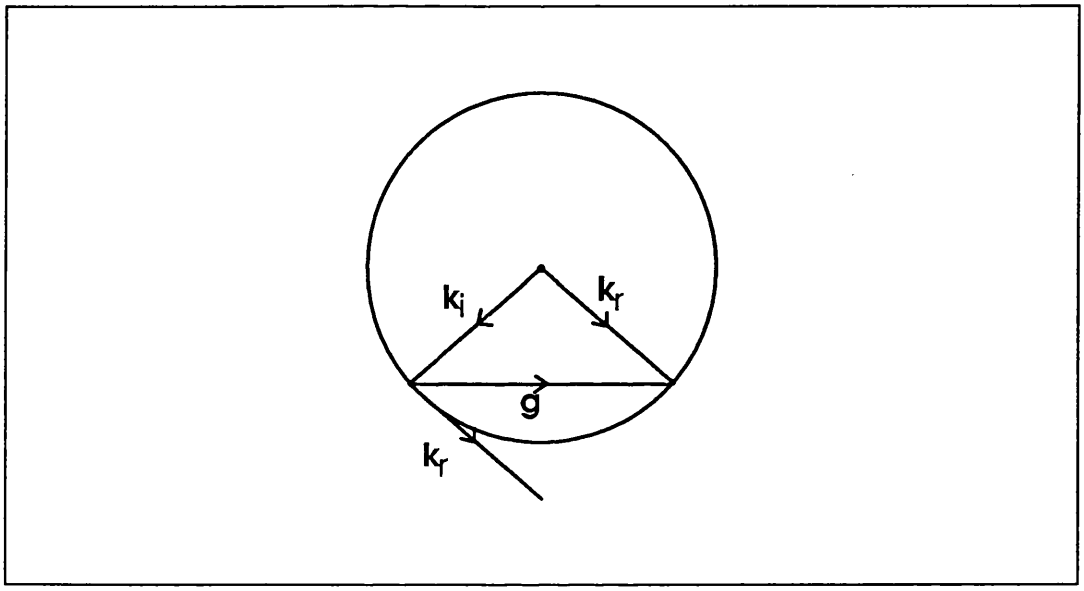

Figure 4.2 Ewald sphere construction of Bragg diffraction in reciprocal space.

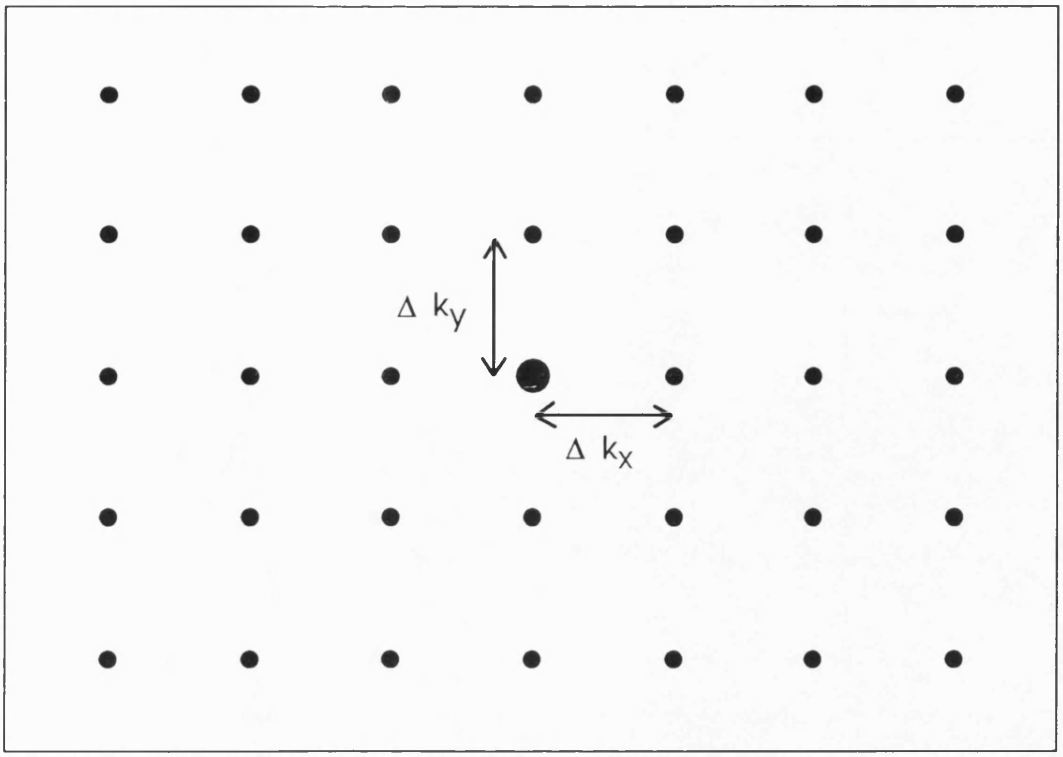

Figure 4.3 Schematic diffraction pattern from a cubic single crystal. Each spot arises from a different set of crystal lattice planes.

Consider a sample that contains two types of material, of planar spacings d_1 and d_2. The corresponding diffraction spots would be separated by $\Delta k_1 = 2\pi/d_1$ and $\Delta k_2 = 2\pi/d_2$, respectively. The two patterns would be superimposed.

Now consider a multilayer made of alternate layers of these two substances. Initially, ignore the crystal structure within each layer, and look only at the periodicity caused by the layering of the substances (Figure 4.4).

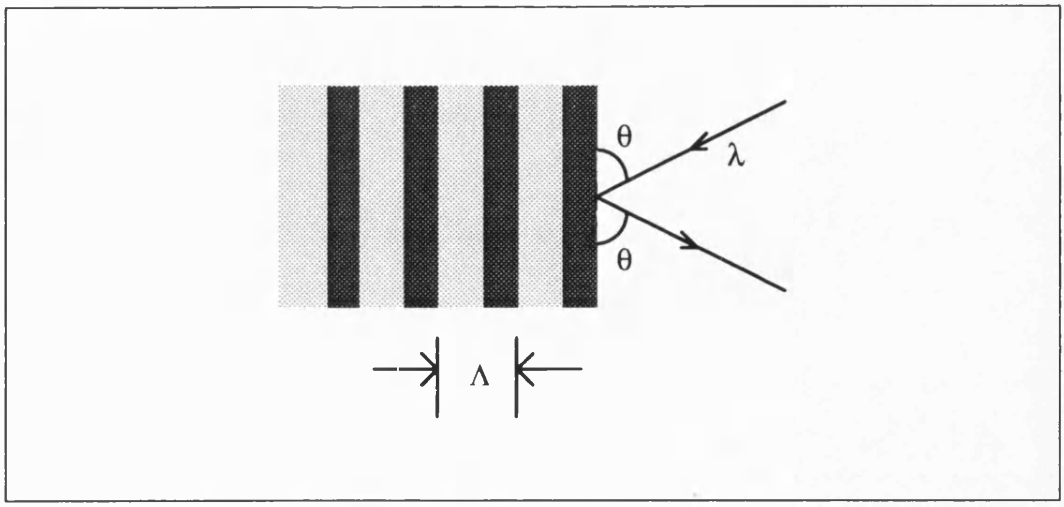

Figure 4.4 Representation of a multilayer with incident and diffracted X-ray beams.

By the same arguments as previously, the multilayer periodicity, Λ, would give rise to diffraction spots at a spacing in reciprocal space of $\Delta k = 2\pi/\Lambda$ (Figure 4.5). Bragg spots can be seen at low angles at positions given by $n\lambda = 2\Lambda\sin\theta$. The spots lie on a single line because the modulation of the multilayer is in one direction only.

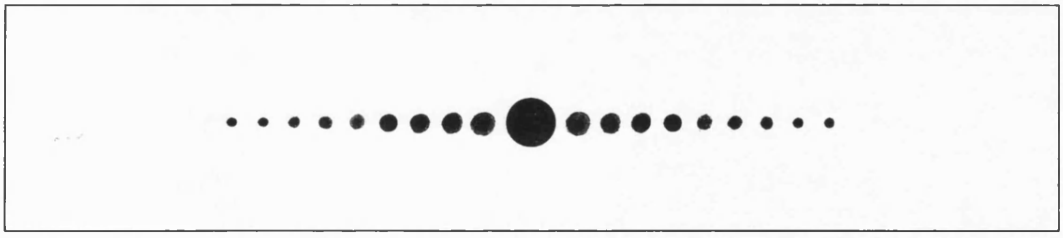

Figure 4.5 Diffraction pattern from a 1D multilayered structure. The spots are different orders of diffraction due to the periodicity, Λ, of the multilayer only.

Now superimpose the effect of the crystal lattice structure of the component materials, to give the diffraction pattern due both to the multilayer periodicity and

to the crystal lattices within each layer. The resulting pattern is illustrated in Figure 4.6.

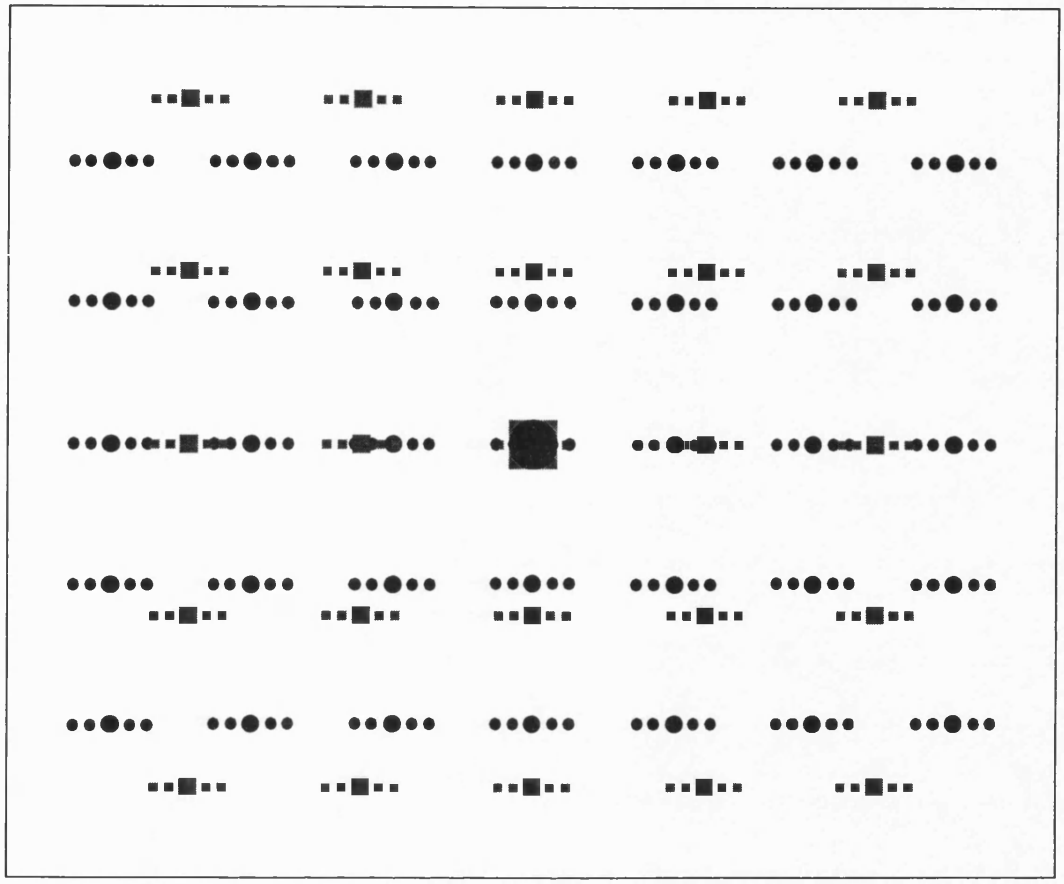

Figure 4.6 Schematic diagram of the diffraction pattern of a multilayer with crystal planes within the layers. The circles represent the spots due to one type of layer, the larger spots being due to the crystal lattice and the smaller spots due to the multilayer periodicity. The squares represent the similar situation with regard to the other type of layer in the multilayer (see Figure 4.4). Spots due to multilayer periodicity only are seen around the centre spot.

The straight-through beam can be diffracted by $\Delta\mathbf{k}_1$ to give the first spot due to the crystal lattice of the first type of layer. Similarly, low-angle spots due to the

multilayer periodicity can also be diffracted by $\Delta\mathbf{k}_1$ to form "satellite" spots near this first spot. Diffraction described by other vectors gives rise to satellites around other spots.

In practise, diffraction spots (intensity peaks registered by a diffractometer) have a finite size (peak width). This is because the sample is not infinitely thick (the width is inversely proportional to the thickness). This restricts the number of rays that can be diffracted coherently. Neither are the d-spacings identical within the region interrogated by the X-ray beam. Also, peaks are not observed at all the predicted values of θ given in Equation 4.1 above; some are "disallowed"; for example, there is no peak from (100) planes in the pattern from a face-centred cubic crystal, although a (200) peak is present. Substances also diffract X-rays with different efficiencies, which vary with the diffraction angle. This scattering factor has the same form for all substances, decreasing as θ increases. Peaks at higher angles are, therefore, less intense. So, peaks have a finite width and a finite number of satellites may be observed around them, with higher order satellites being less intense.

The multilayer periodicity, Λ, can be calculated from the relative positions of low-angle multilayer peaks or of satellite peaks around a main Bragg peak. Consider the Bragg condition for the i^{th} order peak due to the multilayer periodicity:

$$i\lambda = 2\Lambda \sin\theta_i \qquad 4.2a$$

For the next peak,

$$(i+1)\lambda = 2\Lambda \sin\theta_{i+1} \qquad 4.2b$$

Subtracting 4.2a from 4.2b and rearranging gives:

$$\Lambda = \frac{\lambda}{2(\sin\theta_{i+1} - \sin\theta_i)} \qquad 4.3$$

which is the equation given by Meyer *et al.* (1981). This analysis applies to the low-angle peaks which are due solely to the multilayer periodicity, but also applies to satellites around a main Bragg peak since X-rays scattered into the satellite positions from the low-angle multilayer peaks have been scattered by the same scattering vector.

The trace obtained from a diffractometer does not show all diffraction spots, since the X-ray source, sample and detector are coplanar, and the detector does not intercept all possible reflections.

4.2. Simulation of X-Ray Diffraction Scans

Fujii (1987) applied kinematical diffraction theory to diffraction from superlattice structures. This model was used as the basis for a program written to simulate the diffraction patterns obtained from multilayer samples, so that information on lattice strain, sample layer thicknesses and interface roughness might be readily obtained from complex patterns.. The program was written in Q-Basic and compiled. The kinematic model takes no account of differences in refractive index between substances or at different wavelengths.

Some assumptions were made in the theory, which are not likely to be the true physical case in most multilayer systems. For example, it was assumed that the multilayer interfaces were perfectly sharp and flat (the "one-step" model), that each layer was a single crystal and that there was perfect crystallographic texture in the plane of the film for all layers. The d-spacing of the appropriate plane was input to the program, which meant that peaks from other types of plane were not simulated. (Patterns were generally simulated in a small angular range not to include peaks from more than one set of planes from a given layer type). A parameter was included in the simulation to account for interface roughness and so broaden the

peak widths. Its value should be treated with caution, however, as other effects such as inhomogeneous lattice strain and small grain size also cause peak broadening, and these were not accounted for.

Consider a superlattice modulated in the z direction, with layer thicknesses t_a and t_b and modulation period $\Lambda = t_a + t_b$. Let there be N bilayers. As a function of the magnitude of the scattering vector, Q, the diffracted intensity, I, is given as follows:

$$I(Q) = L(Q)|F(Q)|^2 \qquad 4.4$$

$L(Q)$ is the Laue function for the total multilayer (see below). $|F(Q)|^2$ is the intensity of the scattering function of the individual layers, which is a combination of the scattering functions and Laue functions of the individual layers.

$$L(Q) = \frac{\sin^2 N\Lambda Q}{\sin^2 \Lambda Q} \qquad 4.5$$

$$\begin{aligned} |F(Q)|^2 &= \left| \int_0^{t_a} \rho(z)\exp(iQz)dz + \int_{t_a}^{t_a+t_b} \rho(z)\exp(iQz)dz \right| \\ &= f_a{}^2 L_a(Q) + f_b^2 L_b(Q) + 2 f_a f_b [L_a(Q)L_b(Q)]^{\frac{1}{2}} \cos\left(\frac{\Lambda Q}{2}\right) \end{aligned} \qquad 4.6$$

$\rho(z)$ is the electron density as a function of the distance through the thickness of the superlattice, z, and f_a and f_b are the atomic scattering factors for the two layers. $L_a(Q)$ and $L_B(Q)$ are the Laue functions for the two layers, given by:

$$L_i(Q) = \frac{\sin^2(n_i d_i Q/2)}{\sin^2(d_i Q/2)} \qquad 4.7$$

where d_i is the d-spacing of the atomic planes in layer i and n_i is the number of atomic planes.

The atomic scattering factors are also functions of Q and vary from element to element. Scattering factors can be expressed as a series of exponential terms, to a good approximation (Ibers and Hamilton (1974)) and the expressions and

parameters given in this reference were used to calculate f_i in the simulation program.

Interface roughness (or, the fluctuation in modulation period within the multilayer) were taken into account by a Gaussian distribution for non-cumulative disorder:

$$G = \exp\left[\frac{-(\Lambda - \Lambda_0)^2}{\sigma^2}\right] \qquad 4.8$$

where Λ is the superlattice period at a point, Λ_0 is the average superlattice period and σ is the roughness parameter, with units of length. The degree of fluctuation of Λ is given by the FWHM of the distribution, and so can be calculated as follows:

$$\frac{\Delta\Lambda}{\Lambda_0} = 2\frac{\sigma}{\Lambda_0}\sqrt{\ln 2} \qquad 4.9$$

The Laue function for the total superlattice (Equation 4.5) is thus modified to become:

$$L(Q) = \frac{1+\exp(-N\sigma^2Q^2/2) - 2\exp(-N\sigma^2Q^2/4)\cos(N\Lambda_0 Q)}{1+\exp(-\sigma^2Q^2/2) - 2\exp(-\sigma^2Q^2/4)\cos(\Lambda_0 Q)} \qquad 4.10$$

This is the function used in the simulation program. The function $|F(Q)|^2$ is modified by multiplication by the factor $\exp(-\sigma^2Q^2/32)$. The effect of interface roughness is to broaden peaks and to reduce their intensity.

Since Cu-Kα radiation was used in measuring X-ray diffraction patterns, the wavelengths of Kα_1 and Kα_2 were used in the simulation program, and the weighted average result taken. Input parameters were the layer components and their thicknesses, t_a and t_b; their d-spacings corresponding to the principle peaks, d_a and d_b; the number of repeat units in the multilayer, N; and the roughness parameter, σ. The angular range covered and the angle step-size could be altered by the operator. The numbers of lattice planes per layer were calculated from t_i/d_i, rounded to the nearest integer.

In practise, it was found rare that a simulation pattern closely approximated a measured pattern, using the operator's chosen parameters. In response, the program was enlarged to include reading in a measured pattern, subtracting a horizontal background from it, and comparing it to the simulations as the variable parameters were stepped through. It was necessary to ensure that the 2θ range and angle step size were the same in the measured and simulated spectra. Each trace was normalised to the height of the most intense peak in order to facilitate comparison between the two.

The least-squares fit simulation pattern was then stored and plotted at the end, with the fit parameters. Even though small parameter ranges and few steps were used, the compiled program could still take hours to run. The results were sensitive to small changes in d-spacings, particularly (see Section 5.3.1), and a fit was often not improved by fixing the d-spacing of one component at its mid-range best fit value, altering the other and refitting. To make this simulation more routinely useful would require that it be written in a more efficient way and run on faster machines, employing strategies such that not all possible combinations of the fit parameters need be tested. However, some XRD patterns from Co-Pd/Ag multilayers have been fitted reasonably. These multilayers had strong crystallographic texture and their XRD scans showed many satellites, indicating smooth multilayer interfaces and uniform modulation periods.

In simulating the patterns for multilayers containing alloy layers, the scattering factor for the alloy was taken as the weighted average of the atomic scattering factors for the individual components. Below is shown a flow diagram of the program to fit the measured spectrum of a multilayer consisting of elemental layers.

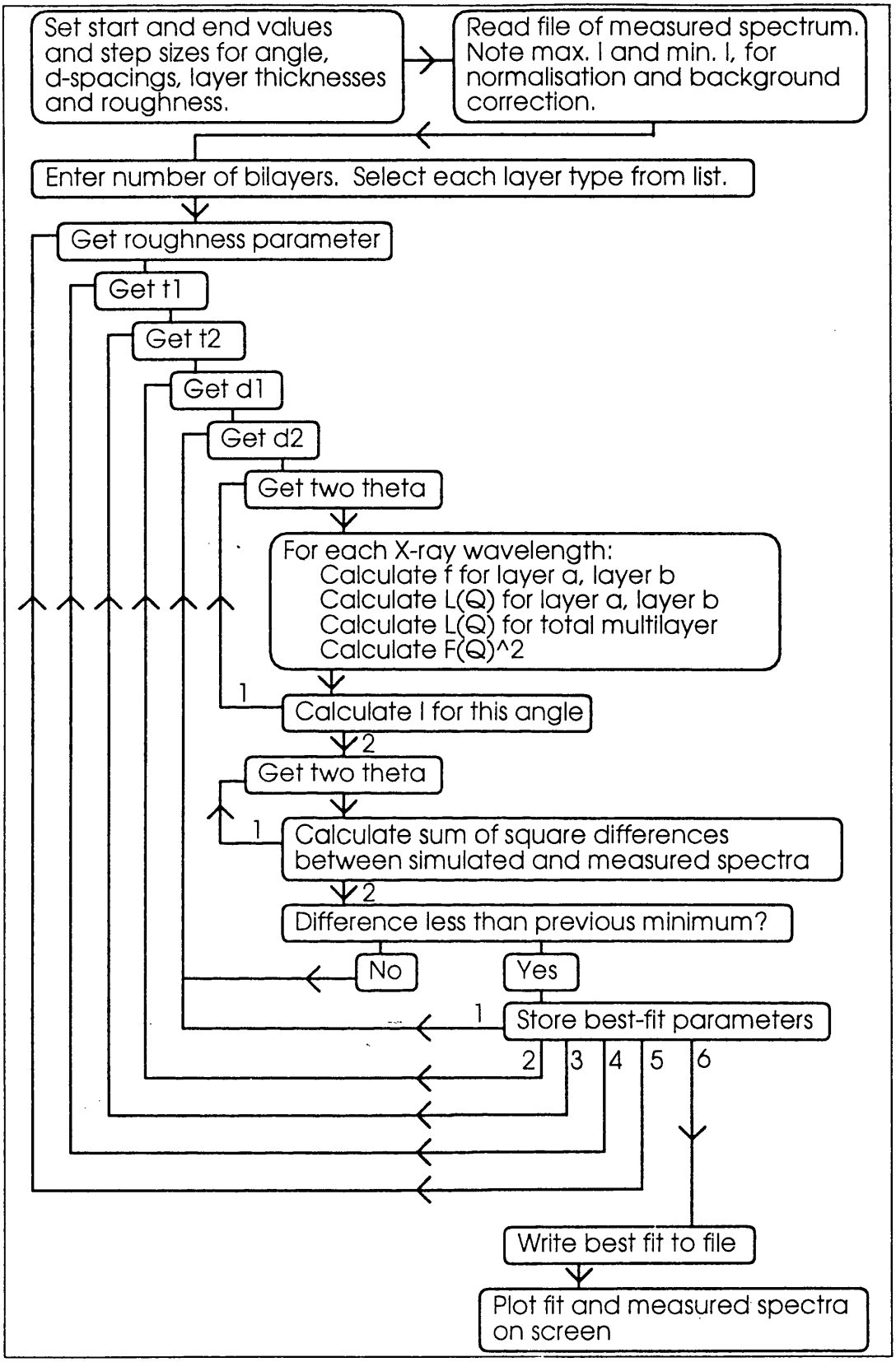

Figure 4.7 Procedure for fitting measured XRD spectra. Symbols used are explained in the text.

4.3. Magnetostriction of Textured Polycrystalline Specimens

In thin layers, it is possible to deposit films which have a preferred crystallographic orientation with respect to the substrate. For example, face-centred cubic systems may grow with the (111) crystal plane parallel to the plane of the film. (It is still possible that the film be polycrystalline, see Section 3.5.1). The standard phenomenological expression of the saturation magnetostriction, λ_s, of cubic single crystals has been presented by e.g. Kittel (1949) and for random polycrystalline materials by Cullity (1972). (Birss (1960) presents a calculation of the saturation magnetostriction of random polycrystals to higher order in the magnetostriction constants; such detail was considered unnecessary here). In this section, working from these expressions, the form of magnetostriction of polycrystalline materials with the crystal axes oriented at a particular angle to the film normal will be calculated.

The expression for the magnetostriction of a single cubic crystal is the following (Kittel (1949)):

$$\lambda_s = \lambda_{100} + 3(\lambda_{111} - \lambda_{100})(\alpha_1^2\alpha_2^2 + \alpha_2^2\alpha_3^2 + \alpha_3^2\alpha_1^2) \qquad 4.11$$

α_i are the direction cosines of the $\mathbf{M}_s$ direction with respect to the crystal axes. The above formula applies only when λ_s is measured in the $\mathbf{M}_s$ direction. Referring to Figure 4.8, $\alpha_1 = \sin\varphi\cos\theta$, $\alpha_2 = \sin\varphi\sin\theta$ and $\alpha_3 = \cos\varphi$.

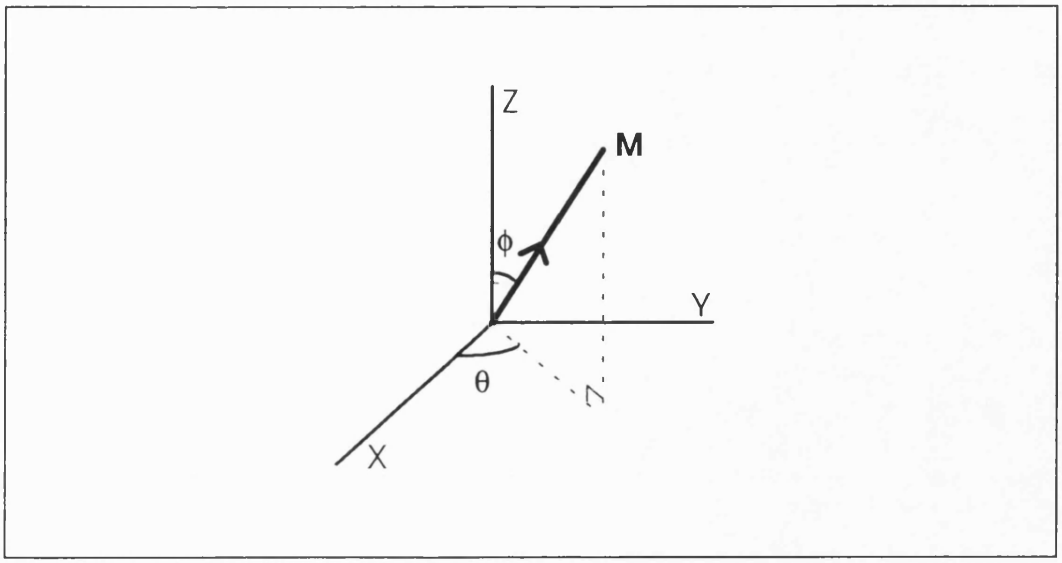

Figure 4.8 λ_s and $\mathbf{M}_s$ orientations with respect to crystal axes.

To obtain the magnetostriction of a *random* polycrystal, the single-crystal expression for λ_s is averaged over all directions of θ, φ as follows (after Cullity (1972)). This formulation is based on the assumption that stress is uniform throughout the polycrystalline sample. The factor $1/4\pi$ arises because 4π is the total solid angle over which the integration is carried out.

$$\overline{\lambda_s} = \frac{1}{4\pi}\int_0^{2\pi} d\theta \int_0^{\pi} d\varphi . \lambda_s \sin\varphi \qquad 4.12$$

λ_s is substituted from Equation 4.11. For a random polycrystal, $\overline{\lambda_s} = (2\lambda_{100} + 3\lambda_{111})/5$. For random polycrystalline Fe (λ_{100} = +21ppm, λ_{111} = -21ppm, Cullity (1972)), the calculation yields $\overline{\lambda_s}$ = -4.2ppm. This compares with the experimental result of -7ppm, which is 67% larger. In the case of Ni, however, the correspondence of theory and experiment is excellent: the calculation gives $\overline{\lambda_s}$ = -33ppm (λ_{100} = -46ppm, λ_{111} = -24ppm) while experiment yields -34ppm (Cullity (1972)). The calculation has limited applicability, therefore. Callen and Goldberg (1965) point out that this approximation gives a poor fit to data, and use more complex reasoning some way between the assumptions of uniform stress

and uniform strain to obtain $\overline{\lambda_s} = \alpha\lambda_{100} + (1-\alpha)\lambda_{111}$ where $\alpha = 2/5 - (\ln c)/8$, where $c = 2c_{44}/(c_{11} - c_{12})$ is a measure of the elastic anisotropy of single crystals. The constants c_{11}, c_{12} and c_{44} are components of the elasticity tensor of a single crystal. Theirs gives a better fit to data than the uniform stress model, but the data are scattered. Callen and Goldberg do not give details of their method. Present consideration will be confined to the simpler approach; caution should be exercised in quantitative application of the following model to experimental data, in view of the considerations mentioned above.

Magnetostriction is assumed to be measured in the plane of the film, as this is the geometry for SAMR measurements (see Section 3.4.1). It is also assumed that the film structure is isotropic in the plane, i.e. that the angle that one cubic crystal axis makes with the film plane is the same in all directions. The other two cubic crystal axes are free to lie in any direction, subject to remaining orthogonal to the first. Figure 4.9 illustrates the arrangement.

The reason for choosing the geometry such that β is constant and so located is that data from Mössbauer spectroscopy may, in certain circumstances, give this angle. Mössbauer spectra (see Section 3.8) yield the value of the average angle of the magnetic moments to the direction of the incident γ-ray. If the γ-ray is incident normal to the film plane, and the magnetic moments may be considered to lie along a (001) axis, then the (average) angle β between the film normal and the (001) axis is known, and the analysis detailed below can be applied. In some cases, the magnetic moments may be considered to lie along the (111) axis, and a more complex analysis is required to calculate $\overline{\lambda_s}$.

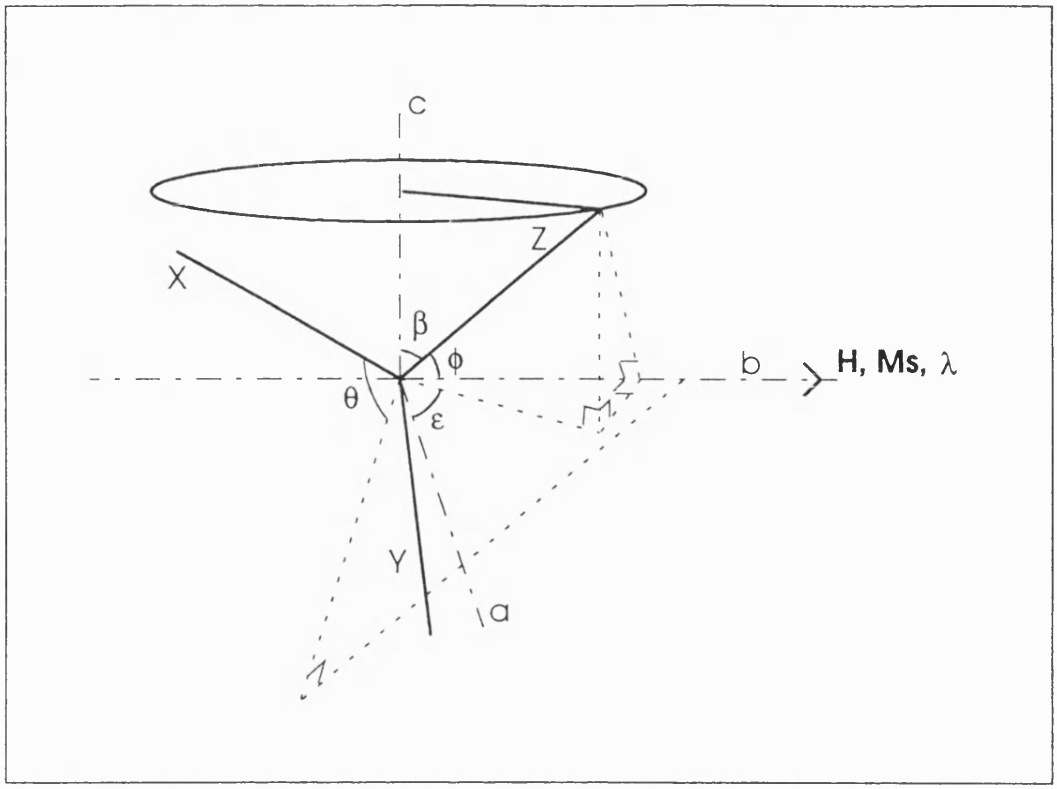

Figure 4.9 Crystal axes XYZ and applied field direction relative to the film plane *ab*. The axes *abc* form an orthogonal set with *c* normal to the film plane and *b* in the direction of the λ_s measurement. One crystal axis, taken as Z(001), is inclined at an angle β to the film normal, *c*, and so may lie anywhere on the cone thus defined. λ_s is measured in the *b* direction in which the saturating field is applied, i.e. in the direction of $\mathbf{M}_s$. The angle φ is the angle between the Z(001) crystal axis and $\mathbf{M}_s$. The angle θ is the angle between the projection of $\mathbf{M}_s$ onto the XY crystallographic plane, and the X axis. The angle ε is the angle between the projection of the Z(001) axis onto the *ab* plane, and the axis *a*.

In the case considered, the crystal axes are the usual <100> set of directions. The resulting values of $\overline{\lambda_s}$ for the textured polycrystal apply when the angle of the Z(001) axis is at a given angle to the film normal and the X(100) and Y(010) axes positions are unknown, and so assumed to be randomly oriented subject to their

being orthogonal to Z(001). Since the crystal system considered is cubic, the three crystal axes are interchangeable and equivalent, so the same results would be obtained if either X(100) or Y(010) were known to be at angle β to the film normal (the other two axes randomly oriented) with λ_s measured in the film plane.

It can be seen from Figure 4.9 that:

$$\cos\varphi = \sin\beta\sin\varepsilon$$
$$\therefore -\sin\varphi d\varphi = \sin\beta\cos\varepsilon d\varepsilon \qquad 4.13$$
$$\sin\varphi = \sqrt{1-\sin^2\beta\sin^2\varepsilon}$$

$\overline{\lambda_s}$ for a textured polycrystalline sample with constant angle β between the Z(001) axis and the film normal *c* can be calculated in a similar way to previously, but the expression 4.12 must be modified. The integral over ϕ may be done either by substituting for φ in terms of ε and β (above) and integrating over ε from 0 to π, or by integrating over φ as before but with new limits (π/2 - β) to (π/2 + β). The latter will be followed here. The multiplying factor must also be altered, as it is not now the full solid angle over which the integration is to be carried out. The new factor, 1/*A*, is found from the following:

$$A = \int_0^{2\pi} d\theta \int_{\frac{\pi}{2}-\beta}^{\frac{\pi}{2}+\beta} d\varphi \sin\varphi \qquad 4.14$$
$$= 4\pi\sin\beta$$

The revised expression to be integrated is thus:

$$\overline{\lambda_s} = \frac{1}{4\pi\sin\beta}\int_0^{2\pi} d\theta \int_{\frac{\pi}{2}-\beta}^{\frac{\pi}{2}+\beta} d\varphi . \lambda_s \sin\varphi \qquad 4.15$$

Substituting for λ_s and including the expressions for α_1, α_2 and α_3 gives:

$$\overline{\lambda_s} = \frac{1}{4\pi\sin\beta}\int_0^{2\pi} d\theta \int_{\frac{\pi}{2}-\beta}^{\frac{\pi}{2}+\beta} d\varphi \left[\begin{array}{l} \lambda_{100}\sin\varphi + \\ 3(\lambda_{111}-\lambda_{100}) \\ \quad \times\{\sin^5\varphi\cos^2\theta\sin^2\theta + \cos^2\varphi\sin^3\varphi\} \end{array}\right] \qquad 4.16$$

Integration of the terms gives the following results:

$$\int_0^{2\pi} d\theta \int_{\frac{\pi}{2}-\beta}^{\frac{\pi}{2}+\beta} d\varphi \sin\varphi = 4\pi\sin\beta \qquad 4.17a$$

$$\int_0^{2\pi} d\theta \int_{\frac{\pi}{2}-\beta}^{\frac{\pi}{2}+\beta} d\varphi \sin^5\varphi \cos^2\theta \sin^2\theta$$

$$= \frac{\pi}{4}\left\{\frac{2}{5}\cos^4\beta\sin\beta + \frac{8}{15}\cos^2\beta\sin\beta + \frac{16}{15}\sin\beta\right\} \qquad 4.17b$$

$$\int_0^{2\pi} d\varphi \int_{\frac{\pi}{2}-\beta}^{\frac{\pi}{2}+\beta} d\varphi \cos^2\varphi \sin^3\varphi$$

$$= 2\pi\left\{\frac{2}{5}\cos^2\beta\sin^3\beta + \frac{4}{15}\sin^3\beta\right\} \qquad 4.17c$$

These integrals were performed analytically, and numerically using Maple V version 2.0a® mathematical software (Waterloo Maple Software).

After integration, the variables remaining are $\cos\beta$, $\sin\beta$, λ_{100} and λ_{111}. The results of this magnetostriction calculation for the case of bcc α-Fe are shown below (Figure 4.10). Values of λ_{100} and λ_{111} were taken from Cullity (1972), to be compared with the experimental value of $\overline{\lambda_s}$ for a random polycrystalline sample of Fe presented there: λ_{100} = +21ppm and λ_{111} = -21ppm, while for the random polycrystalline sample, $\overline{\lambda_s}$ = -7ppm. In the calculation, the random polycrystalline case is reproduced when $\beta = 90°$, for which the calculation yields -4.2ppm.

The case for iron illustrates how the saturation magnetostriction of a sample can change both magnitude and sign, depending on the degree of crystallographic texture in the sample.

The results of the calculation for a particular cubic iron-cobalt alloy are given in Section 5.2.2 along with experimental data from multilayers made using that alloy. Mössbauer spectroscopy was used to find β with the assumption that that represented the (001) axis, after the report from Hall (1960) of the easy axis direction observed in a similar alloy.

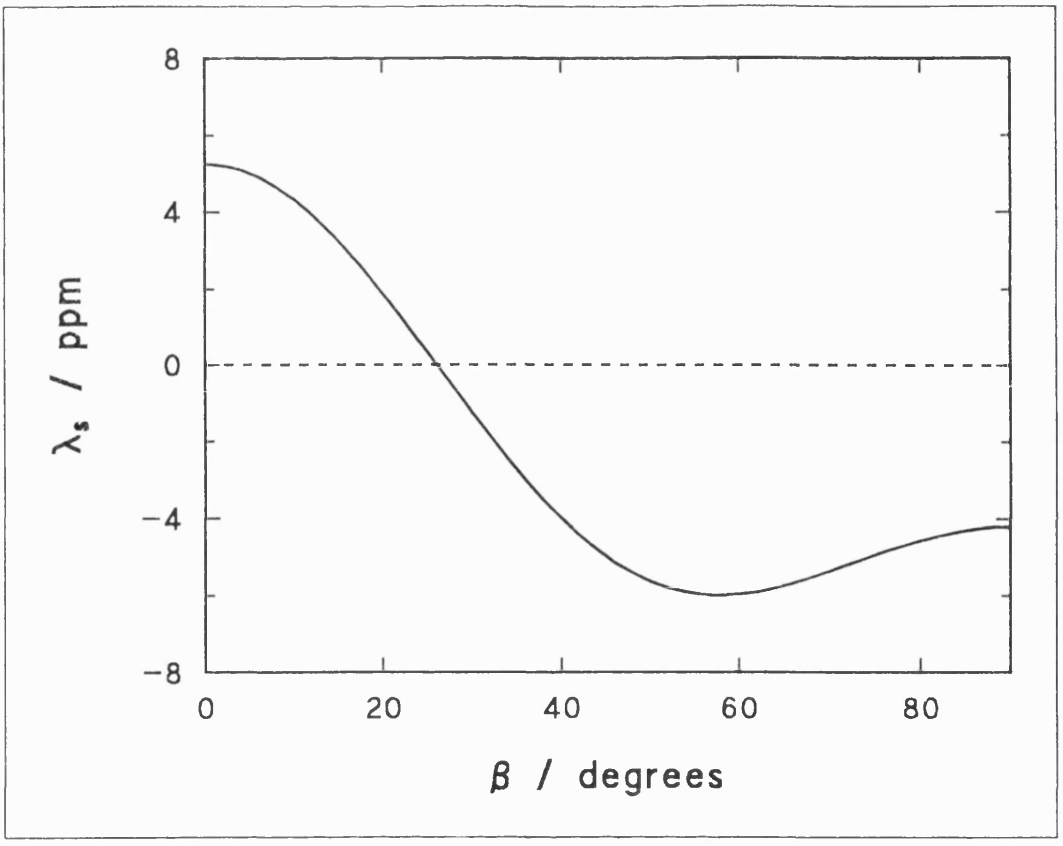

Figure 4.10 Calculated saturation magnetostriction of textured polycrystalline Fe when the Z(001) axis is at an angle β to the normal to the plane in which λ_s is measured, in-plane isotropy assumed.

4.4. Magnetostriction of Multilayer Films

Two phenomenological expressions for the magnetostriction of multilayers have been proposed. Szymczak *et al.* (1988) discuss magnetic/non-magnetic multilayers while the expression of Nagai *et al.* (1989) refers to magnetic/magnetic multilayers. The model of Nagai *et al.* has been extended in this work to apply to magnetic/non-magnetic multilayer systems. The models are detailed in Section 2.4.

5. Results and Discussion

Brief comment is made on some initial investigations, much of which was done in collaboration with Dr. A. P. Thomas. This is followed by a detailed presentation of results on three multilayer systems: two iron-cobalt alloys multilayered with silver, and a cobalt-palladium alloy multilayered with silver. Results on the first Fe-Co alloy/Ag multilayers are compared with those for Fe-Co/Cu multilayers (courtesy Dr. C. Shearwood) and those for films in which particles of Ag were randomly dispersed in the alloy.

5.1. Preliminary Multilayers

To test the deposition system and to make preliminary investigations into magnetic and structural characteristics of some multilayer systems, a few series of multilayers were deposited, starting with systems reported in the published literature. None produced the magnetic softness or the high magnetostriction desired, but practical knowledge was gained from the study of multilayers r.f. magnetron sputtered onto glass and Kapton substrates, as described below.

Ni/Ag (111) textured polycrystalline multilayers were made. These were magnetically hard and could not be saturated in the d.c. magnetometer. The multilayered structure was observed using cross-sectional transmission electron microscopy (TEM) (Figure 5.1, top), although some damage to the thin section appears to have occurred during the preparation. X-ray diffraction (XRD) satellite peaks around the Ag (111) peak of heat-treated samples (see Section 3.5) confirmed the multilayer structure. The layer thicknesses observed with the TEM and by the position of the XRD satellites were in agreement. Discontinuous rings in the selected area electron diffraction image confirmed the XRD result that the Ni/Ag multilayer had a textured polycrystalline structure (Figure 5.1 bottom).

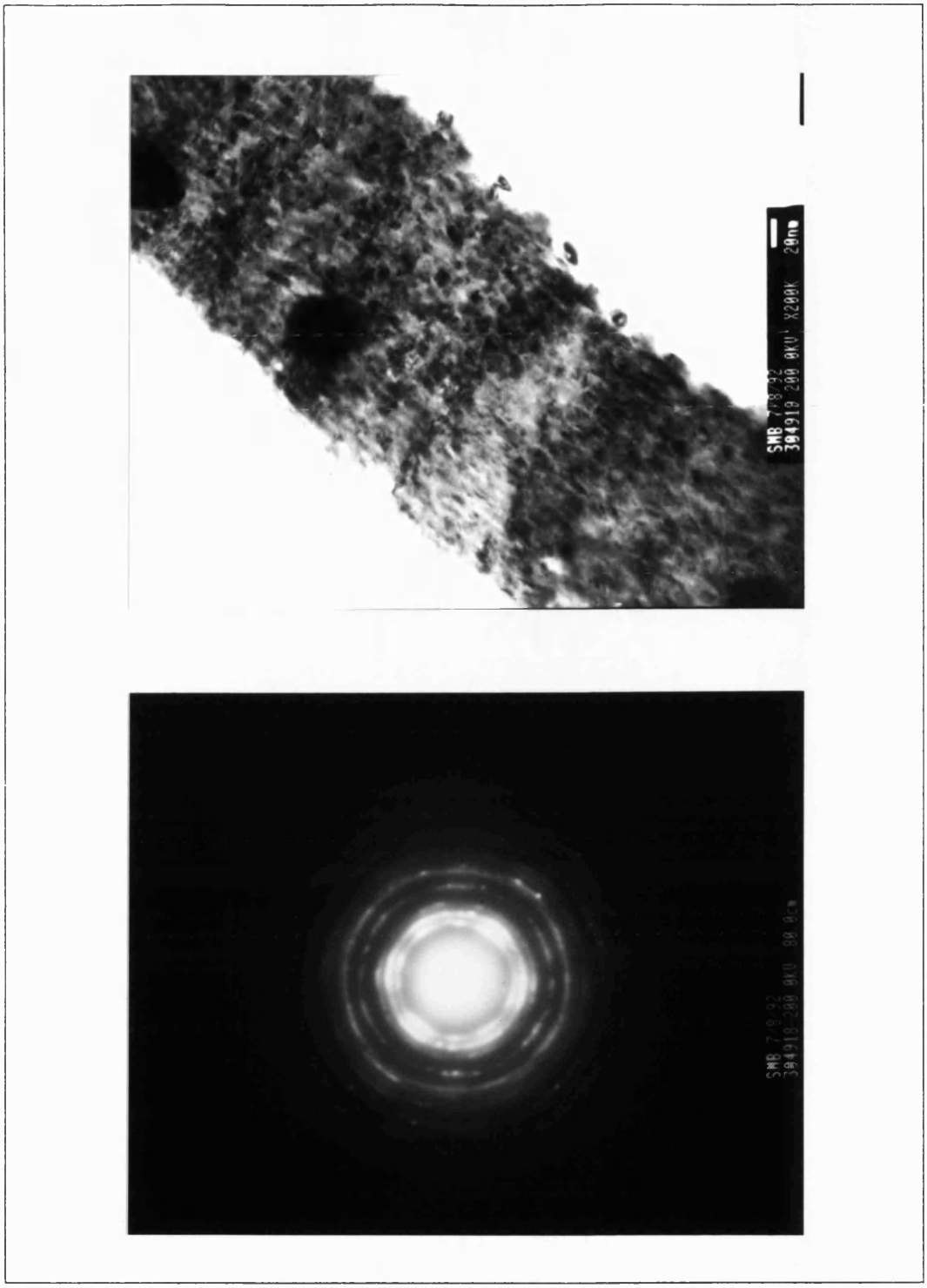

Figure 5.1 Transmission electron micrograph (top: magnification is ×200 000) and selected area electron diffraction image (bottom) of a Ni/Ag multilayer on glass. The rough film top surface and cross-section surface in the TEM image are due (at least in part) to the handling during sample preparation.

Two series of Fe/Co multilayers were fabricated, with either t_{Fe} = 2-20nm, t_{Co} = 2nm (fixed) or t_{Fe} = 5nm (fixed), t_{Co} = 2-10nm. XRD satellite peaks were observed when the number of bilayers deposited was sufficient to give good coherency of scattered X-rays, and the layers were thick enough to give clear periodicity. The multilayers showed bcc structure, with peaks close to those for pure α-Fe. In assessing texture, therefore, reference was made to the standard α-Fe pattern. Although Kapton is amorphous, the XRD trace showed three strong, broad peaks ($\Delta 2\theta \approx 2°$) on top of the diffuse peak ($\Delta 2\theta \approx 20°$) due to its amorphous nature (Figure 5.2).

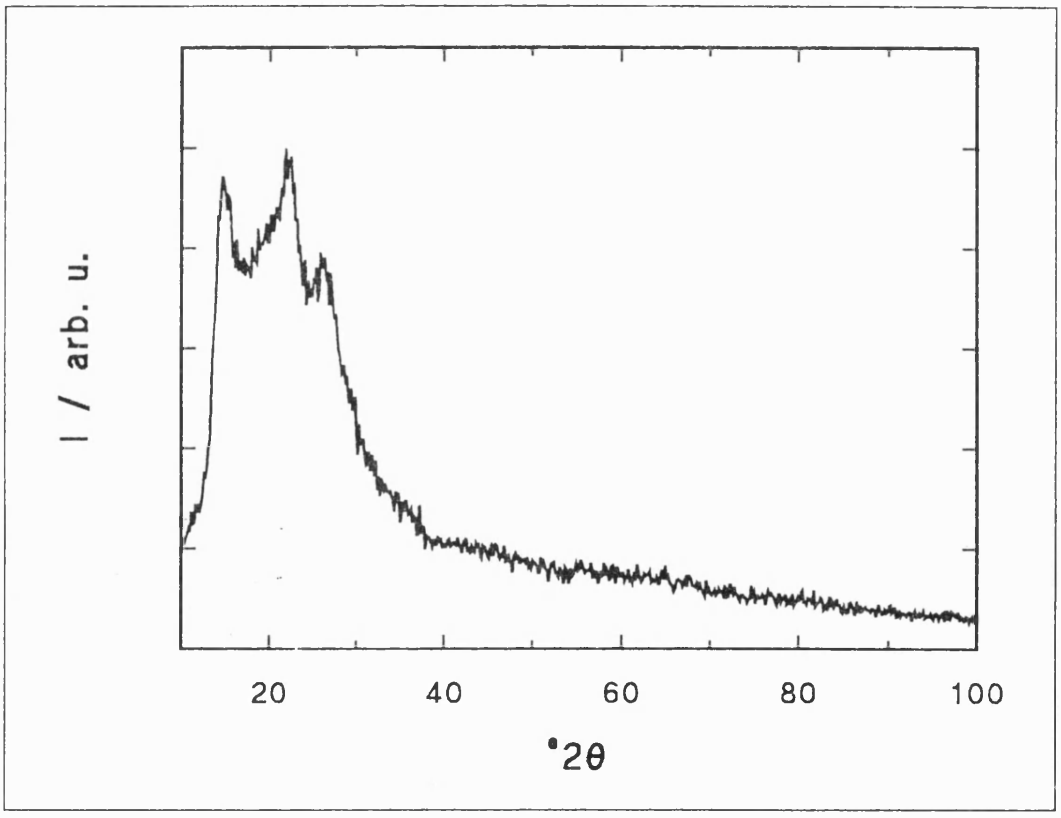

Figure 5.2 X-ray diffraction scan of 26μm thick Kapton polyimide, used as a substrate for the multilayers.

The XRD peaks for Kapton corresponded to d-spacings of 0.599nm, 0.400nm and 0.340nm, which are, respectively, 3.0, 2.0 and 1.7 times the bulk α-Fe (110) d-spacings. This may account for the stronger (110) texture observed in the polycrystalline Fe/Co multilayers deposited on Kapton, while those on glass substrates showed no strong crystallographic texture (Figure 5.3). A plain 195nm Fe film on glass showed strong (200) texture; the Co layers appear to have interrupted the textured growth of Fe.

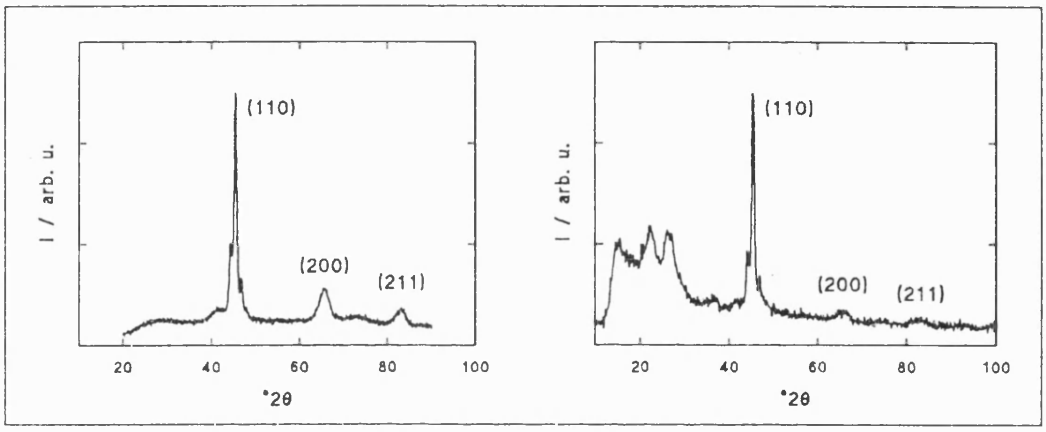

Figure 5.3 XRD patterns of 100(5nm Fe/5nm Co) on Corning 7059 glass (left) and Kapton (right) where the scattering due to the Kapton substrate is clearly observed at 2θ less than about 30°. The satellites around the (110) peaks correspond to a periodicity of 5nm, which reflects the individual layer thicknesses here, since $t_{Fe} = t_{Co}$.

The Fe/Co films could not, in general, be saturated in the d.c. magnetometer ($H_{max} \approx 10 kAm^{-1}$ at this stage); the coercive fields found from the minor loops were higher than the H_c values found in the literature. Squarer MH loops were obtained for multilayers deposited on glass than on Kapton. This was attributed to stress in the films, which was partially accommodated by the Kapton substrate, while the glass held the film rigidly. The published observations that thicker Fe

layers and thinner Co layers gave softer films (see Section 2.4.1) were confirmed. For example, the coercive field for 25(5nm Fe/2nm Co) was 3.6kAm^{-1} while for 25(20nm Fe/2nm Co) it was 1.7kAm^{-1}. The loop obtained for 25(5nm Fe/10nm Co) was too hard and noisy to be able to extract a meaningful coercive field. Annealing was carried out under rough vacuum at 200°C to 350°C for lengths of time up to several hours. These temperatures were chosen following published experiments, e.g. Senda and Nagai (1989a) (see also Section 2.4). On the XRD traces, satellite peaks gradually disappeared as Fe and Co atoms interdiffused at the interfaces. The multilayers were rendered saturable in the d.c. magnetometer and H_c was reduced to a few hundred Am^{-1}. For the multilayer 50(5nm Fe/5nm Co), the coercive field in the as-deposited state was more than 6kAm^{-1}, which reduced to 0.35kAm^{-1} after annealing at 200°C for 4 hours. Further annealing, to a total of 7 hours, did not improve H_c further. The time required for changes in properties was longer for the lower temperature treatments. Following these annealing studies, and some on Fe/Co/Fe/Ag multilayers, anneals were generally carried out at 300°C because the time-scale for reduction of the coercivity was several tens of minutes. Heating over such lengths of time is readily controlled. SAMR measurements were carried out on only the 50(2nm Fe/2nm Co) multilayer (other multilayers required fields larger than those attainable in the SAMR apparatus). A saturation magnetostriction of $\lambda_s \approx +24$ppm was found. This is higher than published values (see Figure 2.6 in Section 2.4.1).

Fe/Ag multilayers were deposited with $t_{Fe} = t_{Ag} = 1$nm to 5nm. Magnetostriction values ranged from +0.4ppm to +4.7ppm (larger values for thinner t_{Fe}). This is possibly a crystallographic texturing effect, although this is unconfirmed. As discussed in Chapter 2, saturation magnetostriction constants are different along different crystallographic axes, so the magnetostriction of a textured polycrystalline multilayer may differ from that of a random polycrystalline film.

The coercivities of the Fe/Ag multilayers ranged from 2.0kAm^{-1} to 0.5kAm^{-1} with higher H_c for thicker t_{Fe}.

It was observed in Ni/Ag multilayers that the Ag layer was more likely to strain than the Ni layer. This was assessed on the basis of XRD peak positions. The Ni (111) spacings (for planes parallel to the film plane) were strained up to +1% for thin t_{Ni}, falling sharply to zero strain for $t_{Ni} > 5$nm. The Ag (111) planes were strained by -4% to -1% independent of t_{Ni}. Fe/Mo multilayers were then deposited with $t_{Fe} = t_{Mo} = 1$nm to 5nm in an attempt to force the magnetic layer to strain. Molybdenum has a higher Young's modulus than Ag: $E_{Mo} = 335$GPa, $E_{Ag} = 76$GPa, while $E_{Fe} = 212$GPa, $E_{Ni} = 202$GPa (Tottle (1984)). The Fe/Mo multilayers did not display clear hysteresis loops in the d.c. magnetometer, however. The loops were slightly open. The signals were low and noisy, indicative of a poor magnetic signal; a reduced magnetic moment in the interface region has been suggested by Ge *et al.* (1991) in r.f. sputtered Fe/Mo multilayers. In bulk form, Mo and Fe both take the bcc structure. The Fe/Mo multilayers formed polycrystalline body-centred cubic structures, and the XRD patterns, with satellite peaks, evolved with layer thickness in a similar way to those observed by Khan *et al.* (1983) for their Mo/Ni superlattices. The complexity of the traces hindered assessment of the crystallographic strain.

Fabricating and measuring these preliminary multilayers built confidence in using the sputtering machine and equipment used to characterise the films. It was demonstrated that multilayered films could be produced on both glass and Kapton substrates, and that different crystallographic textures could be obtained on the different substrates, although both were nominally amorphous. This meant that XRD information from samples on glass could not be used to correlate with magnetic measurements taken on samples prepared on Kapton. The rigid glass

also tended to keep the films stressed, whereas the Kapton could flex to accommodate this partially. In taking XRD traces, it was found that larger numbers of bilayers were required if satellite peaks were to be observed; more magnetic material also increased the signal-to-noise ratio for magnetic measurements. In measuring MH loops of many of these preliminary multilayers, it was found that the maximum field available was insufficient to saturate the samples. As the project developed, the magnetometer was improved to give higher H_{max}. The materials examined did not show high λ_s and so further studies proceeded using alternative component layers.

5.2. Iron-Cobalt/Silver Multilayers

Iron-cobalt alloys were selected because they have saturation magnetostriction values in the random polycrystalline form which can be larger than those attainable in the corresponding random polycrystalline single elements. Two commercially available alloys were used for the Fe-Co targets: HiSat50 (50%Fe, 50%Co with less than 0.2%Ta) and Permendur24 (75%Fe, 24%Co, 0.6%Cr). These were supplied by Telcon Ltd., U.K. The trace elements were present to improve the mechanical strength and enhance the saturation magnetisation.

Experimental values of saturation magnetostriction, λ_s, for similar Fe-Co alloys were read from graphs presented by Bozorth (1951). Bozorth quotes data from Williams (1932). The structure of the samples is not known, but is likely to have been polycrystalline, although possibly with some crystallographic texture induced in the production process. Analysis of impurities present is not given, nor is the strength of the field in which the measurements were taken, although it is stated that the data are saturation magnetostriction constants. The λ_s values are about +65ppm and +39ppm, for the HiSat50 and Permendur24 cases respectively. Williams' λ_s values are affected by about ±1% and ±20%, respectively, for

compositions within ±5% of the nominal. Values of λ_s were also calculated from the engineering magnetostriction data, which Bozorth quotes from Masiyama (1932). Assuming $\lambda_e = \lambda_e^{max}$ and using $\lambda_s = 2\lambda_e^{max}/3$, lower values of λ_s are obtained: +45ppm ($\lambda_e \approx$ 68ppm) and +23ppm ($\lambda_e \approx$ +35ppm), respectively. That these values are lower indicates that the samples were not saturated (so $\lambda_e \neq \lambda_e^{max}$), but the data were taken at fields of 1100G = 87.5kAm^{-1}, which are of the same order as those used in the SAMR apparatus used to measure λ_s in this work.

By electron probe microanalysis, the composition of films sputtered from the HiSat50 target was found to be 45wt.%Fe, 55wt.%Co with approximately 0.2wt.%Ta. The variation between measurements for Fe and Co on different films and sample sections was 0.2%, while the average error on a measurement was 1.8%. By analogy, the composition of films sputtered from the Permendur24 target was 72wt.% Fe, 28wt.%Co (this calculation does not take Cr content into account). These compositions would be expected to have λ_s = +66ppm and λ_s = +39ppm, respectively. From the λ_e data, $\lambda_s \approx$ +47ppm ($\lambda_e \approx$ +70ppm) and $\lambda_s \approx$ +27ppm ($\lambda_e \approx$ +40ppm), respectively.

Values of $\overline{\lambda_s}$ for random polycrystalline samples were calculated from the expression given by Cullity (1972) and using the values of λ_{100} and λ_{111} for single crystal Fe-Co alloys read from Hall (1960) for compositions like those of HiSat50 and Permendur24 in the as-deposited state. Hall does not disclose the field at which the measurements were taken, although it is stated that the saturation magnetostriction constants were measured. The following values were obtained: for HiSat50, random polycrystalline $\overline{\lambda_s}$ = +84±4ppm (λ_{100} =+154ppm, λ_{111} = +38ppm) and for Permendur24, $\overline{\lambda_s}$ = +42±4ppm (λ_{100} =+89ppm, λ_{111} = +11ppm). The errors are given based on the estimated error of ±4ppm for reading the data from the original figure. These values are higher than the experimental results of Williams and much higher than values deduced from Masiyama's data, both cited

by Bozorth. In the figures below for the Fe-Co/Ag multilayers, the experimental λ_s data on polycrystalline samples (Williams') and the values calculated from Masiyama's λ_e results will be used for comparison; the latter, because the data were taken in fields of the same order as those attainable in the SAMR apparatus. Comment will be made with reference to the values calculated from the magnetostriction constants of Hall. The assumptions underlying the calculation of $\overline{\lambda_s}$ of random polycrystalline materials have been shown to be inadequate in many cases, giving limited applicability of the results (see Section 4.3).

5.2.1. HiSat50/Ag Multilayers

The multilayers were sputtered at 75W, P_{Ar} = 5mtorr onto 26μm thick Kapton substrates. The background pressure was 3-6×10^{-7}torr. Two main series were deposited: t_{Ag} = 2nm fixed, with $t_{HiSat50}$ = 2nm to 12nm; and $t_{HiSat50}$ = 12nm fixed, with t_{Ag} = 0 to 10nm. For the series with t_{Ag} fixed, 50 bilayers were deposited on each side of the substrate (except $t_{HiSat50}$ = 12nm: 25 bilayers); for the series with fixed $t_{HiSat50}$ there were 25 bilayers each side. There were no buffer or capping layers. HiSat50 was the first layer deposited and Ag the last. A film was also made of 600nm plain HiSat50 on one face of the Kapton. Measurements were taken on multilayers in the as-deposited state and after annealing for 30 minutes at 300°C in a flow of forming gas. In calculating λ_s, the saturation induction and Young's modulus of HiSat50 were used (2.44T and 230GPa - from manufacturer's data sheet). This seemed reasonable considering that the alloy composition was little changed in the film from that of the target, and also since Ta was present. If a Young's modulus value of E ≈ 205GPa for a Fe-Co alloy of similar composition was taken from Honda (1919), the λ_s result was not altered beyond the experimental error bars. Faraday balance data showed that all the multilayers had the same saturation magnetisation within experimental error.

Some representative XRD traces are shown below (Figure 5.4). The Fe-Co alloy layers in the multilayers are polycrystalline with a body-centred cubic structure and are not appreciably textured (comparison was made to the trace of bulk bcc α-Fe, since this alloy is bcc with lattice parameters similar to α-Fe). Diffraction peaks from fcc Ag (other than the Ag (111) peak) generally fall on top of the bcc peaks, so it is not possible to say whether the Ag is textured. Satellite peaks were not seen around the main peak, indicating that the alloy-silver interfaces were rough. This conclusion was supported by low-angle XRD (Donovan (1993)), which also showed that the multilayering was present, and kinematic modelling (Harrell and Sharp (1993)). It is likely that the Ag layers were not continuous for $t_{Ag} < 5$-6nm (Chopra and Randlett (1968)).

The broad peak(s) around $2\theta = 20°$-$30°$ are from the Kapton substrate. Peaks due to Ag appear for sufficiently large proportions of Ag. For bulk single crystal fcc Ag, the peak positions expected are: (111) $2\theta = 38.15°$; (200) $2\theta = 44.32°$; (220) $2\theta = 64.48°$; (311) $2\theta = 77.55°$; (222) $2\theta = 81.62°$.

Using the d-spacings of the plain HiSat50 film and of bulk Ag, the nearest neighbour distances were found for the (110) and (111) planes, respectively. These figures were used to calculate the lattice mismatch between the two species: 4.5%. This is rather large to be expected to be accommodated only by lattice strain at the interfaces. Dislocations may occur.

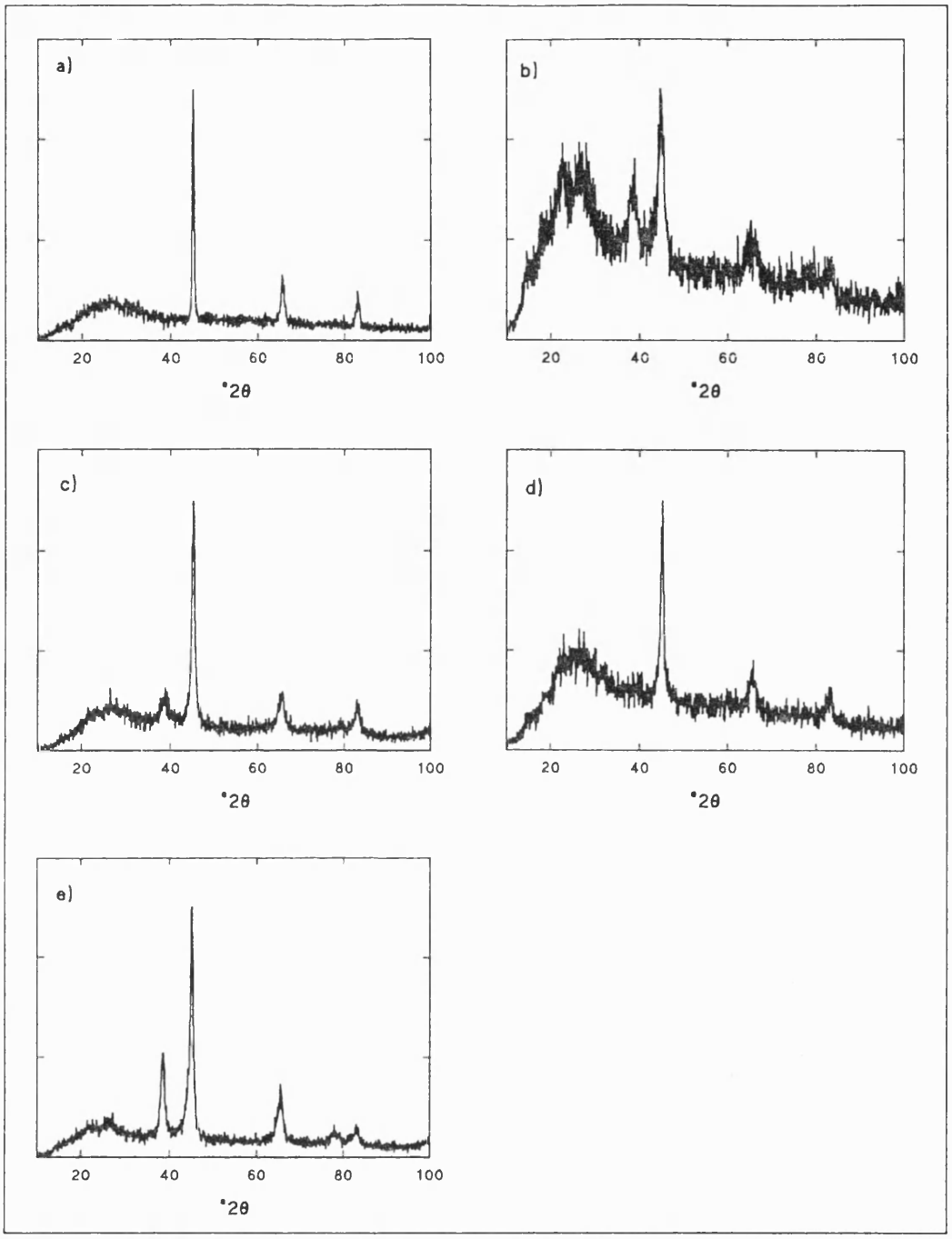

Figure 5.4 X-ray diffraction scans of HiSat50/Ag multilayers on Kapton substrates. Vertical scales are diffracted intensity in arbitrary units (linear scale): each pattern has been normalised to the height of its most intense peak. a) 600nm HiSat50; b) 2×50(4nm HiSat50/2nm Ag); c) 2×50(8nm HiSat50/2nm Ag); d) 2×25(12nm HiSat50/2nm Ag); e) 2×25(12nm HiSat50/6nm Ag).

The peak positions and widths were obtained by fitting each peak using the X-ray diffractometer software. From the peak positions, the average plane spacings were calculated, and the peak widths were used to estimate the grain sizes in the films by the Scherrer equation (Guinier (1963) - see Section 3.5.1). See Figures 5.5 and 5.6. The lattice planes referred to are those which are parallel to the substrate surface, so the spacings are in a direction perpendicular to the substrate. Expansion or contraction of the plane spacings in one sense does not necessarily imply the reverse in an orthogonal direction, as Jankowski (1992) has found.

Trends in lattice plane d-spacings with layer thickness are weak, but, in general, the spacings tend toward the bulk values (the value for the thick film, in the case of d_{110} for HiSat50) as the layer thickness increases. When t_{Ag} = 2nm (fixed), there is a trend towards larger grain sizes, calculated from both bcc (110) and Ag (111) peaks, as the HiSat50 layer thickness increases. For fixed $t_{HiSat50}$ = 12nm, however, the grain size is approximately independent of t_{Ag} except for $t_{Ag} < 2$nm. The largest grain sizes (about 18-20nm) are seen in the plain HiSat50 film. Annealing generally increased the grain size but had no clear effect on the d-spacings.

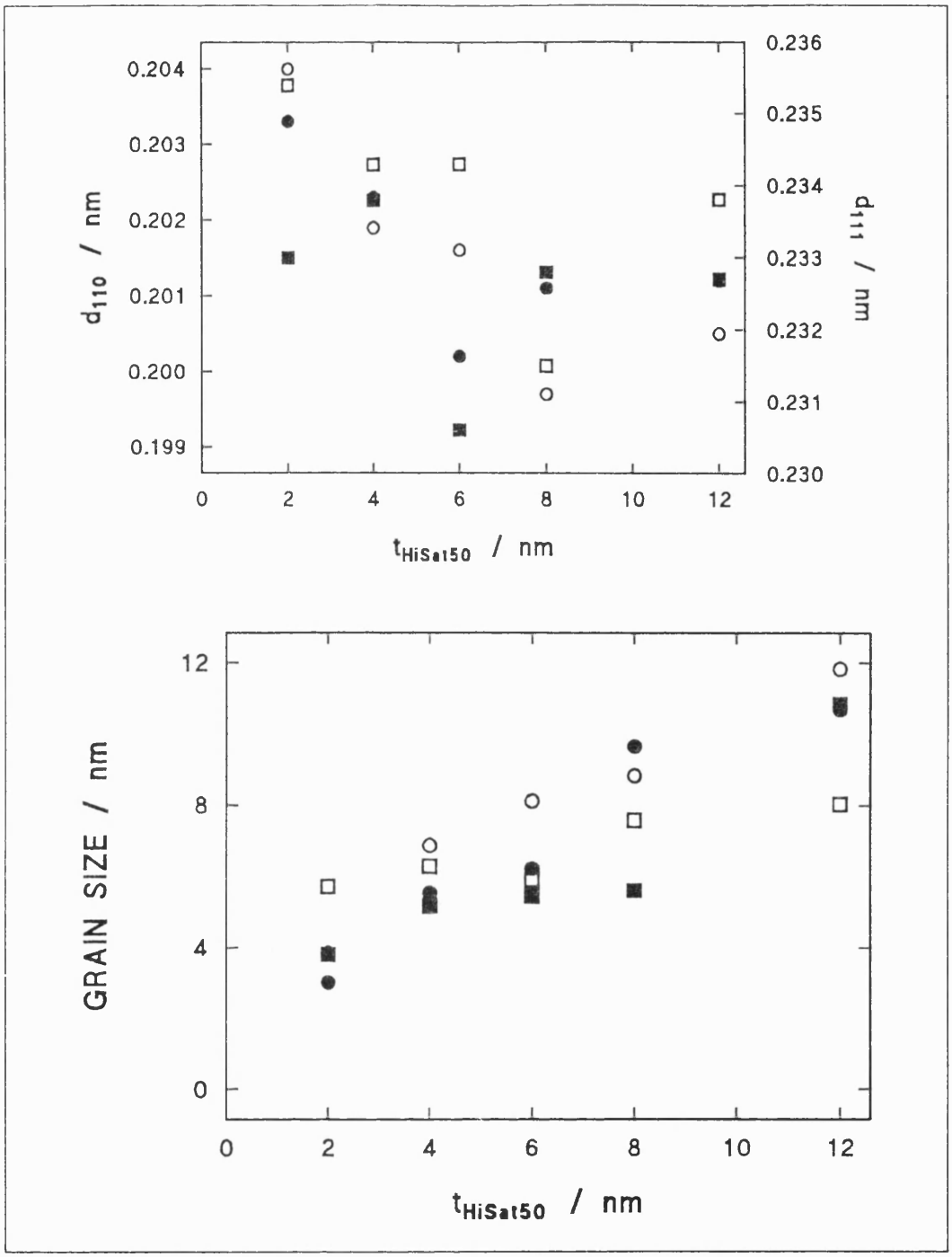

Figure 5.5 Lattice plain spacings (top) and grain sizes (bottom) for HiSat50/Ag multilayers with fixed t_{Ag} = 2nm. Data from Fe-Co (110) peaks from ● as-deposited multilayers and ○ annealed; from Ag (111) peaks from ■ as-deposited and □ annealed samples. For bulk Ag, d_{111} = 0.2359nm. From the thick HiSat50 film, bulk d_{110} = 0.20137nm.

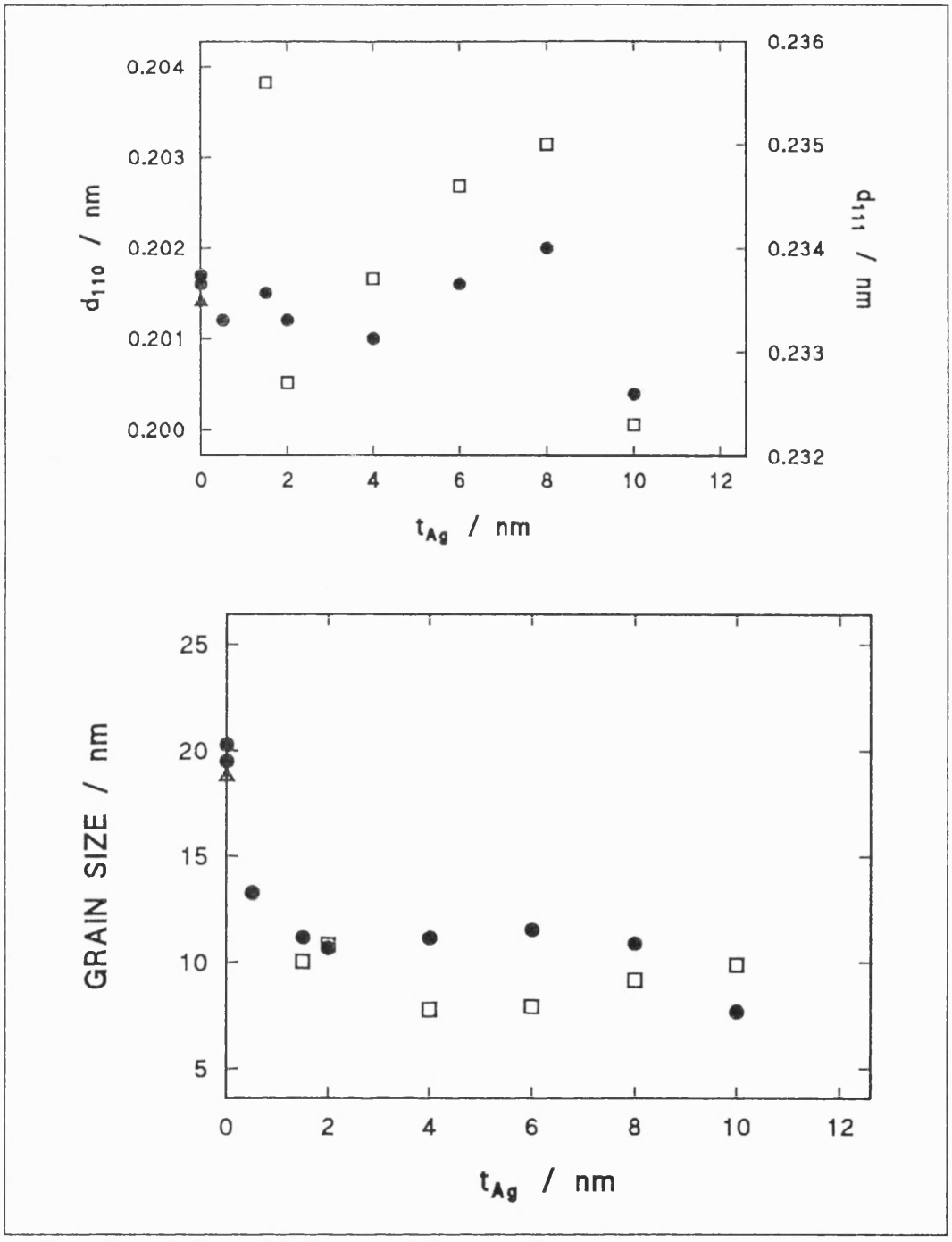

Figure 5.6 Lattice plain spacings (top) and grain sizes (bottom) for HiSat50/Ag multilayers with fixed $t_{HiSat50}$ = 12nm. Data from ● Fe-Co (110) peaks, □ Ag (111) peaks and Δ (110) peak of the plain 600nm HiSat50 film (d_{110} = 0.20137nm). All as-deposited multilayers. For bulk Ag, d_{111} = 0.2359nm.

The magnitude of the grain sizes has been confirmed by high-resolution TEM through the thickness of the film by Heyderman (1994). A single layer of 48nm HiSat50 was grown on top of a 2nm Ag layer on an amorphous silicon nitride substrate, and also a multilayer of 4(2nm Ag/12nm HiSat50) on an identical substrate. The multilayer was grown to mimic a film from the HiSat50/Ag multilayer series discussed above, and the film was deposited to contain the same total thickness of magnetic material. The same results were obtained from both samples. The grain size was shown to be about 9nm. Selected area electron diffraction indicated that there was isotropy of crystallographic orientation in the plane of the film. The central ring was indexed as Ag (111), any further rings from Ag being either too faint to see, or masked by rings from HiSat50. All rings corresponding to a bcc structure were present, with lattice parameters within approximately 2% of those of bulk α-Fe. Tilting the sample with respect to the electron beam showed that there was no texturing perpendicular to the sample plane. Differential phase contrast electron microscopy was then performed on the samples after they had been demagnetised from fields applied in different directions. There was no magnetic anisotropy in the film plane, and domain walls were observed to be separated by a distance of the order of 10μm - much greater than the grain size. Small cross-tie domain walls were seen, giving indirect support to the proposal that an Ag layer 2nm thick gives incomplete coverage. See Figure 5.7.

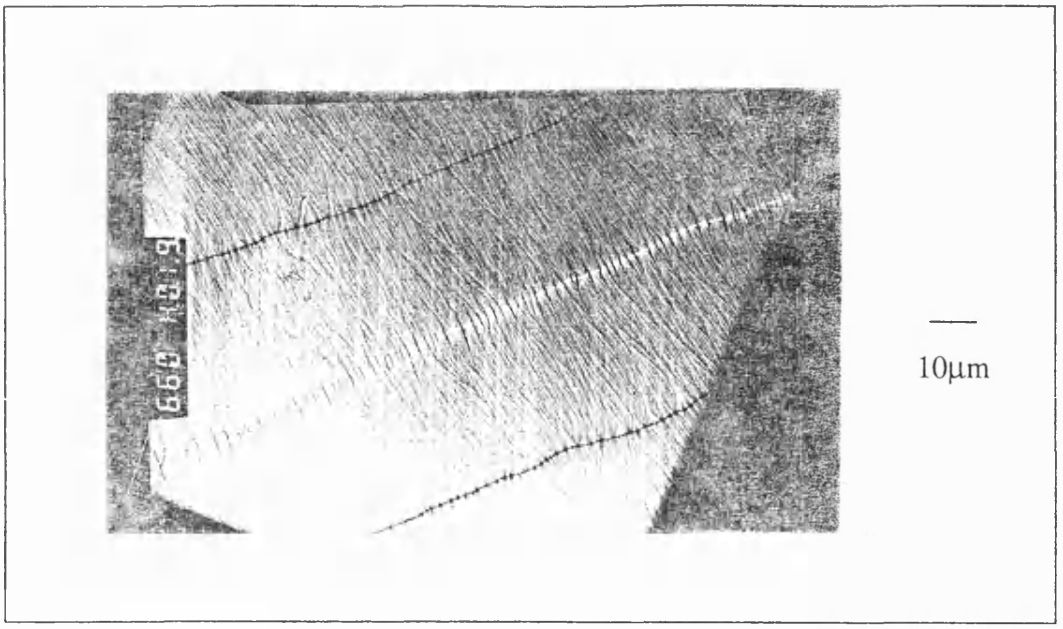

Figure 5.7 Domain image obtained by differential phase contrast electron microscopy on (2nm Ag/48nm HiSat50) on a silicon nitride substrate. Courtesy Dr. L. Heyderman, Glasgow University.

Figure 5.8 shows a selection of hysteresis loops from the multilayer series. The loop squareness is not strongly correlated with the layer thickness, but squareness is also affected by film stress which may not be the same for each. Annealing generally left the loop squareness the same or reduced it slightly for the series with t_{Ag} = 2nm. Films containing larger quantities of silver gave similar or slightly squarer loops on annealing. The plain 600nm HiSat50 film could not be saturated in the d.c. magnetometer. The coercive field of this film was measured on reducing the applied field from H_{max} = 22kAm^{-1}. As-deposited, it had a coercive field of 6.6kAm^{-1}. This was reduced to 4.2kAm^{-1} on annealing. The coercivities would be higher than these values.

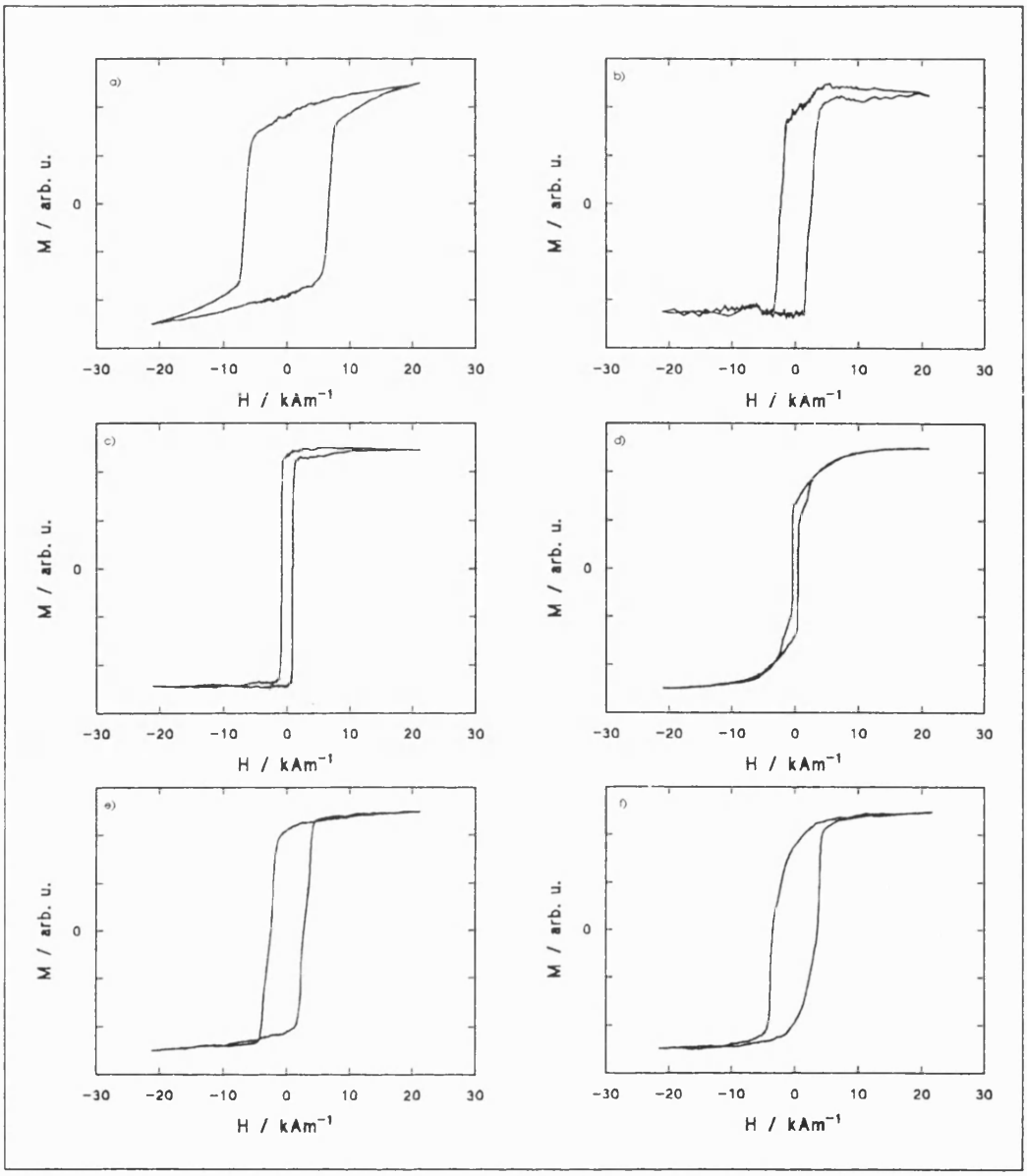

Figure 5.8 MH loops of HiSat50/Ag multilayers on Kapton substrates. a) 600nm plain HiSat50 film; b) 2×50(2nm HiSat50/2nm Ag); c) 2×50(6nm HiSat50/2nm Ag); d) 2×25(12nm HiSat50/2nm Ag); e) 2×25(12nm HiSat50/6nm Ag); f) 2×25(12nm HiSat50/10nm Ag). Shape factor b = 0.9, except (e) and (f), for which b = 0.8.

For some samples, the variation of M with H was not smooth, and there appeared to be two switching fields. This was thought to be due to

inhomogeneities in the film composition. There might be two "phases" with different magnetic characteristics, e.g. an iron-rich phase and a cobalt-rich phase. The same might be observed if the thickness of the deposits were substantially different on the two sides of the substrate (which might occur if the repositioning of the substrate prior to the second deposition was inaccurate) or if film stress levels were different on the two sides. These would cause the films on the two faces of the substrate to switch at different applied fields. Annealing reduced or removed the "double loop" effect. Annealing would be expected to promote interdiffusion between Fe and Co atoms but to sharpen interfaces with Ag, as Ag is immiscible with Fe and Co, and also to reduce film stress. This supports the suggestion that there are differential stresses in the samples, or two phases in the alloy layers, rather than different thicknesses on the two faces of the substrate. Figure 5.9 shows the effect of annealing on a 2×50(4nm HiSat50/5nm Ag) multilayer.

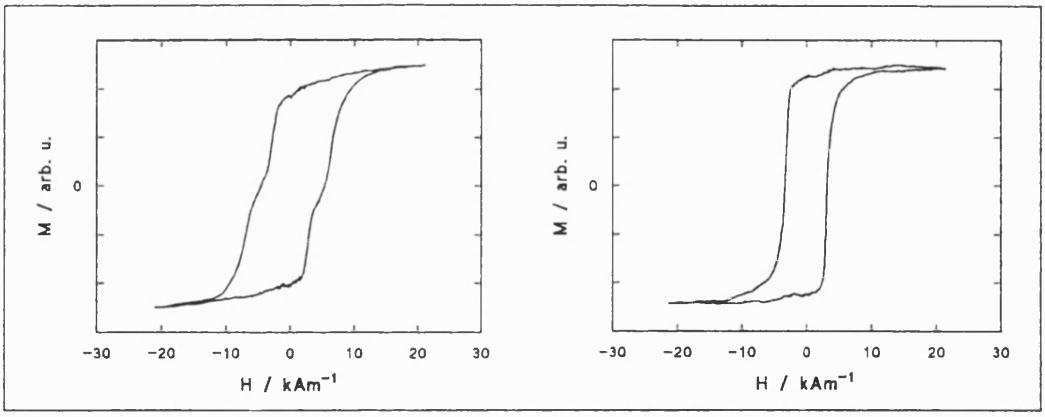

Figure 5.9 MH loops of 2×50(4nm HiSat50/5nm Ag) as-deposited (left) and annealed (right).

Other workers have observed "double loops" in sandwich structures consisting of two magnetic layers separated by a single non-magnetic layer, e.g. Haga *et al.*

(1993) working on d.c. sputtered Fe/Ag and Fe/Ta; Köbler *et al.* (1992), epitaxial Fe/Cr/Fe on GaAs(100), with the Cr layer wedge-shaped; Grünberg *et al.* (1991), various epitaxial wedge-shaped sandwich structures; and Fuß *et al.* (1992), Fe/Al and Fe/Au grown epitaxially by UHV electron gun evaporation. Haga *et al.* attribute the two steps in the MH loop to the two Fe layers which were separated by such a thickness of Ta as to prohibit any interaction between them (160nm in the example given). The other researchers explain the loop shapes for different interlayer thicknesses (i.e. at different positions along the wedge) by the degree of coupling between the magnetic layers, and the extent to which the magnetisation vectors are aligned. Köbler *et al.* and Grünberg *et al.* fit experimental data for Fe/Cr/Fe with theory. Epitaxial growth techniques result in cleaner interfaces than in sputtered films. The coupling effects between magnetic layers in a multilayer with rougher interfaces would be expected to be more complex in description. The number of steps in the loops of Fuß *et al.* depended on the interlayer thickness, being only one step for t_{Al} = 0.4nm, and two to three steps as the Al thickness increased to 0.9nm.

Coercivities for the series with t_{Ag} = 2nm (fixed) are plotted in Figure 5.10. Annealing left H_c unchanged or slightly reduced, except for $t_{HiSat50}$ = 2nm, for which H_c increased sharply. Each multilayer in the series had a lower coercivity than the plain HiSat50 film. The lowest H_c values in this multilayer series were for 2×25(12nm HiSat50/2nm Ag): 450Am^{-1} as-deposited, reduced to 340Am^{-1} after annealing.

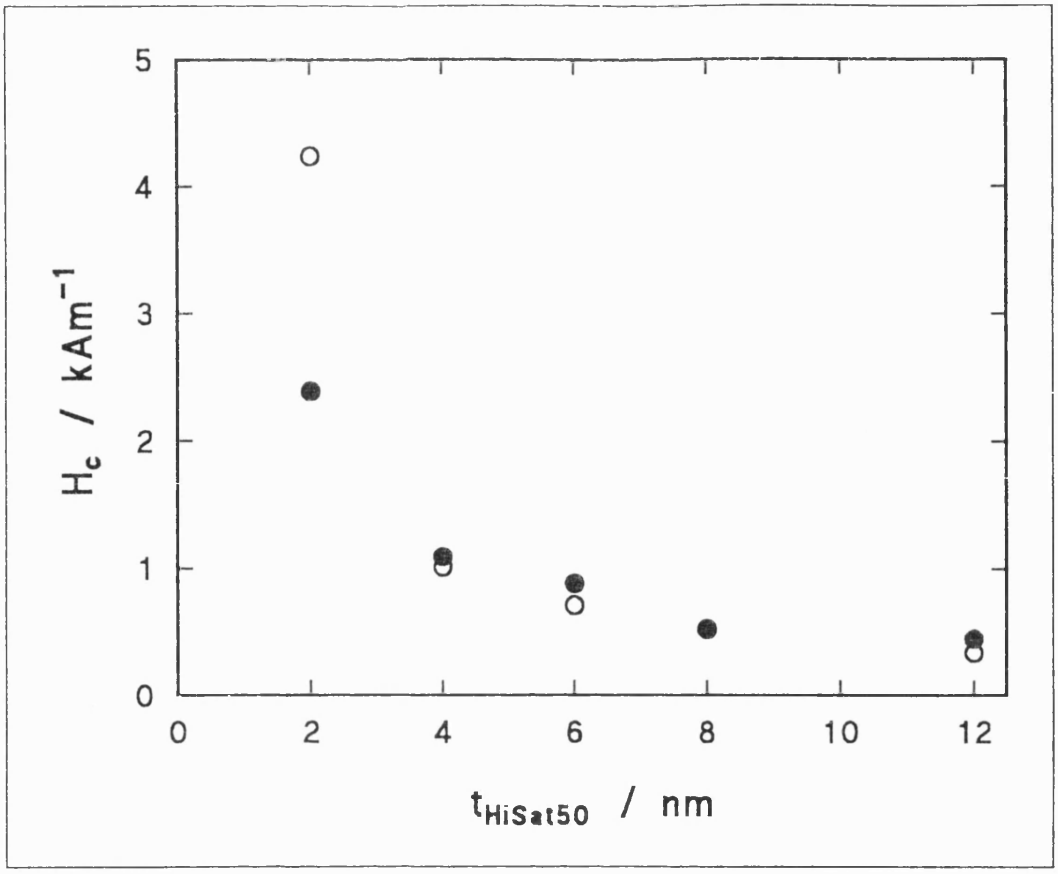

Figure 5.10 Coercivity of HiSat50/Ag multilayers on Kapton with t_{Ag} = 2nm. ● As-deposited, O annealed.

The coercivity is correlated with the inverse of the estimated HiSat50 grain size (Figure 5.11). Larger grains resulted in lower coercivity in the multilayers although the largest grains observed were in the plain HiSat50 film, for which H_c was highest (coercive field 6.6kAm^{-1} as-deposited, with grain size 18nm, reduced to 4.2kAm^{-1} on annealing, with grain size 20nm). It is unclear whether the correlation is significant, in the light of Heyderman's results which show the magnetic domains in the films to be orders of magnitude larger than the grains.

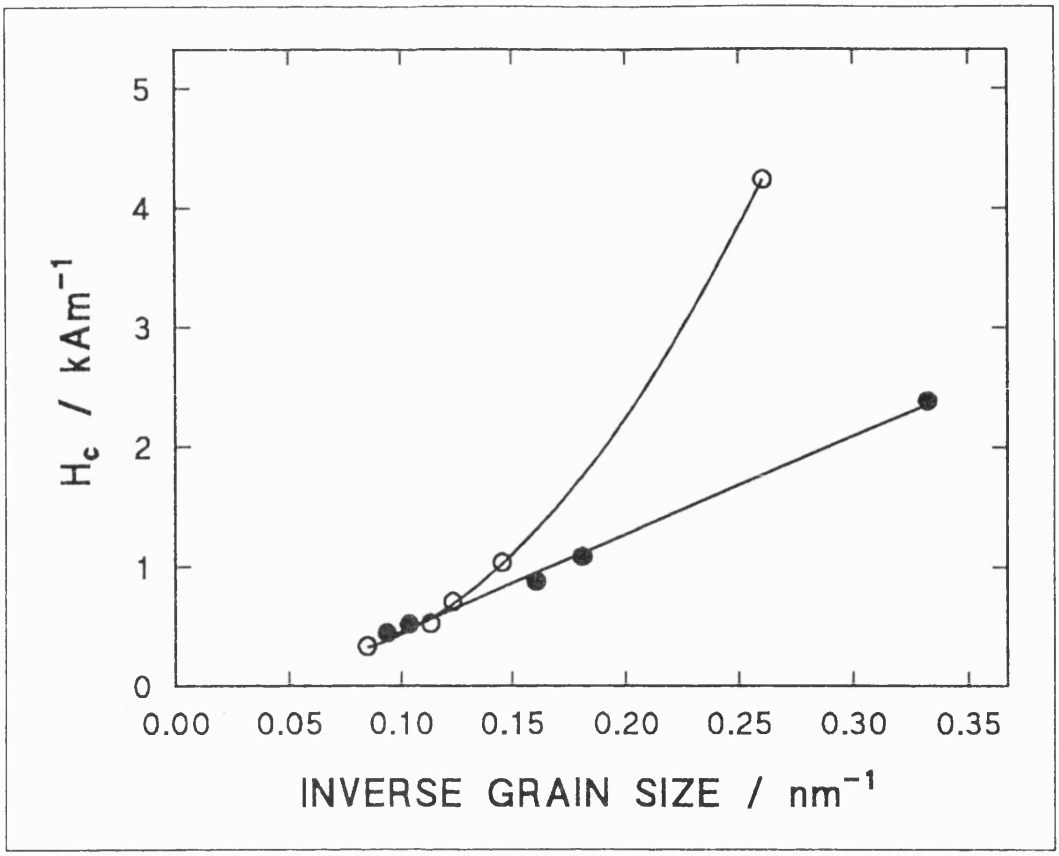

Figure 5.11 Coercivity vs. inverse (110) grain size for multilayers only (t_{Ag} = 2nm). ● As-deposited (regression line shown), ○ annealed (2nd order polynomial fit shown to guide the eye).

For the series with fixed $t_{HiSat50}$ = 12nm, H_c is plotted in Figure 5.12. The coercivity minimum occurs for t_{Ag} = 1.5-2nm. The points at t_{Ag} = 0 are from films made by interrupting the HiSat50 growth. In one case (with the lower H_c values) the plasma was struck over the Ag target but the shutter remained to prevent deposition. The plasma was not struck in the other case. Neither film was quite saturable in the d.c. magnetometer, so these H_c values are underestimated. Annealing reduced H_c in all cases. No correlation of H_c with grain size was found, using either the bcc (110) or the Ag (111) peaks to estimate the grain size (compare Figure 5.4 above).

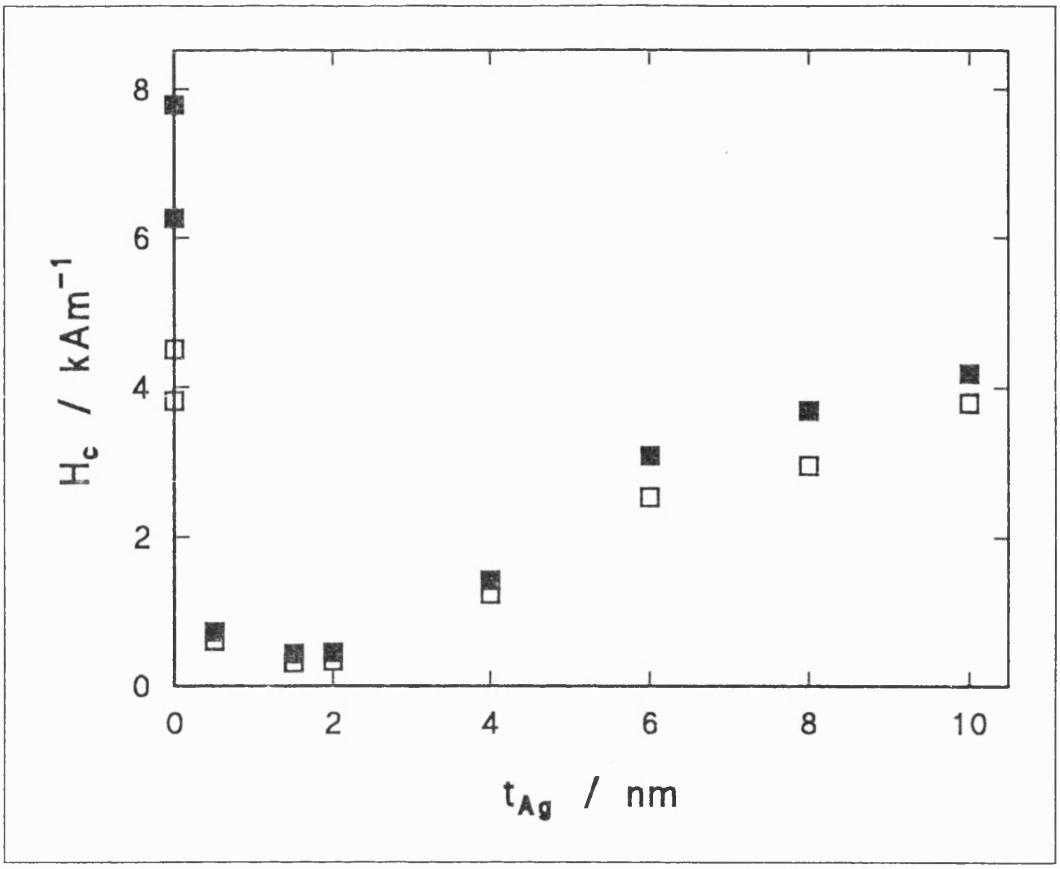

Figure 5.12 Coercivity of HiSat50/Ag multilayers with $t_{HiSat50}$ = 12nm. ■ As-deposited, □ annealed. (Some samples and data courtesy Dr. C. Shearwood).

The saturation magnetostriction data for the series with fixed t_{Ag} = 2nm are presented in Figures 5.13 a and b, using axes suggested by the possible interpretations put forward in Section 2.4. The comparability of the two interpretations has been commented on, but both are used here to reflect what may be encountered in published literature. Results from SAMR measurements are plotted along with data taken by SMFMR on annealed samples, which confirm the SAMR data. Error bars for the SAMR data arise from repeated measurements on the same sample, repositioned each time. For the SMFMR data, the experimental error is ±15% (Zuberek (1993)).

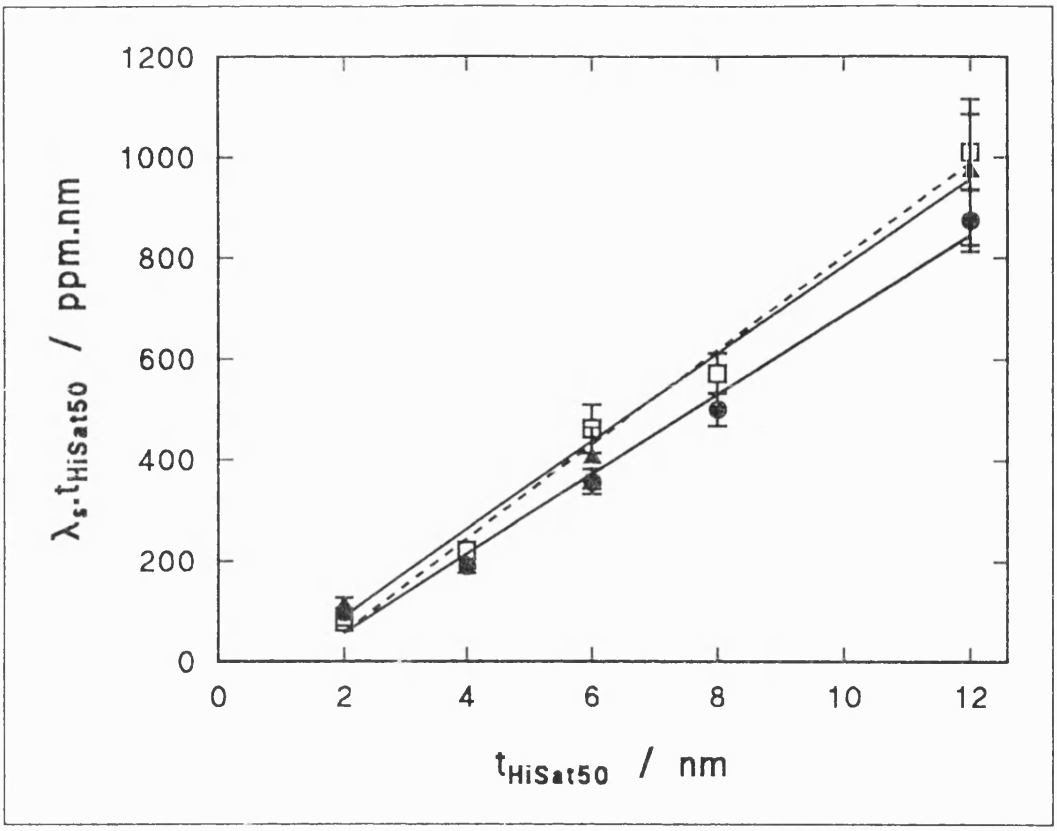

Figure 5.13a Saturation magnetostriction of HiSat50/Ag multilayers with fixed t_{Ag} = 2nm. Presented with reference to Equation 2.3. ● As-deposited (SAMR), -□- annealed (SAMR), ▲ annealed (SMFMR). Regression lines are (λ_s in ppm, $t_{HiSat50}$ in nm):

● $\lambda_s t_{HiSat50} = 79 t_{HiSat50} - 101$, correlation coefficient r = 0.9942;

□ $\lambda_s t_{HiSat50} = 93 t_{HiSat50} - 128$, r = 0.9957;

▲ $\lambda_s t_{HiSat50} = 87 t_{HiSat50} - 84$, r = 0.9977.

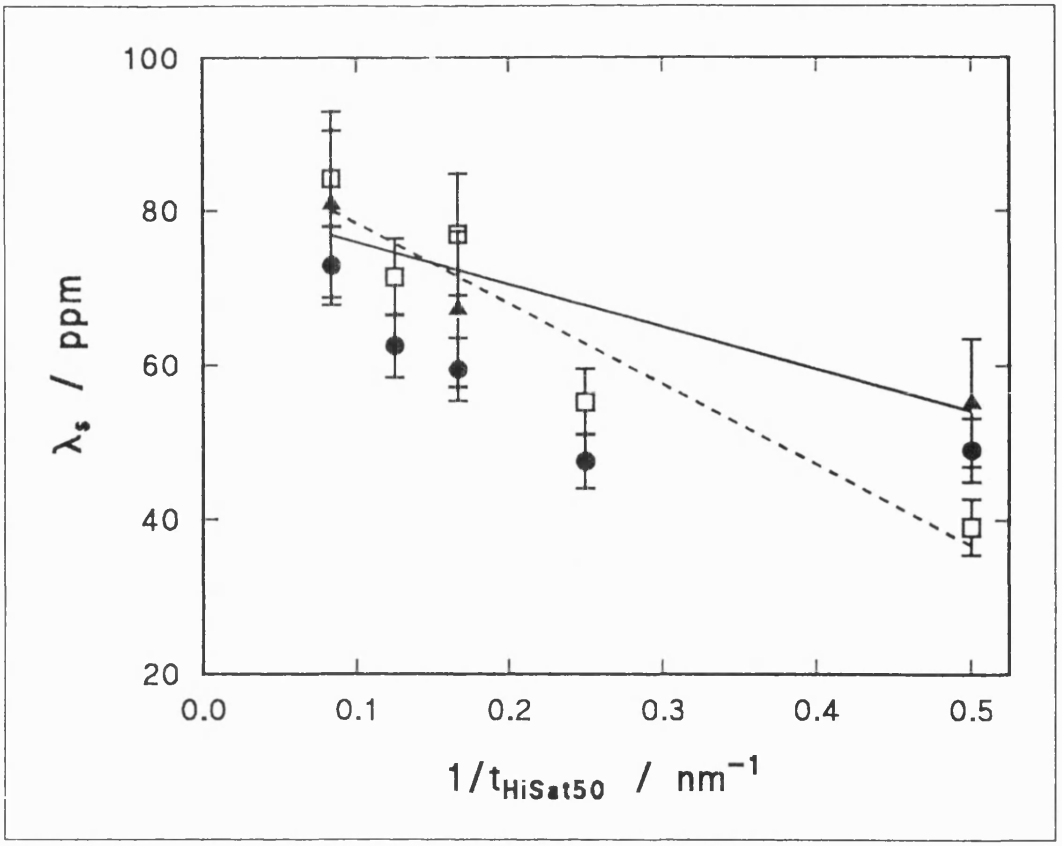

Figure 5.13b Saturation magnetostriction of HiSat50/Ag multilayers with fixed t_{Ag} = 2nm. Presented with reference to Equation 2.2. ● As-deposited (SAMR), -□- annealed (SAMR), ▲ annealed (SMFMR). Lines are regressions (not shown for ●). λ_s in ppm, $t_{HiSat50}$ in nm.

● $\lambda_s = -49/t_{HiSat50} + 69$, r = 0.7786;

□ $\lambda_s = -105/t_{HiSat50} + 89$, r = 0.9500;

▲ $\lambda_s = -55/t_{HiSat50} + 81$, r = 0.9326.

Although the two methods of presenting the λ_s data are essentially equivalent, higher correlation coefficients are obtained when $\lambda_s t_{mag}$ is plotted against t_{mag} because the values involved are larger and the range of t_{mag} is much greater than the range of $1/t_{mag}$. The appropriateness of treating λ_s of multilayers as arising from magnetic volume and interface effects is more readily recognised from the presentation of $\lambda_s t_{mag}$ vs. t_{mag}. Although a perfectly straight line is never expected

from Equation 2.3, given that t_{mag} appears in the intercept, the good linearity of this data set implies that the interface effects are small and that information on λ_s^{mag} obtained from this plot is accurate. The intercept is non-zero, however, and λ_s values for multilayers with thinner HiSat50 layers are lower than for those with thicker HiSat50 layers, implying that interface effects are not negligible, especially at lower $t_{HiSat50}$. An independent measure of t_{int} would be required, however, to help establish the significance of the interfaces effects.

The regression equations using Equation 2.3 (Figure 5.13a caption) indicate that the contribution from the magnetic HiSat50 layers is λ_s^{mag} = +79±10ppm in the as-deposited state, rising to λ_s^{mag} = +93±10ppm (+87±12ppm by SMFMR) on annealing. (Errors are given as two standard errors of the gradient). The analysis applies if the alloy layer makes the same contribution to λ_s in each case, implying that the crystallographic texture in each multilayer is the same. The XRD patterns showed no strong texture in any sample, i.e. random distributions of crystallite orientations, so such an interpretation is valid here.

The values of λ_s^{mag} returned by the regression equations are significantly greater than the experimental λ_s values for such a polycrystalline Fe-Co alloy obtained by Williams (λ_s = +66ppm) or Masiyama ($2\lambda_e/3 \approx$ +47ppm) (Bozorth (1951)). They agree within experimental error, however, with the calculation of $\overline{\lambda_s}$ for a random polycrystalline Fe-Co of this composition (+84±4ppm). In the calculation, saturation magnetostriction constants of single-crystal Fe-Co alloys were taken from Hall (1960): λ_{100} = +154±4ppm, λ_{111} = +38±4ppm for a composition similar to that of deposited HiSat50. Doubts have been expressed as to the applicability of this calculation in many situations, but the agreement here with the multilayer experimental data is good.

Masiyama's λ_e data were taken in fields of 87.5kAm^{-1}; that the data yield lower values of λ_s than Williams' indicates that the samples were not saturated. The

HiSat50 multilayers were saturated in fields much lower than this, and the λ_s values obtained are higher, confirming that the insertion of Ag interlayers in HiSat50 films soften them significantly, as seen when the MH loops of the multilayers are compared with that of a plain HiSat50 film. The multilayer λ_s values are also higher than that found by Williams; the field for those measurements is not mentioned, although saturation is asserted. The samples may have contained some crystallographic texture due to the production process; there is no information given on this.

The highest saturation magnetostriction observed in the multilayers was +84± 6ppm for 2×25(12nm HiSat50/2nm Ag) after annealing. This sample also had the lowest H_c (340Am^{-1}). This λ_s represents an increase of nearly 30% over the experimental λ_s value for a bulk polycrystalline alloy of similar composition to deposited HiSat50 (+66ppm; Bozorth (1951)) but is in accord with the calculated random polycrystalline value. This multilayer value has been achieved whilst also achieving magnetic softness. The multilayer λ_s data have been shown to fit an interpretation based on taking the volume average of contributions from the magnetic layer and interface regions, with λ_s^{mag} in line with the calculation of $\overline{\lambda_s}$ using published single-crystal values of λ_{100} and λ_{111}. Coercivity has been dramatically reduced in HiSat50/Ag multilayers compared to that of a plain HiSat50 film.

The saturation magnetostriction of the series with fixed $t_{HiSat50}$ = 12nm is plotted in Figure 5.14. According to Equation 2.2, t_{Ag} should not influence λ_s at all, while Equation 2.3 is independent of t_{Ag} once the layer thicknesses are sufficient to support the maximum interface thickness. It is thought that the Ag layer may not be continuous for t_{Ag} < 5-6nm (Chopra and Randlett (1968)) giving rise to an HiSat50 network with islands of Ag. A dip in the pattern of λ_s values occurs in the $t_{Ag} \approx$ 5-6nm region. This suggests that the wide variation in

magnetostriction values is more than scatter about an average value due to the HiSat50, but may be linked to the continuity of the Ag layer. The multilayers are all more magnetostrictive than samples containing no silver, although their relative magnetic hardness may mean that the magnetostriction value is underestimated. The multilayer λ_s values are similar to those of Williams for a similar Fe-Co alloy (Bozorth (1951)) and some are as high as the calculated $\overline{\lambda_s}$ value for such a Fe-Co alloy (+84ppm).

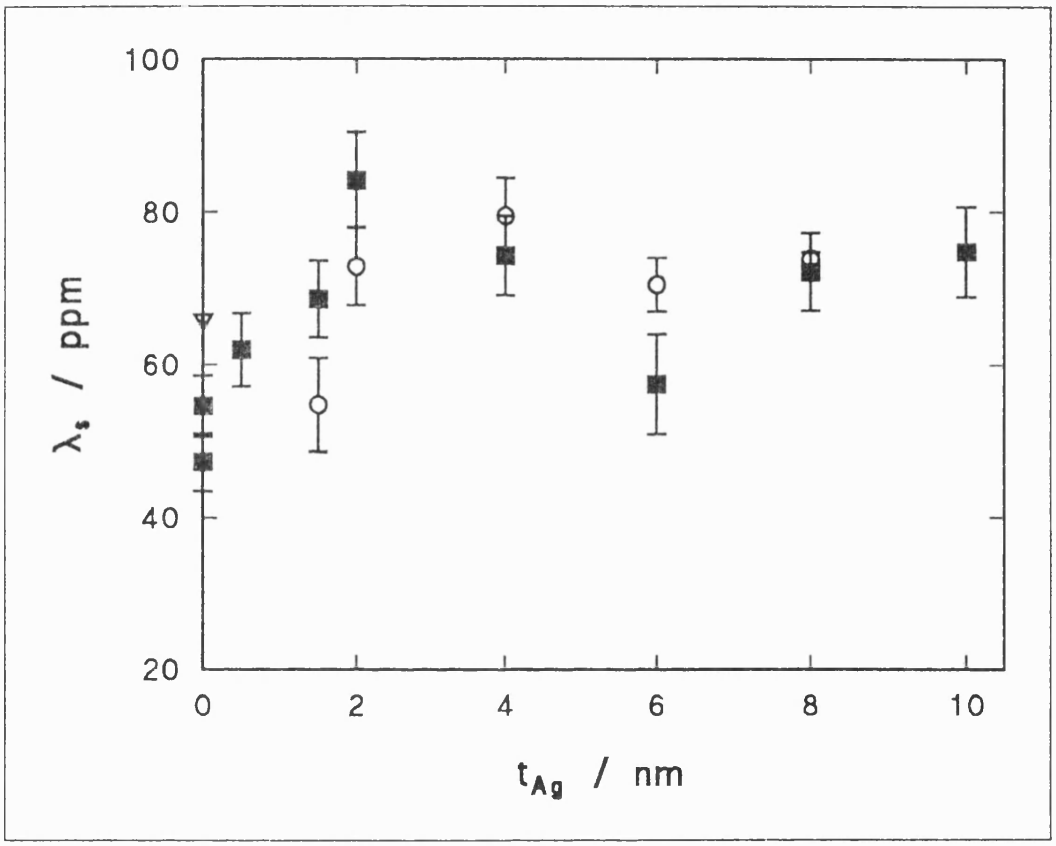

Figure 5.14 Saturation magnetostriction of HiSat50/Ag multilayers with fixed $t_{HiSat50}$ = 12nm. ○ As-deposited; ■ annealed; ∇ Williams' data, Δ Masiyama's data (Bozorth (1951)).

Note that, although the silver layers may not be continuous in the series with $t_{Ag} = 2nm$, $t_{HiSat50}$ is still a measure of the volume of magnetic material present and so presentation of the λ_s data as above remains valid.

No correlation is seen in either HiSat50/Ag series between the λ_s or H_c values and the crystallographic plane spacings, indicating that a strain mechanism is not influencing λ_s here. There is no evidence from XRD of any crystallographic texture in the samples, although a single scan like those shown would highlight only strong texture; more sophisticated techniques are required to obtain a full description of the crystallographic texture in all directions in a sample. Further work is proceeding in this research group regarding the effect of crystallographic texture in the multilayers on λ_s as the sputtering power and pressure are varied widely beyond the conditions used in this project. Texturing in the (100) sense may increase λ_s of the multilayers towards the single-crystal value $\lambda_{100} = +154ppm$ reported by Hall (1960).

Although the XRD patterns of the HiSat50/Ag multilayers do not indicate any strong crystallographic texturing, further information may be gained from Mössbauer spectroscopy measurements (taken by Dr. J. Z. Jiang, University of Liverpool). These give the average magnetic moment angle in the sample, compared to the incident γ-ray beam (normal to the film). The spread of moment angles is not obtained, however. After Hall (1960), the easy direction of magnetisation in an Fe-Co alloy of this composition is expected to be along the <111> set of crystallographic directions. Thus one might interpret the average moment angle as the average angle of the <111> axes. Further work is required to link this geometry with the calculation of λ_s in textured polycrystalline systems described in Section 4.3. However, results are presented below (Figure 5.15) which plot λ_s against the average angle, β, of the moments with respect to the film normal. Caution should be exercised in treating the angle of the magnetic moment

as the angle of the crystallographic axes in multilayer samples because of the sample geometry. The shape anisotropy in thin films tends to align the magnetic moments towards the film plane, and this is in competition with the magnetocrystalline anisotropy when the crystallographic directions do not coincide with the film plane. Hall's samples were disks cut from ingots of ordered and disordered Fe-Co alloys. The dimensions of the disks were not given.

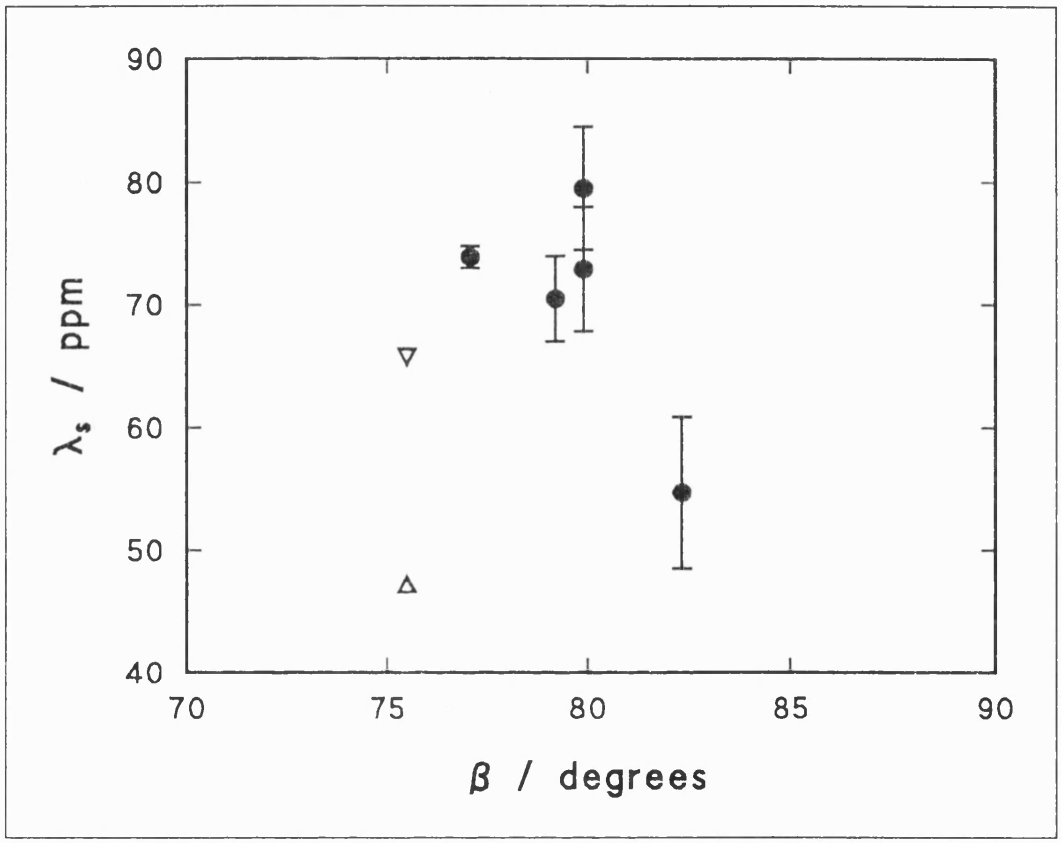

Figure 5.15 Saturation magnetostriction of as-deposited HiSat50/Ag multilayers with fixed $t_{HiSat50}$ = 12nm, vs. β, the average magnetic moment angle with respect to the film normal. ● multilayers; Δ plain HiSat50 film (β from measurement, $\lambda_s = 2\lambda_e/3$ from Bozorth (1951)); ∇ plain HiSat50 film (β from measurement, λ_s from Bozorth (1951)).

There is no correlation between λ_s and β, above. The data are crowded in a small angular range and the model with which to compare the data has yet to be elucidated. Since the multilayers considered here all had $t_{HiSat50}$ = 12nm, it is not surprising that the moment angles are similar. The smaller β angles, that is, moments more out-of-plane, were observed for multilayers with thicker t_{Ag}. If these data are interpreted as the inclination of the <111> axes to the plane, the crystallographic textures of the samples are similar. On this basis, the contribution to λ_s from the HiSat50 layers should be similar in all cases (notwithstanding possible effects linked to the continuity of the Ag layers, mentioned above). Data for the series with fixed t_{Ag} = 2nm and varied $t_{HiSat50}$ are not currently available. From Hall (1960) the expected magnetostriction constants along the crystallographic axes for a single crystal Fe-Co alloy of similar composition to deposited HiSat50 are λ_{111} = +38ppm, λ_{100} = +154ppm. (Estimated error in reading the data from the original is ±4ppm). Thus larger λ_s values are expected when the <100> crystallographic axes are nearer the film plane. The angle between a <100> axis and a <111> axis is 54.7°. Although the average inclination to the film plane of a <111> axis may be known (φ, say), the inclination of a <100> axis may be any angle between (φ-54.7°) and (φ+54.7°) and may well lie in-plane, although not necessarily in the direction of the λ_s measurement. The average positions of <100> axes in these films is not established, and is not necessarily the same in each film. Further, more sophisticated structural observations on each multilayer would be required to confirm any link between λ_{100} and λ_{111} of the single-crystal alloy and the observed λ_s in these multilayers.

The XRD traces showed random crystallographic texture and the λ_s data for the HiSat50/Ag series with fixed t_{Ag} = 2nm are in good agreement with the calculation of $\overline{\lambda_s}$ for such a random polycrystalline Fe-Co alloy. This indicates that the Mössbauer data above cannot be interpreted as giving the positions of <111>

axes. The moments lie predominantly in the film plane, as would be expected in a thin film from shape anisotropy considerations.

Ferromagnetic resonance measurements were performed on the two series of HiSat50/Ag multilayers. The g-factors were calculated using the measured resonant fields and $B_s = 2.44T$ (manufacturer's data for HiSat50). According to Reck and Fry (1969), an alloy of 50wt.%Fe, 50wt.%Co (the closest they present to the HiSat50 composition at the substrate) has a g-factor of 1.92 (g = 2 corresponds to pure spin magnetism). Considering the data taken at 9.73GHz, the g-factors of the multilayers tend toward this value for higher $t_{HiSat50}$ and lower t_{Ag} (Figure 5.16). However, the lower values are probably an artefact of the measurement, since low resonant fields were encountered, and their precise values were not known due to remanence in the magnet pole-pieces (see Section 3.7). The data taken at 34.0GHz is considered more reliable, and these values are more level, averaging g $\approx$ 1.85 for the multilayers. The pure alloy film has a g-factor slightly higher than the value reported by Reck and Fry, although the composition is slightly different, being 45% Fe, 55% Co for deposited HiSat50.

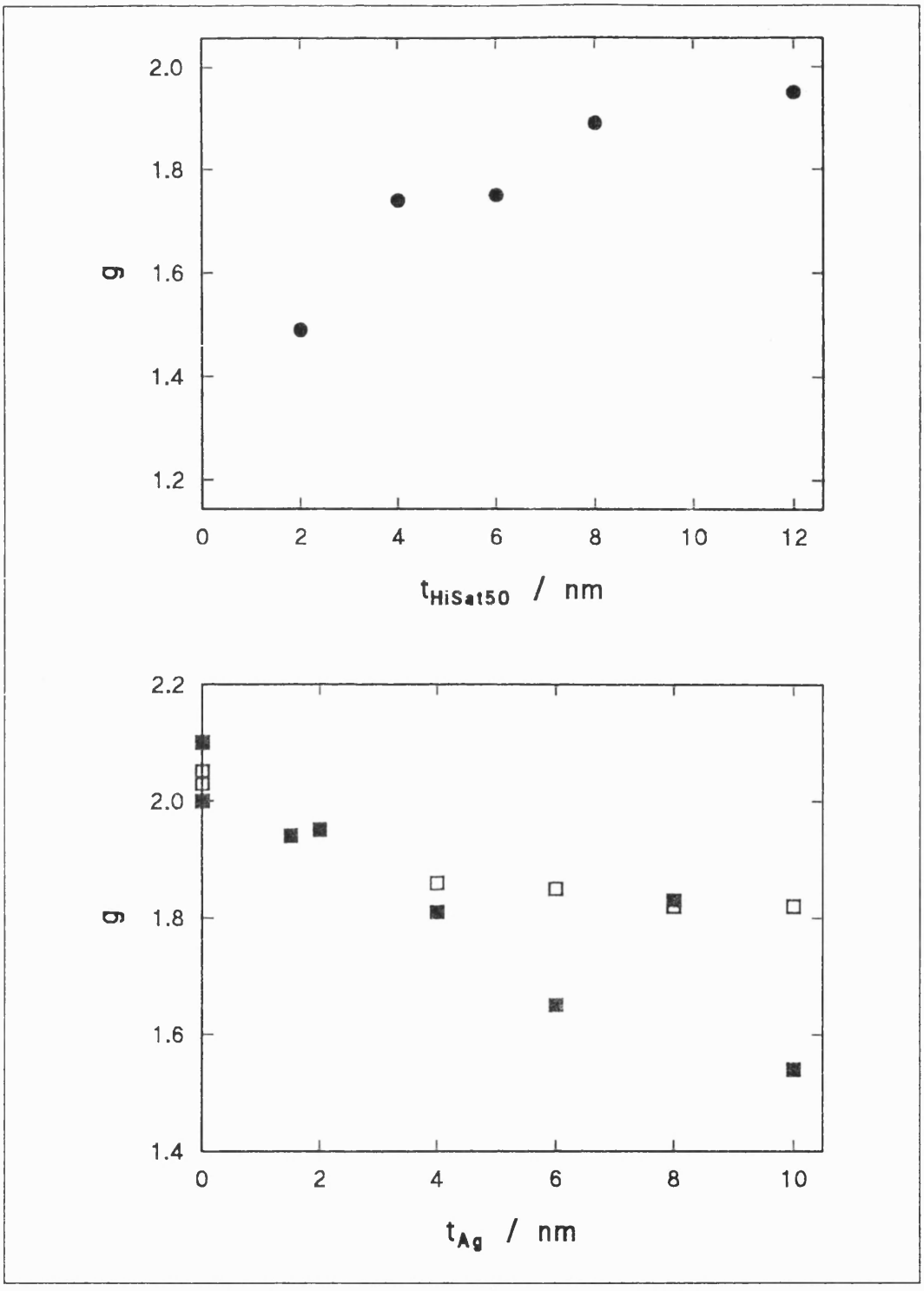

Figure 5.16 g-factors for HiSat50/Ag multilayers, measured by FMR. Top: fixed t_{Ag} = 2nm, f = 9.73GHz; bottom: fixed $t_{HiSat50}$ = 12nm, ■ f = 9.73GHz, □ f = 34.0GHz.

Under the same deposition conditions, a series of HiSat50/Cu multilayers was made, with fixed t_{Cu} = 2nm (Shearwood (1993)). Copper is also immiscible with Fe and Co, but has a higher Young's modulus than silver: E_{Cu} = 118GPa while E_{Ag} = 76GPa (Tottle (1984)) and a smaller lattice constant. Copper forms the fcc structure in the bulk, with d_{111} = 0.2088nm. Thus the lattice strain between HiSat50 (110) nearest neighbours and Cu (111) nearest neighbours is 2.9% - less than between HiSat50 and Ag. Copper also wets Fe and Co more easily than Ag does. Again, the coercivities of the multilayers were much less than that of the plain HiSat50 films (Figure 5.17) but the trend is opposite to that observed in the HiSat50/Ag multilayers. In the HiSat50/Cu series, H_c was observed to be lower in multilayers with *thinner* HiSat50 layers; these were the ones with *smaller* grain sizes. There was no relation between H_c and grain size after the samples were annealed for 30 minutes at 300°C in a flow of forming gas. The range of H_c values seen is narrower than in HiSat50/Ag multilayers. In the as-deposited multilayers, the d_{110} spacing was increased by up to 1% at thin $t_{HiSat50}$.

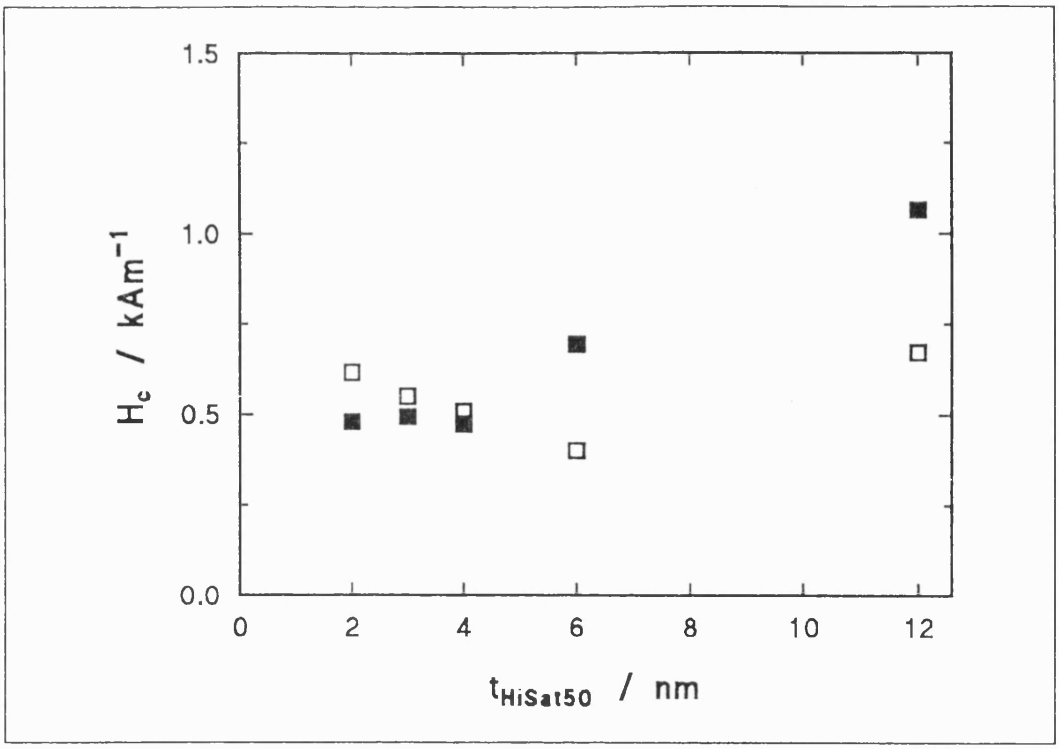

Figure 5.17 Coercivity of HiSat50/Cu multilayers with t_{Cu} = 2nm. ■ as-deposited, □ annealed.

The magnetostriction was similar to the experimental value expected for the polycrystalline alloy (λ_s = +66ppm; Bozorth (1951)) but lower than that obtained by calculation from single-crystal magnetostriction data. Unlike the HiSat50/Ag case, λ_s was not systematically affected by the thickness of HiSat50 (Figure 5.18, top). The average λ_s value for the as-deposited multilayers was +61±5ppm. Plotting λ_s against $1/t_{HiSat50}$ (as per Equation 2.2) gave no correlation, whereas plotting $\lambda_s t_{HiSat50}$ vs. $t_{HiSat50}$ clearly showed the applicability of this interpretation. The fits to Equation 2.3 (Figure 5.18 caption) give λ_s^{mag} = +60±3ppm for multilayers in the as-deposited state and λ_s^{mag} = +56±5ppm after annealing. The intercept became greater on annealing, indicating a more significant rôle of the interfaces in determining the magnetostriction of the multilayers. The very small

intercept found for the as-deposited multilayers explains why the λ_s values are so similar for all the multilayers in that series. In this case, either t_{int} is very small or $\lambda_s^{int} \approx \lambda_s^{mag}$. Annealing was expected to sharpen the interfaces between the immiscible metals, but it appears that the interfaces have a greater influence on λ_s after annealing. Annealing had a greater effect on λ_s for the multilayers with thinner $t_{HiSat50}$.

XRD traces of HiSat50/Cu multilayers showed that the alloy layers were polycrystalline with no significant crystallographic texture, and no satellite peaks were observed, indicating rough interfaces, as in the HiSat50/Ag multilayers.

The different effects on λ_s of multilayering HiSat50 with Ag rather than with Cu are tentatively ascribed to the different wetting characteristics and atomic sizes of the two elements. In studying granular alloys of various materials, including Ag, Bi and Mg with Fe, Maeda *et al.* (1993) consider the difference in size between Ag, Bi and Mg atoms to be one of the reasons for the different magnetoresistance behaviours observed in the three systems. Arai *et al.* (1991) comment similarly on the different MR and H_c behaviour of Fe-Ag and Fe-Cu granular systems.

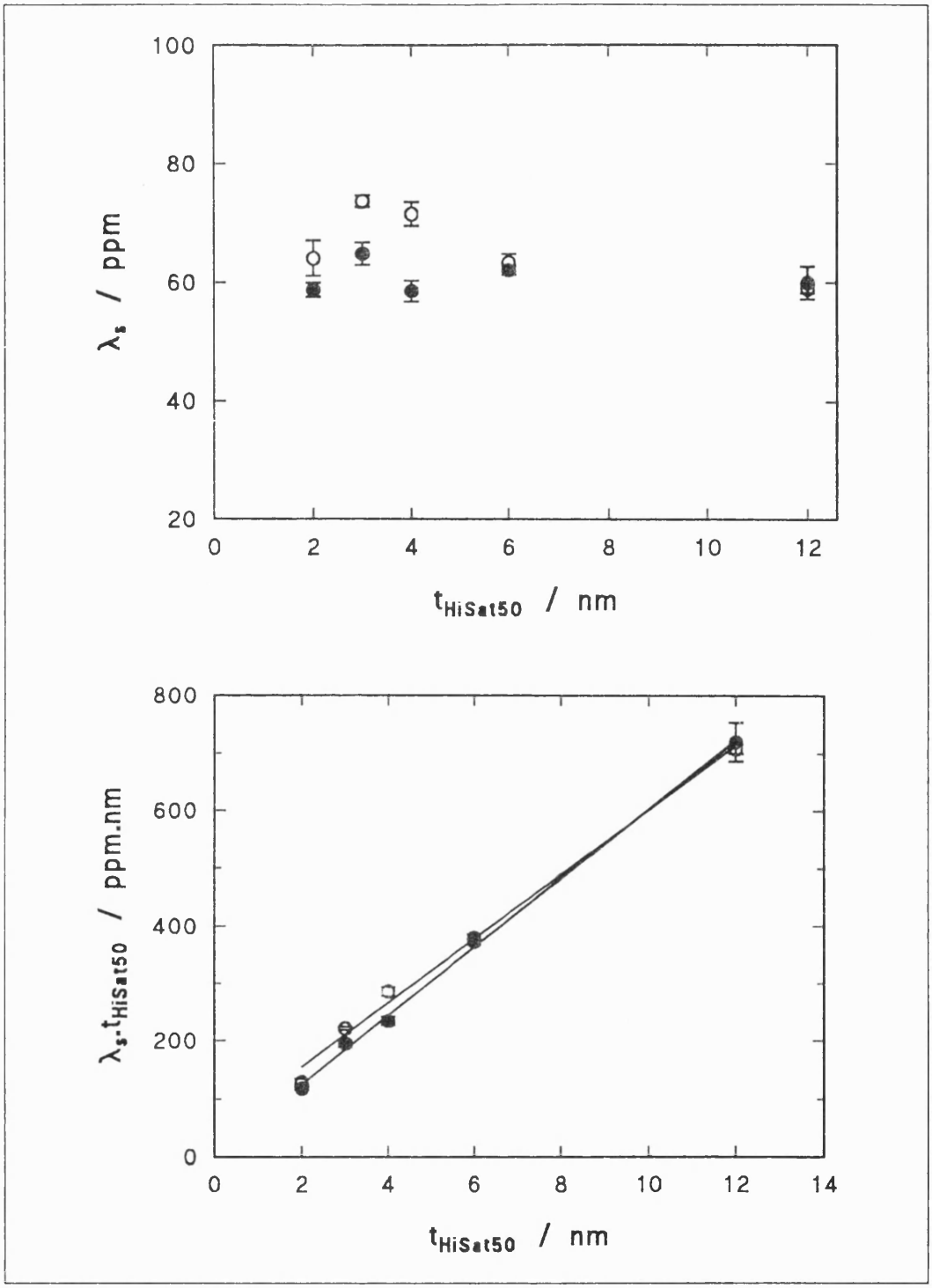

Figure 5.18 Saturation magnetostriction of HiSat50/Cu multilayers with fixed t_{Cu} = 2nm. ● as-deposited, ○ annealed. The regression lines in the bottom plot are: ● $\lambda_s t_{HiSat50} = +60t_{HiSat50} + 5$, r = 0.9993; ○ $\lambda_s t_{HiSat50} = +56t_{HiSat50} + 43$, r = 0.9969 ($\lambda_s$ in ppm, $t_{HiSat50}$ in nm).

Cross-sectional TEM of HiSat50/Ag multilayers has proved unsuccessful. The process described in Section 3.5.2 did not produce good sections. Multilayers were then deposited on a plastic cover slip, which were successfully cut and imaged. The contrast between the HiSat50 and the Ag layers was insufficient to distinguish them, however, although the total film could be seen.

It was observed in the HiSat50/Ag multilayer series that the minimum coercivity occurred with t_{Ag} = 1.5-2nm, a thickness at which it is thought unlikely that the silver layer is continuous. To establish whether the multilayer structure were significant in producing this effect, or whether it were necessary merely to interrupt the growth of the magnetic component, films were produced with small Ag particles randomly dispersed in the HiSat50 alloy. (Giant magnetoresistance has been observed in both multilayered and granular films - see Section 2.3). The dispersion was achieved by sputtering from a target consisting of a HiSat50 disc with square chips of 99.999% pure Ag (0.5mm thick) scattered evenly over the surface. The amount of silver required to give films containing 9vol.% Ag to 50vol.% Ag were calculated from the calibrated deposition rates of the two materials at 75W and 5mtorr Ar pressure. The volume percentages were chosen to reflect the range of thickness combinations in the HiSat50/Ag multilayer series. Each film was approximately 500nm thick. The chamber pressure prior to deposition was 6.0-7.5$\times 10^{-7}$torr.

None of the dispersed HiSat50-Ag films was saturable in the d.c. magnetometer, thus proving them all magnetically harder than the HiSat50/Ag multilayers. Two example loops are shown in Figure 5.19. Coercive fields were estimated on reducing the applied field from H_{max} = 22kAm^{-1}, and values ranged from 1.3kAm^{-1} to 4.2kAm^{-1}. These figures are lower than the coercivities which

would be obtained on reducing M to zero from M_s. The minimum coercive field occurred for a film with a nominal Ag content of 25vol.%.

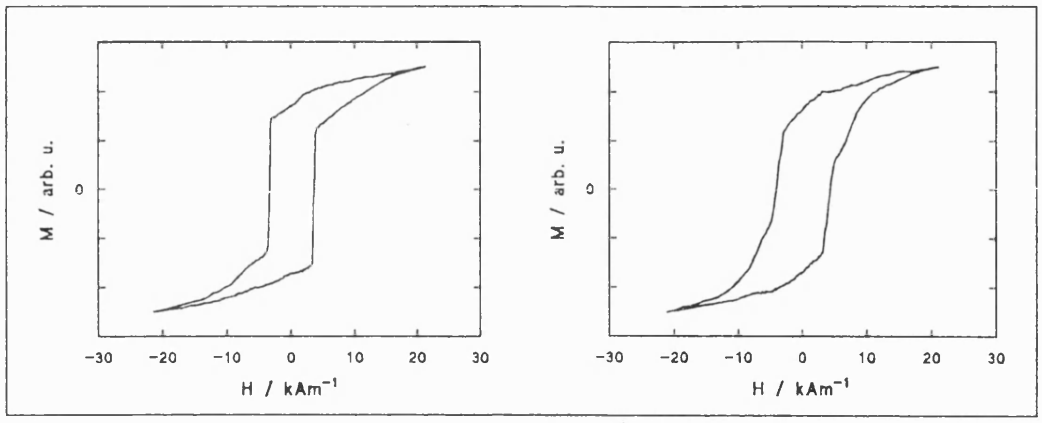

Figure 5.19 In-plane MH loops of two HiSat50-Ag dispersed films, in H_{max} = 22kAm^{-1}. Left: film with nominally 14vol.% Ag; right: film with nominally 45.4vol.% Ag.

The films were annealed for a total of 130 minutes at 300°C. The coercive field of the film with nominally 14vol.% Ag was reduced from 1.4kAm^{-1} to 0.9kAm^{-1}, but all the films remained unsaturable in H_{max} = 22kAm^{-1}. The MH loop of this film was quite square (M_r/M_{max} = 0.9) with a sharp initial transition in M at the coercive field followed by a slow increase in M as H increased. This is indicative of a two-phase material in which there is one magnetically soft phase (giving the sharp transition) and a magnetically harder one (giving the slow increase of M with H). This shape was typical of films containing lower amounts of Ag. As the amount of Ag increased, loops became smoother.

The HiSat50-Ag dispersed films were polycrystalline with weak (110) crystallographic texture. The (110) plane spacing showed no pattern with the nominal fraction of Ag present (Figure 5.20). If a uniform alloy had been formed, a dependence of the lattice constant on the Ag content would have been expected.

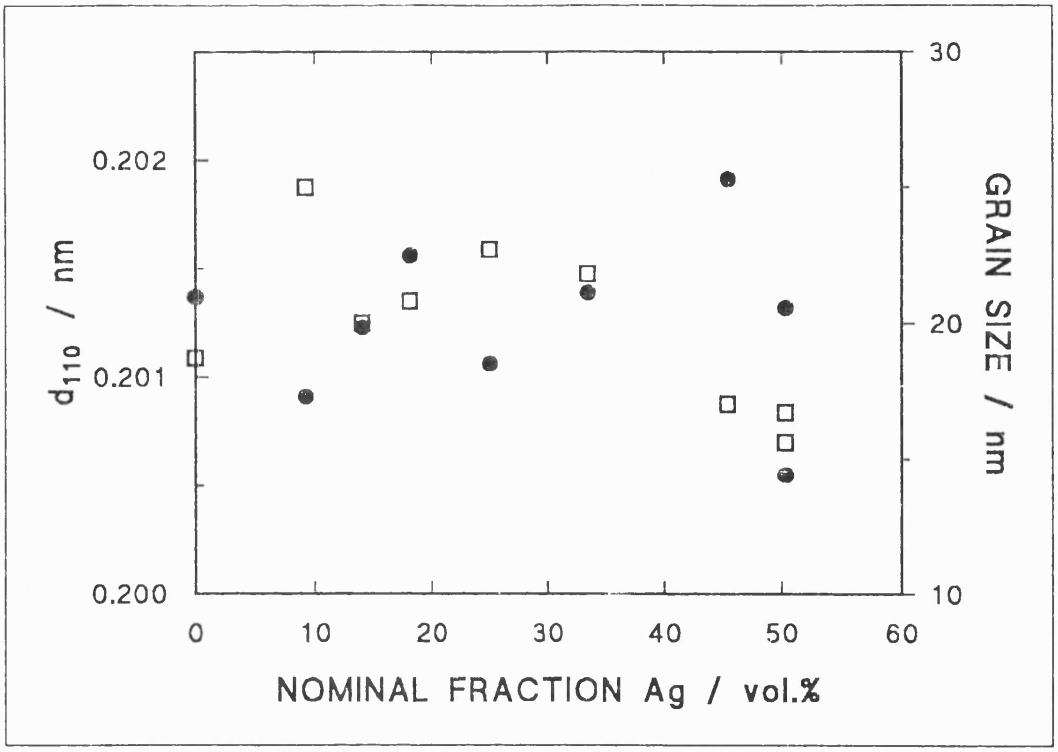

Figure 5.20 (110) plane spacing and estimated Fe-Co grain size in as-deposited HiSat50-Ag dispersed films. ● d_{110}, □ grain size estimated from (110) peak.

The average d-spacing was 0.20129±0.00073nm. The (110) d-spacing of the plain 600nm HiSat50 film was 0.20137nm, well within the scatter of the results from the dispersed films. The grain sizes of the dispersed films, estimated from the (110) peak widths using the Scherrer equation (Guinier (1963)), decrease as the amount of silver in the films increases. This is in line with the observation of Arai *et al.* (1991) on r.f. magnetron sputtered Fe-Ag dispersed films. It is to the decreasing grain size that those authors attributed the reduction of H_c, although the variation of H_c with grain size observed here is not monotonic. The grain sizes observed in these HiSat50-Ag dispersed films were all larger than the grain sizes observed in the HiSat50/Ag multilayers, and some were larger than that seen in the

plain HiSat50 film (see Figure 5.20). The Ag (111) XRD peak appeared for fractions of Ag greater than 30vol.%.

Values of λ_s taken by SMFMR, by Dr. R. Zuberek, await confirmation. The traces show an asymmetric resonance line. Results calculated on the basis of B_s = 2.44T (the manufacturer's value for HiSat50) yielded very high values of λ_s. Dr. Zuberek then calculated λ_s using an effective magnetisation calculated from the resonance position, assuming a g-factor of 2.1, which gave reduced values for B_s. Values varied from +60ppm to +112ppm with no clear correlation with the Ag content. The largest λ_s was found for the film containing 25vol.% Ag nominally.

Compositional analyses of the HiSat50-Ag dispersed films by electron probe microanalysis (EPMA) have not agreed with the designed compositions of the dispersed films. All measured values of the Ag content are lower than the designed proportions, but by varying factors. EPMA measurements repeated on different dates did not show good self-consistency. After sputtering, a black powder coating developed on the Ag chips used on the HiSat50-Ag mosaic target. A diffraction pattern taken in a Laue Powder Camera showed this to be pure Ag, but the form it took may have inhibited sputtering from the Ag metal, reducing the amount deposited from that expected. The film thicknesses obtained were close to those expected from the deposition rates of the components, implying Ag contents similar to those designed.

The dispersion of Ag particles in HiSat50 films has been shown not to produce the magnetic softening observed in the HiSat50/Ag multilayers. No attempt was made to optimise growth conditions or post-deposition treatments, however, which may be avenues for further work. One attraction of granular materials over multilayers is the relative simplicity of production; in this case, continuous sputtering from a single target rather than alternating between two.

5.2.2. Permendur24/Ag Multilayers

Typically 50 bilayers of Permendur24/Ag were deposited on each side of a Kapton substrate 26μm thick. The substrate platen was water-cooled. The r.f. power was 75W, and the argon pressure 5mtorr. The background pressure prior to deposition was $1\text{-}3\times10^{-7}$torr. No buffer or cap layers were laid down; Permendur24 was the first layer to be deposited, and the top layer was Ag. The first series had t_{Ag} = 2nm fixed while $t_{Permendur24}$ was varied from 2nm to 15nm, and the second had $t_{Permendur24}$ = 10nm fixed, t_{Ag} = 2nm to 10nm. Two plain alloy films were also fabricated: 600nm Permendur24 on each side of the substrate.

As with the HiSat50/Ag multilayers, the XRD traces show the Permendur24/Ag multilayers to be polycrystalline, with bcc structure and no particular crystallographic texture; except in multilayers with thin t_{Ag} and thicker $t_{Permendur24}$, where there may be some slight (110) texture. (Comparison was made with the trace for α-Fe since the alloy is also bcc and has lattice parameters similar to those of α-Fe). Satellite peaks are not observed around the main peaks, indicating rough interfaces and possible incomplete coverage by the Ag layers for thinner t_{Ag}. Specimen XRD patterns are shown in Figure 5.21. The peaks below $2\theta \approx 30°$ are from the Kapton substrate. The Ag (111) peak appears at $2\theta \approx 38°$-39° as the Ag content increases, as do Ag peaks at higher angles. (The positions of peaks from bulk fcc silver are given in Section 5.2.1). The peak at $2\theta \approx 44°$ is due to the bcc (110) planes of the Fe-Co alloy.

The d-spacings of the Permendur24 (110) planes and of bulk Ag were used to calculate the nearest neighbour distances in these most closely-packed planes. Lattice mismatch was calculated from this to be 4.1%-4.7%, depending on which plain alloy film was used to obtain d_{110}. This is large to be accommodated by lattice strain at interfaces, so some dislocations and interface roughness are expected.

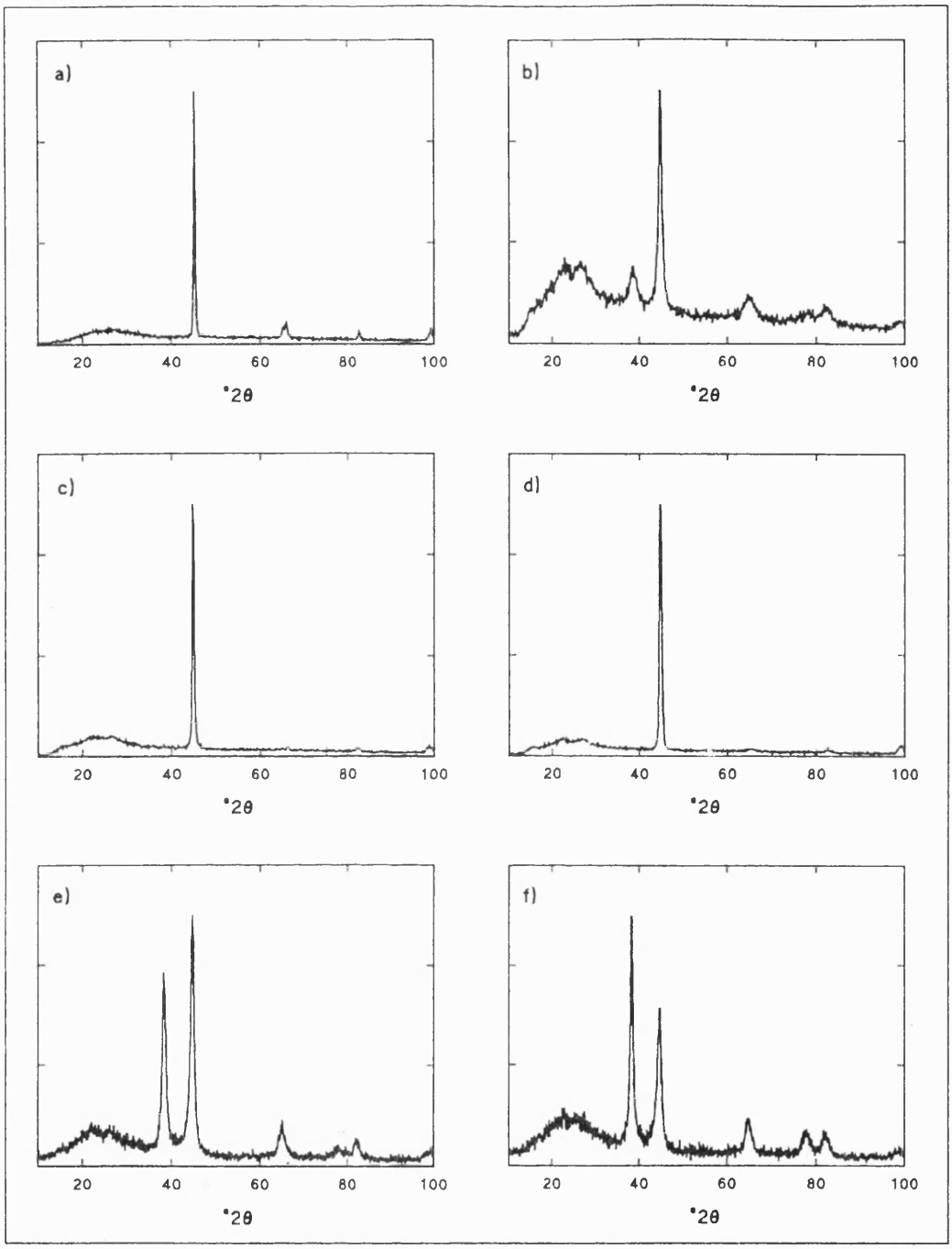

Figure 5.21 X-ray diffraction patterns of Permendur24/Ag multilayers on Kapton substrates. The vertical axes are diffracted intensity in arbitrary units (linear scale); each trace has been normalised to the intensity of its highest peak. a) 2×600nm Permendur24 plain alloy film; b) 2×75(4nm Permendur24/2nm Ag); c) 2 ×50(8nm Permendur24/2nm Ag); d) 2×50(10nm Permendur24/2nm Ag); e) 2× 50(10nm Permendur24/5nm Ag); f) 2×40(10nm Permendur24/10nm Ag).

The average d-spacings of the (110) and (111) planes parallel to the substrate were calculated from the peak positions returned by the peak fitting routine in the diffractometer software. The Scherrer equation (Guinier (1963)) was used to estimate the grain sizes in the films from the XRD peak widths. The results for the two multilayer series are shown in Figures 5.22 and 5.23. The bcc (110) d-spacings for the two plain Permendur24 films were 0.20179nm and 0.20061nm. The (111) plane spacing of bulk Ag is 0.2359nm.

It was generally found that, in fitting the pattern profile using the diffractometer software, two peaks were required to fit well a single observed peak, from either the alloy or Ag. One peak was usually ten or more times smaller than the other, at a small angular distance from the first, and with a larger width. It could be that the shape of the peak used in the fit (two half-Lorentzian distributions) is unsuitable for polycrystalline multilayers; alternatively, in some cases, the second peak may arise from the substrate, seen through the multilayer. In calculating the d-spacings and grain sizes, the larger of the two peaks only was used, except where the two fitted peaks were of similar amplitudes. In that case, the average was taken and error bars drawn to the points resulting from calculations on the two separate fitted peaks.

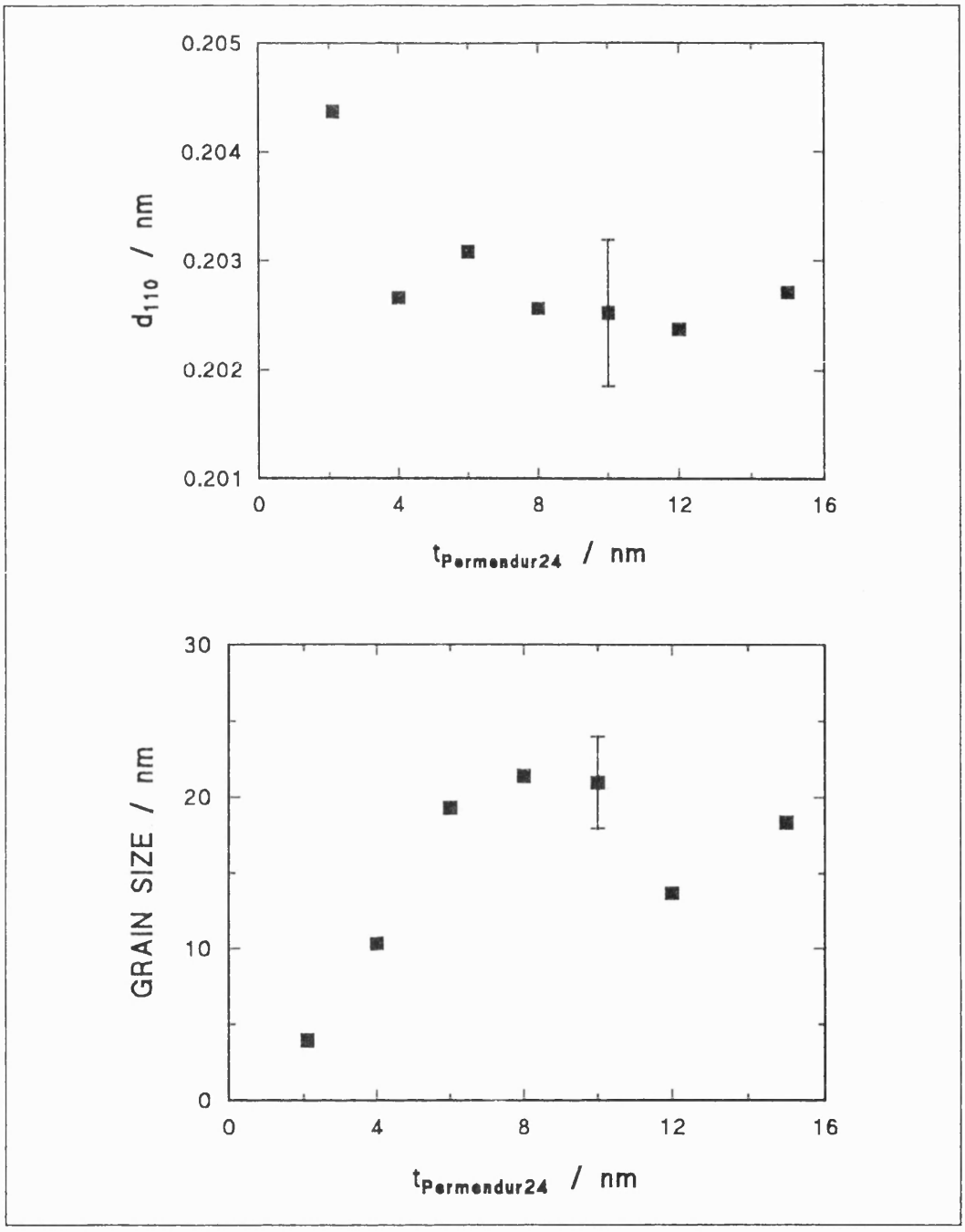

Figure 5.22 Lattice plane spacings (top) and grain sizes (bottom) for the series with fixed t_{Ag} = 2nm. The data are taken from the Fe-Co (110) peaks, the Ag (111) peaks being unobserved for most of the samples.

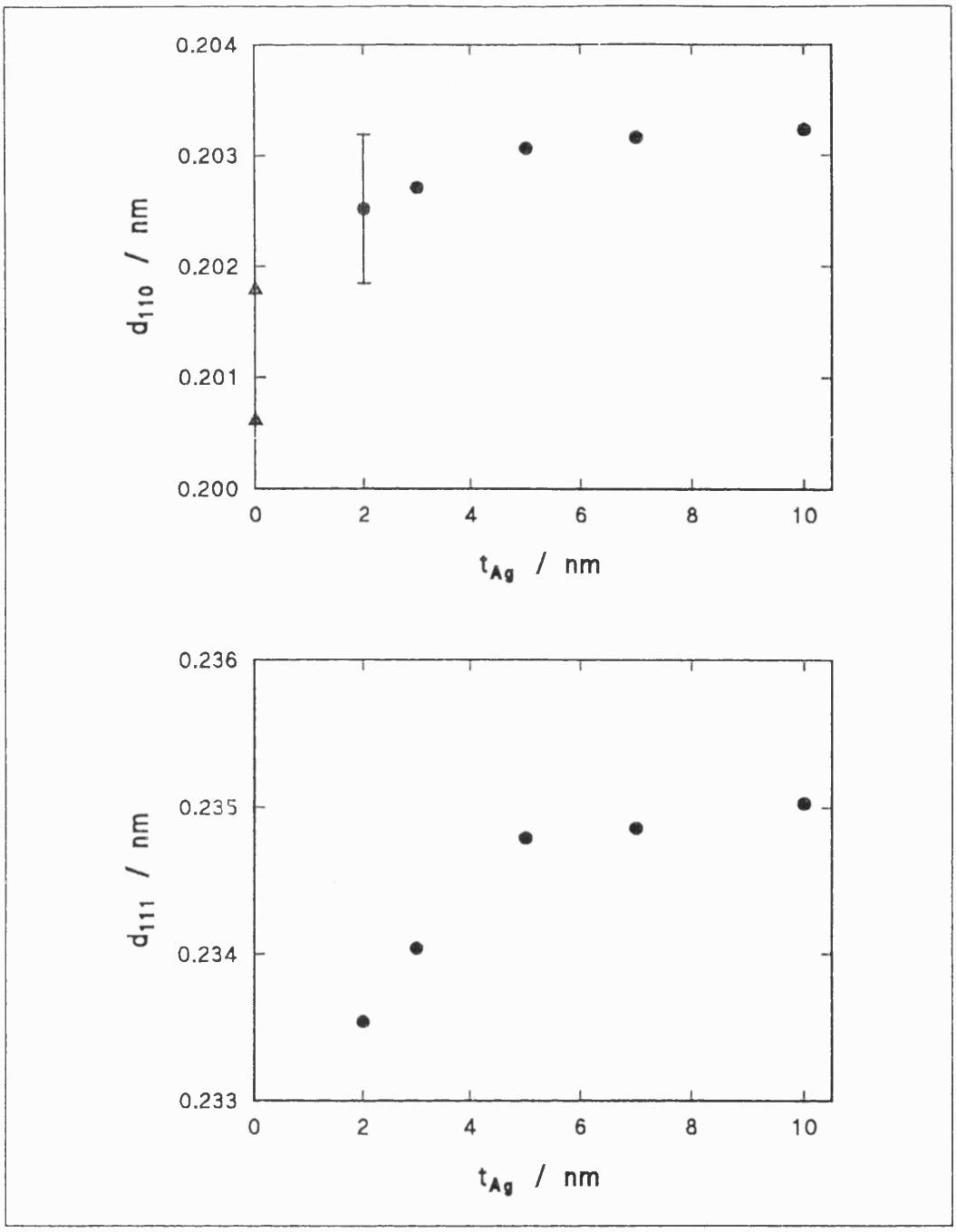

Figure 5.23a Lattice plane spacings for the multilayer series with fixed $t_{Permendur24}$ = 10nm (●), as-deposited. Top: data from the bcc Fe-Co (110) peaks; Δ plain alloy films. Bottom: data from Ag (111) peaks.

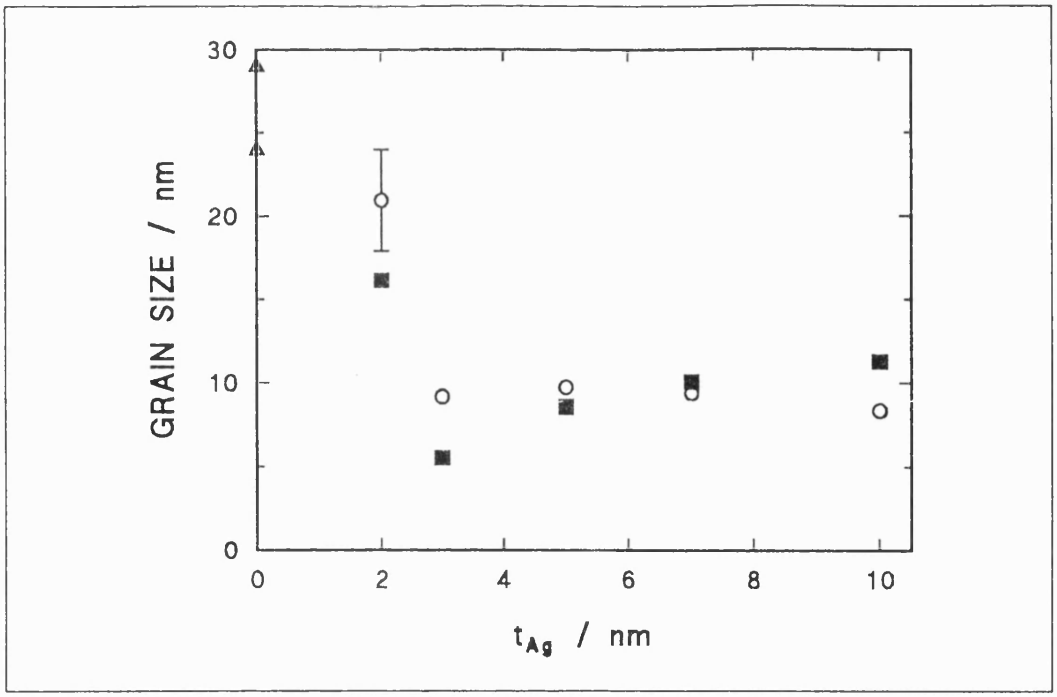

Figure 5.23b Grain sizes for the Permendur24/Ag series with fixed $t_{Permendur24}$ = 10nm. ○ from bcc (110) peaks; ■ from Ag (111) peaks; Δ bcc (110) peaks, plain alloy films.

In the series with fixed t_{Ag} = 2nm, (111) peaks were not generally visible in the XRD traces, in contrast to the case with HiSat50/Ag multilayers discussed above. The bcc (110) d-spacing relaxes from expansion towards the value observed in the thick plain alloy films as $t_{Permendur24}$ increases. A similar trend is seen in the series with constant $t_{Permendur24}$ = 10nm, where d_{111} of the Ag layers increases towards the bulk Ag d_{111} value of 0.2359nm as t_{Ag} increases, having been compressively strained perpendicular to the substrate plane at thinner t_{Ag}. In this latter series, the bcc (110) spacing of the Permendur24 layers also expands as t_{Ag} increases and d_{111} expands.

The trend in grain sizes in the two series are not so smooth. The grain size in the series with fixed t_{Ag} = 2nm is small at thin $t_{Permendur24}$, increasing to a plateau as the Permendur24 thickness increases. In the other series, the grain size calculated

from both the bcc (110) and Ag (111) peaks is larger for $t_{Ag} \leq 2$nm, the largest grains being observed in the plain alloy films. The grain size calculated from the (110) peaks is approximately constant as t_{Ag} increases beyond 2nm, while the grain sizes from (111) peak data increase slightly after an initial drop.

A selection of in-plane magnetic hysteresis loops are shown in Figure 5.24. Some show the "double-loop" effect seen, to a lesser extent, in some HiSat50/Ag multilayers. The multilayers may contain two phases of material (a soft one with a low coercivity and a harder one) or the effect may be due to different film stresses on the two sides of the substrate, giving rise to different switching fields. The MH loop for $t_{Permendur24} = 2.1$nm is noisy because of the low amount of magnetic material present. Multilayers with thinner Permendur24 layers tended to produce squarer MH loops; this may have resulted from stress imposed by the substrates on positively magnetostrictive films, where the stress is more effective on thinner films.

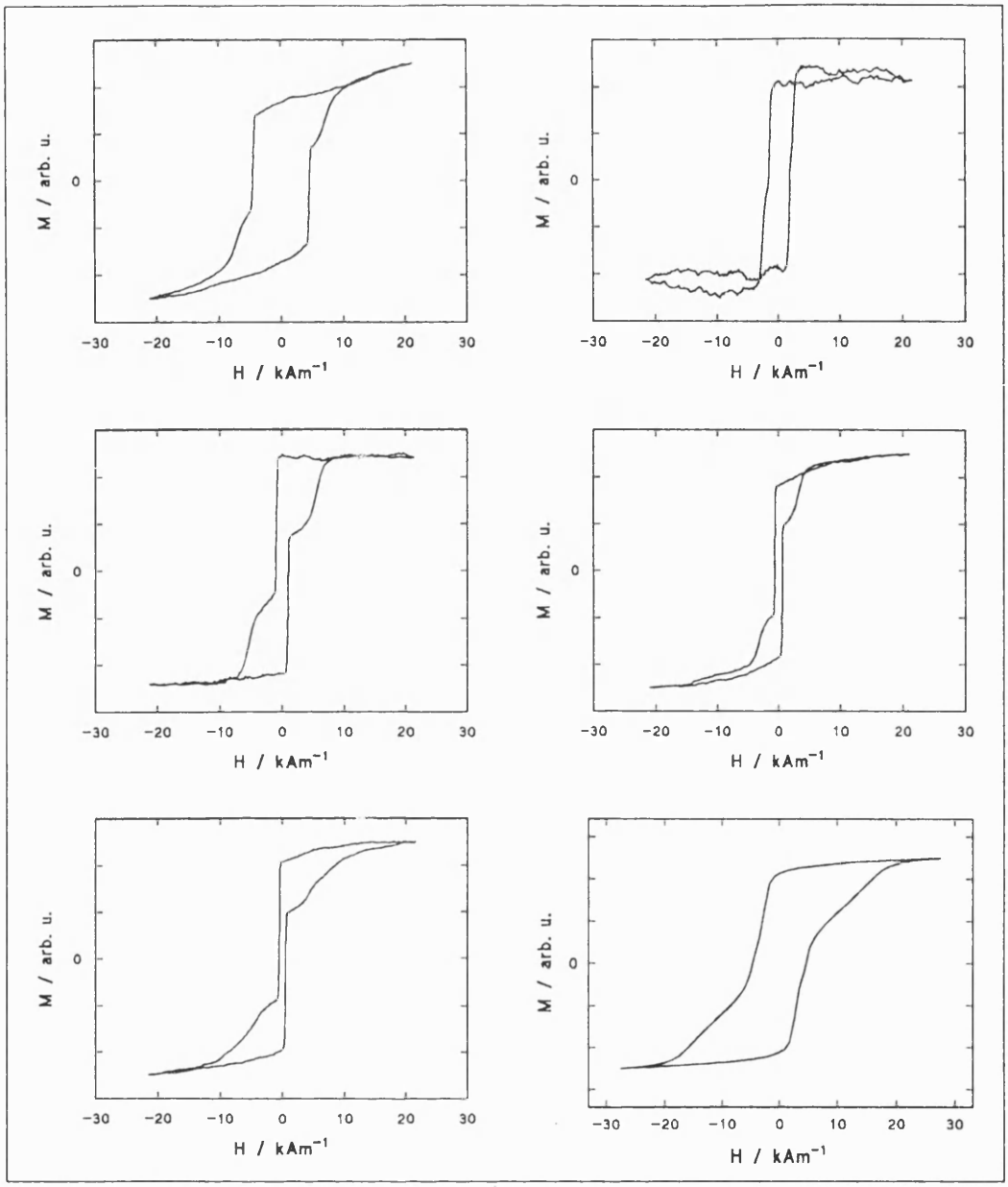

Figure 5.24 MH loops of Permendur24/Ag multilayers on Kapton substrates. Top left: plain 2×600nm Permendur24 film; top right: 2×50(2.1nm Permendur24/2nm Ag); middle left: 2×50(6nm Permendur24/2nm Ag); middle right: 2×50(10nm Permendur24/2nm Ag); bottom left: 2×40(15nm Permendur24/2nm Ag); bottom right: 2×40(10nm Permendur24/10nm Ag). Shape factor b = 0.5.

The coercivity was taken to be the value of H at M = 0, as H was reduced from H_{max} = 22kAm^{-1}, which referred to the sharp transition in the loops. The plain alloy films could not be saturated in the d.c. magnetometer, so H_c values quoted for them are underestimates of the coercivity: values of 5.67kAm^{-1} and 4.64kAm^{-1} were measured on the two films made. Multilayers with larger amounts of silver were more difficult to saturate, but most showed that moment rotation was the magnetisation mechanism in operation at the highest fields, so H_c values given are expected to be close to coercivity values.

The coercivities of the series with t_{Ag} = 2nm are shown in Figure 5.25. Films with thicker $t_{Permendur24}$ have lower H_c values; these films are the ones in which d_{110} is closest to that in the plain film (see above). No clear correlation with grain size was observed, however (Figure 5.26). All the Permendur24/Ag multilayers had lower coercivities than the coercive fields measured for the plain Permendur24 films. The lowest was 560Am^{-1}, of the multilayer 2×50(12nm Permendur24/2nm Ag). This value is higher than the minimum observed in the HiSat50/Ag multilayer series discussed above.

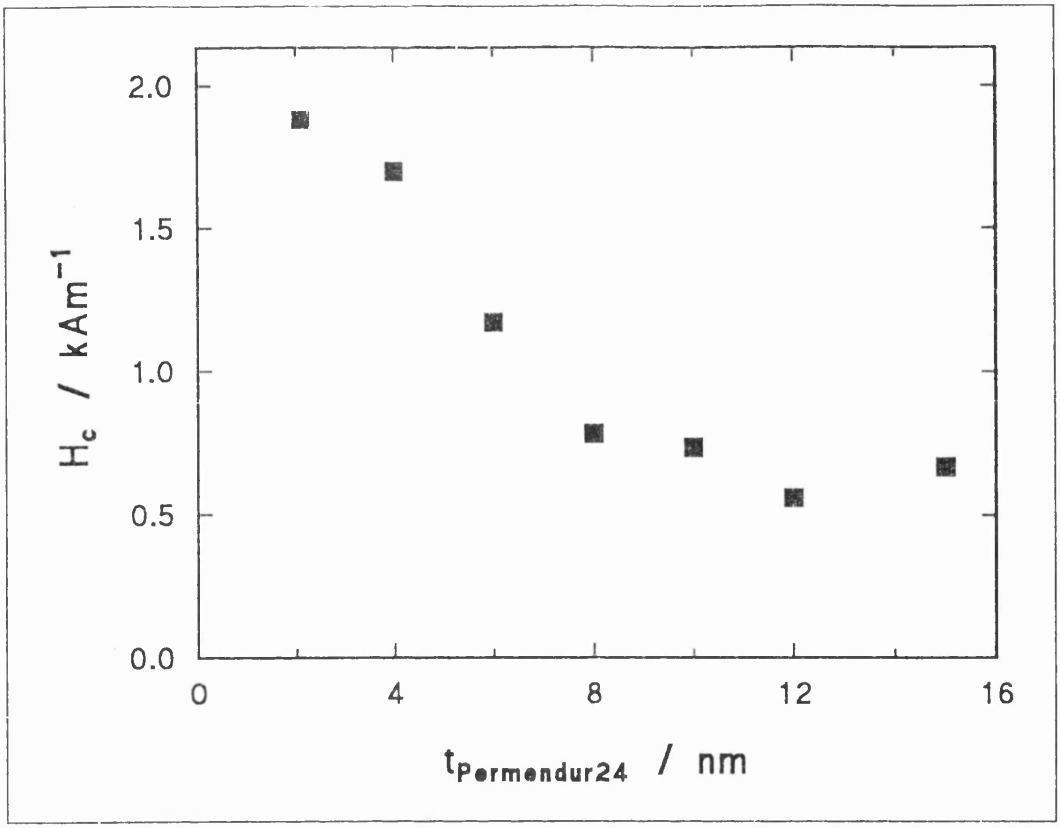

Figure 5.25 Coercivity of Permendur24/Ag multilayers on Kapton substrates, with fixed t_{Ag} = 2nm.

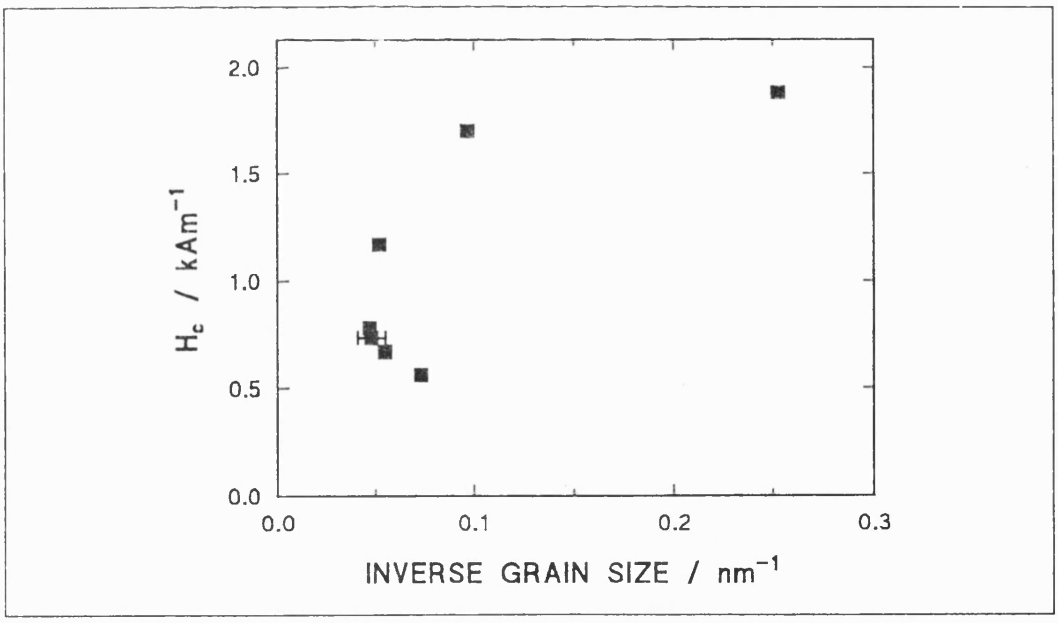

Figure 5.26 Coercivity vs. inverse estimated grain size for Permendur24/Ag multilayers on Kapton substrates. Constant t_{Ag} = 2nm.

The coercivity data for the multilayer series with fixed $t_{Permendur24}$ = 10nm are presented in Figure 5.27. The H_c values increase steadily with t_{Ag}, approaching the plain film values for t_{Ag} = 10nm. The lowest H_c in this series is 734Am^{-1}, for 2× 50(10nm Permendur24/2nm Ag). There was no correlation of H_c with grain size, considering either (110) peaks or (111) peaks for the grain size estimate.

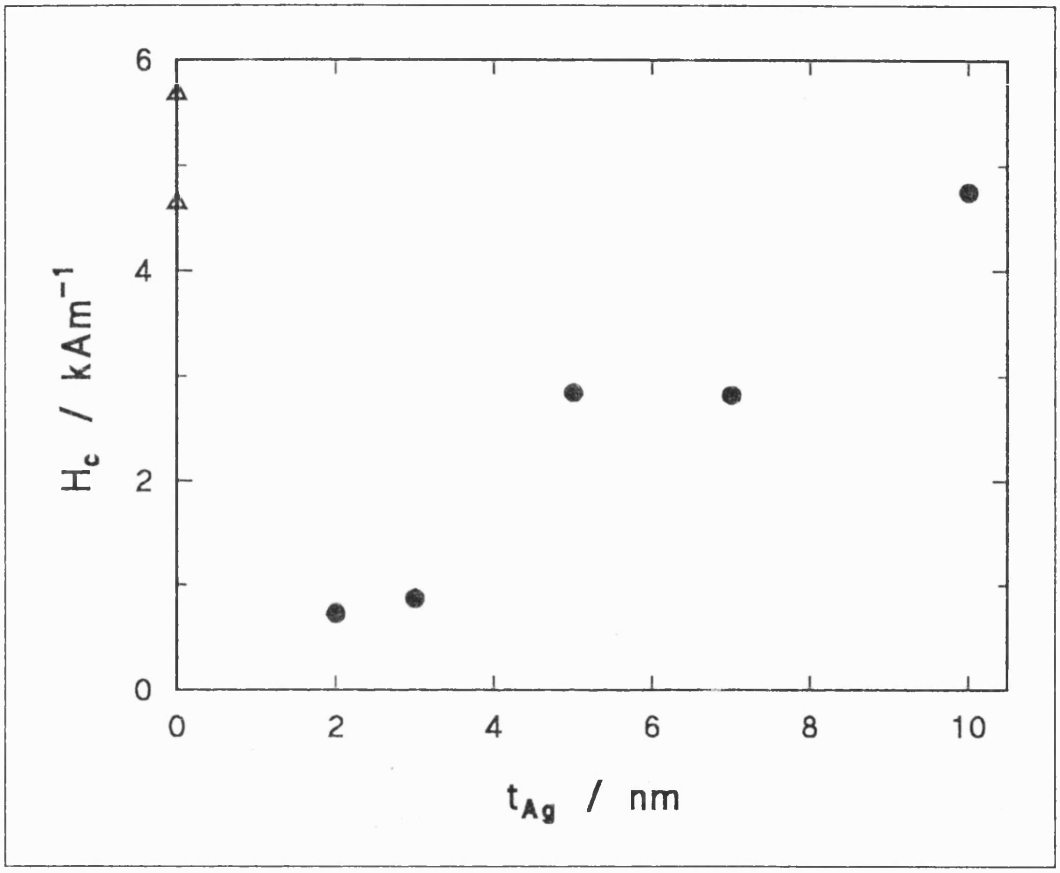

Figure 5.27 Coercivities of Permendur24/Ag multilayers on Kapton, with fixed $t_{Permendur24}$ = 10nm. ● as-deposited multilayers; Δ plain Permendur24 films.

Saturation magnetostriction was measured by the SAMR technique. The saturation induction and Young's modulus were taken from the manufacturer's data sheet for Permendur24 as B_s = 2.34T and $E_{Permendur24}$ = 230GPa respectively. These were regarded as the best information, considering that the alloy

composition at the substrate was thought to be similar to that of the target, and since Cr was present. Using the data from Honda (1919) for the Young's modulus of an iron-cobalt alloy of similar composition ($E_{Fe\text{-}Co} \approx 215GPa$) would not have changed the λ_s values beyond the error bars. The results for the multilayer series with constant $t_{Ag} = 2nm$ are shown in Figures 5.28 a and b, according to the two interpretations of data described before (Section 2.4). The comparability of the two interpretations has been noted.

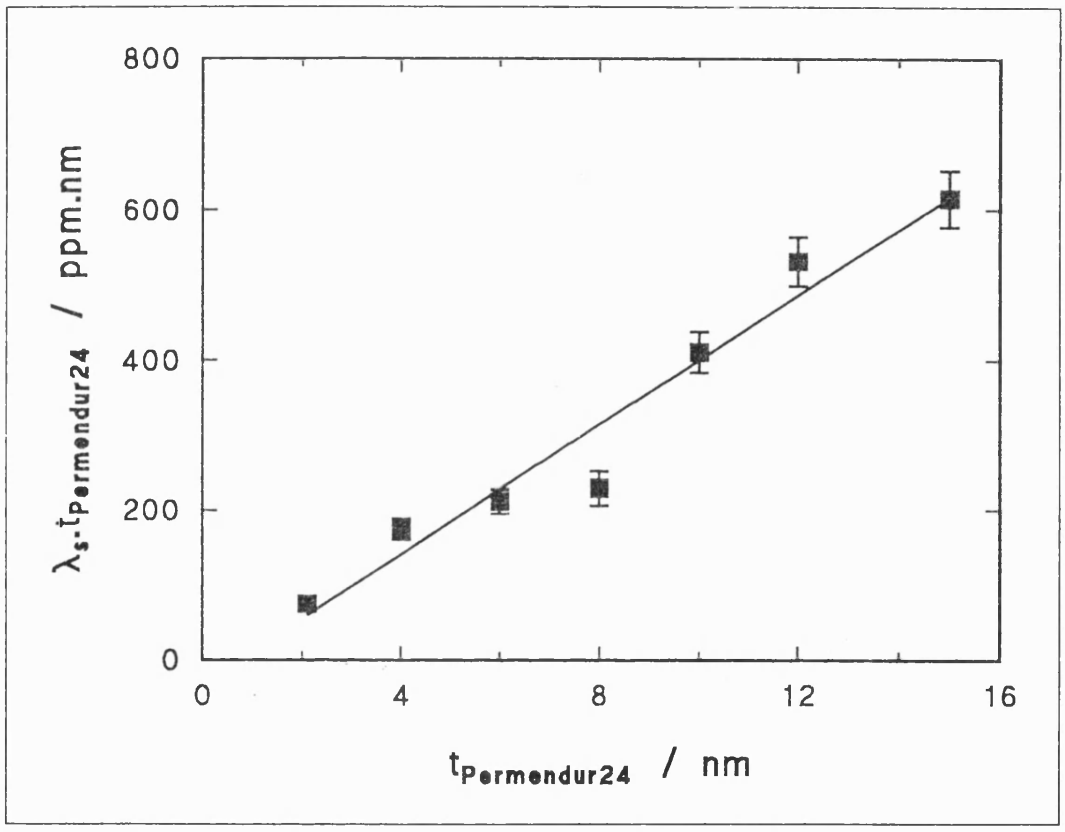

Figure 5.28a Saturation magnetostriction of Permendur24/Ag multilayers with fixed $t_{Ag} = 2nm$, with reference to Equation 2.3. The regression line is: $\lambda_s t_{Permendur24} = 43 t_{Permendur24} - 31$, $r = 0.9768$. λ_s in ppm, $t_{Permendur24}$ in nm.

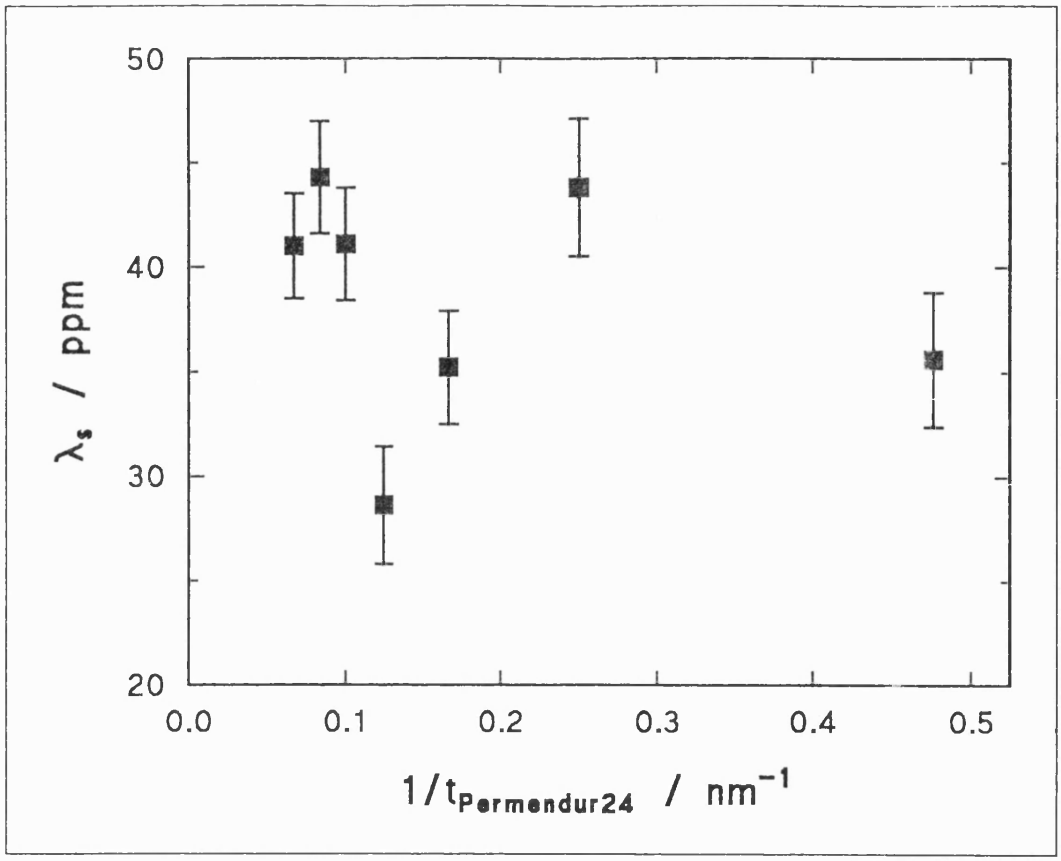

Figure 5.28b Saturation magnetostriction of Permendur24/Ag multilayers with fixed t_{Ag} = 2nm, with reference to Equation 2.2. The equation for the regression line (not shown) is:

$\lambda_s = -8/t_{Permendur24} + 40$, r = 0.1947. λ_s in ppm, $t_{Permendur24}$ in nm.

An interpretation of the λ_s data based on magnetic volume and interface contributions is valid, as can be seen more clearly from the presentation of the data in the form in Figure 5.28a than in Figure 5.28b. The above analyses (Equations 2.3 and 2.2 respectively) apply only when the contributions to λ_s from the magnetic layers and the interface regions are the same for each sample. As mentioned above, the XRD traces indicate random polycrystallinity in the multilayers (except possibly in multilayers with thin t_{Ag} and thicker $t_{Permendur24}$ where they may be some slight (110) texture) so such an interpretation is legitimate as regards different λ_s

values along different crystallographic axes. From the regression according to Equation 2.3 (Figure 5.28a) the contribution to λ_s from the bulk of the magnetic layers is λ_s^{mag} = +43±8ppm. This agrees within experimental error with the value of $\overline{\lambda_s}$ for a random polycrystalline Fe-Co alloy of this composition calculated using the expression given by Cullity (1972) and taking single-crystal values of the magnetostriction constants from Hall (1960). The magnetostriction constants are λ_{100} = +89±4ppm and λ_{111} = +11±4ppm, giving $\overline{\lambda_s}$ = +42±4ppm (errors are those estimated as being incurred in reading the data from the original figure). That there is a non-zero intercept and that λ_s values are lower in multilayers with thinner Permendur24 layers indicate that the interfaces have a non-negligible effect on the magnetostriction of these multilayers; compare the case of as-deposited HiSat50/Cu multilayers, discussed in Section 5.2.1, for which the magnetostriction is similar in each multilayer of the series. For thicker $t_{Permendur24}$ the interface effects are proportionately smaller and hence λ_s values are higher.

The application of the random polycrystalline expression to both HiSat50 and Permendur24-type alloys seems valid, as the agreement in both cases between calculation and experimental determination of λ_s^{mag} is excellent. This gives confidence in using the single-crystal magnetostriction constants in any model predicting values of $\overline{\lambda_s}$ in textured polycrystalline multilayers based on the expression presented by Cullity (1972).

The experimental value of $\overline{\lambda_s}$ quoted by Bozorth for a similar polycrystalline Fe-Co alloy in the bulk is +39ppm, while the value deduced from Masiyama's data is $2\lambda_e/3 \approx$ +27ppm. It seems likely that the samples of the latter could not be saturated in the 87.5kAm^{-1} field used, so measurements yield values lower than the saturation magnetostriction. It is significant, therefore, that measured values of

λ_s^{mag} for these multilayers agree with the calculated $\overline{\lambda_s}$ value, which is higher, whilst achieving magnetic softness. The maximum field in the SAMR apparatus used to measure λ_s is 18kAm^{-1}.

The largest value of λ_s in the series with fixed t_{Ag} = 2nm was +44±3ppm, for the multilayer 2×50(12nm Permendur24/2nm Ag), for which H_c = 560Am^{-1}, the lowest observed. As with the HiSat50/Ag multilayer series, the sample with the highest magnetostriction is also the one with the lowest coercivity. The same λ_s value was measured for the sample 2×75(4nm Permendur24/2nm Ag) but H_c = 1.70kAm^{-1}. It has been suggested that the highest λ_s values are measured in the softest films because the fields available in the apparatus could drive these films further into saturation. This reasoning would imply that other measured values of λ_s are lower than they should be. However, that the measurements were taken in the SAMR region was checked for each sample, and it has been shown above that the data fit well the Equation 2.3 which returns a value for λ_s^{mag} in line with the calculation of $\overline{\lambda_s}$ using experimental single-crystal values of λ_{100} and λ_{111} at saturation from Hall (1960). Also, SAMR data from the HiSat50/Ag series have been confirmed by SMFMR measurements, an independent technique.

The saturation magnetostriction values of the Permendur24/Ag series with constant $t_{Permendur24}$ = 10nm are shown in Figure 5.29. The general trend is for λ_s to be greater in multilayers with thicker t_{Ag}. This behaviour does not follow either of the data interpretations proposed above for magnetic/non-magnetic multilayers, which suggest that multilayers with a fixed magnetic layer thickness should have a constant magnetostriction, regardless of the non-magnetic layer thickness, provided that there is sufficient Ag to provide the full interface thickness, t_{int}. As mentioned before regarding HiSat50/Ag multilayers, the continuity of the Ag layer may affect λ_s in this series. The XRD traces show no especial crystallographic texture, so

texture is probably not the explanation for the λ_s variation seen here, although simple XRD scans are not a sensitive probe of texture.

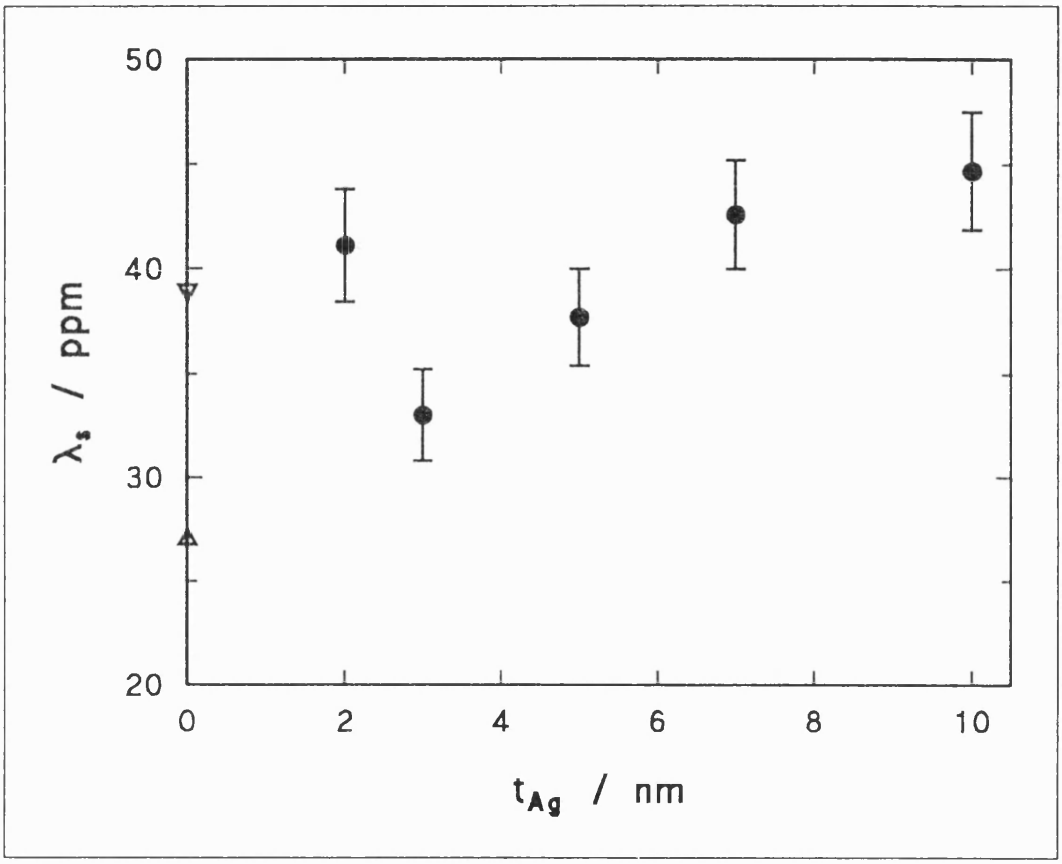

Figure 5.29 Saturation magnetostriction of Permendur24/Ag multilayers with fixed $t_{Permendur24}$ = 10nm (●). Δ Masiyama's $2\lambda_c/3$ value, ∇ Williams' λ_s value for bulk alloy from Bozorth (1951).

The largest λ_s value in this series was +45±3ppm, for the multilayer 2×40(10nm Permendur24/10nm Ag), which had H_c = 4.75kAm^{-1}, the highest coercivity of this series. This magnetostriction represents a slight increase over the experimental value of saturation magnetostriction of a bulk polycrystalline alloy of similar composition (+39ppm; Bozorth (1951)), but agrees within experimental error with $\overline{\lambda_s}$ calculated from single-crystal Fe-Co alloy magnetostriction constants ($\overline{\lambda_s}$ = +42

±4ppm). In the series with fixed t_{Ag} = 2nm, however, large magnetostriction was achieved simultaneously with low coercivity. In both multilayer series, observation of strained layers did not coincide with observation of high magnetostriction, so it appears that lattice strain does not influence high magnetostriction here. (Strain perpendicular to the plane is assessed, however, and this does not necessarily translate to strain of the opposite sense parallel to the film plane).

Mössbauer spectroscopy measurements (performed by Dr. J. M. Williams and Prof. J. Adetunji, University of Sheffield) on the multilayers have given the average angle, β, of the magnetic moments to the direction of the incident γ-ray, which was normal to the multilayer surface. In single-crystal Fe-Co alloys of composition similar to that of Permendur24 as deposited at the substrate, the easy direction of the magnetic moment is along the <100> set of crystallographic directions (Hall (1960)). Thus the likely average angle of the set of <100> crystallographic axes with respect to the film normal may be known, and the model calculation described in Section 4.3 can be applied (NB in the model, the moment is considered to lie along the [001] axis only, and simultaneous population of the [100] and [010] axes is not accounted for). Values of λ_{100} = +89ppm and λ_{111} = +11ppm were taken from Hall (1960). The error in reading these values from the paper is estimated at ±4ppm. This error is not shown in the diagram below (Figure 5.30). The points shown are from measurements on Permendur24/Ag multilayers with various Permendur24 and Ag layer thicknesses. When interpreting the data in this way, however, it must be remembered that the geometry of thin films is such that shape anisotropy tends to align the magnetic moments in the film plane. The magnetic moment direction is the result of the competition between these anisotropies (plus others) and is not necessarily in the <100> set of directions in this case. Also, the spread of moment angles is not known. For a sample in which the moment angles

are completely randomly distributed, the angle obtained would be $\beta = 54.7°$. XRD patterns showed no strong texture, although these θ-2θ scans are not particularly sensitive to it.

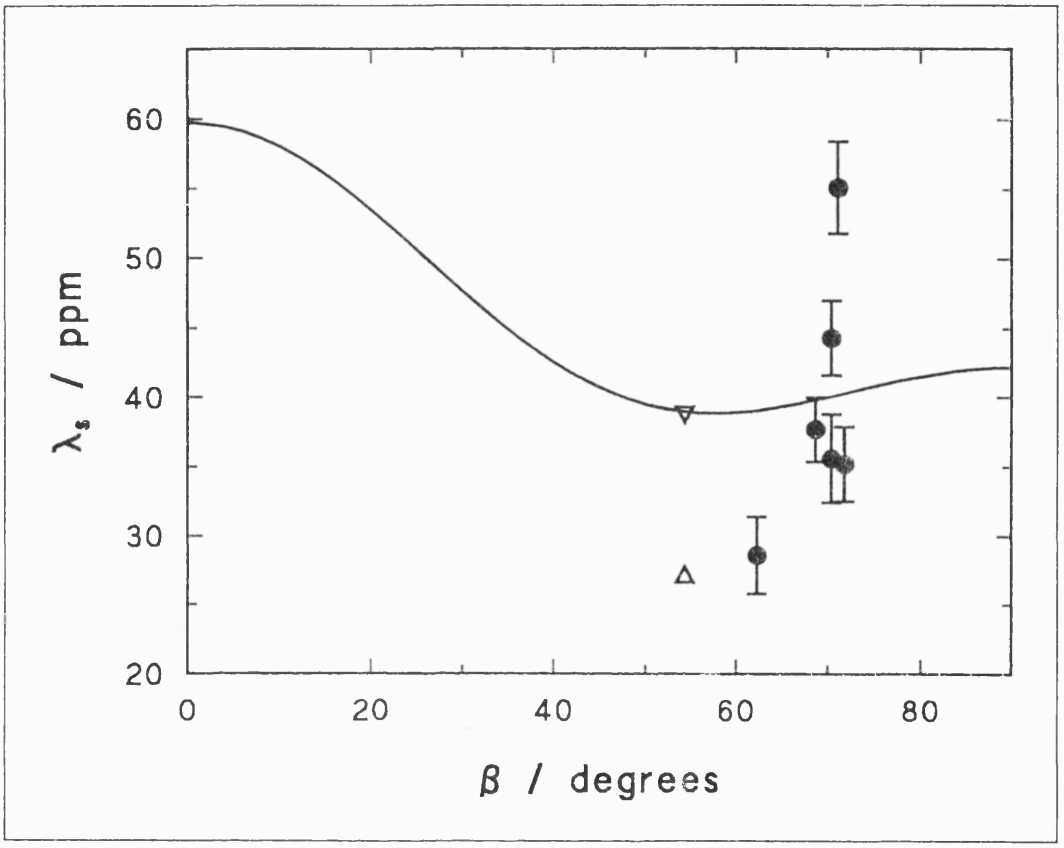

Figure 5.30 Saturation magnetostriction calculated from the model presented in Section 4.3 (solid line) for a Fe-Co alloy with the same composition as deposited Permendur24 at the substrate. In the model, the angle β is the angle of the [001] axis to the normal to the multilayer film; this is identified with the average moment angle measured by Mössbauer spectroscopy. ● SAMR and Mössbauer data for Permendur24/Ag multilayers; ∇ plain Permendur24 film (β from Mössbauer, Williams' λ_s from Bozorth (1951)); Δ plain Permendur24 film (β from Mössbauer, Masiyama's $2\lambda_s/3$ from Bozorth (1951)).

From the expression presented by Cullity (1972) and using the λ_s values along crystallographic axes from Hall (1960) the saturation magnetostriction of a random polycrystalline bulk Fe-Co alloy such as this is calculated to be $\overline{\lambda_s}$ = +42±4ppm. In the model above, the random polycrystalline case is described at $\beta = 90°$. This $\overline{\lambda_s}$ is to be compared with William's experimental value of +39ppm (Bozorth (1951)). It is coincidence, therefore, that the published λ_s value, coupled with the Mössbauer data for β, coincide with the model calculation. The Permendur24/Ag multilayer data are scattered around the model value. In view of the correspondence between experimental λ_s values for the multilayers and the calculated random polycrystalline $\overline{\lambda_s}$, and since the β values are similar, it would appear that β should be identified only with the moment angles, and not with the <100> directions. Thus the moment angles are largely in the film plane, as would be expected for thin-film geometry. The λ_s values are diverse, but this is explained in terms of Equation 2.3 (see Figure 5.28) for multilayers with fixed t_{Ag} and varied $t_{Permendur24}$. To apply the model calculation of $\overline{\lambda_s}$ for textured polycrystalline multilayers to experimental λ_s data successfully would require more sophisticated structural measurements in order to be able to identify the positions of the crystallographic axes. The present model is not suitable for comparison with data obtained from Mössbauer spectroscopy. XRD scans indicate that these multilayers are probably random polycrystalline, in which case it is more instructive to compare the multilayer λ_s results with the calculation of random $\overline{\lambda_s}$ mentioned above.

Work is in train in the group to establish whether λ_s can be enhanced over the calculated random polycrystalline $\overline{\lambda_s}$ by crystallographic texturing, with reference to the model calculation above. Multilayers are being fabricated at a wide range of r.f. powers and Ar pressures to give films with different, pronounced crystallographic textures and interface qualities. In suitably crystallographically

textured multilayers, it might be expected that the saturation magnetostriction could reach +89ppm, the experimental value of λ_{100} for a single-crystal Fe-Co alloy of similar composition (Hall (1960)).

The model was set up in this way to fix only the [001] axis with respect to the film normal, and leave other axes randomly oriented, since this was thought to match the experimental information obtainable. The physical situation may be different, however. When more is known about the crystal structure distribution, the model calculation may be modified to reflect this. At that point, application of the calculation to experimental λ_s data will provide deeper insight into the mechanisms producing the λ_s values observed in multilayers such as these.

5.3. Cobalt-Palladium/Silver Multilayers

Following the observation that silver or copper interlayers in iron-cobalt alloy films reduced the coercivity, multilayers were fabricated of a cobalt-palladium alloy with silver interlayers. Co-Pd alloys can be highly magnetostrictive, but are magnetically hard. The alloy of composition around $Co_{30}Pd_{70}$ has $\lambda_s \approx -170$ppm for a film about 200nm thick, r.f. magnetron sputtered onto glass at $P_{Ar} = 25$mtorr (Hashimoto *et al.* (1989a)). This film had (111) crystallographic texture. The coercivity, measured perpendicular to the film plane, was $H_c \approx 58 kAm^{-1}$. The sputtering pressure used in this project was $P_{Ar} = 5$mtorr, and it has already been noted that higher sputtering pressures increase H_c in Co/Pd and Co/Pt multilayers and Co-Pd alloy films (Section 2.3). For a film of $Co_{27}Pd_{73}$ grown at about 5mtorr Ar pressure, Hashimoto *et al.* report $H_c^{\perp} \approx 16.1 kAm^{-1}$. The effect of P_{Ar} on λ_s was not recorded.

A mosaic target of Co sectors on a Pd disc was made, the area of the Co sectors having been calculated to give an alloy composition at the substrate of

$Co_{30}Pd_{70}$ (at%) when deposited at 75W, P_{Ar} = 5mtorr. Electron probe microanalysis of films showed that the resultant deposit was $Co_{32}Pd_{68}$, with an error within about ±1at%. From Hashimoto *et al.* (1989a), this composition would be expected to have $\lambda_s \approx$ -160ppm. Multilayers were deposited with fixed t_{Ag} = 2nm and t_{CoPd} = 1, 2, 3, 4, 6, 8, 12nm, and also with fixed t_{CoPd} = 6nm, t_{Ag} = 5nm and 10nm. Fifty bilayers were deposited on each side of 26μm Kapton substrates, except for t_{CoPd} = 1nm (2×100 bilayers) and t_{CoPd} = 2nm and 3nm (2×75 bilayers). There were no cap or buffer layers. The first layer was Co-Pd and the last was Ag in each case. A plain alloy film was also fabricated: 400nm Co-Pd on each side on the substrate. The background pressure was 4.5-6.5×10^{-7}torr.

The multilayers could not be saturated in the d.c. magnetometer, although minor loops could be traced for some. An example of an in-plane loop is shown in Figure 5.31. It is clear that saturation is not approached, from the slant on the loop. To obtain MH data, therefore, loops were measured in the plane of the films using a Faraday balance at room temperature. Figure 5.32 shows a typical loop. The coercivities were obtained from loops where many data points were taken around H = 0.

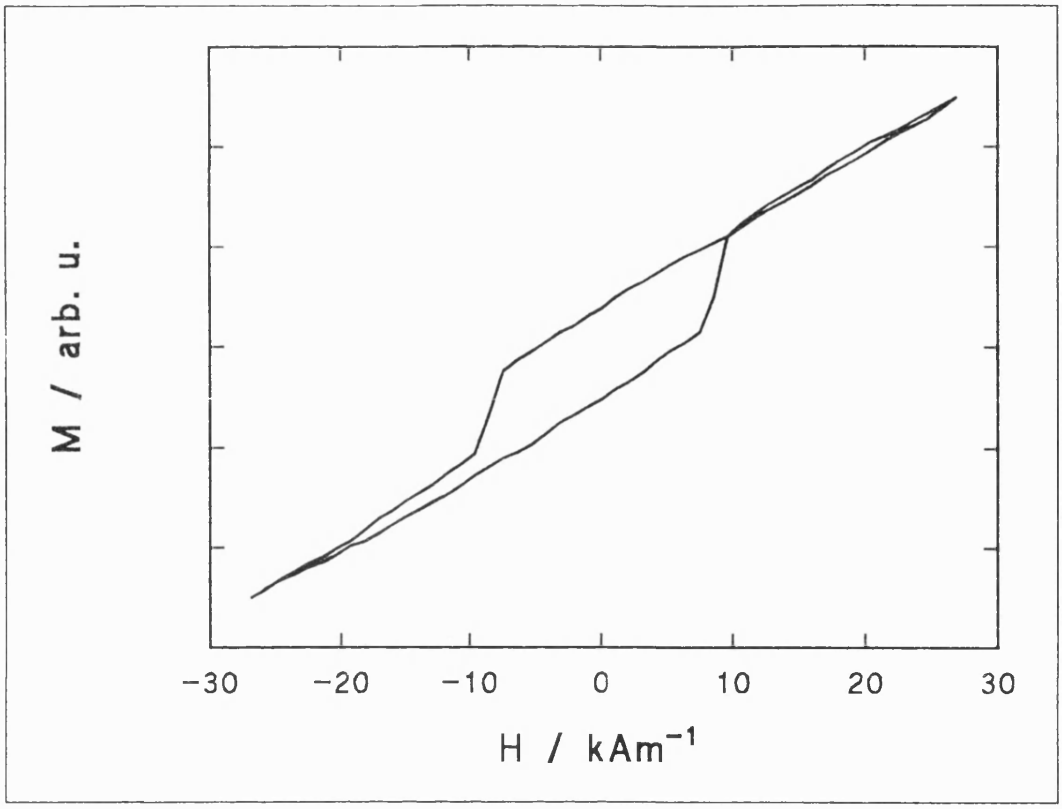

Figure 5.31 Minor hysteresis loop for 2×75(3nm Co-Pd/2nm Ag) on Kapton.

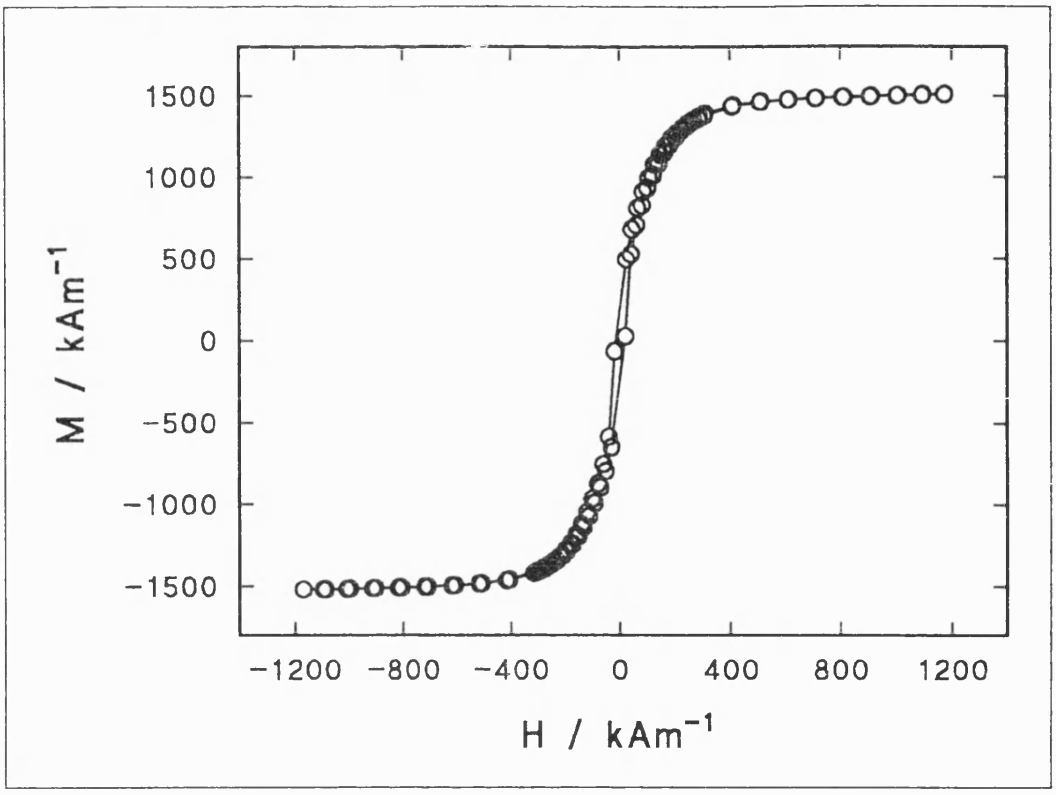

Figure 5.32 Hysteresis loop of 2×50(8nm Co-Pd/2nm Ag) on 26μm Kapton.

Values of coercivity and saturation magnetisation obtained from the Faraday balance hysteresis loops are plotted in Figure 5.33. The Ag interlayers do soften the Co-Pd films, a minimum H_c of 10.7kAm^{-1} being observed for the multilayer 2× 75(3nm Co-Pd/2nm Ag). The plain 2×400nm Co-Pd film had H_c = 17.2kAm^{-1}; some of the multilayers had higher coercivities than this. M_s does not much vary with the Co-Pd layer thickness for t_{CoPd} > 2nm, being close to the value for the plain alloy film. For t_{CoPd} = 1nm, however, M_s is much reduced. The reduction is too great to be attributed to magnetically dead layers, considering the M_s values measured for the other thin Co-Pd multilayers.

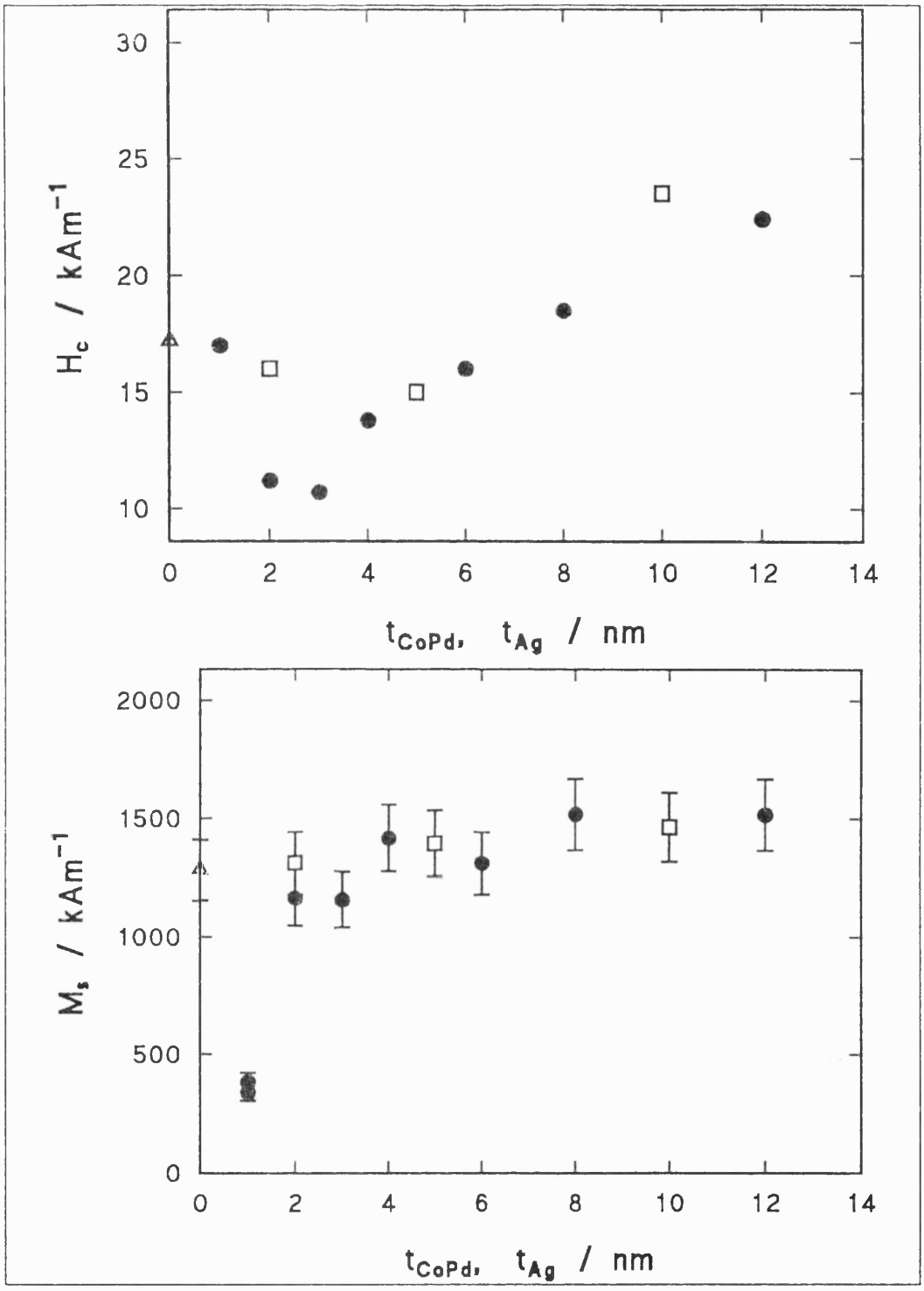

Figure 5.33 Coercivity (top) and saturation magnetisation (bottom) of Co-Pd/Ag multilayers vs. Co-Pd or Ag layer thickness. ● t_{Ag} = 2nm (vs. t_{CoPd}); □ t_{CoPd} = 6nm (vs. t_{Ag}); Δ plain Co-Pd film.

The Co-Pd alloy films of Hashimoto *et al.* are magnetically harder to saturate parallel to the film plane, although H_c may be lower in this direction. The fields required to saturate a $Co_{25}Pd_{75}$ alloy film were around 350kAm^{-1} perpendicular to the film plane and more than 800kAm^{-1} parallel to the plane. Figure 5.34 shows the fields required to bring the Co-Pd/Ag multilayers to 95% and 97% of M_s in-plane.

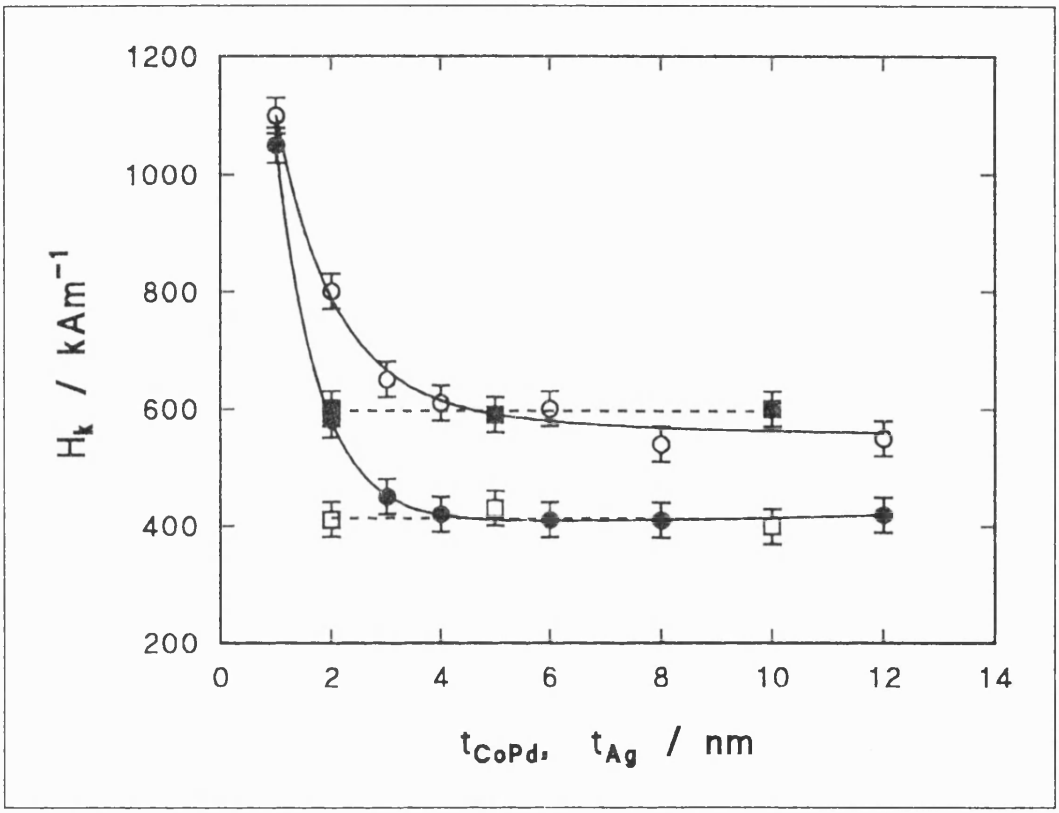

Figure 5.34 Fields, H_k, required to bring Co-Pd/Ag multilayers to magnetic saturation. ●, ○ t_{Ag} = 2nm (vs. t_{CoPd}); □, ■ t_{CoPd} = 6nm (vs. t_{Ag}). The higher H_k values are those required to bring the sample to 97% of M_s; the lower values, to 95% of M_s. The curves are fitted double decaying exponentials to guide the eye; the straight lines show the average H_k values for the multilayers with t_{CoPd} = 6nm.

The H_k values are lower than those obtained from the published data of Hashimoto *et al.*, for $t_{CoPd} \geq 3$nm. For $t_{CoPd} \geq 4$nm, H_k is unaffected by Co-Pd layer thickness. Below $t_{CoPd} = 3$nm, however, H_k rises sharply. For multilayers with $t_{CoPd} = 6$nm, H_k is independent of t_{Ag}, being 410kAm^{-1} to reach 95% of saturation or 600kAm^{-1} for 97% saturation.

Saturation magnetostriction was measured by the strain modulated ferromagnetic resonance technique (SMFMR) by Dr. R. Zuberek of the Polish Academy of Sciences, Warsaw. The M_s values required for the calculation were taken from the Faraday balance measurements. The volume of Co only in the multilayers was used in calculating M_s; this brought the λ_s values in line with bulk values expected (Hashimoto *et al.* (1989a)). Using the volume of Co only in calculating M_s, the average g-factor found from conventional FMR measurements (performed in Bilbao at 34.0GHz) was 1.57±0.35 for the series with $t_{Ag} = 2$nm, indicating mixed electron spin and orbit contributions to the magnetism. If the volume of Co-Pd alloy was used, the average g-factor became 1.99±0.21, indicating almost pure spin magnetism. Magnetostriction values were then reduced by about two-thirds, taking them well out of line with expected values.

In accordance with the two (comparable) models proposed in Section 2.4 for the interpretation of λ_s data on magnetic/non-magnetic multilayers, the magnetostriction data for the Co-Pd/Ag multilayers are presented in Figures 5.35a and b, below.

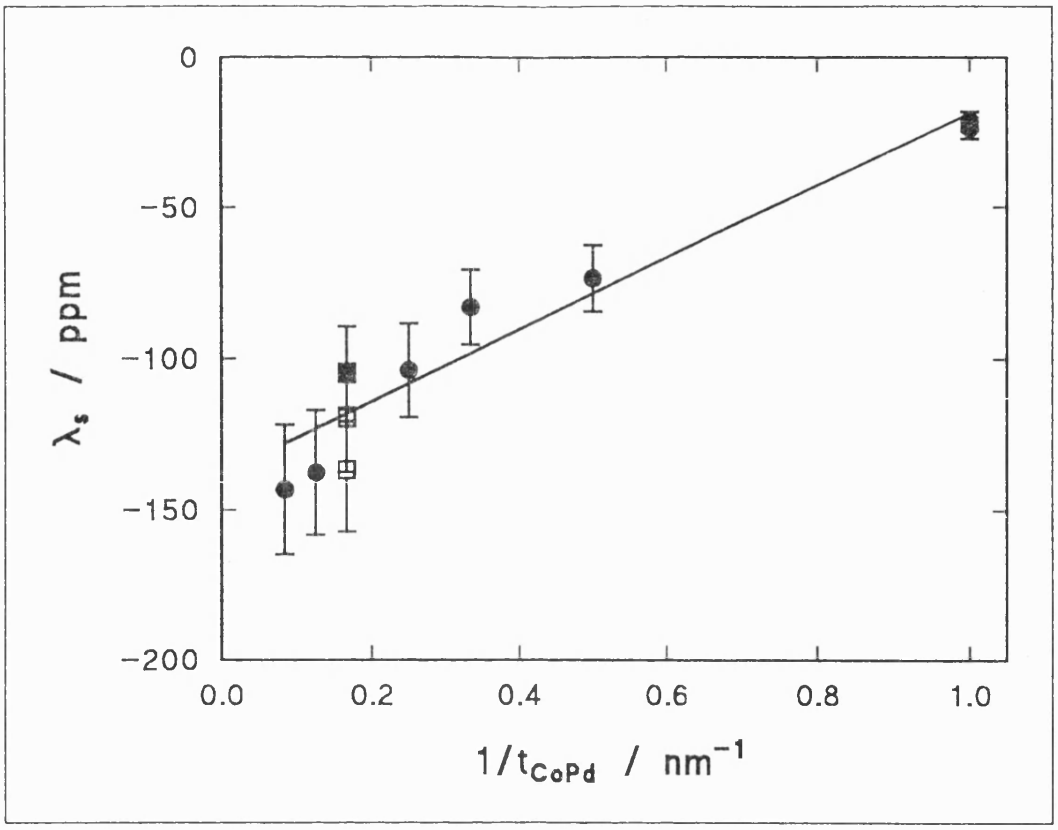

Figure 5.35a Saturation magnetostriction data, taken by SMFMR, for Co-Pd/Ag multilayers on 26μm Kapton substrates; after Equation 2.2. Regression line refers only to data for the series with t_{Ag} = 2nm. $\lambda_s = 119/t_{CoPd} - 138$ (λ_s in ppm and t_{CoPd} in nm; correlation coefficient r = 0.9684). ● t_{Ag} = 2nm; □ t_{CoPd} = 6nm.

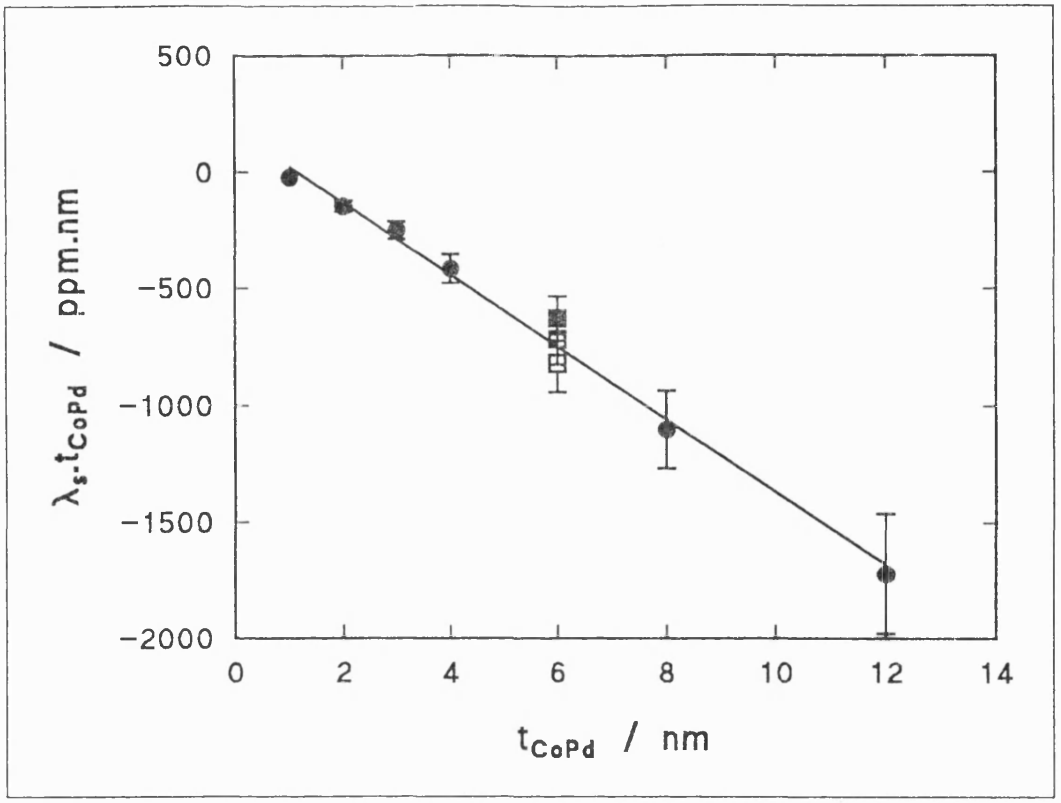

Figure 5.35b Saturation magnetostriction data, taken by SMFMR, for Co-Pd/Ag multilayers on 26μm Kapton substrates; after Equation 2.3. Regression line refers only to data for the series with t_{Ag} = 2nm. $\lambda_s t_{CoPd} = -155 t_{CoPd} + 176$ (λ_s in ppm, t_{CoPd} in nm; r = 0.9952). ● t_{Ag} = 2nm; □ t_{CoPd} = 6nm.

From Figure 5.35a the contribution to λ_s from the magnetic layer is λ_s^{v} = -138± 6ppm. The corresponding value obtained from the second presentation is λ_s^{mag} = -155±12ppm. These values are to be compared with the saturation magnetostriction reported by Hashimoto *et al.* for a Co-Pd alloy film of similar composition: $\lambda_s \approx$ -160ppm. On the second plot, the non-zero intercept is assigned to effects at the interfaces, for which λ_s^{int} and t_{int} are not uniquely defined. In that model, the data are not expected to be perfectly linear when plotted as $\lambda_s t_{mag}$ vs. t_{mag}; curvature in the data set occurs when the interface thickness is not negligibly small compared to the magnetic layer thicknesses.

The models apply independently of t_{Ag}, although for Equation 2.3 it is required that the individual layer thicknesses be sufficient to incorporate the whole of the interface region. Therefore, all the data points can be included in the regressions, regardless of t_{Ag}. Such analysis leads to:

1) $\lambda_s = 123/t_{CoPd} - 142$ ($r = 0.9652$), giving $\lambda_s^{\nu} = -142 \pm 10$ppm; and

2) $\lambda_s t_{CoPd} = -155 t_{CoPd} + 175$ ($r = 0.9942$), giving $\lambda_s^{CoPd} = -155 \pm 12$ppm once more.

Data analysis by these models is applicable whilst the same contribution to λ_s from the magnetic layers is made in all the multilayers, which implies that they should all have the same crystallographic texture. When the texture varies, λ_s is affected, since magnetostriction constants may be different in different crystallographic directions. XRD showed that all the multilayers were fcc polycrystalline, exhibiting strong (111) crystallographic texture, i.e. the (111) crystallographic planes lay predominantly parallel to the substrate. Both the Co-Pd alloy and Ag in bulk form take the fcc structure. The plain 2×400nm Co-Pd film was particularly strongly (111) textured. (A weak peak can also be seen at $2\theta = 36.8°$, due to Cu-Kβ radiation). A selection of XRD patterns is presented in Figure 5.36. Other authors also report (111) texture in Co-Pd alloy films and Co/Pd multilayers, e.g. Takahashi *et al.* (1993), Bennett *et al.* (1991), Hashimoto *et al.* (1989a), den Broeder *et al.* (1987). Taking the plain Co-Pd film as a reference, and comparing bulk d-spacing values from Ag, the lattice mismatch is calculated to be 7.1%, again too high to be expected to be completely accommodated by lattice strain at the interfaces.

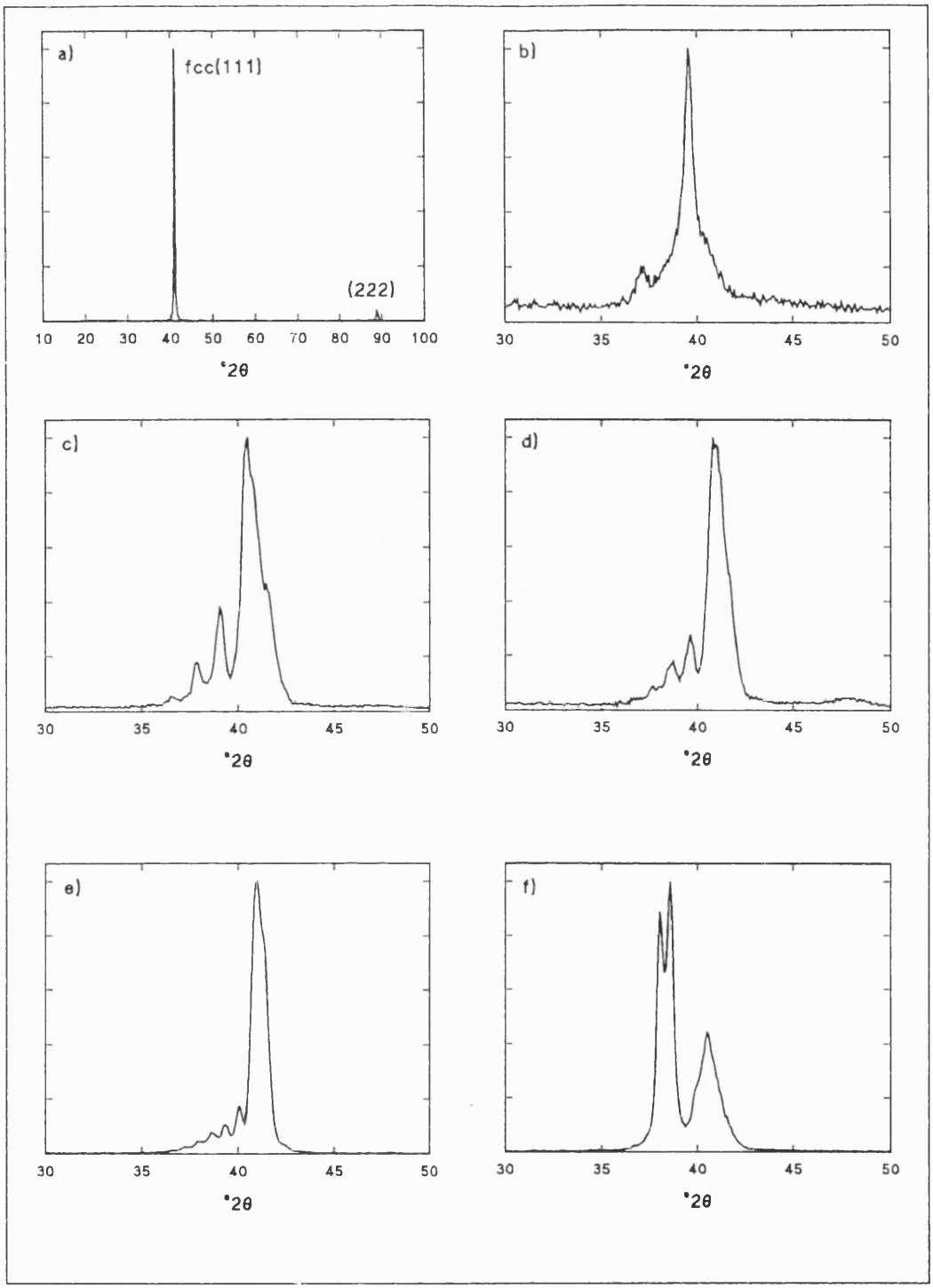

Figure 5.36 XRD patterns: a) Plain 2×400nm Co-Pd film; b) 2×75(2nm Co-Pd/2nm Ag); c) 2×50(6nm Co-Pd/2nm Ag); d) 2×50(8nm Co-Pd/2nm Ag); e) 2×50(12nm Co-Pd/2nm Ag); f) 6nm Co-Pd/10nm Ag). The vertical axes are X-ray intensity in arbitrary units (linear scale, each trace normalised).

For the 2×100(1nm Co-Pd/2nm Ag) multilayer, a single peak at $2\theta \approx 39°$ was observed, corresponding to the average spacing of the Ag and Co-Pd (111) planes. As t_{CoPd} increased, this peak separated into Ag (111) and Co-Pd (111) peaks. Satellite peaks appeared around the Ag (111) peak for $t_{CoPd} \geq 4$nm. Smaller, broad satellites were distinguishable around the Co-Pd (111) peak. For thinner layers, the satellites disappeared and the main peak bases were broadened. Up to seven orders of satellites were visible for thicker t_{CoPd}. The presence and sharpness of the satellites indicates that the interfaces were smooth and the modulation period uniform throughout the multilayer stack. Modulation periods calculated from the satellite peak positions agree with the designed layer thicknesses to within 5%-10%. It appears that Ag wets the fcc Co-Pd alloy more readily than the bcc Fe-Co alloys of Section 5.2, where XRD satellite peaks were not observed.

All the samples were annealed for a total of 130 minutes at 300±4°C in forming gas (flow rate greater than $50cm^3min^{-1}$). There was no tarnishing.. The XRD patterns were unaltered, and the multilayers still could not be saturated in the d.c. magnetometer, so annealing studies were not pursued.

The highest λ_s value observed in the Co-Pd/Ag multilayers was -143±21ppm, for the multilayer 2×50(12nm Co-Pd/2nm Ag) for which $H_c = 22.4kAm^{-1}$. The softest multilayer, 2×75(3nm Co-Pd/2nm Ag) had λ_s = -83±12ppm (H_c = $10.7kAm^{-1}$). These saturation magnetostriction values have been shown to be consistent with the value obtained by Hashimoto *et al.* (1989a) for a plain alloy film of the same Co-Pd composition, of approximately -160ppm, using a description based on assuming contributions to λ_s from the volume of the Co-Pd layer and from the interface regions. The film of Hashimoto *et al.* also had strong (111) crystallographic texture.

Multilayers with smooth interfaces and controlled periodicities were produced, as evidenced by the appearance of XRD satellite peaks for multilayers with thicker

component layers. Modulation periods calculated from the XRD satellite peak positions were consistent with designed layer thicknesses. Although the λ_s variation is monotonic with t_{CoPd}, H_c is not. Magnetostriction is sacrificed in softening the Co-Pd films, but softness is not necessarily sacrificed in films with higher λ_s values. To obtain softer multilayers containing Co-Pd, it might be profitable to try making Co-Pd/Co or Co-Pd/Fe multilayers. Magnetostriction would still be sacrificed to some extent, but the Co or Fe layers might be expected to soften the films more than Ag layers.

5.3.1. Simulation and Fitting of XRD Patterns of Co-Pd/Ag Multilayers

Simulations and fits to the XRD traces were performed for some of the samples. Those with clear satellites were chosen, as the goodness of fit and the variation in the pattern due to changes in layer thickness parameters were more readily assessed visually than for patterns with no satellites (e.g. Fe-Co/Ag multilayers). The "best fit" choice of the program was thus monitored. The simulation/fit program took many hours to run, and many iterations with different ranges of the fit parameters were required to produce a pattern which approached the original measured data. The simulated pattern was very sensitive to changes in the fit parameters, and individual features in the patterns were generally affected by alterations to any of the parameters, making it difficult to converge towards a suitable range of parameters to test. Below are shown the measured and fitted patterns for two samples. The trace of the 400nm thick plain Co-Pd film (Figures 5.37a and b) also contained very weak peaks due to Cu-Kβ radiation (e.g. (111) peak at $2\theta = 36.8°$ - see Figure 5.36a). The fit program did not take this into account, nor was it possible to strip these lines out using the XRD software. Their

amplitude, however, is more than 200 times weaker than the peaks from Cu-Kα radiation.

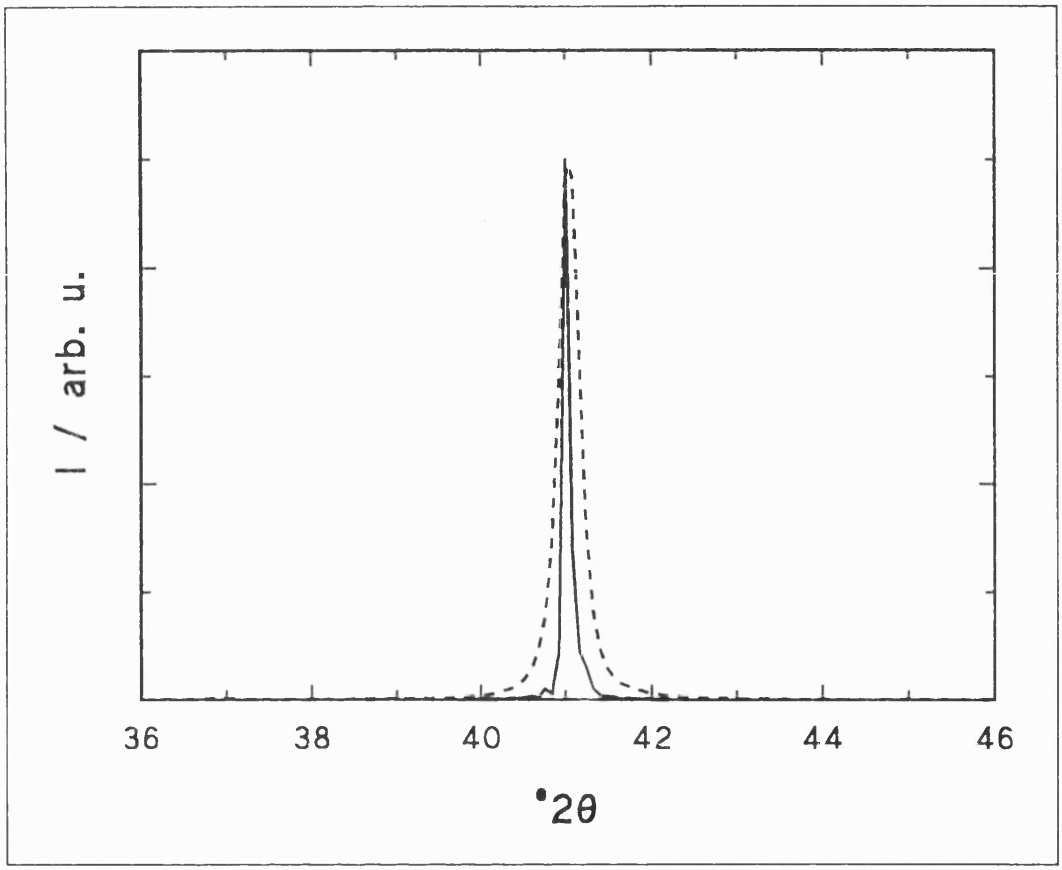

Figure 5.37a Fitted (solid line) and measured (dashed line) X-ray diffraction spectra (background subtracted) of a 400nm Co-Pd film. The X-rays do not see the film deposited on the reverse side of the substrate. Fit parameters: d_{111}(Co-Pd) = 0.2198nm, roughness = 0. The layer thickness was fixed at 400nm.

In fitting this trace, the Co-Pd layer thickness was fixed at the design thickness of 400nm. Although the width of this peak is not well fitted, increasing the roughness parameter did not alter it, but only introduced low, sharp oscillations at the lower end of the angular range used. Increased peak width with increased roughness would not be expected in the pattern of a single film. The peak

broadening in the measured trace may be caused by a range of d-spacings present in the film, and/or by film stress and/or by a limited grain size. If the Scherrer equation (see Guinier (1963)) is used here, the estimated grain size is 38nm. The fit procedure was carried out again, investigating with the layer thickness around 38nm. This yielded the result shown in Figure 5.37b, in which the peak width is more closely fitted, using t_{CoPd} = 29nm, reflecting the grain size in the film. Another problem with simulating XRD patterns is thus highlighted: the grain size is not accounted for in the simulation, and the layer thicknesses affect the peak widths as well as the positions of any satellites in the case of multilayer samples. (The roughness parameter also affects peak width). This causes difficulties in fitting the experimental traces, or can cause the traces to be fitted reasonably with physically improbable values of the fit parameters. This contributed to the great difficulty in obtaining any reasonable fits for patterns from Fe-Co/Ag multilayers where there were no satellite peaks to help fix the individual layer thicknesses by their positions and where grain sizes and layer thicknesses were similar values.

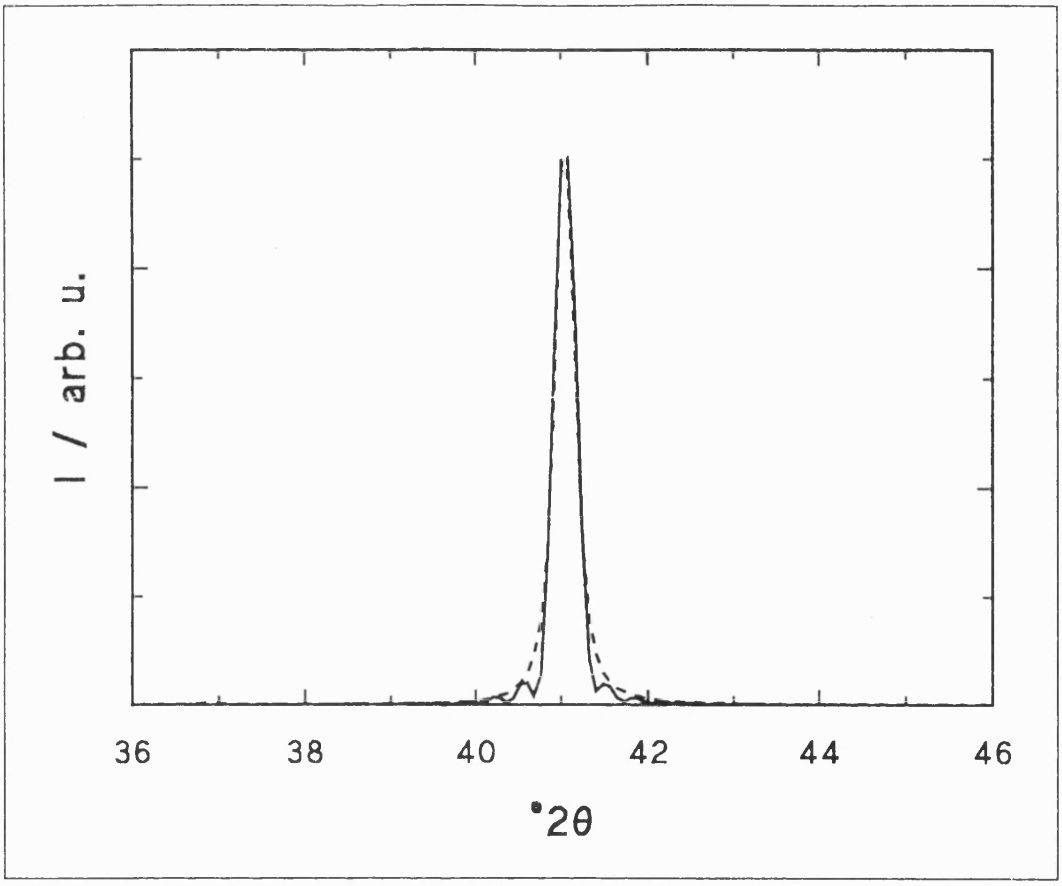

Figure 5.37b Fitted (solid line) and measured (dashed line) XRD pattern of a 400nm Co-Pd film (background corrected). The fit parameters were: d_{111}(Co-Pd) = 0.2199nm, roughness = 0 and t_{CoPd} = 29nm, which reflects the grain size in the film.

The experimental and fitted patterns of the multilayer 2×50(6nm Co-Pd/5nm Ag) are shown in Figure 5.38. The clear satellite peaks helped to fit the layer thickness parameters. It was chosen to aim to fit the Ag peak height and width, the Co-Pd peak intensity and the satellite peak positions as closely as possible.

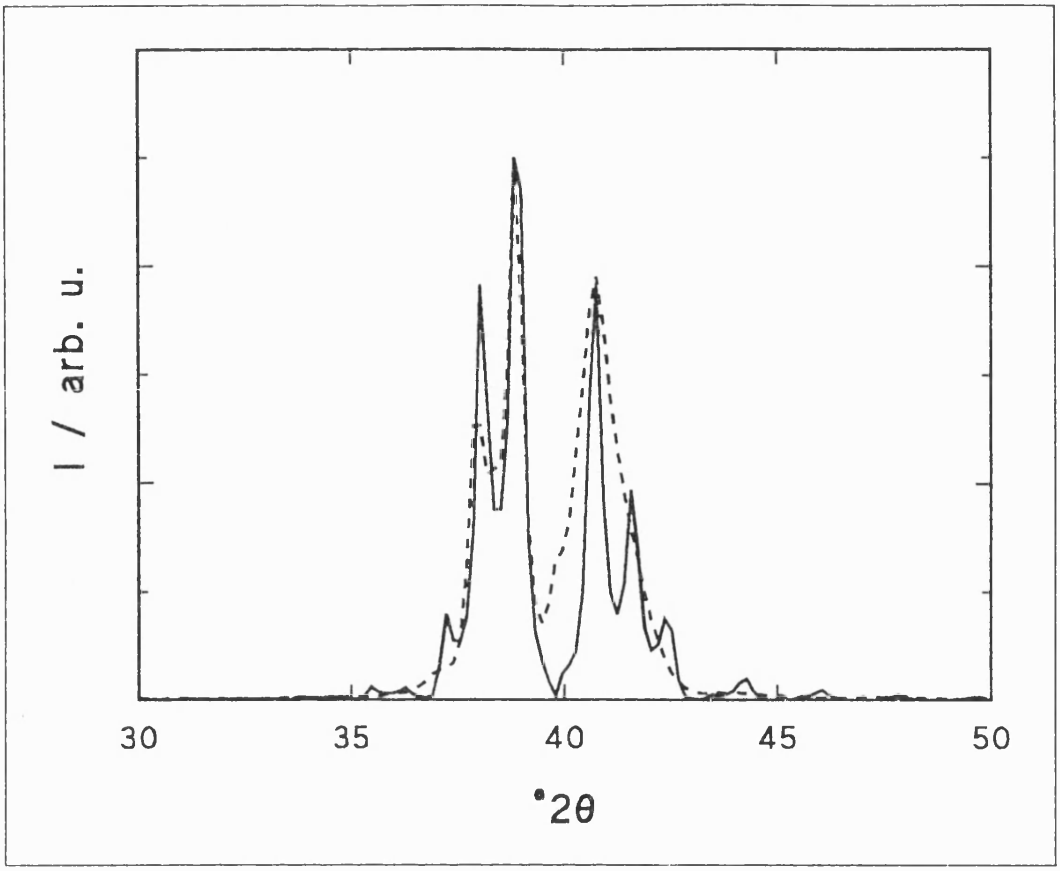

Figure 5.38 Fitted (solid line) and measured (dashed line) X-ray diffraction spectra (background subtracted) of 50(6nm Co-Pd/5nm Ag). The X-rays do not see the part of the multilayer deposited on the reverse side of the substrate. Fit parameters: d_{111}(Co-Pd) = 0.2192nm, d_{111}(Ag) = 0.2340nm, t_{CoPd} = 4.94nm, t_{Ag} = 5.50nm, roughness = 0.078nm.

The fitted d-spacings correspond to lattice strains of -0.3% in the Co-Pd (111) planes, compared to the thick film, and -0.8% in the Ag (111) planes, compared to bulk Ag. These refer to planes which lay parallel to the film surface, so the strain is measured normal to the film. That the width of the Ag main peak is well fitted while that of the Co-Pd peak is not implies that the roughness parameter as it stands is inadequate. At present, the roughness parameter allows for variation through the multilayer stack of the multilayer periodicity, $\Lambda = t_a + t_b$. It is

anticipated that the two peak widths would be better fitted if two roughness parameters were included, one for each layer thickness. The modulation period calculated from the two layer thickness fit parameters is $\Lambda = 4.94 + 5.50$ nm = 10.44nm, compared to the designed period of 6 + 5nm = 11nm. This represents a modulation period only 5% different from the design value.

To arrive at these fit parameters, it was necessary to impose a strategy on the simulation program by judicious choice of parameter ranges and of which should be varied when. Due to the method employed in the program of testing all combinations of parameters, it took too long to run over ranges of parameters wide enough to include all the possibilities one might anticipate. However, to include a strategy to converge on the correct set of fit parameters might prove complex, as small changes in one parameter can have a dramatic effect on the resulting simulated pattern (see below). The process by which the above results were obtained was as follows: first, the roughness range was set, and various d-spacing values based on those returned by the XRD software were tested to establish the combination of these which most closely fitted the spectrum, along with reasonable values of layer thicknesses, bearing in mind the value of Λ calculated from the satellite peak positions. Such preliminary fits were run overnight. After these, the roughness was set at 0.08nm, and the layer thicknesses at $t_{CoPd} = 5.0$nm and $t_{Ag} =$ 5.5nm, while the d-spacings were varied over small ranges, in steps of 0.0001nm. When one peak was fitted well for position and amplitude, its d-spacing was fixed while the other was varied to obtain a good peak position. With that then fixed, t_{CoPd} and t_{Ag} were varied to establish their best values, in steps of 0.1nm. The important factor here is the position of satellite peaks. Once a peak and satellite position had been fitted with the layer thickness parameters, little adjustment of t_{Ag} or t_{CoPd} was necessary. Different values of t_{CoPd} and t_{Ag} or roughness could also alter the relative amplitudes of peaks. The thicknesses were then set constant, and

the process of varying the d-spacings was repeated. This procedure was iterated until the fit was judged by eye to be good. The final stages were to investigate around the best fit layer thickness parameters so far in finer steps of 0.01nm, and to vary the roughness parameter. The best roughness value selected by the program was not necessarily the one which fitted well any single peak. Thus, the roughness parameter was altered step by step, viewing the resulting pattern each time; it was chosen here such that the Ag peak width was well fitted. Further fine adjustment of the d-spacings was necessary after the roughness was altered. To obtain a reasonable fit to the data, it was necessary for the operator to guide the process.

Considering the amount of operator judgement exercised in producing this fit, it is possible that other combinations of fit parameters might also produce good fits to the experimental data. If other criteria had been employed, e.g. that the Co-Pd peak width should be well fitted with preference over the Ag peak width, other results would have been obtained for the roughness parameter at least.

Figure 5.39 illustrates how sensitive the result of the simulation could be to changes in fit parameters. Changes in parameters did not always produce such dramatic changes in simulated spectra, but the possibility of such unpredictable behaviour complicated the task of fitting a measured spectrum.

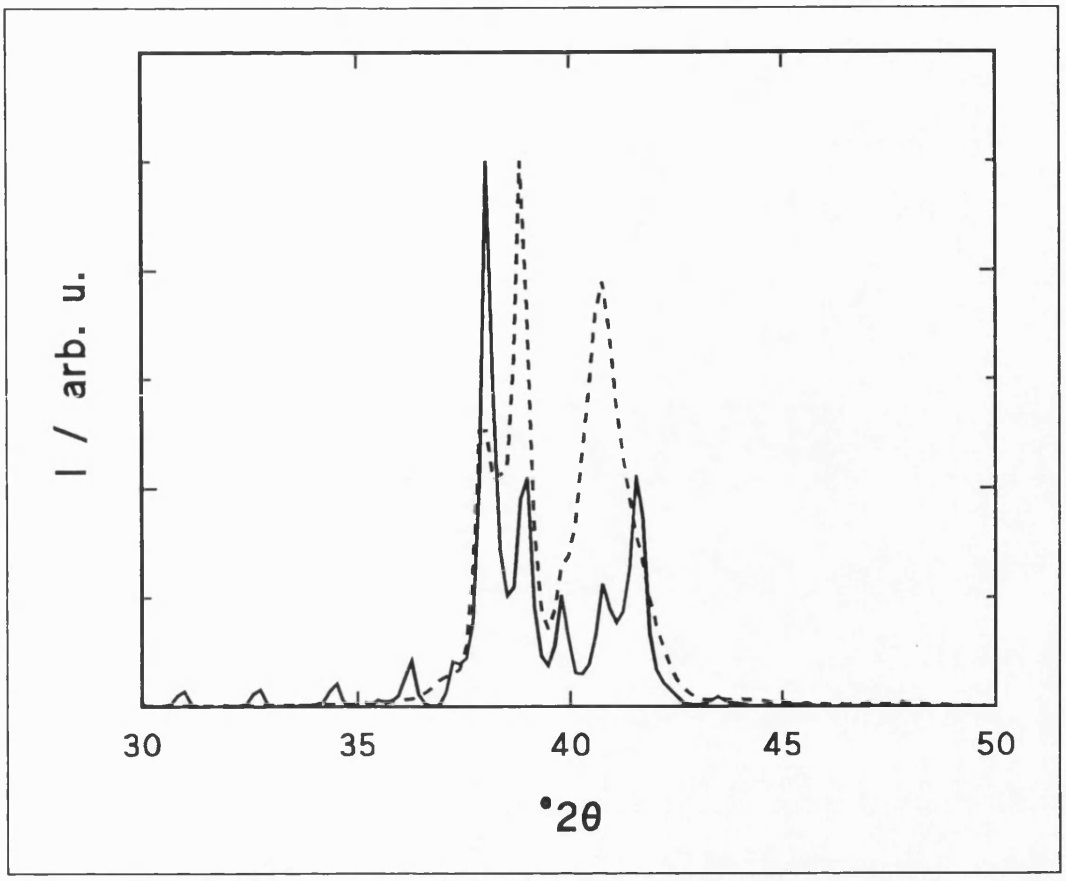

Figure 5.39 Illustration of the sensitivity of the simulated spectrum (solid line) to a change in one fit parameter (cf. Figure 5.38). The only fit parameter which has been changed is $d_{111}(Ag)$. Here, $d_{111}(Ag) = 0.2341nm$, whereas in Figure 5.38, $d_{111}(Ag) = 0.2340nm$. Measured data: dashed line (background corrected).

Attempts to fit patterns from Fe-Co/Ag multilayers were unsuccessful. "Best fits" were poor and layer thickness values returned improbable. This problem may be linked with the effects of grain size on experimental traces, as mentioned above; an effect which is not accounted for in the simulation. The lack of satellite peaks made identifying good layer thicknesses difficult and the broad bases of main peaks could not be well fitted even if the shape of the upper part of the peak was matched.

For this pattern-fitting program to be useful on a routine basis, the program must be re-coded. It will be necessary that it be written in a faster language and run on computers designed for carrying out repeated calculations. The most significant improvement would be to include in the program some strategy to converge on the best fit. This would markedly accelerate arrival at a solution. It may also be useful to include some criterion on the choice of the roughness parameter, e.g. that the width of the most intense peak should be well fitted. It would be useful if the operator were to input "seed" values of d-spacing, layer thicknesses, etc., based on designed values and information returned by the XRD peak-fitting software, and for the program to investigate around these. The investigation could be guided if code were included to recognise if, for example, a main peak position was at too low and angle, and take appropriate action on the d-spacing parameter, i.e. reduce it in this example. This process would have to be iterated as the layer thickness were altered. Closer fits to data would be expected for multilayers with greater crystallinity, where the grain size is much greater than the layer thicknesses and does not so severely affect the shape of the peaks. Problems arise as small parameter changes can cause significant modification of the resulting pattern. Some patterns have, however, been simulated with moderate success.

<u>Summary.</u> All multilayers containing **Fe-Co alloys** (that is, **HiSat50** or **Permendur24**) with **Ag** interlayers were bcc polycrystalline with no or little crystallographic texture. Interfaces were rough. There were weak trends that the d-spacing of a layer relaxed towards its bulk value as the thickness of that layer increased. Grain sizes increased as layer thickness increased, with plain alloy films having the largest grain sizes. All the multilayers were magnetically softer than the plain alloy films. With fixed Ag thickness and varied Fe-Co thickness, the softest films were those with the thickest alloy layers. Annealing had a small effect on H_c.

For films with fixed alloy thickness and varied Ag thickness, H_c was a minimum for t_{Ag} = 1.5-2nm.

The magnetostriction values for the multilayers with fixed t_{Ag} and varied $t_{Fe\text{-}Co}$ were larger for thicker $t_{Fe\text{-}Co}$. The values were found to be in line with those calculated for random polycrystalline alloys from published single-crystal magnetostriction constants of similar Fe-Co alloys. The most magnetostrictive samples were also those most magnetically soft. There was no evidence that crystallographic strain enhanced λ_s. **HiSat50/Ag** multilayers had higher λ_s than **Permendur24/Ag** multilayers of similar thickness combinations since HiSat50 is an alloy which has a higher λ_s in polycrystalline form than does Permendur24. The λ_s data fit a model constructed on the basis of contributions to the total magnetostriction from the magnetic layer and interface regions. Magnetostriction data for multilayers with fixed Fe-Co alloy thickness and varied t_{Ag} were not fitted by this model. It is tentatively suggested that the variation in λ_s observed is due to the differing degrees of continuity of the Ag layer at different thicknesses.

On inspection of the data, it was concluded that the Mössbauer data could not be interpreted as giving information on crystal structure and texture. Though a model to link textured polycrystallinity to magnetostriction has been developed here (Section 4.3), it is necessary to know the orientation of the (001) axes, so it could apply to Permendur24 but not to HiSat50. Further development of the model and more precise crystallographic information are required for λ_s to be linked directly with crystal structure.

HiSat50-Ag dispersed films were grown which were polycrystalline with weak (110) texture. There was no pattern in the variation of d_{110} with the designed Ag volume concentration, although the grain size decreased as the proportion of Ag increased. The films were all magnetically hard and could not be saturated in the d.c. magnetometer. SAMR was not possible because of this hardness, and SMFMR was inconclusive. There is some doubt as to the actual

volume compositions of the samples, as EPMA data have proved inconsistent.

HiSat50/Cu multilayers with t_{Cu} = 2nm were polycrystalline with rough interfaces. The variation of H_c with $t_{HiSat50}$ was smaller than for the HiSat50/Ag multilayers and the trend was opposite: H_c was lower for thinner t_{Cu}, for which the grain sizes were smaller. There was no strong variation of λ_s across the series, as-deposited, indicating little influence from the interfaces. The average value of λ_s was lower than that expected from the calculation from single crystal magnetostriction constants. The different behaviours observed between HiSat50/Cu and HiSat50/Ag multilayers are tentatively ascribed to the different wetting characteristics and atomic sizes of Ag and Cu.

Co-Pd/Ag multilayers were grown with strong (111) crystallographic texture and sharp, flat interfaces. They were magnetically too hard to be measured in the d.c. magnetometer and so the hysteresis measurements were taken on a Faraday balance. The saturation magnetostriction was measured by SMFMR. The minimum H_c was found for $t_{Co\text{-}Pd}$ = 3nm. Some multilayers were harder than the plain Co-Pd films. The largest λ_s value was found for the thickest Co-Pd layer, and the data were in line with published results on Co-Pd alloy films, using the interpretation of data based on contributions from magnetic layer and interface regions. Unlike the Fe-Co/Ag multilayers, the most magnetostrictive Co-Pd/Ag multilayers were not the most magnetically soft.

The **simulation of XRD patterns** from Co-Pd/Ag multilayers met with moderate success, but much operator intervention was required to produce a reasonable fit to a measured spectrum. Small changes in one parameter can significantly alter a spectrum, which makes automatic fitting difficult. There are many parameters and the present program takes a long time to run. A simulation is, in principle, very useful, as thickness, interface roughness, multilayer periodicity and component d-spacing information can be extracted.

6. Conclusions and Outlook

Metallic multilayers were deposited by radio frequency magnetron sputtering. Magnetic, magnetoelastic and structural measurements were made on them, using principally a quasi-d.c. magnetometer, the Small Angle Magnetisation Rotation (SAMR) technique and X-ray diffraction analysis (XRD) in the θ-2θ configuration. The aim was to produce metallic multilayers which were simultaneously magnetically soft and highly magnetostrictive for potential use in sensor and transducer applications. Several papers have arisen from this work.

During the course of the project, the d.c. magnetometer and software used in the analysis of MH loops were developed to meet the requirements of the thin films studied. The apparatus for SAMR was built and developed, and the technique applied to multilayers deposited on a substrate. The precision of the results was more sensitive to the measurement itself than to the parameters used in the correction for the presence of the substrate. Some λ_s data taken by SAMR were confirmed by Strain Modulated Ferromagnetic Resonance (SMFMR), an independent technique.

The bulk of the investigations centred around two iron-cobalt alloys multilayered with silver or copper and a cobalt-palladium alloy multilayered with silver. The saturation magnetostriction results for these magnetic/non-magnetic multilayers were understood in terms of a model developed from a volume average λ_s expression in the literature, which had been proposed for magnetic/magnetic multilayers.

The Fe-Co/Ag and Fe-Co/Cu multilayers were random polycrystalline in structure. The magnetostriction values attained in the Fe-Co/Ag multilayers were found to agree with a calculation of $\overline{\lambda_s}$ for random polycrystalline Fe-Co alloys of similar compositions within experimental error. The single-crystal saturation

magnetostriction constants used in the calculation were taken from published work. The calculated $\overline{\lambda_s}$ values were higher than experimental values published for such alloys. Values of λ_s measured for Fe-Co/Cu multilayers were lower, and closer to published experimental data on Fe-Co alloys. The differences in results obtained with Ag and Cu interlayers are tentatively ascribed to the different atomic sizes and wetting characteristics of these two noble metals.

The calculation of $\overline{\lambda_s}$ has been shown to have limited accuracy when applied to many materials, but the agreement with these experimental data is excellent. No evidence has been found to link lattice strain at interfaces with λ_s; rather, mixing or roughness at interfaces reduced λ_s in the multilayers studied.

Target values set at the beginning of the project were $|\lambda_s|$ = 100ppm and H_c = 100Am^{-1}. The closest to these was achieved in the multilayer 2×25(12nm HiSat50/2nm Ag) annealed at 300°C for 30 minutes in a flow of forming gas. For this multilayer, λ_s = +84±6ppm and H_c = 340Am^{-1}. As deposited at the substrate, HiSat50 has a composition of 45wt.% Fe, 55wt.% Co with less than 0.2wt.% Ta. For this alloy, the calculated magnetostriction was $\overline{\lambda_s}$ = +84±4ppm. The best achieved with the other Fe-Co alloy was λ_s = +44±3ppm, H_c = 560Am-1, for 2× 50(12nm Permendur24/2nm Ag) as-deposited (no anneals were performed). Permendur24 as deposited has a composition of 72wt.% Fe, 28wt.% Co with a trace of Cr (by comparison with experimental data on HiSat50). This alloy was expected to have a lower λ_s than HiSat50, the calculated value being $\overline{\lambda_s}$ = +42± 4ppm. The composition of HiSat50 was expected to give one of the highest λ_s values attainable in random polycrystalline Fe-Co alloys.

The calculated values of $\overline{\lambda_s}$ have been realised in the above-mentioned multilayers where the magnetic layers are thickest and hence the interface regions, reducing λ_s, have least effect. No higher λ_s values are expected in random polycrystalline samples. In crystallographically textured specimens, however,

saturation magnetostriction values greater than these may be expected , where the higher magnetostriction constants along given crystallographic directions might be exploited. Work along this avenue is being pursued in this research group, and results will be compared with a model developed in this work for the magnetostriction of textured polycrystalline samples. Deposition conditions and post-deposition treatments will be optimised to produce the softest, most magnetostrictive films.

It is significant that high λ_s values have been obtained in soft magnetic multilayers. All the Fe-Co/Ag and Fe-Co/Cu multilayers were markedly softer than the plain alloy films deposited. Also, literature data on magnetostrictive strain in Fe-Co alloys taken at 87.5kAm^{-1} gave considerably lower values, indicating that the samples were not saturated in that field, whereas the Fe-Co/Ag multilayers fabricated in this project were saturated in lower fields. The insertion of Ag or Cu interlayers in Fe-Co films gave rise to pronounced magnetic softening.

The interfaces between the Fe-Co alloy layers and the noble metal layers were shown to be rough. From published research, it is thought likely that the Ag layers were not continuous for $t_{Ag} \leq$ 5-6nm; the degree of continuity may explain the varied λ_s values found for Fe-Co/Ag multilayers with fixed Fe-Co layer thickness and varied Ag thickness. It was demonstrated that, for magnetic softening to occur under these deposition conditions, a degree of multilayering was necessary, or the Ag regions were required to be above some size. Films made of Ag particles finely dispersed in HiSat50 (by sputtering from a mosaic target) were not saturable in the field available in the d.c. magnetometer (H_{max} = 22kAm^{-1} at that time).

Larger saturation magnetostriction values were measured by SMFMR in multilayers of a highly magnetostrictive Co-Pd alloy with Ag. These were shown to be in line with published experimental λ_s data on Co-Pd alloy films of various compositions, using the interpretation of λ_s data mentioned above. The coercivity

values (measured using a Faraday balance) showed a minimum of H_c = 10.7kAm^{-1} in the range of layer thicknesses investigated. This was for 2×75(3nm Co-Pd/2nm Ag), for which λ_s = -83±12ppm. The highest saturation magnetostriction was observed in 2×50(12nm Co-Pd/2nm Ag), where λ_s = -143±21ppm but H_c = 22.4kAm^{-1}. This was the multilayer with the thickest magnetic layer, for which the effects of the interface regions were proportionately less. The coercivity of the plain Co-Pd film was H_c =17.2kAm^{-1}. These multilayers were magnetically hard (in terms of the aims of this work) but the fields required to saturate the multilayers in-plane compared favourably with those reported in the literature for Co-Pd alloy films. Possibilities for exploiting the highly magnetostrictive nature of Co-Pd but producing softer films include examining Co-Pd/Co, Co-Pd/Fe or Co-Pd/Ni-Fe multilayers. The Co, Fe or Ni-Fe layers would improve magnetic softness, but magnetostriction would be sacrificed to achieve this, as with the Co-Pd/Ag multilayers. Further softening might be achieved through optimisation of deposition conditions.

The XRD patterns of the Co-Pd/Ag multilayers showed that they were polycrystalline with (111) texture. Satellite peaks around the main crystal lattice peaks indicated that the interfaces were smooth and that the multilayer periodicity was uniform throughout the stack. Some patterns were simulated using a program developed in this project, based on the kinematic theory of X-ray diffraction. The present program is time-consuming to use, and requires considerable operator intervention to produce good fits to experimental data. The present algorithm takes no account of crystallographic grain size, and this can cause problems fitting the XRD patterns of polycrystalline multilayers where the grain size is similar to or less than the layer thicknesses. To become useful on a routine basis would require that the program be written in a faster language and run on more suitable computers, and that some strategy be employed to converge on the correct fit

parameters. One difficulty with writing a suitable strategy is that small changes in test parameters often cause large modifications to the simulated pattern. Further parameters to simulate variations in the individual layer thicknesses may provide fits closer to measured data, but these would also increase the program's run-time. A pattern simulation program would be useful, however, to extract from measured XRD data information on lattice plane spacings (and hence lattice strain), layer thicknesses and interface roughness.

There is much further work which can be suggested following that presented here. One major area would be to investigate a wide range of deposition conditions (sputtering pressure, power and substrate temperature, principally) as only select conditions were employed here, while the layer materials and thicknesses were varied. Such investigations are proceeding in the research group. The highest λ_s values expected for random polycrystalline materials have been achieved in multilayers studied in this work, but multilayers are now being produced with different crystallographic textures and interface qualities, which can significantly enhance the magnetostriction values obtained. The sputtering conditions also affect the magnetic softness of the films. The λ_s data will be compared with a model developed for the magnetostriction of textured polycrystalline materials, which was set up to accord with experimental data available. The present model has limited applicability to the real physical situation, and more detailed structural information would be required so that a more detailed model could be elucidated.

Further investigations into multilayers of highly magnetostrictive alloys with magnetic interlayers may be profitable. It has been shown that highly magnetostrictive multilayers can be produced with Co-Pd/Ag, but they have been magnetically hard. Magnetic interlayers may soften the alloy films, at the expense

of some of the magnetostriction. Layer thickness combinations and deposition conditions for producing the softest, most highly magnetostrictive multilayers could be optimised. Other magnetostrictive alloys might be investigated with various interlayer materials.

To further understand the mechanisms for magnetostriction in multilayers, and the links with crystal structure, it would be instructive to study multilayers in which each layer is a single element. It is not expected that such multilayers would be highly magnetostrictive, on the basis of experimental data published on the magnetostriction constants of single-crystal and random polycrystalline elements, although soft multilayers may be produced. Such investigations would also give further understanding of the models and expressions used to interpret the magnetostriction data presented here while eliminating any possible effects arising from the nature of an alloy layer (e.g. ordered/disordered). Further understanding of the nature and rôle of the interface regions would be gained if conjoined with appropriate structural characterisation.

7. Acknowledgements

This work has been supported financially by the UK Engineering and Physical Sciences Research Council (formerly the Science and Engineering Research Council) and British Technology Group (which holds certain intellectual property rights in this area). Trips to Bilbao to use the Faraday Balance and FMR facilities were funded by the Spanish Government and the British Council under the Acciones Integradas initiative.

I would like to thank warmly my family and friends for their moral support and encouragement, in particular Mum and Dad and my friend Ian, and all those who have prayed for me at various times - you are deeply appreciated. God is faithful. Many thanks to my supervisor, Dr. Mike Gibbs, who has been supportive and encouraging throughout the progress of this project. Also thanks to all the past and present members of the magnetics groups at Bath and Sheffield Universities, especially Dr. Chris Shearwood and Dr. Andy Thomas - it was very helpful to discuss with them and to learn from watching them working - and Dr. Patrick Squire; and to all the technicians in both places, in particular Barry Chapman, in charge of the X-ray diffraction facilities at Bath University. Thanks too to Dr. Pam Donovan (Birkbeck College, London) and to Ruth Harrell and Kelly Sharp, for their various contributions to X-ray analysis and modelling, and to Dr. R. A. L. Sullivan and Dr. Richard James for helping me to understand the XRD satellites equation. Ian Houghton and Nick Semmett from Nordiko Ltd. installed the sputtering machine and took Radio Railways off the air early in its career! Ursula Potter and Dr. Hugh Perrott (University of Bath) and Dr. Geoff Cope (University of Sheffield) helped significantly in sample preparation, imaging and interpretation in Electron Microscopy. For work with the Faraday balance, thank you to Prof.

Manu Barandiarán and Pilar Rodriguez (Departamento de Electricidad y Electrónica, Universidad del País Vasco, Bilbao, Spain) for helping me; also to Luis Lezama, who operated the ESR apparatus; and for SMFMR work, thanks to Henryk Szymczak and especially to Ryszard Zuberek (Institute of Physics, Polish Academy of Sciences, Warsaw, Poland). Mössbauer spectroscopy was kindly carried out by Dr. Jianzhong Jiang at Liverpool University and by Dr. John Williams and Prof. Jacob Adetunji (Amhadu Bello University, Zaria, Nigeria) at Sheffield University.

"God has made everything beautiful in its time. He has also set eternity in the hearts of men, but they cannot fathom what God has done from beginning to end".

Ecclesiastes 3 v. 11, The Holy Bible.

8. References

Aldén, M., S. Mirbt, H. L. Skriver, N. M. Rosengaard and B. Johansson, "Surface magnetism in iron, cobalt and nickel", *Phys. Rev.* **B 46** (1992) 6303-6312.

Arai, K. I., Y. Hayashi and M. Yamaguchi, "Magnetic properties of Fe-Cu and Fe-Ag sputtered films", *phys. stat. sol. (a)* **125** (1991) 313-318.

Awano, H., Y. Suzuki, T. Yamazaki, T. Katayama and A. Itoh, "Magnetostriction and in-situ measurement of stress of Co/Pd compositionally modulated multilayer films during fabrication", *IEEE Trans. Mag.* **MAG-26** (1990) 2742-2744.

Awano, H., O. Taniguchi, T. Katayama, F. Inoue, A. Itoh and K. Kawanishi, "Magnetostriction of 3d-transition metal/noble metal compositionally modulated multilayer films", *J. Appl. Phys.* **64** (1988) 6107-6109.

Azároff, L. V., "Elements of X-Ray Crystallography", International Student Edition, McGraw-Hill, New York/Kõgakusha Co. Ltd., Tokyo (1968) pp. 467-469.

Bennett, W. R., C. D. England, D. C. Person and C. M. Falco, "Magnetic properties of Pd/Co multilayers", *J. Appl. Phys.* **69** (1991) 4384-4390.

Berry, B. S. and W. C. Pritchet, "Vibrating reed internal friction apparatus for films and foils", *IBM J. Res. Develop.* **19** (1975) 334-343.

Birss, R. R., "The saturation magnetostriction of polycrystals", *Proc. Phys. Soc.* **75** (1960) 8-16.

Bloemen, P. J. H. and W. J. M. de Jonge, "Magnetic anisotropy of Co/Ni/Co/Pt multilayers" *J. Magn. Magn. Mat.* **116** (1992) L1-L6.

Bozorth, R. M., "Ferromagnetism", D. Van Nostrand, Princeton, New Jersey (1951). Magnetostriction (λ_e) data for iron-cobalt alloys quoted from Masiyama, Y., "On magnetostriction of Fe-Co alloys", *Sci. Repts. Tôhoku Imp. Univ.* **21** (1932) 394-410. Saturation magnetostriction (λ_s) data for Fe-Co alloys quoted from Williams, S. R., "Joule magnetostriction effect in a group of Fe-Co alloys", *Rev. Sci. Instruments* **3** (1932) 675-683.

den Broeder, F. J. A., H. C. Donkersloot, H. J. G. Draaisma and W. J. M. de Jonge, "Magnetic properties and structure of Pd/Co and Pd/Fe multilayers", *J. Appl. Phys.* **61** (1987) 4317-4319.

Bruno, E. and B. L. Gyorffy, "Oscillatory coupling between interfaces inmetallic multilayers", *J. Phys.: Condens. Matter* **5** (1993) 2109-2136.

Bruno, P. and J.-P. Renard, "Magnetic surface anisotropy of transition metal ultrathin films", *Appl. Phys.* **A 49** (1989) 499-506.

Bunshah, R. F., "Deposition Technologies for Films and Coatings", Noyes Publications, Park Ridge, New Jersey (1982).

Callen, E. and C. Chase, Prologue to E. du Trémolet de Lacheisserie, "Magnetostriction: Theory and Applications of Magnetoelasticity", CRC Press, Boca Raton, Florida (1993).

Callen, H. B. and N. Goldberg, "Magnetostriction in polycrystalline aggregates", *J. Appl. Phys.* **36** (1965) 976-977.

Carcia, P. F. and W. B. Zeper, "Sputtered Pt/Co multilayers for magneto-optical recording", *IEEE Trans. Mag.* **MAG-26** (1990) 1703-1705.

Carlotti, G., D. Fioretto, G. Socino, B. Rodmacq and V. Pelosin, "Interface effects and elastic constants of Ag/Ni superlattices studied by Brillouin scattering", *J. Appl. Phys.* **71** (1992) 4897-4902.

Celinski, Z. and B. Heinrich, "Exchange coupling in Fe/Cu, Pd, Ag, Au/Fe trilayers", *J. Magn. Magn. Mat.* **99** (1991) L25-L30.

Chin, G. Y. and J. H. Wernick, in E. P. Wohlfarth (ed.), "Ferromagnetic Materials", vol. 2., North-Holland, Amsterdam (1980).

Chopra, K. L. "Thin Film Phenomena", McGraw-Hill, New York (1969).

Chopra, K. L. and I. Kaur, "Thin Film Device Applications", Plenum Press, New York (1983).

Chopra, K. L. and M. R. Randlett, "Influence of deposition parameters on the coalescence stage of growth of metal films", *J. Appl. Phys.* **39** (1968) 1874-1881.

Clarke, R., S. Elagoz, W. Vavra, E. Schuler and C. Uher, "Epitaxial strain, metastable structure, and magnetic anisotropy in Co-based superlattices", *J. Appl. Phys.* **70** (1991) 5775-5779.

Coehoorn, R., "Period of oscillatory exchange interactions in Co/Cu and Fe/Cu multilayer systems", *Phys. Rev.* **B 44** (1991) 9331-9337.

Cullity, B. D., "Fundamentals of magnetostriction", *J. Metals* **23** (1971) 35-41.

Cullity, B. D., "Introduction to Magnetic Materials", Addison-Wesley, Reading, Massachusetts (1972)

Daalderop, G. H., P. J. Kelly and F. J. A. den Broeder, "Prediction and confirmation of perpendicular magnetic anisotropy in Co/Ni multilayers", *Phys. Rev. Lett.* **68** (1992) 682-685.

Dekoster, J., E. Jedryka, M. Wójcik and G. Langouche, "Structure and magnetism in bcc Co/Fe superlattices", *J. Magn. Magn. Mat.* **126** (1993) 12-15.

Delsanto, P. P., V. Provenzano and H. Überall, "Coherency strain effects in metallic bilayers", *J. Phys.: Condens. Matter* **4** (1992) 3915-3928.

Dieny, B., V. S. Speriosu, S. S. P. Parkin, B. A. Gurney, D. R. Wilhoit and D. Mauri, "Giant magnetosresistance in soft ferromagnetic multilayers", *Phys. Rev.* **B 43** (1991) 1297-1300.

Dirne, F. W. A. and C. J. M. Denissen, "Interface mixing in Fe/Co multilayers", *J. Magn. Magn. Mat.* **78** (1989)122-128.

Dirne, F. W. A., J. A. M. Tolboom, H. J. de Wit and C. H. M. Witmer, "Structural and soft-magnetic properties of Fe/CoNbZr and Fe/FeCrB multilayers", *J. Appl. Phys.* **66** (1989) 748-755.

Dirne, F. W. A., J. A. M. Tolboom, H. J. de Wit and C. H. M. Witmer, "Soft magnetic multilayers: the role of the magnetostriction", *J. Magn. Magn. Mat.* **83** (1990) 399-401.

Donovan, P., private communication (1993).

Egelhoff, W. F. jr. and M. T. Kief, "Antiferromagnetic coupling in Fe/Cu/Fe and Co/Cu/Co multilayers on Cu(111)", *Phys. Rev.* **B 45** (1992) 7795-7804.

Fabricius, G., A. M. Llois and M. Weissman, "Calculation of electronic and magnetic properties of metallic superlattices", *Phys. Rev.* **B 44** (1991) 6870-6877.

Falicov, L. M., D. T. Pierce, S. D. Bader, R. Gronsky, K. B. Hathaway, H. J. Hopster, D. N. Lambeth, S. S. P. Parkin, G. Prinz, M. Salamon, I. K. Schuller and

R. H. Victora, "Surface, interface and thin-film magnetism", *J. Mater. Res.* **5** (1990) 1299-1340.

Fartash, A. and H. Oesterreicher, "Magnetic properties of Co-Cr films and the effects of heat treatment", *J. Appl. Phys.* **66** (1989) 3275-3281.

Fu, C. L., A. J. Freeman and T. Oguchi, "Prediction of strongly enhanced two-dimensional ferromagnetic moments on metallic overlayers, interfaces and superlattices", *Phys. Rev. Lett.* **54** (1985) 2700-2703.

Fujii, Y., "X-ray diffraction studies on metallic superlattices", in "Metallic Superlattices - Artificially Structured Materials", *Studies in Physical and Theoretical Chemistry* **49**, ed. T. Shinjo and T. Takada, Elsevier, Amsterdam (1987).

Fuß, A., S. Demokritov, P. Grünberg and W. Zinn, "Short- and long period oscillations in the exchange coupling of Fe across epitaxially grown Al- and Au-interlayers", *J. Magn. Magn. Mat.* **103** (1992) L221-L227.

Ge, S. H., C. X. Li, Z. Y. Wang, F. S. Li, J. C. Gao and B. N. Li, "Structural and interface studies of Fe/Mo multilayered films", *phys. stat. sol. (a)* **127** (1991) 397-404.

Gleiter, H., "Diffusion in nanostructured metals", *phys. stat. sol. (b)* **172** (1992) 41-51.

Glocker, D. A., W. E. Yetter and J.-S. Gau, "The role of atomic mobility during film growth in the structural and magnetic properties of CoCr", *IEEE Trans. Mag.* **MAG-22** (1986) 331-333.

Greaves, S. J., A. K. Petford-Long, Y.-H. Kim, R. J. Pollard, P. J. Grundy and J. P. Jakubovics, "A magnetic and high resolution structural investigation of Pt/Co multilayers", *J. Magn. Magn. Mat.* **113** (1992) 63-71.

Greig, D., M. J. Hall, C. Hammond, B. J. Hickey, H. P. Ho, M. A. Howson, M. J. Walker, N. Wiser and D. G. Wright, "The giant magnetoresistance of Co/Cu superlattices grown by MBE", *J. Magn. Magn. Mat.* **110** (1992) L239-L246.

de Gronckel, H. A. M., K. Kopinga, W. J. M. de Jonge, P. Panissod, J. P. Schillé and F. J. A. den Broeder, "Nanostructure of Co/Cu multilayers", *Phys. Rev.* **B 44** (1991) 9100-9103.

Grünberg, P., J. Barnas, F. Saurenbach, J. A. Fuß, A. Wolf and M. Vohl, "Layered magnetic structures: antiferromagnetic type interlayer coupling and magnetoresistance due to antiparallel alignment", *J. Magn. Magn. Mat.* **93** (1991) 58-66.

Grünberg, P., S. Demokritov, A. Fuss, R. Schreiber, J. A. Wolf and S. T. Purcell, "Interlayer exchange, magnetotransport and magnetic domains in Fe/Cr layered structures", *J. Magn. Magn. Mat.* **104-107** (1992) 1734-1738.

Grundy, P. J., D. Greig and E. W. Hill, "Multilayered magnetic materials", *Endeavour* **17** (1993) 154-159.

Guinier, A., "X-Ray Diffraction in Crystals, Imperfect Crystals and Amorphous Bodies", Freeman, San Francisco (1963). Translated by P. Lorrain and D. Sainte-Marie Lorrain.

Gumbsch, P., M. S. Daw, S. M. Foiles and H. F. Fischmeister, "Accommodation of lattice mismatch in a Ag/Ni heterophase boundary", *Phys. Rev.* **B 43** (1991) 13833-13837.

de Haan, P., Q. Meng, T. Katayama and J. C. Lodder, "Magnetic and magneto-optical properties of sputtered Co/Pd multilayers", *J. Magn. Magn. Mat.* **113** (1992) 29-35.

Haeiwa, T., H. Negoro and M. Matsumoto, "Soft-magnetic properties of compositionally modulated Fe/Al films", *J. Appl. Phys.* **69** (1991) 5346-5348.

Haga, Y., T. Sugiyama and O. Nittono, "Magnetic and structural properties of Fe/Ag and Fe/Ta multilayer films prepared by dc sputtering", *J. Magn. Magn. Mat.* **126** (1993) 19-21.

Hall, M. J., B. J. Hickey, M. A. Howson, C. Hammond, M. J. Walker, D. G. Wright, D. Greig and N. Wiser, "Interface scattering and the giant magnetoresistance of MBE-grown Co/Cu superlattices", *J. Phys.: Condens. Matter* **4** (1992) L495-L502.

Hall, R. C., "Magnetic anisotropy and magnetostriction of ordered and disordered cobalt-iron alloys", *J. Appl. Phys.* **31** (1960) 157S-158S.

Hansen, M., "Constitution of Binary Alloys", 2nd ed., McGraw-Hill, New York (1958).

Harrell, R. and K. Sharp, University of Bath, private communications (1993).

Hashimoto, S., Y. Ochiai and K. Aso, "Perpendicular magnetic anisotropy in sputtered CoPd alloy films", *Jpn. J. Appl. Phys.* **28** (1989) 1596-1599.

Hashimoto, S., Y. Ochiai and K. Aso, "Perpendicular magnetic anisotropy of sputtered Co/Pd and Co/Pt multilayered films", *J. Appl. Phys.* **66** (1989) 4909-4916.

Hashimoto, S., Y. Ochiai and K. Aso, "Film thickness dependence of magneto-optical and magnetic properties in Co/Pt and Co/Pd multilayers", *J. Appl. Phys.* **67** (1990) 4429-4431.

He, P., W. A. McGahan, S. Nafis, J. A. Woollam, S. H. Liou, F. Sequeda, T. McDaniel and H. Do, "Sputtering pressure effect on microstructure of surface and interface and on coercivity of Co/Pt multilayers", *J. Appl. Phys.* **70** (1991) 6044-6046.

Heyderman, L., University of Glasgow, private communication (1994).

Honda, K., "On some physical constants of iron-cobalt alloys", *Sci. Repts. Tôhoku Imp. Univ.* **8** (1919) 51-58.

Honda, S., H. Tanimoto, J. Ago, M. Nawate and T. Kusuda, "Origin of coercivity in Co/Pt sputtered multilayers", *J. Appl. Phys.* **70** (1991) 6047-6049.

Houdy, Ph., P. Boher, F. Pierre, C. CHappert, P. Beauvillain, K. Le Dang, P. Veillet and E. Velu, "Magnetic and structural properties of r.f.-sputtered Co/Fe and Co/Cr multilayers", *J. Appl. Phys.* **69** (1991) 5667-5669.

Hultgren, R., P. D. Desai, D. T. Hawkins, M. Gleiser and K. K. Kelley, "Selected Values of the Thermodynamic Properties of Binary Alloys", American Society for Metals, Ohio (1973).

Hylton, T. L., K. R. Coffey, M. A. Parker and J. K. Howard, "Giant magnetoresistance at low fields in discontinuous NiFe-Ag multilayer thin films", *Science* **261** (1993) 1021-1024.

Ibers, J. A. and W. C. Hamilton (eds.), "International Tables for X-Ray Crystallography", vol. 4 pp.71ff, Kynoch Press (1974).

Jankowski, A. F., "Modelling the supermodulus effect in metallic multilayers", *J. Phys. F.: Met. Phys.* **18** (1988) 413-427.

Jackson, T. J. and S. B. Palmer, "Oxide superconductor and magnetic metal thin film deposition by pulsed laser ablation", *J. Phys. D: Appl. Phys.* **27** (1994) 1581-1594

Jankowski, A. F., "Lattice spacing variations in gold-nickel superlattices", *Superlattices and Microstructures* **6** (1989) 427-429

Jankowski, A. F., "Measurement of lattice strain in Au-Ni multilayers and correlation with biaxial modulus effects", *J. Appl. Phys.* **71** (1992) 1782-1789.

Jankowski, A. F. and T. Tsakalakos, "The effect of strain on the elastic constants of noble metals", *J. Phys. F.: Met. Phys.* **15** (1985) 1279-1292.

Jimbo, M., E. Sobue, S. Tsunashima and S. Uchiyama, "Structure and soft magnetic properties of Fe/CoZr multilayer films", *Japan. J. Appl. Phys.* **30** (1991) 2756-2760.

Khan, M. R., C. S. L. Chun, G. P. Felcher, M. Grimsditch, A. Kueny, C. M. Falco and I. K. Schuller, "Structural, elastic and transport anomalies in molybdenum/nickel superlattices", *Phys. Rev.* **B 27** (1983) 7186-7193.

Kittel, C., "Physical Theory of Ferromagnetic Domains", *Rev. Mod. Phys.* **21** (1949) 541-583.

Kittel, C., "Introduction to Solid State Physics", 4th ed., Wiley, New York (1971).

Köbler, U., K. Wagner, R. Weichers, A. Fuß and W. Zinn, "Higher order interaction terms in coupled Fe/Cr/Fe sandwich structures", *J. Magn. Magn. Mat.* **103** (1992) 236-244.

Komuro, M., Y. Kozono, S. Narishige, M. Hanazono and Y. Sugita, "Structures and magnetic properties of Fe/Co multilayer films", *Japan. J. Appl. Phys.* **27** (1988) L2105-L2107.

Kozono, Y., M. Komuro, S. Narishige, M. Hanazono and Y. Sugita, "Structures and magnetic properties of Fe/Cu multilayered films prepared by a magnetron sputtering method", *J. Appl. Phys.* **61** (1987) 4311-4313.

Kozono, Y., M. Komuro, S. Narishige, M. Hanazono and Y. Sugita, "Structures and magnetic properties of Fe/Ag multilayer films prepared by sputtering and ultrahigh-vacuum depositions", *J. Appl. Phys.* **63** (1988) 3470-3472.

Krishnan, R., V. Cagan, M. Tessier and S. Visnovsky, "Magnetic and magneto-optical studies in Fe/AlN multilayers", *J. Magn. Magn. Mat.* **101** (1991) 205-206.

Krishnan, R., H. O. Gupta, H. Lassri, C. Sella and M. Kaabouchi, "Structural and magnetic properties of Fe/Ni and Fe/Co multilayers", *J. Appl. Phys.* **70** (1991) 6421-6423.

Le Dang, K., P. Veillet, E. Vélu, S. S. P. Parkin and C. Chappert, "Influence of crystal structure on the magnetoresistance of Co/Cu multilayers", *Appl. Phys. Lett.* **63** (1993) 108-110.

Li, Z. G., P.F. Carcia and Y. Cheng, "Co thickness dependence of the microstructure of Pt/Co multilayers", *J. Appl. Phys.* **73** (1993) 2433-2437.

Lindley, R. A., University of Sheffield , private communication (1994).

Maeda, A., M. Kume, S. Oikawa, T. Tanuma, Y. Shimizu and M. Doi, "Magnetoresistance characteristics of grain-type alloy thin films of various compositions", *J. Phys.: Condens. Matter* **5** (1993) 6745-6752.

Mathon, J., D. M. Edwards, R. B. Muniz and M. S. Phan, "Theory of oscillatory exchange coupling in magnetic multilayers", *J. Magn. Magn. Mat.* **104-107** (1992) 1721-1724.

Mattox, D. M., "Surface cleaning in thin film technology", *SAND* **74-0344** (1975) (Sandia Labs., Albuquerque, New Mexico).

Meyer, K. E., G. P. Felcher, S. K. Sinha and I. K. Schuller, "Models of diffraction from layered ultrathin coherent structures", *J. Appl. Phys.* **52** (1981) 6608-6610.

Nafis, S., J. A. Woollam, Z. S. Shan and D. J. Sellmyer, "Temperature and thickness dependence of coercivity and magnetization of Co/Cu and Co/Si multilayers", *J. Appl. Phys.* **70** (1991) 6050=6052.

Nagai, Y., M. Senda and T. Toshima, "Properties of ion-beam sputtered Ni/Fe artificial lattice film", *J. Appl. Phys.* **63** (1988) 1136-1140.

Nagakubo, M., T. Yamamoto and M. Naoe, "Magnetic properties and structure of Fe/Al multilayered films prepared by ion-beam sputtering", *J. Appl. Phys.* **64** (1988) 5751-5753.

Nakatani, R. and T. Kobayashi, "Changes in soft magnetic properties of Fe multilayered films due to lattice mismatches between Fe and intermediate layers", *J. Appl. Phys.* **66** (1989) 4338-4344.

Narita, K., J. Yamasaki and H. Fukunaga, "Measurement of saturation magnetostriction of a thin amorphous ribbon by means of small angle magnetization rotation", *IEEE Trans. Mag.* **MAG-16** (1980) 435-439.

Néel, L., "Anisotropie magnétique superficielle et surstructures d'orientation", *J. de Phys. et le Radium* **15** (1954) 225-239.

Nguyen Chi Thanh and R. Krishnan, "Anisotropy of magnetostriction in coevaporated $Co_{1-x}Zr_x$ amorphous thin films", *phys. stat. sol (a)* **90** (1985) 313-323.

Niimura, Y. and N. Naoe, "The dependence of magnetostriction of sputtered Co-Cr thin films on crystal structure", *IEEE Trans. Mag.* **MAG-21** (1985) 1447-1449.

Ohnuma, S., H. Fujimori, N. Yano, S. Furukawa, S. Fujii and T. Matsumoto, "Soft magnetic multilayers for micromagnetic devices", *J. Magn. Magn. Mat.* **126** (1993) 556-562.

Okuyama, T. and T. Shinjo, "Magnetic properties of Fe/Co multilayered films", *J. Phys. Soc. Japan* **61** (1992) 286-292.

Pan, F., K. Tao and B. X. Liu, "Enhancement of magnetic moment of iron atoms in the Fe/Au nanomultilayers", *J. Appl. Phys.* **74** (1993) 1929-1932.

Pan, F., K. Tao, T. Yang and B. X. Liu, "Microstructure and magnetic properties of the Fe/Cu nano-multilayers by vapour deposition", *phys. stat. sol. (a)* **135** (1993) 573-580.

Pan, F., T. Yang, K. Tao and B. X. Liu, "Magnetic properties of Fe/Ag nano-multilayers", *J. Phys.: Condens. Matter* **4** (1992) L519-L524.

Pan, F., T. Yang, J. Zhang and B. X. Liu, "Fe/Pd nano-multilayers prepared by vapour deposition, and their magnetic anomaly", *J. Phys.: Condens. Matter* **5** (1993) L507-L514.

Parkin, S. S. P., Z. G. Li and D. J. Smith, "Giant magnetoresistance in antiferromagnetic Co/Cu multilayers", *Appl. Phys. Lett.* **58** (1991) 2710-2712.

Peng, C., Y. Cao and D. Dai, "Magnetic properties of Ag/Ni multilayered films", *J. Appl. Phys.* **71** (1992) 3457-3461.

Philipp, H. R. and J. J. Tiemann, "Magnetic properties of sputtered Ni-Fe and Fe-Co alloy layers", *J. Appl. Phys.* **43** (1972) 3542-3545.

Reck, R. A., and D. L. Fry, "Orbital and spin magnetization in Fe-Co, Fe-Ni and Ni-Co", *Phys. Rev.* **184** (1969) 492-495.

Richardson, G., J. L. Makous, H. Y. Yu and A. S. Edelstein, "Elastic-constant softening in nonperiodic Mo/Ni superlattices", *Phys. Rev.* **B 45** (1992) 12114-12117.

Rodmacq, B., "X-ray diffraction study of silver-nickel superlattices", *J. Appl. Phys.* **70** (1991) 4194-4201.

Rodmacq, B. and C. Dos Santos, "Magnetic properties of ultrathin Ni layers in Ag/Ni superlattices", *J. Magn. Magn. Mat.* **104-107** (1992) 1739-1740.

Ruggiero, S. T., "Review of synthetic metal multilayers", *Superlattices and Microstructures* **1** (1985) 441-446.

Ruud, J. A., A. Witvrouw and F. Spaepen, "Bulk and interface stresses in silver-nickel multilayered thin films", *J. Appl. Phys.* **74** (1993) 2517-2523.

Schelp, L. F., G. Tosin, M. Carara, M. N. Baibich, A. A. Gomes and J. E. Schmidt, "Co/Ag multilayer film: role of annealing on the magnetic properties", *Appl. Phys. Lett.* **61** (1992) 1858-1860.

Senda, M. and Y. Nagai, "Magnetic properties of Fe/Co, Fe/CoFe and (Fe/Co)/SiO_2 multilayer films", *J. Appl. Phys.* **65** (1989) 3151-3156.

Senda, M. and Y. Nagai, "Magnetic properties of multilayer films consisting of Fe and nonmagnetic layers", *J. Appl. Phys.* **65** (1989) 3157-3160.

Senda, M. and Y. Nagai, "Influences of noble gases (Ne, Ar, and Kr) on magnetic properties of ion-beam-sputtered Fe/SiO_2 multilayer films", *J. Vac. Sci. Technol.* **A8** (1990) 13-18.

Shearwood, C., University of Sheffield, private communication (1993).

Shearwood, C., University of Sheffield, private communication (1994).

Slonczewski, J. C., "Magnetostatic mechanism for field sensitivity of magnetoresistance in discontinuous magnetic multilayers", *J. Magn. Magn. Mat.* **129** (1993) L123-L128.

Squire, P. T., S. M. Sheard, C. H. Carter and M. R. J. Gibbs, "Digital M-H plotter for low coercivity metallic glasses", *J. Phys. E.: Sci. Instrum.* **21** (1988) 1167-1172.

Swab, P. and R. E. Klinger, "Preparation of multilayer optical coatings for TEM cross-sectional microanalysis by ultramicrotomy", *Mat. Res. Soc. Symp. Proc.* **115** (1988) 229-234.

Szymczak, H., R. Zuberek, R. Krishnan and M. Tessier, "Magnetostriction constant of multilayer Co/Ag films", *IEEE Trans. Mag.* **26** (1990) 2745-2746.

Szymczak, H., R. Zuberek, R. Krishnan, M. Tessier, K. B. Youn and C. Sella, "Interfacial effects in multilayer Ni-C and Ni-Ag films", 12th ICMFS, Le Creusot, France, 1988. Abstracts pp.266-267.

Takahashi, H., S. Tsunashima, S. Iwata and S. Uchiyama, "Measurement of magnetostriction constants in polycrystalline alloy and multilayer films of PdCo and PtCo", *J. Magn: Magn. Mat.* **126** (1993) 282-284.

Thomassen, J., F. May, B. Feldmann, M. Wuttig and H. Ibach, "Magnetic live surface layers in Fe/Cu(100)", *Phys. Rev. Lett.* **69** (1992) 3831-3834.

Tottle, C. R., "An Encyclopædia of Metallurgy and Materials", MacDonald and Evans, Plymouth (1984).

Tsunashima, S., M. Hasegawa, K. Nakamura and S. Uchiyama, "Perpendicular magnetic anisotropy and coercivity of Pd/Co and Pt/Co multilayers with buffer layers", *J. Magn. Magn. Mat.* **93** (1991) 465-468.

Vossen, J. L. and W. Kern (eds.), "Thin Film Processes", Academic Press, New York (1978).

Wan, H. and G. C. Hadjipanayis, "Thickness dependence of coercivity in Co-Ni thin films", *J. Appl. Phys.* **70** (1991) 6059-6061.

Wang, D. and D. J. Sellmyer, "Magnetic and structural properties of Co/Cr multilayers with in-plane anisotropy", *J. Appl. Phys.* **70** (1991) 6053-6055.

Wenda, J., H. Jankowski and A. Kulak, "Measurement of the saturation magnetostriction of a thin amorphous film by means of small angle magnetization oscillation", *Thin Solid Films* **148** (1987) 1-6.

de Wit, H. J., "Soft magnetic multilayers", *Rep. Prog. Phys.* **55** (1992) 113-155.

Wosik, J., K. Nesteruk, W. Zbieranowski and A. Sienkiewicz, "Composite transducer for longitudinal strain modulation", *J. Phys. E.: Sci. Instrum.* **11** (1978) 1200-1202.

Wu, Y., J. Stöhr, B. D. Hermsmeier, M. G. Samant and D. Weller, "Enhanced orbital magnetic moment on Co atoms in Co/Pd multilayers: a magnetic circular dichroism study", *Phys. Rev. Lett.* **69** (1992) 2307-2310.

Xiao, G., J. Q. Wang and P. Xiong, "Giant magnetoresistance and its evolution in the granular Fe_xAg_{1-x} system ($0 \leq x \leq 100$)", *Appl. Phys. Lett.* **62** (1993) 420-422.

Yamaguchi, A., S. Ogu, J. Zhang and R. Yamamoto, "Perpendicular magnetic anisotropy of the multilayer films Ag/Co/Pd and Pd/Co/Ag", *J. Magn. Magn. Mat.* **126** (1993) 300-302.

Yang, W. M. C., T. Tsakalakos and J. E. Hilliard, "Enhanced elastic modulus in composition-modulated gold-nickel and copper-palladium foils", *J. Appl. Phys.* **48** (1977) 876-879.

Zuberek, R., H. Szymczak, R. Krishnan, H. O. Gupta, C. Sella and M. Kaabouchi, "Magnetostriction of sputtered Co/C multilayers", *J. Magn. Magn. Mat.* **101** (1991) 219-220.

Zuberek, R., H. Szymczak, R. Krishnan, C. Sella and M. Kaabouchi, "Interface magnetostriction of sputtered Fe/C multilayers", *J. Magn. Magn. Mat.* **121** (1993) 510-512.

Zuberek, R., H. Szymczak, R. Krishnan and M. Tessier, "Magnetostriction constant of multilayer Ni-Ag films determined by ferromagnetic resonance", *J. de Phys.* **49** (1988) C8-1761 to C8-1762 (Colloq. C8, supplement to no. 12).

Zuberek, R., H. Szymczak, R. Krishnan, K. B. Youn and C. Sella, "Magnetostriction of multilayer Ni-C films", *IEEE Trans. Mag.* **MAG-23** (1987) 3699-3700.

Zuberek, R., H. Szymczak, G. Suran and K. Ounadjela, "Investigations of magnetostriction in $Co_{0.86}Ti_{0.14}$ amorphous thin films", *Thin Solid Films* **188** (1990) 1-5.

Zuberek, R., Institute of Physics, Polish Academy of Sciences, Warsaw, Poland, private communication (1993).